2004

Novel Apparatus to Control Electrospinning Fiber Orientation for the Production of Tissue Engineering Scaffolds

Eugene David Boland
Virginia Commonwealth University

NOVEL APPARATUS TO CONTROL ELECTROSPINNING FIBER ORIENTATION FOR THE PRODUCTION OF TISSUE ENGINEERING SCAFFOLDS

A dissertation submitted in partial fulfillment of the requirements for the degree of Doctor of Philosophy at Virginia Commonwealth University.

by

EUGENE DAVID BOLAND
Bachelor of Science, Marquette University, 1994

Director: Gary L. Bowlin, PhD
Associate Professor
Department of Biomedical Engineering

Virginia Commonwealth University
Richmond, Virginia
May 2004

Acknowledgement

I would like to begin by thanking my wife, Lisa, for all her love and support through the years and for her willingness to follow me as my jobs and dreams have dragged us around the country. I am especially grateful for the financial hardship she, and my children, Alexandra, Derek and Jasper, have accepted for me to pursue this degree.

I would like to thank the faculty and staff in the Department of Biomedical Engineering for allowing me to follow my dream through support and instruction. My mentor and director, Dr. Gary Bowlin, has provided advising, leadership, structure and discipline but most importantly friendship. Dr. David Simpson provided me with a research "home away from home" in the Department of Anatomy and Neurobiology and so much more. Members of both laboratories, especially Todd Telemeco, Jamil Matthews, Andy Anderson and Mike McManus, have made the experience rewarding and definitely unforgettable. Sushi Fridays will live forever in my memories. I would also like to include Johnny Owens for his morning wit and wisdom, at times much more stimulating then the coffee he shared it over.

Family is where it all comes back. For everything my parents have done not least of all for teaching me that I can do anything I put my mind to and never being afraid to follow a dream and my sister for her "been there, done that" advise when the words wouldn't come. And finally for Lisa's parents and sister who have done so much to help through the years.

Table of Contents

List of Tables

Page

List of Figures

Page

List of Abbreviations

°C	degrees Celsius
3-D	three-dimensional
AC	alternating current
AFM	atomic force microscopy
ANOVA	analysis of variance
BMSC	bone marrow stromal cells
cm	centimeter
COM1	serial communication port number 1
cos	cosine
cP	centipoise
DC	direct current
DMEM	Delbecco's Modified Eagle Medium
EC	endothelial cell
ECM	extracellular matrix
ESCA	electron spectroscopy for chemical analysis
FB	fibroblasts
FBS	fetal bovine serum
FDA	Food and Drug Administration
g	gram

HCl	hydrochloric acid
HFIPA, HFIP, HFP	1,1,1,3,3,3 hexafluoro-2-propanol
hr	hour
ID	internal diameter
in (")	inch
ITS+l	Insulin-Transferrin-Sodium Selenite media with linoleic acid
KRB	Kreg's-Ringer buffer solution
kV	kilovolt
L	liter
ln	natural log
m	meter
m/s	meters per second
M	Molar
MEM	Minimum Essential Medium
mg	milligram
ml, mL	milliliter
mm	millimeter
mm/s	millimeters per second
mM	millimolar
MPa	megapascal

MRI	magnetic resonance imaging
ms	millisecond
N	Newton
NaOH	sodium hydroxide
ng	nanogram
NIH	National Institutes of Health
nm	nanometer
OD	outer diameter
P/N	part number
PCL	poly(ε-caprolactone)
PDLA	poly(D-lactic acid)
PDS	Polydioxanone
PEG	poly(ethylene glycol)
PEO	poly(ethylene oxide)
PGA	poly(glycolic acid)
pH	power of Hydrogen
PLA	poly(lactic acid)
PLLA	poly(L-lactic acid)
RCCS	rotary cell culture system
Revs/sec	revolutions per second

Revs/sec/sec	revolutions per second per second
RPM, rpm, r.p.m.	revolutions per minute
sec	second
SEM	scanning electron microscope
SERS	surface enhanced Raman scattering
SMC	smooth muscle cell
STLV	slow turning lateral vessel
tan	tangent
TEBAC	tetraethyl benzylammonium chloride
TEM	transmission electron microscope
UTHSCSA	University of Texas Health Sciences Center – San Antonio
V	volt
v/v	volume to volume ratio
w/v	weight to volume ratio
wt%	weight percent
µl	microliter
µm	micron
π	Pi (numerical constant)

Abstract

NOVEL APPARATUS TO CONTROL ELECTROSPINNING FIBER ORIENTATION FOR THE PRODUCTION OF TISSUE ENGINEERING SCAFFOLDS

By Eugene David Boland, Ph.D.

A Dissertation submitted in partial fulfillment of the requirements for the degree of Doctor of Philosophy at Virginia Commonwealth University.

Virginia Commonwealth University, 2004

Major Director: Gary Lee Bowlin, Ph.D.
Associate Professor
Department of Biomedical Engineering

The conception of electrospinning can trace its roots back more than 400 years, when it was observed that rubbed amber can deform a droplet of water on a smooth surface, and is based upon simple concepts of charge separation and surface tension. Since that time, considerable effort has been directed at both the cause and utility of this phenomenon. The specific aim of this dissertation project was to develop an automated electrostatic processing apparatus that was capable of controlling the three-dimensional architecture of an electrospun scaffold to further improve its utility in tissue engineering. The efficacy of using this technique has been well documented and can be adapted to produce tissue

engineering scaffolds for a variety of tissues and organs. This apparatus incorporates precise mandrel motion. The system is capable of 0 – 5000 revolution per minute rotation, 0 – 25 inch per second translation and ± 40° rotation about the electrospinning jet axis for repeatable scaffold production. Fiber alignment and scaffold density are precisely controlled by rotating a mandrel along one axis, translation along that same axis, and rotation around the second axis perpendicular to the electrospun fiber stream. The control is accomplished with a PC based "supervisory" control program written partially in the LabVIEW® programming language and partially in SI Programmer supplied by Applied Motion Products. Scaffold thickness and fiber diameters are determined by the syringe metering pump flow rate, material being electrospun and solution concentrations. Through extensive laboratory analysis (mechanical testing and both optical and electron microscopy), parameters such as fiber orientation, diameter and mechanics can be predictive from specific polymer setups. Our laboratory has demonstrated the ability to electrospin natural and synthetic polymers and this apparatus will be utilized to tailor scaffolds to meet specific tissue engineering needs by creating a truly biomimicking scaffold / extracellular matrix.

Chapter 1 Historical Basis of Electrospinning

The ability to electrospin nanofibers began with an observation over 400 years ago when William Gilbert observed that a drop of water on a clean, flat surface can be drawn upward to form a standing cone when amber is rubbed and held at an appropriate distance above the drop (107). The phenomenon remained a curiosity until Lord Rayleigh, in the 1880's, began evaluating the physical and electrical forces present in the droplet (90). Rayleigh began with the supposition that a spherical droplet of water acted upon by only an electrical repulsion is in a state of unstable equilibrium. As long as the droplet remains spherical, its electrical potential is equal to its charge divided by its radius. As the charge and subsequent potential rise, the droplet will begin to deform. This deformation force is opposed by the cohesive tension that is characteristic of the liquid. Rayleigh deduced that the stabilizing surface tension T was related to charge (Q) by the following equation where the spherical radius is a.

$$T > \frac{Q^2}{16\pi a^3} \tag{1}$$

When this equation no longer holds true due to an increase in charge or a decrease in radius, liquid is thrown off in fine jets. Rayleigh did not take inductor distance into consideration except to say that the distance should be adequate to prevent sparks but short enough to cause the effect (90).

This work and a long-known experiment of threads being pulled from highly electrified molten sealing wax provided the basis for John Zeleny to study this phenomenon in the early 1900's (126). In 1914, Zeleny devised a method for evaluating the electrical discharge from liquid points using an apparatus like the one depicted in Figure 1 (125). This experimental apparatus and procedure will be described in detail as it became the standard setup to examine this phenomenon for over 50 years.

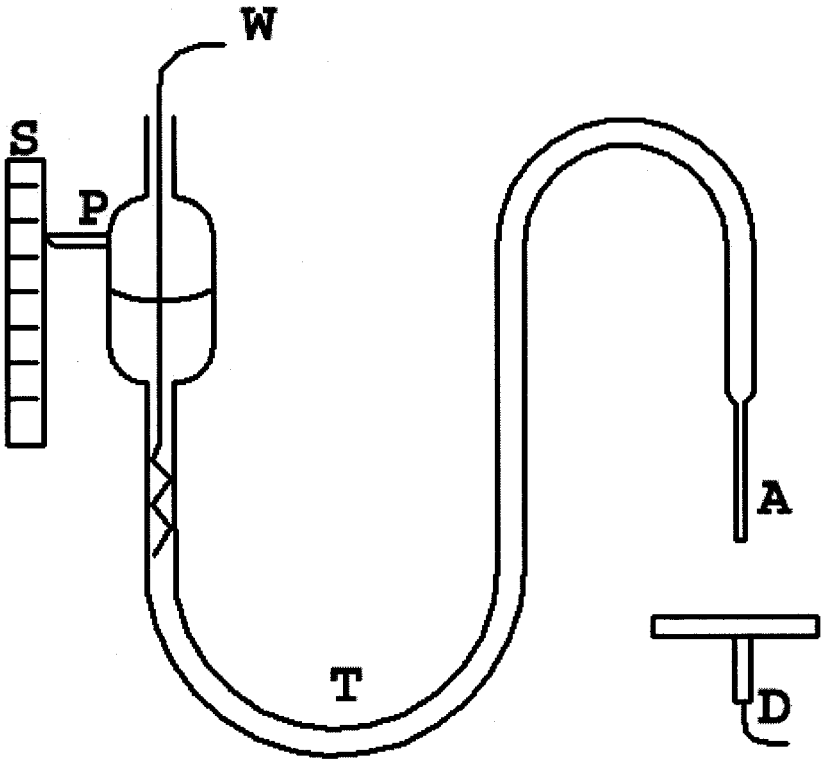

Figure 1. Experimental apparatus: (w) charge source and voltmeter, (s) scale to record reservoir height, (p) reference pointer, (T) rubber and glass tubing, (A) narrow exit tube (nozzle), (D) brass plate attached through a telephone receiver and galvanometer to ground.

This experimental apparatus consists of a voltmeter and static machine providing charge into a nonconductive reservoir and tubing system eventually leading to a narrow tube of uniform diameter not greater that 1mm diameter. The reservoir end was attached to a scale and could be raised or lowered to vary the static pressure in the fluid at the exit of the nozzle. The brass plate was held at 1.5 cm from the nozzle tip and provides a ground and electrical detection. The telephone receive will crackle as current is applied and the galvanometer was capable of measuring current with a resolution of 3×10^{-9} amperes. The static machine contained 15 leyden jars to stabilize the charge and the system was capable of shunting all or part of the current to ground to provide variable potentials to the test apparatus. The fluid of choice in these experiments was a weak hydrochloric acid solution to provide a conductive solution that would not leave a residue on the nozzle upon evaporation. Various acid concentrations were tried with little effect on the outcome (125).

To begin, the reservoir height (h) was adjusted to produce a hemispherical meniscus protruding from the nozzle. Knowing the radius of the tube (r), the density of the liquid (d) and the gravity constant (g), one can calculate the surface tension (T) using the following equation:

$$T = \frac{rhdg}{2} \tag{2}$$

This method proved capable as long as care was taken to assure a square cut end of the nozzle. As charge was gradually applied, the meniscus was stretched so that the reservoir must be lowered to maintain the original shape. If electrical intensity (f) was defined as the electrical pull per unit surface area of the meniscus and the lowered distance (p) was

equal to the distance that the reservoir was lowered to maintain the hemispherical meniscus, we derive the equation:

$$f = \sqrt{8\pi pdg} \tag{3}$$

This holds as long as no current was passing from the fluid to the grounding plate. When the potential reached a certain value, surface tension could no longer counter the electrical intensity and a discharge took place. A single click was heard and the galvanometer recorded a slight current passage. The magnitude of the electrical potential was reported to depend on the diameter of the point and the time that the liquid stood unused. After the discharge, the meniscus collapses and additional pressure was needed to reform the hemispherical shape. The discharge would not repeat itself at the same potential. The second discharge would require a 100 or more volt increase in the potential and again would be accompanied by a collapse of the meniscus. Further discharges occurred at diminishing steps until a potential was reached that produced steady discharges. The frequency of these steady discharges increased with increased potential. Finally, a point was reached when the meniscus became motionless and a steady deflection in the galvanometer was seen. This last stage continued through the 10,000 volt upper limit of the system (125).

Behavior of the oscillating meniscus was noted during the intermittent discharge phase as it was presumed to be attributable to the change in current flow. Although not described mathematically, it was assumed that the previous equations could account for the surface motion with instantaneous changes occurring at each discharge. Of particular interest was the observation that the meniscus rises slightly before a discharge. This

formed a region of greater curvature and it was from this region that the discharge took place. The difficulty arose from the way the surface tension increased immediately following a discharge. This proved difficult to measure. A second difficulty arose from the observation that the surface tension of the meniscus changed on standing while no current was passing. This second observation was partially explained by small currents depositing solids in the meniscus although this idea was not tested experimentally.

To address the apparent change in surface tension in a standing meniscus and since surface tension is used in all the calculations to evaluate electrical intensity; a method was derived to test the presupposed that the surface tension was the same before and after discharge. Assuming no change in composition, it was assumed that temperature would have the greatest impact on surface tension. A thin thermocouple was placed in and through the meniscus to capture these temperatures. Even at the highest current attainable with this system, no temperature change within the meniscus was measured. The droplets, however, were recorded to be up to 2° C lower then the bulk liquid. Since the temperature decreased with increased current, it was presumed that the drop in temperature was a result of an increased rate of evaporation. The final relationship derived in this study was a constant value for the product of the electrical intensity, expressed as electrostatic units per centimeter, multiplied by the square root of the nozzle radius (125).

Zeleny continued this research to examine the instability of electrified liquid surfaces in greater detail (126). When the electrification of a liquid in an apparatus like that in Figure 1 reached a certain limiting value, any slight displacement of the surface

resulted in the rapid increase of that displacement. This electrification potential depended on the surface tension of the liquid and the radius of curvature but the resulting jet was independent of a hydrostatic driving force. Initiation usually began at the lower end of the drop where the electrical density was greatest. At that point, the liquid was pulled out of the drop in a fine jet that then broke into very fine droplets. The specific jet location was explained as a redistribution of the electric charge resulting from any minor perturbation of the surface. It was theorized that a number of these locations could exist on the surface of the liquid and if the voltage provided adequate driving force, multiple jets could form (126).

In addressing his previous research, he inferred that as large droplets left the nozzle tip, a finite amount of charge was also removed from the liquid at the nozzle. This would explain the observation of the meniscus collapse previously attributed to an increased surface tension. Through precise photography, this inference was confirmed but noting that the elongated detached droplets of liquid retained the instability point for a short time even after being separated from the liquid in the nozzle. While these droplets did eventually collapse into spheres, sufficient evidence was acquired to support charge extraction.

Further evidence was gathered by examining the interactions between the fine jets of liquid and previously extracted droplets. These jets often changed direction very rapidly on account of the droplets of liquid ahead of them. The electrical force of these droplets caused large loops in the jet and, upon closer examination smaller more complex loops are evident within the larger loops. As the jet loops it was also observed to thin

until it rather suddenly broke into a fine mist of droplets. The initiating jet was straight and stable for a short distance with a diameter of 0.004 mm after leaving the meniscus. Knowing the rate of emission of the liquid, it was calculated that the jet was being expelled at a rate of 8 meters per second (126).

To induce multiple jets, the hydrostatic pressure was reduced below the requisite pressure to maintain a hemispherical meniscus. As the liquid flattened from a cone, the jet moved to the edge of the meniscus. Under this condition, it was possible to increase the voltage and cause a second point of instability along the edge of the meniscus. This instability quickly formed into a second jet along the edge. With further increases in voltage, it was reported that eight or more independent stationary jets where possible, all of which originated from the meniscus edge.

By 1930 the use of an electric field to form threads was already known. The application of such a field to liquids containing solid materials caused the production of silk-like spun fibers. The utility of these threads to the textile industry was not known. Many people experimented with the extraction of the artificially produced thread but found it too difficult with traditional collecting devices such as reels. Additionally, the fragility of the threads precluded all traditional textile fabrication techniques. In 1934, Anton Formhals was issued the first United States patent for the practical use of a process he coined "electrical spinning" and apparatus for preparing artificial thread (41). He theorized that a movable thread collection device that can support the artificial thread in a stretched form can be combined with the electrode that attracts the fiber. In that way, the thread collecting device itself exerts the attracting power on the thread. The entangled

threads that repel each other in space will stack parallel to each other on this device and can theoretically be removed in such a way as to have solid fibers. The collecting device can be regulated to the size and strength of the thread produced. Formals prepared cellulose acetate (and a softening agent) in a 50% acetone and 50% alcohol mixture to prove his concept. In this model, the receiving wheel catches multiple jets or an inter-tangled jet and combines it into a single fiber. The size of the thread produced is a function of the number of spinning jets and the rate at with the jets are collected. Theoretically, any size from a fine thread to a rope can be produced at any length from such an apparatus (41). Further refinements and a clearer reduction to practice can be seen with the ensuing patents (42, 43). These patents addressed some of the shortcomings of the initial patent, namely, the insufficient time for the fibers to dry before being collected and the effect of stray fibers interfering with the electrical spinning process. This new design (42) addressed these shortcomings. The distance between the electrified source and the collecting device was increased to facilitate drying of the fibers and additional charged strips, wires, screens, or plates will be placed in proximity of the fiber path to induce a higher degree of control on the deposition of these fibers. By altering the electric field, Formhals was able to direct the fiber jets with more precision to the intended target. In addition, multiple jets where used to improve the rate at which useful fibers could be manufactured. A further refinement of this process was realized in 1940 with the issue of a patent for his third iteration of the apparatus to produce artificial thread. This system incorporated a standard thread twisting and reel wrapping system as well as the ability to electrically spin material onto existing thread as it passed in front of

the spinning nozzles creating composites and expanding the utility of electrical spinning (43).

In the 1960's, Sir Geoffrey Taylor experimented with electrically driven jets to develop a more thorough theoretical model as he concluded that all previous work failed to fully describe the phenomenon (107). Taylor had subjected the phenomenon to theoretical postulation. He concluded that a conducting fluid could be held conically in equilibrium under the influence of an electric field. However, this was only possible when the semi-vertical angle of the fluid maintained 49.3° (107). He constructed and apparatus capable of holding such an angle to confirm his findings. An uncharged droplet of water in an electric field will begin spherical but become unstable when the field reaches a value of $1.62(T/r)^{½}$ where T is the surface tension of the specific liquid and r is the initial spherical radius. At this precise field strength, the drop will stretch into an ellipsoid with the major diameter 1.85 times as long as the minor diameter. At higher fields, the droplet will develop pointed ends and narrow jets or small droplets are torn off. Previous authors, such as Zeleny, described these jets but could not discuss their theoretical mechanics, possibly because they could not relate the field to the geometry of their apparatus even before the appearance of these jets.

Taylor chose to modify the apparatus originally designed by Zeleny to a system that could be compared more closely to theoretical calculations as depicted in Figure 2.

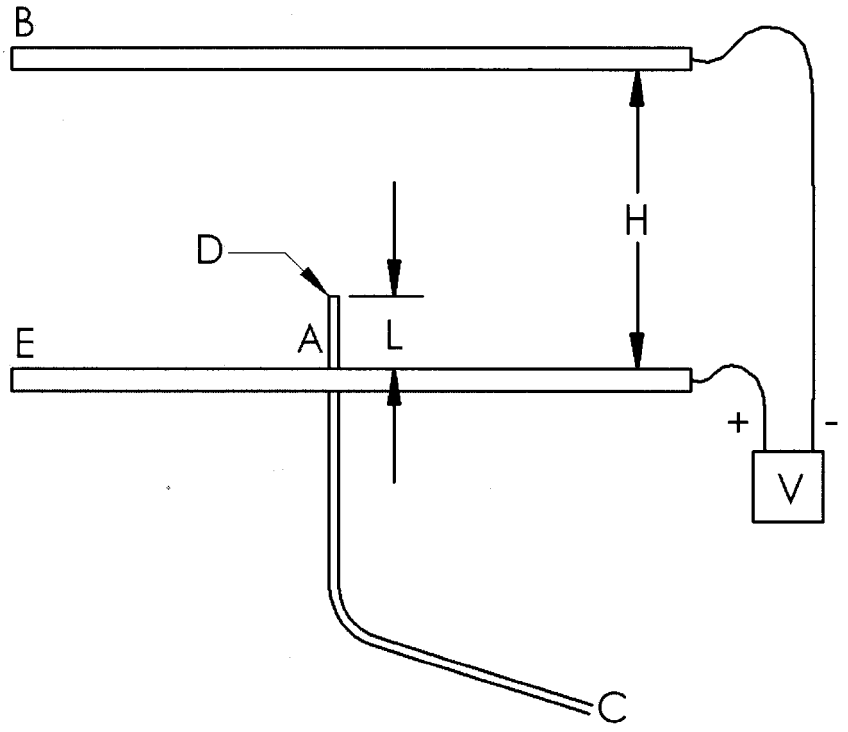

Figure 2. Taylor's two plate apparatus: (A) metal tube used to introduce the fluid to the field, (B and E) parallel plates used to establish the field, (C) reservoir or syringe to deliver fluid connected with non-conducting tubing to (A), (D) diameter of the metal tube, (H) separation of the plates, (L) length of the metal tube passing through plate (E), (V) voltage source.

In this system, two parallel plates established the static field. A metal tube was passed through the lower plate. This metal tube was connected to a pressure syringe or reservoir via non-conducting rubber tubing. The height and radius (R) of the metal tube could be

changed to fully explore the theoretical relationships. The following equation was derived to explain the force, P, exerted on a cylinder of length L.

$$P=\frac{V^2L^2}{4H^2}*\frac{1}{\ln(2L/R)-\frac{3}{2}} \tag{4}$$

This equation could be used to compare experimental values with theory. One possible source of discrepancy in this approach was the theory used infinite plates. The plates were increased in size but no appreciable difference was seen so the experiments were carried forward. Using a solution of glycerin with 5% to 10% sodium chloride a standing cone was possible. This stable meniscus was confirmed to be the predicted value of 49.3° (107). This conical shape continued to the outer edge of the tube which was not derivable from theory. Barring this anomaly, Taylor proceeded to derive an equation to predict the voltage required to develop this standing cone. In the following equation, V_k is the supplied potential in kilovolts with all other variables taken from the diagram in Figure 2.

$$V_k^2=\frac{4H^2}{L^2}\left(\ln\left(\frac{2L}{R}\right)-\frac{3}{2}\right)(1.30\pi RT)(0.09) \tag{5}$$

Experimentation with three metal tubes (radii of 0.05, 0.12, and 0.163) inserted between 1.5 and 21.0 centimeters through the plate yielded observed voltages very close to those predicted by Equation 5 and all the results were within typical experimental error (107). It must be noted that there is very little difference between the voltage needed to form a stable cone and the voltage that will result in instability where the end becomes pointed and starts throwing off drops. This experimentation was repeated with non-conducting fluids (transformer and silicon oils) with similar results.

The constitutive equations developed by Taylor were only capable of considering the normal force that an electric field could exert on a conducting surface. This may have adequately described the initial jet formation but was insufficient in describing the complete phenomenon. One divergence from Taylor's model was the instability seen at the tip of a jet leaving an otherwise stable cone. Taylor went on to theorize that the tip of standing jet slows down and causes the jet to contract longitudinally. The viscous stress in the jet then reversed and the jet became unstable in a manner analogous to an elastic column under compression. Taylor believed that a small amount of crumpling could relieve the stress and prevent the jet from becoming violently unstable. He noted the similarity of the jet tip with the observed oscillation of a viscous fluid being poured slowly onto a stationary plate. While this inference may have satisfied him observationally, he admitted that he too had failed at developing a full mathematical model (107).

Taylor then redirected his efforts to develop a theoretical model for the cylindrical liquid conductor in a radial field. This model would be useful in predicting the behavior of varicose instabilities originally reported by Rayleigh (107). These instabilities cause wave patterns to be observed in an electrified jet. In view of the difficulty Rayleigh and others found in trying to account for these instabilities, Taylor devised an apparatus that could subject a cylindrical soap film to a radial field. This apparatus allowed a film to be produced with a circumference greater than its length. Taylor postulated that this apparatus would mimic the conditions of an electrified jet yet be more controllable thereby allowing Taylor to model the system mathematically and compare these

experimental results with those of pure theory. This testing ended with a mathematically correct model that was of little practical use. The apparatus developed by Taylor was not capable of producing soap films of an adequate geometry to reach a stabilizing potential without first reaching a destabilizing potential. His soap films would simply rupture when destabilized rather than mimic a destabilized jet. A destabilized jet would be characterized by lateral motion, oscillation and Rayleigh varicose instability (107).

Peter Baumgarten, a contemporary of Taylor, focused his research at E. I. du Pont de Nemours & Co. on the applications of electrospinning acrylic resins based in part on the work done by Formhals. The experimental setup was similar to Zeleny except the spinning solution was fed by a positive displacement infusion pump and the high voltage power supply was attached directly to the stainless steel capillary tube being used as the nozzle. The electrospin fibers were collected on a grounded metal screen. Baumgarten was interested in the ability to produce acrylic fibers below 1 micron in diameter as well as the theory behind such fiber formation. Through this experimentation of electrospinning a copolymer of 93.6% acrylonitrile, 6% methyl acrylate and 0.4% sodium styrene sulfonate (a common commercial acrylic resin) in dimethyl formamide, Baumgarten demonstrated that concentration and viscosity of the electrospinning solution significantly effects the diameter of the fibers produced as well as the length of the stable jet (6). High speed photography revealed that a single fiber was produced by the jet and the loops shot out radially at a velocity of 6 to 7 m/s as the jet fell to the screen at a rate of 1.8 to 3.7 m/s (6). Experimentation with feed rate, voltage and spinneret to ground (gap) distance revealed and interdependence with optimum feed rate increasing with

voltage and the jet length increased with increased voltage and with decreased gap distance. Through all these changes, there was very little change in the diameter of the fibers produced. Nozzle diameter and polarity did not have any measurable effects. Baumgarten also examined electrospinning atmosphere and found dry air (relative humidity < 5%) caused the spinneret to clog and in humid air (relative humidity > 60%) the solution did not dry and caused significant entanglement above the grounded screen. A helium atmosphere caused the field to breakdown at 2500V so electrospinning was not possible. At higher voltages, corona discharge could be seen with currents more that 100 times higher than electrospinning in air. Two differences were noted while spinning in a Freon-12 gas environment. The fiber diameters were 1.4 to 2.6 times greater than fibers spun in air at otherwise identical conditions. The other is that numerous side jets were seen as offshoots from the main jet. These offshoots were all seen at sharp bends in the main jet. One additional conclusion reached by Baumgarten in the work was that if the conductivity of the electrospinning solutions was too high only droplets could be formed and if the conductivity was too low the flow rates for sustained spinning would become too small to achieve reasonable geometries (6).

In conclusion, this pioneering work of Lord Rayleigh, John Zeleny, Anton Formhals, Geoffrey Taylor and Peter Baumgarten helped establish the science and practice of electrospinning. Rayleigh introduced the competing equilibrium between surface tension and electrical potential and is also credited with first describing varicose waves in a jet that are now simply referred to as Rayleigh instabilities. John Zeleny devised an apparatus capable of testing and developing electrical force theories and is

very similar to devices used to this day. Anton Formhals reduced the phenomenon to commercial use thus validating the utility of electrospinning outside the world of theoretical physics. This reduction to practice was expanded by Baumgarten who evaluated many of the practical parameters that control fiber size and quality. Geoffrey Taylor built upon the work of Zeleny to examine stabilizing forces present in electrospinning. Although his work originated on a theoretically stable cone that can be formed by electrifying a liquid, his name is attached to the cone that forms during the electrospinning process. His other contributions were a refined apparatus to produce stable jets and predictive equations to determine the voltage requirements to stabilize jet oscillations and Rayleigh instabilities.

Chapter 2 Jet Stabilization and Process Parameters in Electrospinning

Interest in electrospinning has been increasing rapidly in recent years as seen in Figure 3.

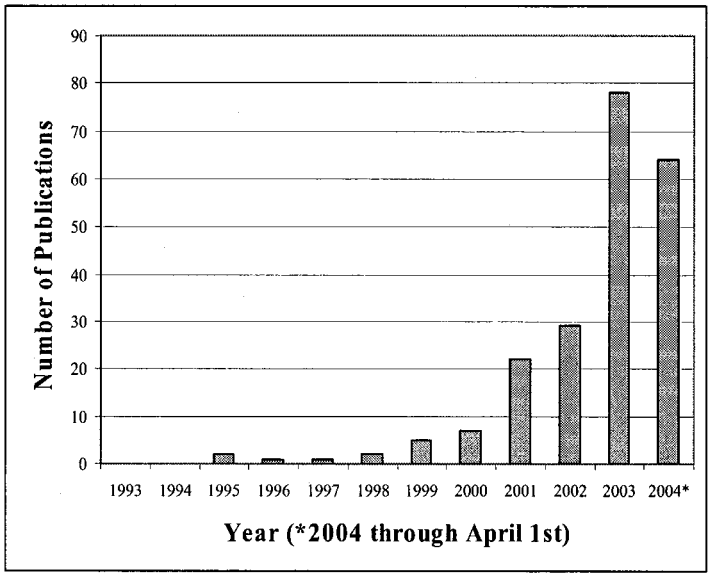

Figure 3. The number of publications using "electrospinning" as a key word using the ISI Web of Knowledge database accessed on April 1, 2004 (http://isi10.isiknowledge.com/portal.cgi).

Much of this interest has been exploring what materials can be electrospun and solvent systems can be used. A small subset of this work has been interested in the processing / property relationships. The key solution parameters include concentration, viscosity and conductivity and the key field parameters include voltage, jet current and nozzle to target distances. An even smaller subset of these papers was concerned with jet and field

stability. This latter work is the continuation of Taylor's study using more precise instrumentation and an improved computational ability to expand the theoretical basis for electrospinning.

A schematic diagram to interpret electrospinning of polymer nanofibers is shown in Figure 4.

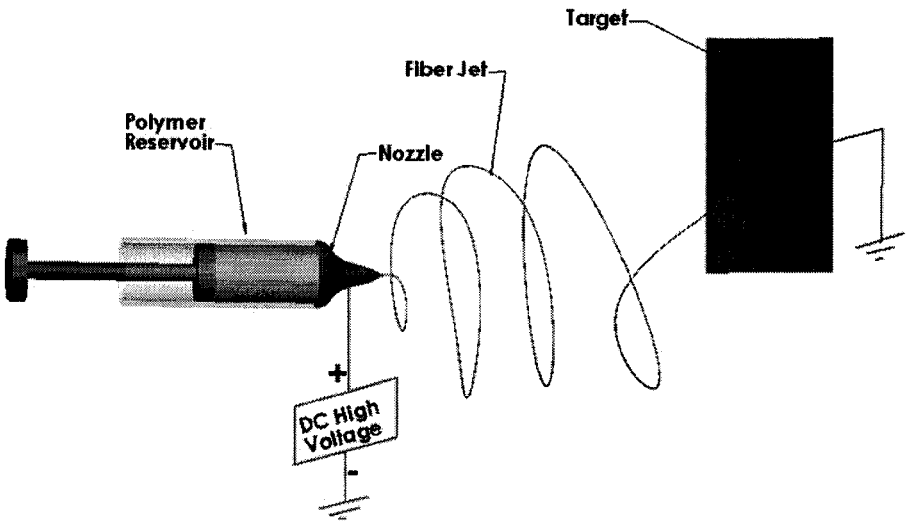

Figure 4. A schematic representation of a typical electrospinning setup.

There are three critical components to establish the process: a high voltage power supply, a reservoir with a small diameter pipette or needle to serve as a nozzle, and a conductive target. In the electrospinning process a high voltage power supply is used to electrically charge the polymer solution and create a static field between the reservoir and the oppositely charged target. Mutual charge repulsion within the polymer solution and the attraction of the surface charges to the countercharged electrode induces a force in direct opposition to the surface tension. This charge-induced force causes the hemispherical surface of the polymer solution at the tip of the nozzle to elongate into a conical shape

known as the Taylor cone. As the driving voltage is increased, a critical value is attained at which time the repulsive electrostatic force overcomes the surface tension and a charged jet of the polymer solution is ejected from the tip of the Taylor cone. The discharged polymer solution jet undergoes an instability and elongation process that stretches and thins the jet. Meanwhile, depending on the volatility of the solvent and the electrospinning environment, the solvent evaporates and a dry fiber is collected on the target. Due to the convoluted path and possible interconnections during the drying phase, the mat produced resembles an interconnected web of nano to micro-scale fibers. With this basic understanding, the individual variables can be examined more closely.

Jet Stabilization

Theoretical postulation about the governance of thin liquid jets in an electric field dates back to the work of Rayleigh. Zeleny advanced the study and more recently, Taylor provided important insight with his combination of theory and experimentation. It has been demonstrated in recent years that Taylor's study of stable cones can also apply to highly viscous uncharged jets as well as thin charged jets (92).

Reneker et al. (92) used the electrospinning of an aqueous solution of high molecular weight polyethylene oxide to study jet stability and downstream bending instability. In their setup, a straight jet was formed as a consequence of electrical forces. As a suspended drop of solution was subjected to an increasing electrical field, a conical protrusion, commonly referred to as a Taylor cone, formed and was the initiation point for the jet. The electrically charged jet traveled in a straight path for a few centimeters.

At the end of this straight jet, a semitransparent shape, also conical, could be detected with proper illumination. This conical region defined the envelope in space where the unstable portion of the jet can be found (92, 100, 103). Images of this conical region with sufficiently short exposure times reveal continuously bending fibers following a tortuous path (6, 92, 100).

To understand this phenomenon in greater detail, an understanding of electrical charge is required. The common assumption that a charge instantaneously traverses metals is not appropriate when dealing with ionic conductivity of moving fluids. In an uncharged ionic solution, equivalent numbers of positive and negative ions exist in each volume element. This produces no external field. However, when a field is applied to such a volume element, the charged ions tend to move in opposite directions. The positive ions are forced toward the negative electrode and the negative ions are forced toward the positive electrode. The difference in number of positive and negative ions in a volume element is referred to as a charge imbalance or simply the charge of the volume. This excess charge can establish electrical fields that span large distances. Techniques such as salt addition can increase the quantity of ions in any giving volume element but has no effect on the excess charge produced. What can be accomplished with this increased conductivity, is an increase in the rate of change in any given volume element. This response can influence the electrical field in a given region of the jet and ultimately affect the shape of the jet (33, 57, 92, 100, 103). Calculations of ion drift velocities in Reneker's system were estimated at 0.1 m/s based on the applied electrical field, polymer conductivity and distance between the suspended drop and the collection plate. The jet

velocity was estimated at 1.0 m/s or approximately 10-times faster then the ability of the ions to move within the solution (92). Due to the velocity disparity, ionic charge was assumed to be stationary for many of the included calculations.

The variables that affected the behavior of the electrified fluid jet during electrospinning could be split into one of two categories: fluid properties and operating parameters. The relevant fluid properties were viscosity, conductivity, dielectric constant and surface tension. The relevant operating parameters were flow rate, jet current, applied electrical potential, and distance between the nozzle and the collector. The applied field was assumed to be the applied voltage divided by the distance between the nozzle and the collector.

As an electric potential was applied to an otherwise unchanging system, two distinct voltages transitions were readily determinable. The first point was the voltage at which a dripping nozzle first formed a stable jet. A narrow window between no jet formation and stable jet formation was observed. As the potential was steadily increased, a second transition voltage was observed. This caused the stable jet to become unstable. This instability was characterized as bending oscillations of the jet centerline. Raising and lowering the voltages demonstrated that very little hysteresis existed in this system. Voltage measurements were reproducible to within 0.2kV independent of the direction of the change in voltage (100).

While experimentation was conducted in the stable jet region, detailed study of varicose waves, or Rayleigh instabilities, could be performed. Perturbations of a stable jet were determined to be the underlying cause of these waves. By applying

electrohydrodymanic theory, it is evident that stable jets preferentially produce axisymmetric instabilities when perturbed (100). This finding was in agreement with observations of Rayleigh, Zeleny and Taylor. Another equally important finding that was made while studying stable jets was a deposition and coalescence of fluid on the collector. No fibers were capable of being produced across a wide range of solution concentrations. Fiber formation only occurred at voltages above the transition to unstable jet formation. Shin postulated that this instability was crucial to accelerate solidification of the jet into fibers (100).

Bending Instability

To study jet instability, Reneker imaged the region containing the vortex of the instability cone at 2000 frames per second (92). This high speed time course allowed the evolution and shape of the jet to be examined with a high degree of temporal and spatial accuracy. After the initially small bending oscillation near the end of the straight jet, the amplitude of the bending increased until the jet broke into a bending, winding, spiraling and looping path within the three dimensional space defined by the previously observed conical envelope. Each cycle of bending instability can be described in a three step process. The first step is the sudden onset of multiple bends in a previously straight or slightly curved jet. The second step is the expansion of each of these bends into a series of spiraling loops. The final step is localized thinning of the fiber as a direct result of the loop expansion. This three step process was observed to continue throughout the jet's travel toward the collector with the length of the initiation region for the first step

continually being reduced. The process ended when the jets were fully dry or in contact with the collector. The overall path toward the collector was determined to be driven by the vector sum of the externally applied electric field, the charge that was momentarily suspended in space by the jets, the drag from the electrospinning atmosphere and the interactions of charged fibers on each other (92). This further confirmed the work of Taylor who indicated that the process was insignificantly affected by gravity (107).

Detailed time course studies on specific regions of the jets were conducted to further develop a governing mathematical model for electrospinning. Observationally, a small region of the jet was followed to verify that the previous three step process was occurring throughout the jet. In one such study, three instability cycles where observed within a 38.5 ms window with an average rate of elongation of approximately 120 mm/s (92). A sketched representation of three instability cycles can be seen in Figure 5.

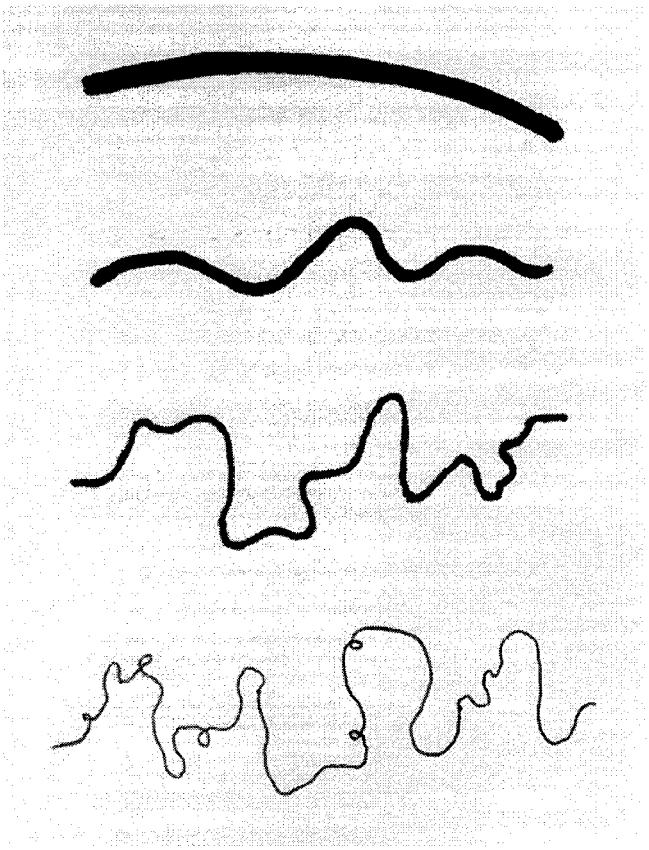

Figure 5. Sketched representation of three instability cycles where a slightly curved jet begins oscillating then each of the subsequent loops begin to oscillate finally leading to a third oscillation and a very complex fiber pathway. Note that fiber thinning takes place at each cycle.

These smaller bending segments continued to elongate, however, the images of these trajectories grew fainter as the less light was reflected by the ever-thinning jet. It can be assumed that this elongation process continues as long as the charge of the jet provided enough force to overcome jet viscosity. Eventually, as the jet dries, the viscosity will be sufficiently high to prevent further elongation. The exact evolution of fiber drying has yet to be described in detail due to limitations in observation schemes.

The advance in video technology from 30 frames per second to several thousand frames per second has changed one commonly held perception of electrospinning, namely splay. Splay is the term to describe the condition of a single jet splitting into multiple jets within the region of bending instability. Reneker discredited this concept as the primary means of jet thinning by photographing the same electrospinning jet with a typical 16.7 ms exposure of a video camera and a 1.0 ms exposure of a high speed video camera. The three dimensional path of rapid segmental expansion appears to be multiple jets in one image and appears as a tortuous path of a single jet in the other. This is not to say that splay does not happen. Throughout Reneker's study, smaller splay jets where observed to branch off the main jet; however, these occurrences were very rare (92).

Only after improvements in illumination were made, could the true jet path be determined. This was the missing element in all previous theories describing electrospinning. The coiling and looping nature of the jet is very much like the well documented tendency of any liquid jet traveling in an axial direction striking a hard plate normal to the surface (92). These observations formed the basis of a viscoelastic model of rectilinear motion for an electrified jet (92, 122, 123). A detailed mathematical evaluation of this theory will not be included in this work. Instead, a summary of the finding as they apply to the practice of electrospinning shall be discussed.

Thin rectilinear liquid jets are made unstable by capillary (varicose) perturbations that are driven by the surface tension of the electrospinning solution. These instabilities can be made stable through longitudinal stretching of the jet (38, 52, 92, 101, 122). In electrospinning, jets are stretched by the applied electrical field as well as repulsion from

nearby charged jets. As long as the jet is capable of elongating, it is capable of resisting these varicose instabilities. The consequence of a jet being unable to continue to elongate will be addressed in following sections.

Another aspect of this theory examines the longitudinal strain within the jet and its affect on molecular orientation. Observationally, it is expected that the large reduction in area coupled with the high longitudinal strain would cause macromolecules to be stretched and axially aligned. Theory suggests that a random coil can be transformed into a stretched macromolecule if the product of the strain rate and the conformational relaxation time of a given molecule is greater than 0.5. Since a typical electrospinning process produces a product between 10 and 1000, there is ample evidence to support the theory that macromolecules will be stretched along the axis of the fiber. This stretching phenomenon could also account for reduced crystallinity in electrospun fibers (72, 91, 92, 121, 128).

All aspects of the electrospinning process as well as individual bending instabilities within an electrospun jet can be viewed as particular examples of the Earnshaw theorem in electrostatics. This very general theorem states that a collection of point charges cannot be maintained in an equilibrium configuration solely by the electrostatic interaction of the charges. This was first stated by Samuel Earnshaw in 1842. Application of this theorem to electrospinning leads to the conclusion that it is impossible to create a stable structure in which the elements of the structure interact only by Coulomb charge forces thus supporting the use of Maxwellian viscoelastic resistance elements in the predictive model developed by Reneker and Yarin (92, 122, 123).

Voltage Dependence

As discussed earlier, electrospinning voltage has a distinct effect on the morphology of the electrospun fibers. It was expected that the degree of instability at the surface of the liquid from which the jet initiates should generate changes in the fibers produced. Deitzel, et al confirmed experimentally, using a solution of polyethylene oxide in water, that applied voltage will change the initiating drop shape which changes the ensuing jet and fibers produced (33). At low voltages (approximately 5.5kV) a droplet of solution remained suspended at the end of the syringe needle, and the fiber jet originated from a conical protrusion at the bottom of the droplet. This protrusion had a semi-vertical angle of about 50.8°, in agreement with Taylor's theoretical prediction and measurements of 49.3° for a viscous fluid in an electric field (33, 107). The fibers produced under these conditions had a cylindrical morphology with very few "bead on a string" defects observed. As voltage was increased and all other parameter held constant, the volume of the droplet decreased. At voltages of 7 kV or more, the cone had receded and the jet originated from the liquid surface within the syringe tip. The electrospun fibers produced still have essentially a cylindrical morphology, but there is a distinct increase in number of "bead on a string" occurrences in the fibrous mat. At 9.0 kV the solution jet appears to be initiating directly from the tip with no externally visible droplet. At this voltage, the jet moves around the edge of the syringe tip. This would indicate that the jet originated on the inside of the syringe needle and probably where the edge of the liquid surface met the needle wall. The fibers produced under these conditions have a high bead density. The rate of occurrence of these defects increase sharply over 7.0 kV

in this system (33). In addition to increased numbers of beads, Zong reported a change in bead morphology from spindle shaped to more spherical. Representative scanning electron micrographs of bead morphologies can be seen in Figure 6.

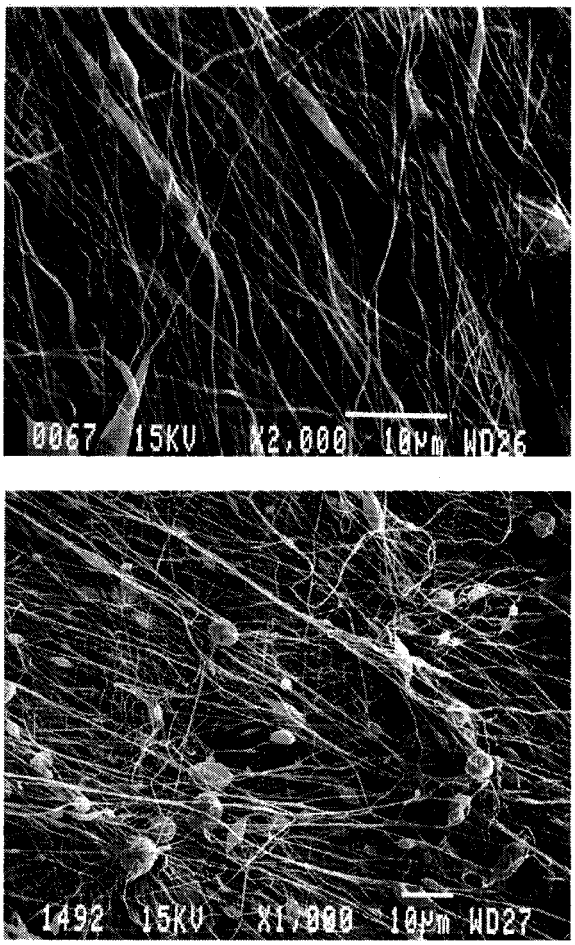

Figure 6. Top micrograph (2000x magnification) depicts spindle shaped bead defects in poly(glycolic acid). Bottom micrograph (1000x magnification) depicts more spherical bead defects also occurring in poly(glycolic acid) at a higher density.

Another observation while electrospinning poly(D-lactic acid) (PDLA) from a dimethyl formamide solution was evidence that higher voltages increased the overall fiber

diameter (127). The cause of the voltage dependence was not determined for either observation.

Solution Dependence

As previously stated, the key solution parameters include concentration, viscosity and conductivity. Many authors have reported that dramatic morphological changes have been found when the concentrations of polymer solutions were changed. That is to say, the concentration or the corresponding viscosity was the most effective variable to control the fiber morphology. In one such study by Zong, as the viscosity of a PDLA solution was increased (lower than the process limiting concentration), larger fibers with more uniform diameters were formed. Additionally, the diameters of the beads became larger and the average distance between the beads also increased as the viscosity of the PDLA solution increased (127, 128). The following reason was offered to explain the concentration effect on the fiber morphology during electrospinning. At lower concentrations, electrospun fibers are harder to dry before they reach the collection drum (127). The visual presence of junctions and fused bundles on the SEM micrographs of electrospun low concentration PDLA solutions indicated that the polymer fibers were still wet at the time that they reach the collector. In addition to junctions and bundles, fibers produced from low concentration solutions tend to have a great deal of variability in diameter along single fibers (33). Since wet fibers are no longer subjected to the field effects as they lay on the grounded target, their solidification process is controlled by surface tension and a viscoelastic relaxation process determined by the material being

electrospun and the degree of dryness of the deposited fibers. This process could produce the observed undulating morphology (127). In contrast, at higher concentrations, the electrospun fibers were mostly dried by the time they were collected. The apparent change in morphology may be reflective of the lower surface tension and solvent content in the high concentration solutions (33). In general, Zong found that the effect of the electric field opposed the effect of viscosity in controlling the morphology of the electrospun fibers (127). Many authors have shown that the relationship between concentration and fiber diameter is directly related. Dietzel has proposed a power law relationship with the exponent of about 0.5 for a polyethylene oxide in water solution (33) while Boland and Matthews have seen a linear relationship for synthetic and natural polymers electrospun from various polar solvents (14-16, 18, 76, 77).

Solution concentration and viscosity are closely coupled variables but conductivity can be readily varied. As previously shown by Taylor and subsequently by Reneker, addition of ions to a electrospinning solution will not change the potential of the solution but does change the charge density (92, 107). It is this charge density that will affect the morphology of the fibers produced from the electrospinning process. Zong demonstrated the effects of salt addition experimentally. The starting solution was 30 weight percent PDLA in dimethyl formamide. Under the experimental setup, this concentration produced "beads on a string" with great regularity. To verify the effects of salt, solutions were made containing potassium phosphate, sodium phosphate or sodium chloride at various weight percentages. It was observed that no "beads on a string" were formed for the solution with the addition of 1 wt% salts. All the resulting fibers exhibit a

uniform diameter ranging from 200 to 1000 nm (127). It was theorized that the addition of salts resulted in a higher charge density on the surface of ejected jet during spinning, thus more electric charges were carried by the electrospinning jet (107, 126, 127). As the charges carried by the jet increased, higher elongation forces are imposed to the jet by both the electrical field and charge repulsion of adjacent fibers. It is known that the overall tension in the fibers depends on the self-repulsion of the excess charges on the jet (39). Therefore, as the charge density increased, the self repulsive forces increased. In all cases, the diameter of the fibers produced were considerably smaller then the solution without the addition of any salts. Likewise, as the ion concentration per weight of the salts increased, the fiber size decreased (potassium phosphate has the lowest ion concentration per weight and sodium chloride has the highest) (127).

One of the most significant parameters yet to be discussed in detail that effect electrospun fibers is surface tension of the electrospinning solution. For the most part, the formation of beads on a string is driven by the surface tension (39). Surface tension forces try to reduce the surface area per unit mass. In electrospinning, charge excess in the fibers produces a self-repulsive force which opposes bead formation and favors thinner jets, resulting in an increase in the surface area per unit mass. These forces are coupled by the viscoelastic force of the polymer jet to resist any rapid change in shape. To better understand surface tension, a more detail examination in needed.

Surface tension acts on an electrospinning fiber the same way it acts on a solid rod. Surface tension attempts to convert rod shapes into sphere shapes to conserve energy. The ability of a solid object to resist this deformation force is generally high

enough that the surface tension forces do not usually produce measurable deformation. The axial force caused by the surface tension is known to be πDT, where D is the diameter and T is the surface tension coefficient. Knowing the cross-sectional area of a cylinder is $\pi D^2/4$, the radial pressure on that circular cross section would be 4T/D. As D approaches the diameter of a single molecule, the effects of surface tension will make the stretched molecular conformation unstable (as opposed to the coiled conformation) (39). The compressive strengths of polymer fibers have not been characterized but information available from other systems suggest that the range of 200–400 MPa would be representative (39). Likewise, the surface tension of an electrospinning jet has not been characterized but it should be adequate to use the value for the electrospinning solution. These values can be used to solve for the diameter of a polymer fiber that is unstable because of its surface tension (39).

When trying to predict or cause specific fiber morphology, it is critical to understand the interactions between all the solution parameters discussed. There is competition between surface tension and viscoelastic force. Increasing viscoelastic force (increased concentration) will favor the formation of smooth fibers with larger diameters. Likewise, reducing the surface tension, such as the addition of ethanol, will favor the formation of larger smooth fibers. Another competition in electrospinning is between electrical force and viscoelastic force. Increasing the charge density such as with the addition of salt will increase the associated electrical forces favors the formation of smaller smooth fibers. Again decreasing the viscoelastic force, such as reducing the polymer concentration, will reduce fiber size. Therefore, a multifaceted approach is

needed to understand all the effects that will occur if the electrospinning solution is modified.

Other parameters

There are a few other process parameters that will affect the outcome of the electrospinning process. Some of these parameters include: nozzle to target distance, solvent choice and infusion rate. As compared to the parameters discussed above, these may have smaller influences on the processes and could best be discussed by recommendations rather than detailed experimental setups. The nozzle to target distance is best left as a variable that is dependent on the drying time of the fibers. Generally, it is preferred that fibers should be dry or nearly dry when collected. Infusion rate is also governed by a general recommendation to infuse polymer into the field at a rate high enough to maintain a stable Taylor cone. These rates vary greatly among solvent – polymer systems and the driving voltage of the system. Solvent choice is based on polymer solubility but can also affect the fibers produced. Figure 7 depicts the same concentration of poly(L-lactic acid) electrospun from chloroform and methylene chloride while all other parameters were held constant.

Figure 7. Top: Poly(L-lactic acid) electrospun from a 143 mg/ml solution in chloroform. Bottom: Poly(L-lactic acid) electrospun from a 143 mg/ml solution in methylene chloride.

Note that the gross fiber size varied but, more interestingly, so did the surface topology. Knowledge of solvent – polymer systems can be very valuable in determining the optimum system for a given application.

In this chapter, the parameters that affect the ability to electrospin fibers as well as the processing parameters have been discussed. It was shown that the morphology of electrospun fibers depends greatly on the processing parameters including: electrospinning voltage, solution concentration, solution viscosity, solution surface tension, charge density, infusion rate and solvent choice. The initiating voltage changes the shape and size of the initiating Taylor cone which is coupled to the infusion rate. This cone determines the stable and unstable regions of the jet and ultimately controls the ability to form fibers. It was also shown that solution variables have a significant impact on the final fiber production and subsequent utility. Even with this knowledge, detailed experimentation is still needed to determine the utility of any solvent – polymer system.

Chapter 3 Electrospinning of Poly(glycolic acid)

The following manuscript appeared in the Journal of Macromolecular Science, 2001, volume 38, pages 1231-1243 (14). The work included demonstrates the relationship between solution concentration and fiber diameter when electrospinning poly(glycolic acid). Additional, uniaxial mechanical testing was performed to quantify a fiber alignment procedure that involved varying the rotational speed of the electrospinning target. Additional details about the chemistry, biodegradation and uses of poly(glycolic acid) can be found in Appendix A.

TAILORING TISSUE ENGINEERING SCAFFOLDS USING ELECTROSTATIC PROCESSING TECHNIQUES:

A STUDY OF POLY(GLYCOLIC ACID) ELECTROSPINNING

Eugene D. Boland [1], Gary E. Wnek [2], David G. Simpson [3], Kristin J. Pawlowski [1], and Gary L Bowlin[1]

[1]Department of Biomedical Engineering
Virginia Commonwealth University
P.O. Box 980694
Richmond, VA 23298-0694

[2]Department of Chemical Engineering
Virginia Commonwealth University
P.O. Box 843028
Richmond, VA 23298-3028

[3]Department of Anatomy
Virginia Commonwealth University
P.O. Box 980709
Richmond, VA 23298-0709

Abstract

Poly(glycolic acid) (PGA) has long been a popular polymer in the tissue engineering field. PGA possesses many favorable properties such as biocompatibility, bioabsorbability, and good tensile strength. The traditional fiber formation techniques of melt extrusion and cold-drawing are generally limited to fibers of 10-12 μm in diameter. Electrostatic spinning, or electrospinning, is an attractive approach for the production of much smaller diameter fibers which are of interest as tissue engineering scaffolds. We demonstrate the ability to control the fiber diameter of PGA as a function of solution concentration and the fiber orientation, and also show a correlation between the fiber orientation and the elastic modulus and strain to failure of PGA in a uniaxial model.

Key Words: Electrospinning; Tissue Engineering; Scaffold; Poly(Glycolic) Acid

Introduction

Poly(glycolic acid), or PGA, is one of a group of biodegradable aliphatic polyesters currently exploited in a variety of medical applications. PGA possesses a moderate degree of crystallinity, a high melting point, and low solubility in organic solvents. Importantly, monofilaments can be degraded *in vivo* in as little as 2 to 4 weeks due to its hydrophilic nature (5, 119).

PGA's inception as a biomaterial came in the 1970's as a degradable suture material. It was found to have better than average tissue compatibility, reproducible mechanical properties such as strength, elongation and knot retention, and predictable bioabsorption (119). Hydrolytic degradation accounts for the nearly 60% loss of strength during the first two weeks, and is characterized by a sharp decrease in local pH and a decrease in crystallinity (27). This mechanism appears to be applicable to a host of semi-crystalline, bioresorbable polymers (5).

The current commercial process of producing PGA for medical applications is a braiding of multiple melt-spun filaments. These braided, multi-stranded fibers are either used as suture material, such as Dexon^{TM} (American Cyanamid Co., Inc.), or woven into mats such as Medisorb^{TM} (Dupont Co., Inc.) to serve as tissue dressings (5, 119). These constructs have also been employed as scaffolds in tissue engineering. One limitation of these commercially prepared PGA products is the relatively large fiber sizes (10–12 μm) due to the limitations of traditional extrusion (82). We believe that the proper *in vivo* phenotype cannot be achieved if cells are presented with fibers that possess diameters equal to the cell size or, in many cases, an order of magnitude greater than the cell size.

Observational evidence for this conclusion comes from a consideration of the native extracellular matrices of various tissues. Cells appear to have a highly intricate 3-D relationship with their extracellular structures. These structures, which are primarily composed of collagens, exhibit varying fiber diameters which are quite frequently one or more orders of magnitude smaller than the cell itself (87). This presents a unique problem and challenge for the fabrication of materials to be used as engineering tissue scaffolds.

Electrostatic spinning represents an attractive means to achieve these small fiber diameters. It is of interest to briefly contrast electrospinning with electrostatic spraying, as spraying or spinning can be achieved depending upon the polymer concentration in solution. In electrostatic spraying, or more simply electrospraying, charged droplets are generated at the tip of a metal needle (or pipette with a wire immersed in the liquid) with a several kV dc field, and are subsequently delivered to a grounded target. The droplets are derived by charging a liquid to ca. 5-20kV (corresponding to electric field strengths of ca. 1,000 V/cm), which leads to charge injection into the liquid from the electrode. The sign of the injected charge depends upon the polarity of the electrode; a negative electrode produces a negatively charged liquid. Electrostatic repulsions within the charged liquid coupled with attraction to the ground electrode of opposite polarity lead to the formation of a so-called Taylor cone at the needle tip. Subsequently, a jet is formed when electrostatic forces between the charged liquid and the ground exceed the liquid's surface tension. The jet, like any unconfined liquid column, is susceptible to a Rayleigh instability which in turn leads in the creation of droplets. If the liquid is relatively volatile, evaporation leads to shrinkage of the droplets and an increase in excess charge

density, affording break-up into smaller droplets. The electrospinning phenomenon is mechanistically similar to electrospraying, a key difference being that chain entanglements in more concentrated polymer solutions or melts help to stabilize the initial jet toward break-up into droplets. Solvent evaporation (or crystallization from the melt) ultimately stabilizes the jet, the result being a continuous fiber.

While electrospinning has been known for some time (6, 41) and attempts have been made to produce vascular grafts by this technique, (75) only recently has interest in electrospinning for polymer biomaterial processing been revived (12, 20, 23, 56, 77, 106). Of particular interest is the ability to generate polymer fibers of sub-micron dimensions, down to about 0.05 microns (50 nm), a size range that is otherwise difficult to access (91). In electrospinning, polymer solutions or melts are deposited as fibrous mats, with advantage taken of chain entanglements in melts or at sufficiently high polymer concentrations in solution to produce continuous fibers (92). The basic elements of a laboratory electrospinning system are simply a high voltage supply, collector (ground) electrode/mold, source electrode, and a solution or melt to be sprayed or spun. The sample is confined in any material formed into a nozzle with various tip bore diameters (such as a disposable pipette tip), with a very thin source electrode immersed in it. The collector can be a flat plate or wire mesh, or in more sophisticated modifications can be a rotating metal drum or plate on which the polymer is wound.

With successes seen in the electrospinning of other polymers, it seemed reasonable to believe that this process could be utilized for bioabsorbable polymers as well. Indeed, we recently demonstrated that poly(glycolic acid), poly(l-lactic acid), their

copolymers, and collagen are readily electrospun (20, 77, 106) and that the products are promising scaffolds for muscle growth and as components of engineered vascular grafts. In the present study, we set out to develop protocols that would demonstrate the effects of various control parameters in the electrospinning of PGA. We desired the ability to produce continuous fibers with diameters significantly smaller than those available through commercial extrusion, as well as the ability to tailor the fiber orientation in the electrospun scaffold. We suggest that the combination of these two parameters can drive the mechanical properties of a spun mat and eventually be used to mimic the natural mechanical and structural properties of a target tissue.

Methods

The prototype electrospinning process that we employed in this study is described schematically in Figure 8.

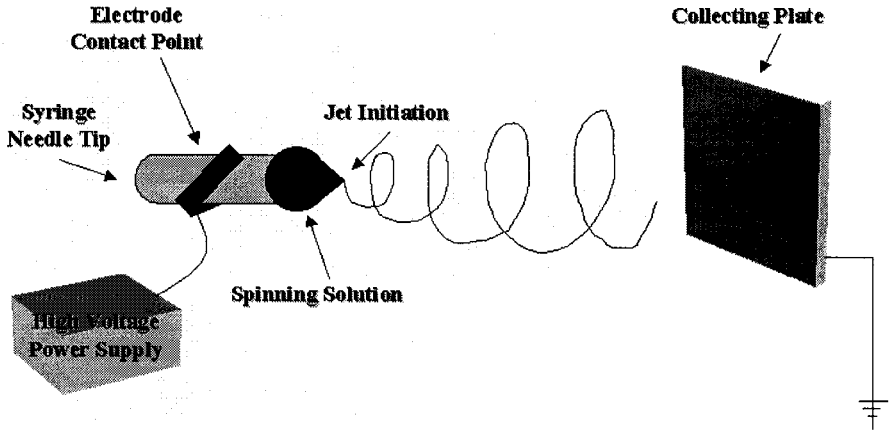

Figure 8. A schematic of the electrospinning system for the production of micro- to nano-scale fibers and subsequent biodegradable polymer tissue engineering scaffolds.

Jet initiation is achieved by charging a polymer solution (or melt) followed by ejection through a small opening or nozzle (a blunt needle in our prototype). Because of its charge, the ejected solution is drawn toward a grounded collecting target (a stainless steel mandrel in our system) as a whipping jet (91). During the jet's travel, the solvent gradually evaporates leaving a continuous polymer fiber that accumulates on the grounded target. Orientation can be controlled through rotation and translation of the mandrel while collecting the fiber. The charges on the fibers eventually dissipate, as they are neutralized by the surrounding environment (91) or can be neutralized with an ionizer. This process results in the production of a non-woven fibrous mat. These mats can have fiber diameters on the order of nanometers to microns.

For this research, poly(glycolic acid) (100 PGA) obtained from Alkermes, Inc. (Cincinnati, OH) was dissolved in 1,1,1,3,3,3 hexaflouro-2-propanol (HFIPA, Sigma Chemical Co.) at concentrations ranging from 1/7 to 1/20 weight/volume (w/v) of PGA in HFIPA. The solutions were then loaded into a Becton Dickinson 1.0-ml syringe and placed in a KD Scientific syringe pump for metered dispensing at 10 ml/hr. The positive output lead of a high voltage supply (Spellman CZE1000R; Spellman High Voltage Electronics Corp.), set to 22 kV, was attached to a blunt 18 gauge needle on the syringe. A grounded target (1" × 4" × 1/8" 303 Stainless Steel) was placed 11 inches from the needle tip and revolved at 100 RPM for random fibrous mats and 1000 RPM for aligned fibrous mats.

An experimental protocol to test the effect of solution concentration and orientation was desired. All other electrospinning parameters were held constant,

including applied voltage, distance between the anode (needle tip) and cathode (grounded mandrel), solution feed rate, HFIPA and PGA manufacturing lots, mandrel material, syringe and needle configuration, translation speed and rotation speed (within each orientation group). Solution concentrations of 1/7, 1/8, 1/9, 1/10, 1/12, and 1/20 w/v PGA to HFIPA were evaluated. This concentration range was selected from preliminary work done in our laboratory that identified 1/7 w/v PGA to HFIPA as an acceptable spinning solution. By reducing the solution concentrations, a low concentration threshold for spinning this solution could be determined and the hypothesis that fiber diameter can be controlled in part by solution concentration could be investigated. Fiber diameters were determined by scanning electron microscopy (SEM) using a JEOL JSM-820 JE electron microscope. The images were digitized and analyzed by UTHSCSA's ImageTool 2.0 to determine the average fiber diameters (average and standard deviation calculated from 60 measurements per micrograph) in the various mats. All measurements were calibrated using the scale on the micrograph as a reference to avoid errors in calculating the magnification of the scanned photos.

The second hypothesis addressed in this experiment was that the material properties of a mat can be altered by changing the fiber orientation and the spinning solution concentration. As previous mentioned, it is believed that the orientation of the mat can be controlled through rotation and translation of the mandrel and that the diameters of the fibers can be varied by changing the solution concentrations. For this experiment, translation speed was held constant (at 10 rpm) and the rotation speed was 100 rpm for random mats of all concentrations tested and 1000 rpm for aligned mats of

all the concentrations tested. The degree of alignment was visually assessed from SEM micrographs. Future work will involve the implementation of methods to quantify the orientation.

Uniaxial material testing was performed on a MTS Bionix 200 mechanical testing system incorporating a 100N load cell with an extension rate of 1.0 mm/minute to failure (MTS Systems Corp.; Eden Prairie, MN). Due to the viscoelastic nature of PGA, a slow loading rate was chosen to mimic static loading conditions. Five (n = 5) test specimen were tested in each of the following orientations at each solution concentration; Longitudinal – along the principal fiber direction in the aligned mat, Orthogonal – perpendicular to the principal fiber orientation in the aligned mat, and Random – taken from the random mat. The specimens were cut out of the mats using a "dog-bone" shaped template to assure uniformity and to isolate the failure point away from the grips. The specimens had a width of 2.75 mm, a gauge length of 11.25 mm and thicknesses that ranged from 0.6 to 1.25 mm. The material properties chosen for comparison were the elastic modulus (tangential method automatically selected by the MTS TestWorks 4.0 software) and the strain to failure (also calculated automatically by the software).

Results and Discussion

A strong linear relationship between fiber diameter and concentration in electrospun PGA was observed (Figure 9).

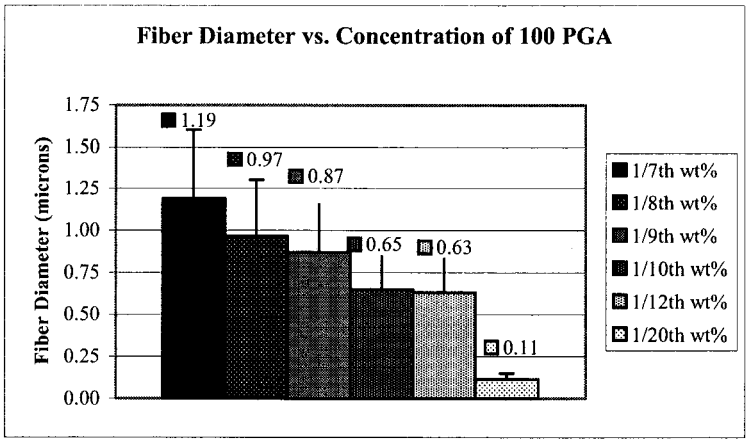

Figure 9. The PGA fiber diameters as a function of solution concentration produced by electrospinning.

Remarkably, the fiber diameters ranged a full order of magnitude from 110 nanometers to 1.19 microns with relatively small error over the concentrations evaluated. Even the largest diameters produced by electrospinning are more than 10 times smaller then those that can be extruded to manufacture braided thread and woven mats (82).

The electrospinning results show peak fiber diameters of 1.19 ± 0.41 microns for the 1/7 w/v concentration of PGA in HFIPA. With a drop in concentration to 1/10 w/v (4.3% drop in concentration), the mean fiber diameters drop to 0.65 ± 0.21 microns (45.4% drop in mean diameter). This trend continues between the 1/10 w/v concentration and the 1/20 w/v concentration (5% drop in concentration) since the mean fiber diameter drops to 0.11 ± 0.04 microns (83% drop in mean diameter). A curve fit of these data (Figure 10) could be used predict the concentration needed to produce a desired fiber diameter within the concentration range that is capable of being spun.

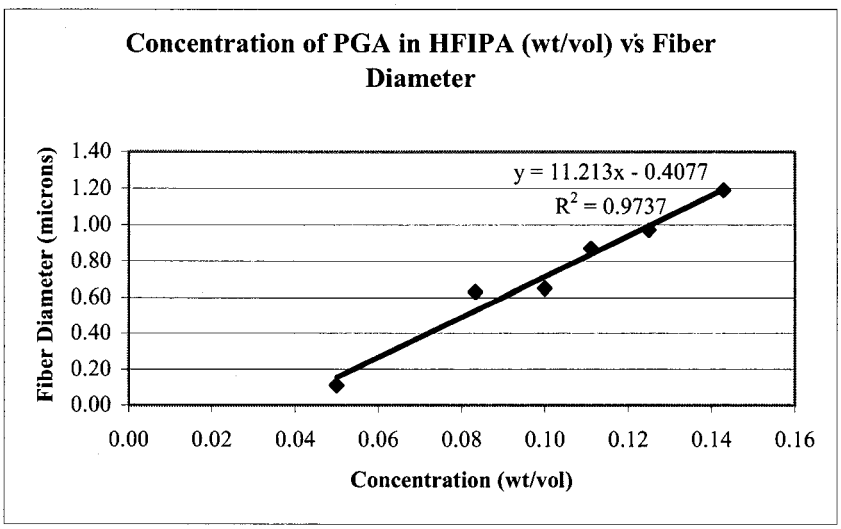

Figure 10. A linear regression of the concentration of PGA in HFIPA vs. the fiber diameter. The R^2 value of 0.9737 supports the correlation hypothesis.

This equation (Diameter (microns) = 11.213 * concentration (wt/vol) –0.4077) is valid only at the experimental conditions listed in this protocol and would need to be regenerated for any additional polymer/polymer blend or protocol of interest.

The results clearly support the first hypothesis of a significant (R^2 = 0.9737) dependence of fiber diameter on concentration. The low concentration threshold was also determined to be at or near a 1/20 w/v. As previously stated, when the solution concentration drops, electrostatic spinning reverts to the historically described electrostatic spraying discussed earlier. A threshold is defined as the observance of three distinct product morphologies: the presence of fibers, a phenomenon termed "beads on a string", and the presence of droplets resulting from electrospraying (77, 106).

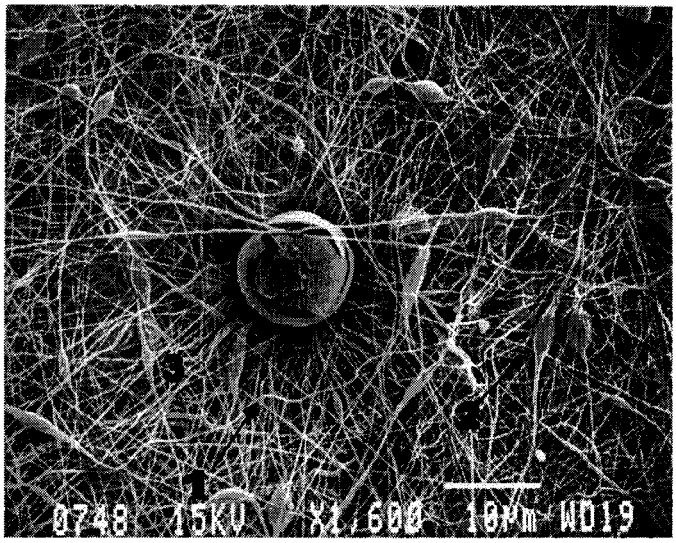

Figure 11. A SEM of electrospun PGA illustrating (1) Fibers, (2) "beads on a string", and a (3) droplet (ruptured during SEM scan) (1,600X magnification).

Figure 11 shows a representative sample of these three morphologies. The true threshold would be the concentration at which a further reduction would first cause "beads on a string" to form. This transitional region, as illustrated in Figure 11, has a gradual increase in beads and droplets until no more fibers or beads form. This concentration would define the upper threshold of electrospraying, or the lower threshold of electrospinning.

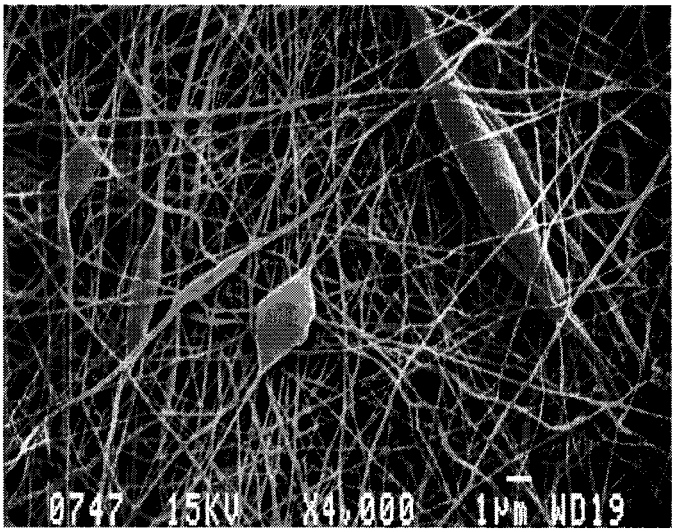

Figure 12. A SEM micrograph (4,000X magnification) of 1/20 w/v concentration of PGA in HFIPA illustrating the fiber size uniformity (110 ± 35 nm).

Figure 12 is a higher magnification view of the same mat spun from a 1/20 w/v solution. From this micrograph, we can see that there is a high degree of uniformity in the fibers aside from the bead formation. This leads to the conclusion that bead formation may be a localized effect, possibly caused by variation in field strength or localized solution concentration in the needle tip, and may not grossly affect the properties of the scaffold if the density of beads is not very high. Future mechanical testing at and just below the spinning threshold will be able to test this hypothesis.

After biocompatibility and tissue incorporation are addressed, traditional engineering principals such as stress and strain may ultimately govern the success of a tissue engineering scaffold (8). The mechanical properties of interest in this study were the modulus of elasticity and strain at failure. We believe that these are two of the key characteristic properties that must be addressed in the design of a structural tissue

engineering scaffolds. These characteristics, together with maximum stress, are commonly reported for soft tissues in various literature sources and will form a basis of comparison for future work.

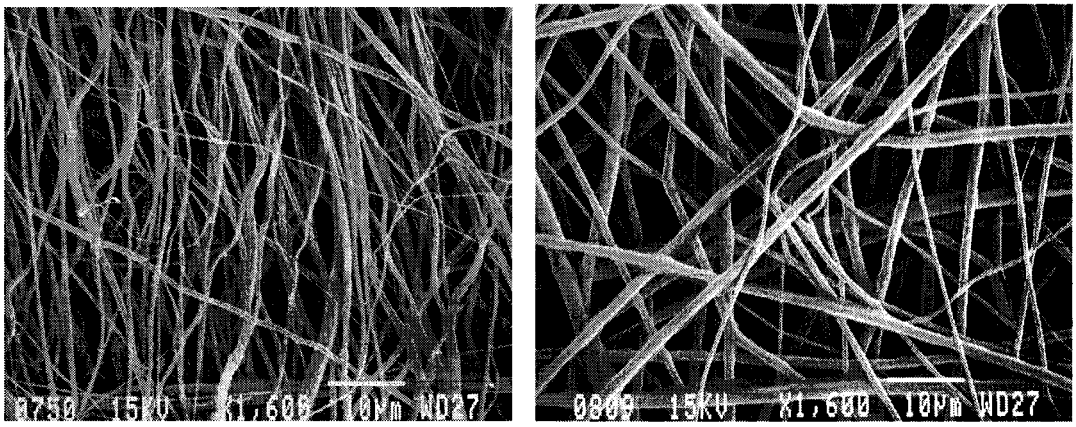

Figure 13. (Left) Electrospun 1/7 w/v PGA in HFIPA illustrating aligned fibers (mandrel rotation of 1000 rpm), (Right) Electrospun 1/7 w/v PGA in HFIPA showing the random fiber orientation (mandrel rotation of 100 rpm). Both micrographs are at 1,600X magnification.

Figures 13 exemplify the ability to align the fibers in a spun mat. The only variable changed between the two mats is the rotational velocity of the mandrel picking up the fiber that is whipping around within the developed static electric field.

As evident by the micrographs in Figure 13, a visual distinction can be made between the aligned and random mats. Also evident is the incomplete alignment seen in Figure 4a. As previously discussed, a method for quantifying the orientation will be needed to gage scaffold orientation with the native tissue orientation. Future studies will address this issue.

Elastic moduli calculations were made and averaged from the 15 groups (5 specimens from each test category). The results of these calculations are shown in Figure 14.

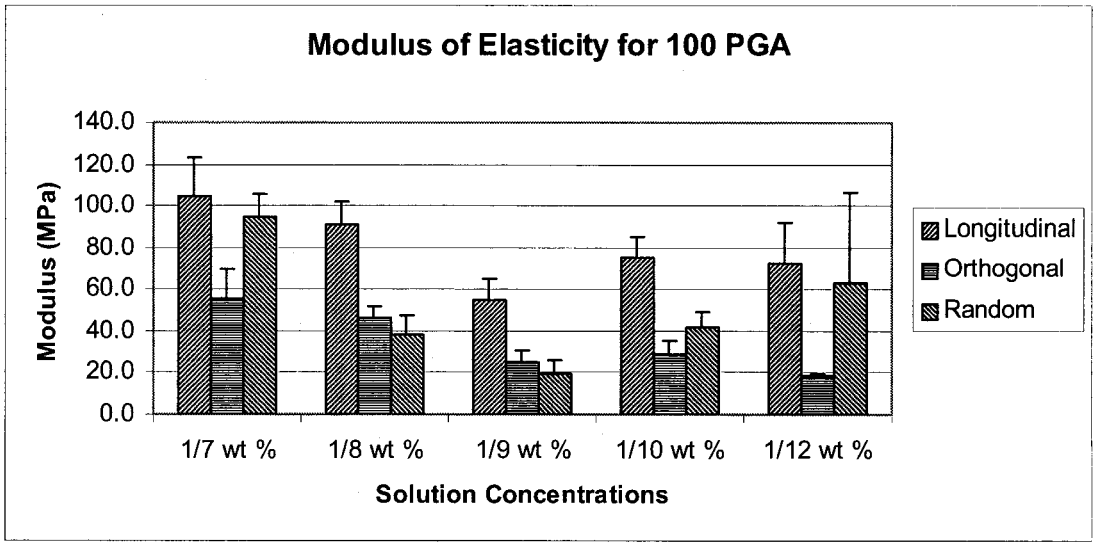

Figure 14. Tangential modulus of elasticity for various concentrations of PGA tested along the longitudinal and orthogonal axes and in a random mat.

A statistical analysis comparing the moduli at the different orientations and concentrations was performed using the Student's T-test. The 1/7 w/v concentration showed a significant difference between the longitudinal and orthogonal directions ($P < 0.001$) and between the longitudinal and random directions ($P < 0.001$). The 1/8 w/v concentration showed a significant difference between the longitudinal and orthogonal directions ($P < 0.001$) and between the orthogonal and random directions ($P < 0.001$). The 1/9 w/v concentration showed a significant difference between the longitudinal and orthogonal directions ($P < 0.001$) and between the longitudinal and random directions ($P < 0.001$). The 1/10 w/v concentration showed a significant difference between the

longitudinal and orthogonal directions ($P < 0.001$) and between the longitudinal and random directions ($P < 0.005$). The 1/12 w/v concentration showed a significant difference only between the longitudinal and orthogonal directions ($P < 0.005$). The *a priori* level of significance for all tests was set equal to $P < 0.01$. Generalizing for elastic moduli testing, the longitudinal direction always possessed a greater stiffness then the orthogonal direction and the random scaffolds typically exhibited moduli similar to either the longitudinal or the orthogonal directions.

A similar T-test was performed to compare the modulus of a particular orientation to the solution concentrations. Significant differences in the longitudinal direction was found only at 1/7 w/v ($P < 0.005$). Similarly, only the 1/9 w/v yielded a significant difference in the orthogonal direction ($P < 0.005$). In the random orientation both the 1/7 w/v concentration ($P < 0.005$) and the 1/9 w/v concentration ($P < 0.001$) were significantly different. These statistical tests support the hypothesis that strength is a function of orientation.

The highest modulus of 104.9 MPa was seen in the longitudinal axis of the 1/7 w/v concentration. This would follow reason since the fiber diameters are the greatest and the alignment would present the maximum resistance. The lowest moduli were observed along the orthogonal axis for most of the concentrations, again as expected.

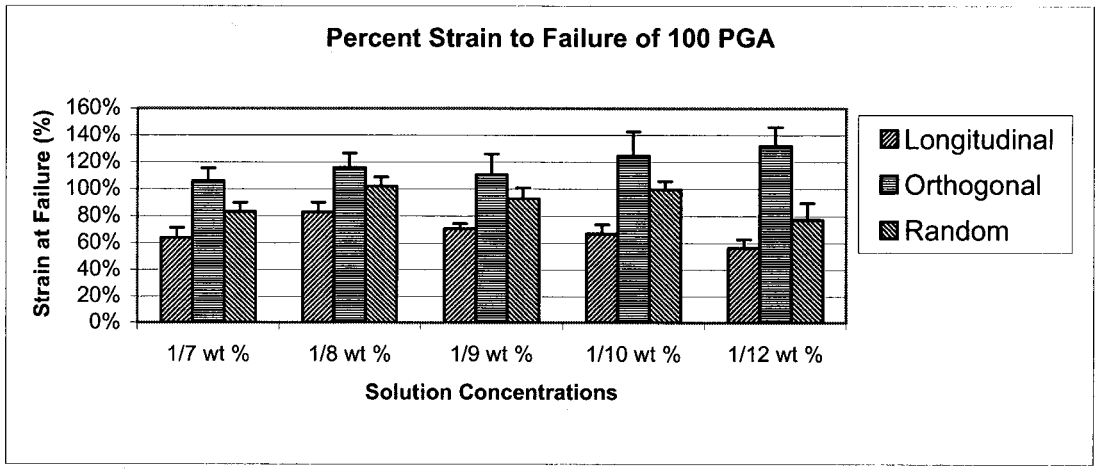

Figure 15. Maximum strain measurements for various concentrations of PGA.

Additionally, the peak strains were calculated from the same sample groups with the results presented in Figure 15. All five solutions concentrations produced equivalent results with the strain to failure being highest for the orthogonal specimens and lowest for the longitudinal specimens. A Student's T-test was performed to compare the strain to failure at the three orientations to the solution concentrations. The only significant differences were seen in the 1/7 w/v concentration ($P < 0.001$) and the 1/8 w/v concentration ($P < 0.005$) in the random orientation. This also correlates to the suspected orientation in the mats since strain values are higher when the specimens are not loaded along the principal axis of the fibers but are similar across the solution concentrations. Future studies with larger sample sizes are needed to verify the difference measured in the 1/7 and 1/8 w/v concentrations.

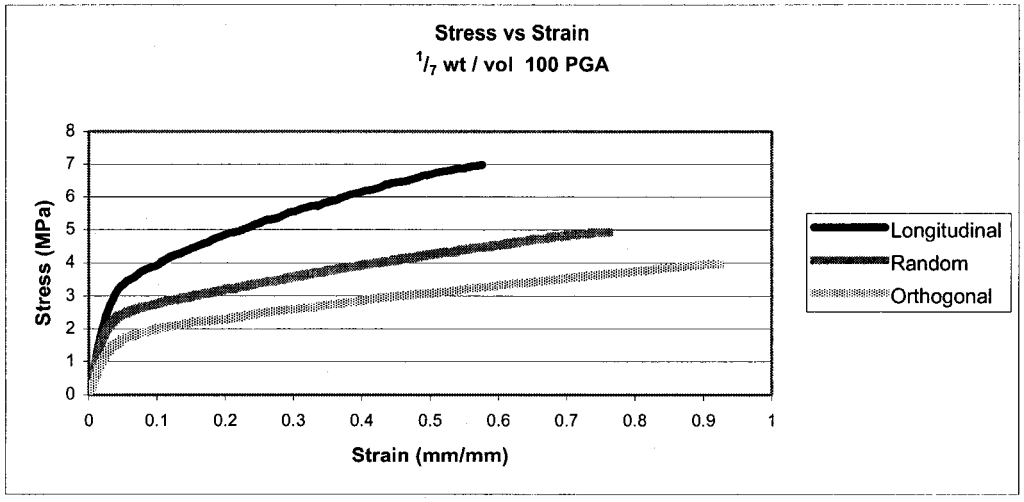

Figure 16. Ensemble Averaged Stress vs. Strain Plot for all Three Orientations of 1/7 Wt/Vol Concentration of PGA.

The ensemble average of engineering stress versus strain is included in Figure 16 for the 1/7 w/v concentration along the longitudinal and orthogonal axes and with random orientation. This chart is included to illustrate the general mechanical response as a function of fiber orientation. It is evident that the stress handling ability of the mat is related to the degree of orientation. Energy or toughness (area under the load - elongation curve) is another measurement that can be used to compare bulk mechanical properties of the scaffolds. The toughness values for the 1/7 w/v concentrations are 10.2 N*mm, 11.2 N*mm, and 11.8 N*mm, respectively for the longitudinal, orthogonal and random orientations. A Student's T-Test was performed and there was no significant difference between these values (significance $P < 0.1$). This is as expected since the energy a material can absorb before failure is a fundamental material property dependant principally on composition and processing. Similar results were achieved in the comparison of energy versus orientation for the remaining test concentrations of PGA in

HFIPA. Paired T-Tests were computed comparing the energy of each orientation and concentration and again no significant differences were found (significance $P < 0.1$).

Through the course of these experiments, the ability to electrostatically process PGA was demonstrated at various concentrations. These concentrations were directly related to the fiber diameters produced from the process. The fiber scale achieved was one to two orders of magnitude smaller than commercially available fibers. Future cell culture experiments will be needed to determine if creating smaller diameter fibers in a scaffold is just novelty or improves phenotypic expression or construct viability. One may argue that that the pore sizes in these scaffolds are too small to promote tissue ingrowth or vascularization. There may be other factors at work with cell migration, we have demonstrated (unpublished data) that cells (smooth muscle cells) can migrate into a scaffold with pore sizes less than the previously reported 10 micron threshold.

When reviewing the alignment of the mats depicted, it is apparent that the alignment is not 100%. Refinement of the aligning process will be undertaken through the implementation of additional control on the mandrel rotation and location (next generation electrospinning apparatus). These constitutive models in conjunction with advanced processing systems will provide the critical next step in our ability to tailor scaffolds that truly mimic the target tissue.

After alignment is achieved, the tissue mechanics will need to be satisfied. Clear trends were shown in the strain to failure and elastic modulus of the various constructs. As mentioned previously, the orthogonal and random orientations of 1/8 and 1/9 w/v concentrations did not follow the pattern of the other concentrations. One possible reason

for the deviation could be the quality of alignment of the scaffold. While these appear aligned by visual examination, there may be underlying fibers which are not. Another, and more probable, reason is that the solvent used for the solutions (HFIPA) did not fully evaporate and we saw the effect of solvent bonding or welding which would make the orthogonal and random mats structurally similar.

Conclusion

Poly(glycolic acid) is readily electrospun to afford fibers ranging from about 0.15 to 1.5 μm in diameter, the latter being related to the concentration of the spinning solution. Oriented electrospun mats were achieved using a rotating collection plate, and mechanical testing revealed anisotropic properties of the oriented mats. We believe that the fine fiber diameters make electrospun PGA an attractive candidate as a tissue engineering scaffold, and experiments are underway to evaluate this prospect.

Acknowledgements

The authors would like to thank the Whitaker Foundation (RG-98-0465) for the support of this research, as well as Alkermes, Inc. for the donation of the PGA used in this study. We would also like to thank Ms. Judy Williamson for her assistance obtaining the SEM micrographs.

Chapter 4 Electrospinning Polydioxanone

The following manuscript has been submitted to *Acta Biomaterialia*. The work included demonstrates the ability to electrospin polydioxanone and the relationship between solution concentration and fiber diameter. Additional calculated parameters including surface area to volume ratio and porosity. Again, uniaxial mechanical testing was performed to quantify a fiber alignment procedure that involved varying the rotational speed of the electrospinning target.

Electrospinning Polydioxanone for Biomedical Applications

Eugene D. Boland[1], Branch D. Coleman[1], Catherine P. Barnes[1], David G. Simpson[2], Gary E. Wnek[3], and Gary L. Bowlin[1]

[1.] Department of Biomedical Engineering
Virginia Commonwealth University
Richmond, VA 23298-0694

[2.] Department of Anatomy and Neurobiology
Virginia Commonwealth University
Richmond, VA 23298-0709

[3.] Department of Chemical Engineering
Virginia Commonwealth University
Richmond, VA 23284-3028

Corresponding Author:
Gary L. Bowlin
Associate Professor
Department of Biomedical Engineering
Virginia Commonwealth University
P.O. Box 980694
Richmond, VA 23298-0694
Phone (804) 828-2592
Fax (804) 828-4454
Email: glbowlin@vcu.edu

Disclosure: The authors have several patents pending concerning technology presented in this manuscript and this technology has been licensed to NanoMatrix, Inc. of which several authors have a financial interest.

ABSTRACT

Polydioxanone (PDS) is a colorless, crystalline, bioabsorbable polymer that was first developed specifically for wound closure sutures. Electrospinning is a polymer processing technique that utilizes an electric field to form fibers from a polymer solution or melt and allows the fabrication of nanofibrous non-woven structures. Over the years a variety of synthetic and natural polymers have been electrospun to form non-woven structures, this research presents the electrospinning of PDS to fabricate unique nano-fibrous structures for a variety of biomedical applications. Results demonstrate the ability to control the fiber diameter of PDS as a function of solution concentrations and the fiber orientation with our prototype electrospinning apparatus. The results also show dependence between the fiber orientation and the elastic modulus, peak stress, and strain to failure of PDS in a uniaxial model.

Key Words: electrospinning, tissue engineering, scaffold, polydioxanone

INTRODUCTION

Polydioxanone (PDS) is a colorless, crystalline, bioabsorbable polymer that was developed specifically for wound closure sutures. Ethicon, A Johnson and Johnson Company markets it in the United States. PDS, also known as poly (p-dioxanone) is derived from the monomer paradioxanone via a ring-opening polymerization with heat and an organometallic catalyst like zirconium acetylacetone, diethylzinc, or zinc L-lactate (ZnLac2) resulting in a poly (ether-ester) with a molecular structure of (-O-CH2-CH2 -O-CH2-C=O)n (70). This is diagrammatically represented in Figure 17.

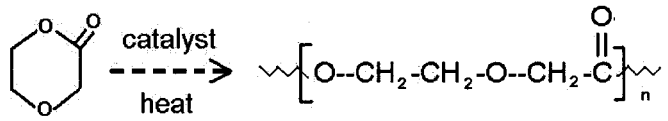

p-dioxanone Poly(dioxanone)

Figure 17. PDS polymerization reaction.

Polydioxanone exhibits a crystalline fraction of 55% and a glass-transition temperature between -10° and 0°C (79). Special precautions should be undertaken to process the material at the lowest possible temperature to prevent spontaneous depolymerization back to paradioxanone. PDS is typically extruded into a monofilament for use as a suture. As a suture, it exhibited high flexibility in any suture diameter and exhibited higher strength retention, slower absorption rates and lower inflammatory response rates when compared to Vicryl (poly(glycolic-co-lactic acid)) and Dexon (poly(glycolic acid)). The flexibility of monofilament polydioxanone is obtained by the incorporation of an ether oxygen group in the backbone structure (89). The monofilament suture typically loses 50% of its initial breaking strength after 3 weeks and

is completely absorbed within 6 months. This provides an advantage over Dexon for slower healing wounds but is not retained as long as poly(lactic acid) based suture (79). One key disadvantage of PDS suture is shape memory. Due to its shape memory, PDS often coils to retain its spooled shape and can be difficult to use. PDS has low surface friction so it can glide through tissues easily, but the lack of friction coupled with shape memory makes knots retention difficult (1). Other downsides of PDS suture include degradation rates too rapid to provide a durable closure for abnormally healing wounds and the suture ends may be sharp when cut. Since the initial use as a suture, PDS has been used in orthopedics, plastic surgery, drug delivery, cardiovascular applications and bone repair applications. These other applications have had mixed results which has slowed the expansion of PDS applications (9, 11, 19, 24, 63, 69, 96, 115).

While the disadvantages of PDS have limited its use as a suture; its compatibility, flexibility, degradation rate and, to some extent, its memory may make it suitable for tissue engineering applications. In this study, we characterized the mechanical properties of PDS scaffolds produced by the electrospinning methods previously described by our laboratory [13-19]. Briefly, electrospinning occurs by inducing a large electric potential (15 to 30 kilovolts DC) in a polymer solution or melt. This charged polymer reservoir is separated from an oppositely charged target creating a static electric field. As the field strength grows, the electric potential overcomes the surface tension of the solution and a thin jet with entangled polymer chains is ejected from the polymer reservoir. This jet travels around in space toward the target as a function of charge repulsion between and within the jet. If the polymer concentration is optimized, the solvent will evaporate and a

continuous filament (or multiple filaments) will be collected dry on the target. The utility of this resulting fibrous mat can be improved through target motion.

MATERIALS AND METHODS

PDS Preparation

The PDS used for electrospinning in this study was obtained as PDS II violet monofilament sutures from Ethicon, Inc (Somerville, NJ) with the needles were removed prior to processing. The sutures are manufactured with a cosmetic violet No. 2 dye that is uniformly distributed throughout the suture. Although only a cosmetic addition to the suture, the dye was removed to prevent the addition of an unknown variable to the electrospinning process. To remove the dye, the PDS II violet monofilament sutures were soaked in airtight jars of methylene chloride for approximately three days until the dye had been completely extracted (88). The clear sutures were removed from the solvent and air dried for 2 to 5 minutes, allowing the remaining methylene chloride to evaporate. The sutures were then cut into small, 1 to 4 cm lengths, and stored at –20°C until use.

Electrospinning

The solutions used in this experiment were made from dye extracted PDS suture and 1,1,1,3,3,3 hexafluoro-2-propanol (HFP, Sigma Aldrich Chemical Co.). Concentration of 42, 50, 56, 71, 83, 100, 125, and 167 mg/ml of PDS in HFP were chosen to determine the absolute and optimal fiber forming range. This range was chosen from previous experience by the authors with other resorbable suture materials

and visual inspection of the solution viscosity (16, 18, 20, 106). The viscosity of PDS in HFP (42-170 mg/ml) solutions was quantified at 25°C using a Brookfield Digital Rheometer Model DV-III+ at a shear rate of 200 r.p.m. For electrospinning, the solutions were loaded into either a Becton Dickinson 3.0 or 10.0 ml syringe and placed in a KD Scientific syringe pump for metered dispensing between 4-12 ml/hr (dispersing rate varies inversely with electrospinning concentration). The positive output lead of a high voltage supply (Spellman CZE1000R; Spellman High Voltage Electronics Corp.), set to 22 kV, was attached to a blunt 18 gauge needle on the syringe as depicted diagrammatically in Figure 18.

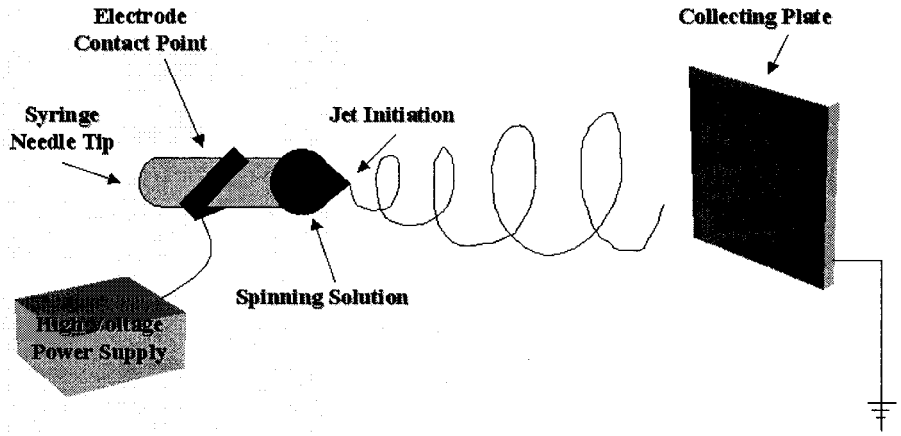

Figure 18. Schematic diagram of electrospinning apparatus.

A grounded target (1" Wide × 4" Long × 1/8" Thick; 303 stainless steel) was placed 8 inches from the needle tip and revolved at 100 revolutions per minute (r.p.m.) to produce randomly arranged fibers and 4000 RPM to produce aligned fibers.

Scaffold Characterization

After the scaffolds were electrospun, 1 cm diameter samples were cut from each mat for characterization. A representative sample from each was sputter coated in gold (Electron Microscope Sciences model 550) for scanning electron microscopy (SEM) (JEOL JSM-820 JE Electron Microscope) and evaluated at 1000 to 3000 times magnification. The images were digitized with a flat bed scanner (Hewlett – Packard Scanjet 6200C) and analyzed by ImageTool 3.0 (Shareware provided by University of Texas Health Science Center in San Antonio) to determine the average fiber diameters (average and standard deviation calculated from 60 measurements per micrograph) in the various electrospun structures. All measurements were calibrated using the scale on the micrograph as a reference to avoid errors in calculating the magnification after digitization. In addition to fiber diameter, pore areas for the random fiber orientations were also calculated. Pore area is a subjective approximation of surface pores in the SEM micrographs that were at least 15 μm deep. Current quantitative methods for determining porosity of electrospun scaffolds are in development. Porosity and surface area to volume ratios were calculated for the random orientation mats knowing the supplied material density (1.34 g/cm3), mass of the electrospun scaffolds, volume of the electrospun scaffold and the calculated equivalent fiber length using the following equations:

$$Porosity = \frac{(1 - calculated\ scaffold\ density)}{(known\ material\ density)} * 100\%$$

$$Equivalent\ Fiber\ Length = \frac{(measured\ mass\ of\ scaffold)}{(known\ material\ density) * \pi * (average\ fiber\ radius)^2}$$

$$Surface\ Area\ to\ Volume\ Ratio = \frac{(equivalent\ fiber\ length) * 2 * \pi * (average\ fiber\ radius)}{(calculated\ scaffold\ volume)}$$

Mechanical Evaluation

Uniaxial material testing was performed on a MTS Bionix 200 mechanical testing system incorporating a 100N load cell with an extension rate of 10.0 mm/minute to failure (MTS Systems Corp.; Eden Prairie, MN). Eight (n = 8) test specimen were tested in each of the following orientations at each solution concentration; Longitudinal – along the principal fiber direction in the aligned mat, Orthogonal – perpendicular to the principal fiber orientation in the aligned mat, and Random – taken from the random mat. The specimens were cut out of the mats using a "dog-bone" shaped template to assure uniformity and to isolate the failure point away from the grips (18). The specimens had a width of 2.75 mm, a gauge length of 11.25 mm and ranged in thickness from 0.07 to 0.69 mm. The material properties chosen for comparison were the elastic modulus (tangential method automatically selected by the MTS TestWorks 4.0 software), peak stress (engineering stress: based on the uncorrected cross-sectional area) and the strain to failure (also calculated automatically by the software) (18). The final mechanical testing of the electrospun PDS structures was to perform mechanical testing on 100 mg/ml PDS in HFP samples hydrated overnight in phosphate buffered saline to determine the impact of hydration on the mechanical properties.

Statistical Analysis

Unless otherwise noted, all statistics are based on a Kruskal-Wallis one way analysis of variance on ranks then subjected to a pair-wise multiple comparison procedures (Tukey Test). The a priori alpha value was set at 0.05 with significance defined as $P < 0.05$. This methodology was chosen to address uneven sample sizes and distributions that may not be normal.

RESULTS

Viscosity

The change in solution viscosity (change in polymer concentration and subsequent chain entanglements) is the most effective method of altering fiber diameter during electrospinning (18, 46). The results of the PDS/HFP solution viscosity measurements are presented in Figure 19 with the viscosity ranging from 50 to 2856 cP over the PDS concentration range of 42 to 170 mg/ml.

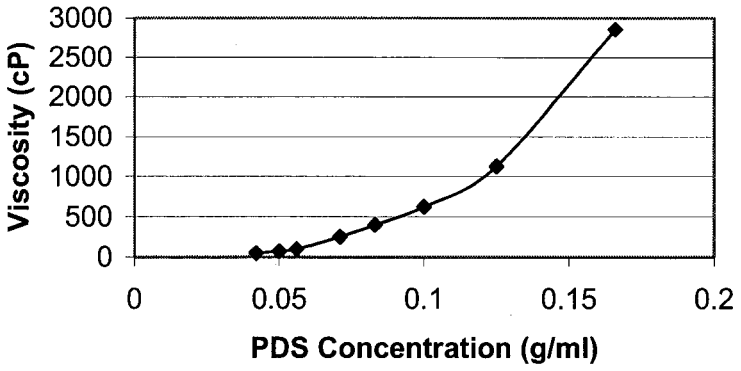

Figure 19. The viscosity (cP) versus PDS in HFP solution concentration (g/ml).

This region evaluated is the classical "heal" region of the viscosity versus concentration curve where electrospinning is optimum due to the appropriate number of chain entanglements. However, there are limits to the electrospinning ability of PDS from HFP due to viscosity. At viscosities lower than 50 cP, the solution was not viscous enough to electrospin a uniform fibrous structure. This is in the transition zone between electrospinning and electrospraying, which results in what is commonly referred to as "bead-on-a-string" structure. At viscosities over 2850 cP, the solution was too viscous to flow through the nozzle.

Scaffold Characterization

Fiber diameter is dependant on many electrospinning variables including electric field strength and polymer concentration. The results of electrospinning with all variables constant except the PDS concentration are shown in Figures 20-21 and Table 1.

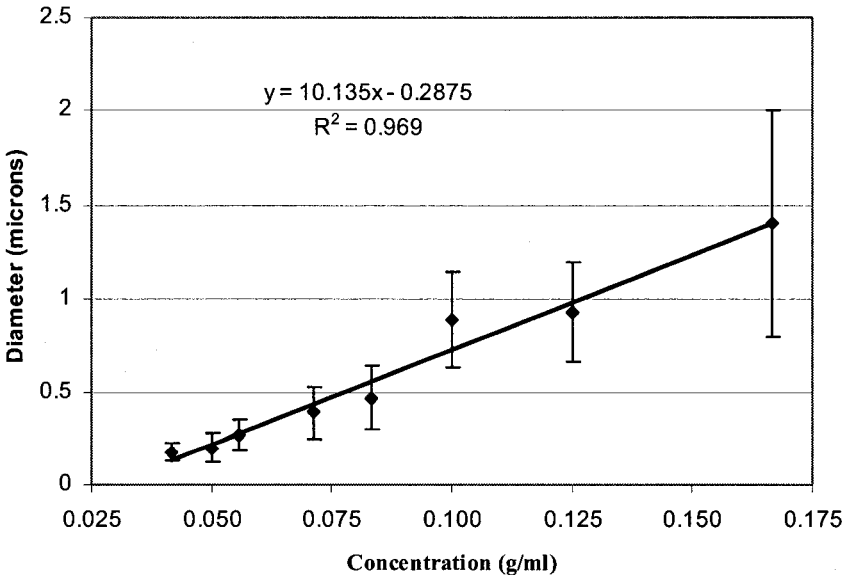

Figure 20. Results of the fiber dimension analysis versus the electrospinning PDS concentration illustrating the linear relationship between electrospinning solution concentration and fiber diameter.

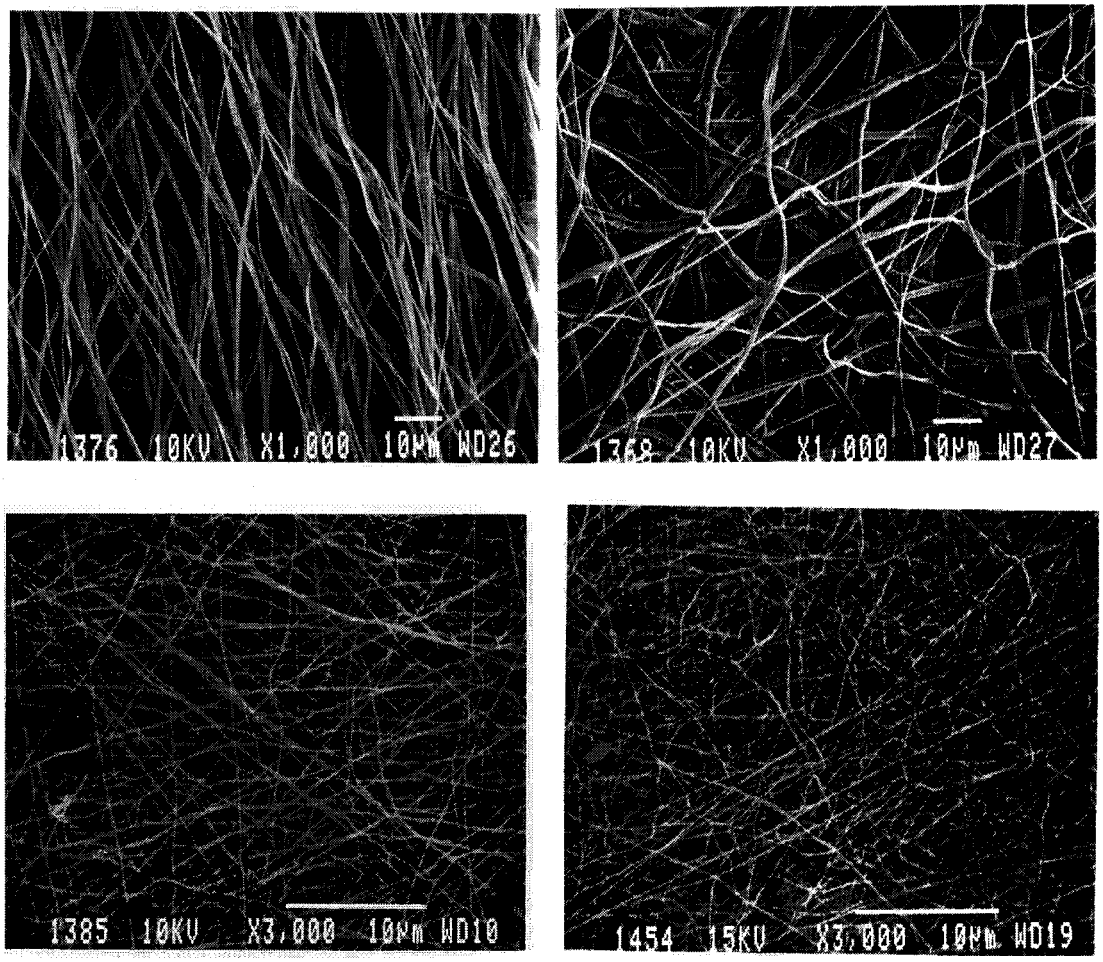

Figure 21. Top: Micrographs of aligned and random fibrous structures produced from 167mg/ml PDS in HFP at 1000x magnification consisting of 1.4 μm diameter fibers. Bottom: Micrographs of aligned and random fibrous structures produced from 42mg/ml PDS in HFP at 3000x magnification consisting of 0.18 μm diameter fibers.

Concentration (mg/ml)	Fiber Diameter (μm)	Pore Area (μm^2)	Porosity (%)	Surface area/volume (m^2/cm^3)
167	1.4 ± 0.6	24.5 ± 18.8	80.1 ± 4.5	0.55 ± 0.13
125	0.93 ± 0.27	19.3 ± 10.9	78.0 ± 5.8	0.94 ± 0.25
100	0.89 ± 0.26	14.0 ± 8.2	62.8 ± 6.3	1.7 ± 0.3
83	0.47 ± 0.17	3.6 ± 2.6	70.3 ± 5.0	2.5 ± 0.4
71	0.39 ± 0.14	1.9 ± 0.9	78.4 ± 5.5	2.2 ± 0.6
56	0.27 ± 0.08	0.9 ± 0.4	77.6 ± 3.6	3.3 ± 0.5
50	0.20 ± 0.08	0.9 ± 0.5	73.6 ± 10.1	5.3 ± 2.0
42	0.18 ± 0.05	0.5 ± 0.3	81.4 ± 8.0	4.1 ± 1.8

Table 1. Average Fiber Diameters (μm), pore area (μm^2), porosity (%), and surface are to volume ratios (m^2/cm^3) for the electrospun PDS from HFP structures.

As the solution concentration decreased, the fiber diameter decreased linearly ($R^2 = 0.97$) from 1.4 to 0.18 μm over the 167 - 42 mg/ml concentrations, respectively. Thus, the PDS concentration in HFP for electrospinning is an important factor in manufacturing non-woven structures. The statistical analysis of this data indicates that the 42-56 mg/ml fibers are significantly different from the 71-167 mg/ml fibers with fibers diameters within each of those groups not significantly different from each other.

Another variable of interest while electrospinning these non-woven structures of PDS for potential biomedical applications is the pore size (area). In general, the pore area decreases as the concentration of PDS decreases with the results of this analysis illustrated in Figure 22.

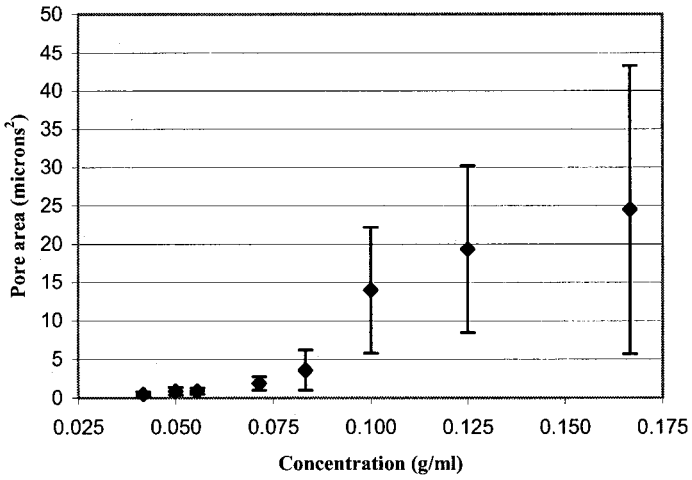

Figure 22. The results of the pore area measurements to illustrate the relationship between electrospinning concentration and pore area.

In this study as the solution concentration decreased, the electrospun non-woven structures had pore areas that decreased, non-linear, from 24.5 to 0.5 μm^2 over the 167 - 42 mg/ml concentrations, respectively. The statistical analysis of this pore area data indicates that the 42-56 mg/ml pore areas were significantly different from the 71-167 mg/ml pore areas with the pore areas within each of those groups not significantly different from each other. This demonstrates the ability to fabricate a variety of pore areas of electrospun PDS, which will play a critical role in mass transfer, diffusion across the structure, and probably most importantly overall cell interaction and migration into the structure.

Porosity and surface area are two important variables upon interaction of structures with the host environment. For example, a highly porous structure with a large

surface area may be more conducive to cell attachment and infiltration of cellular components. The results of the porosity measurements are presented in Figure 23.

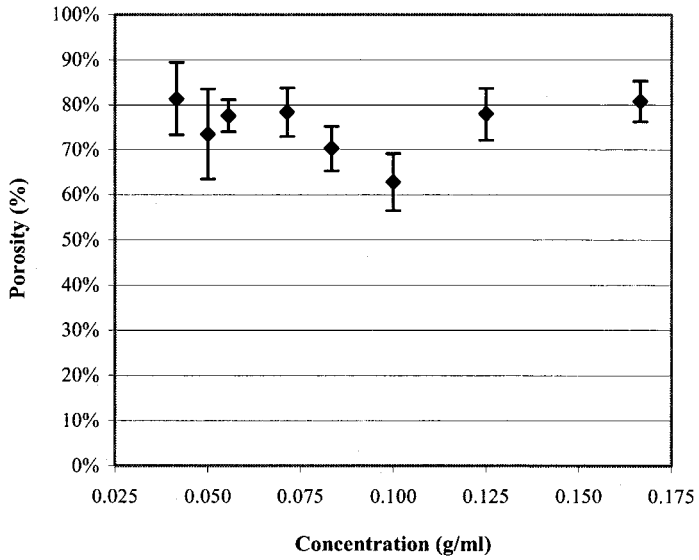

Figure 23. The results of the calculation of the porosity of the randomly orientated electrospun PDS structures to illustrate the relationship between electrospinning concentration and percent open area.

The porosity of the electrospun structures ranged from 63 – 82% with no clear relationship to the PDS concentration. This result indicates that there is still the need for finer process controls, particularly a well-defined electric field, during electrospinning, which was not achieved with the prototype electrospinning system in this study.

Unlike the porosity, the study did indicate a relationship between PDS concentration and surface area to volume ratios of the electrospun structures. In general, the surface area to volume ratio decreases as the concentration of PDS increases with the results of this analysis illustrated in Figure 24.

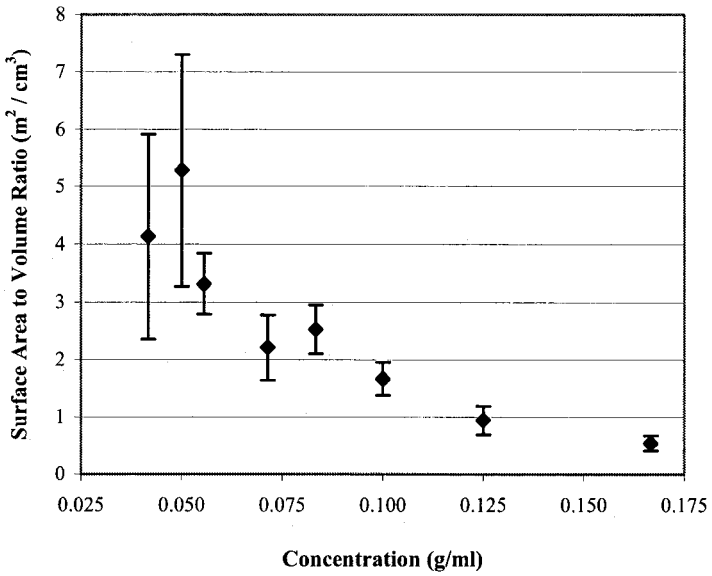

Figure 24. The results of the surface area to volume ratio calculations are presented to illustrate the relationship between concentration and the surface area to volume ratio for the electrospun structures.

As the PDS concentration decreased, the electrospun non-woven structures had surface area to volume ratios that increased, non-linear, from 5.3 to 0.5 m^2/cm^3 over the 42-167 mg/ml concentrations, respectively. This demonstrates the ability to fabricate a wide variety of surface areas of electrospun PDS, which may play a critical role in cell-matrix interactions. The statistical analysis of this data indicates that the 42-56 mg/ml surface area to volume ratios are significantly different from the 71-167 mg/ml surface area to volume ratios, within each of those groups no significant difference was detected.

Mechanical Evaluation

The results of the mechanical testing of the electrospun PDS structures are presented in Figures 25-27.

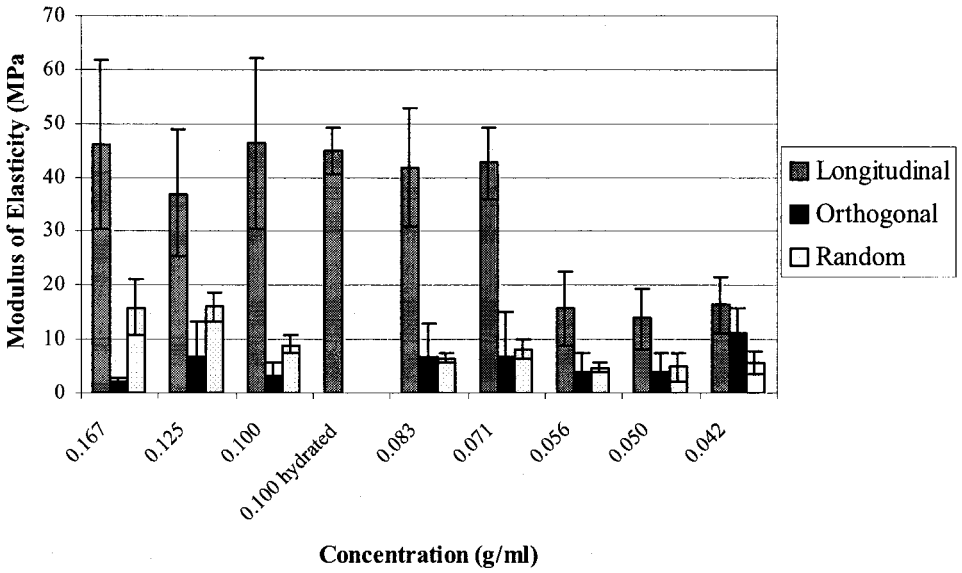

Figure 25. The results of the mechanical testing, dry and hydrated, are illustrated in terms of elastic modulus vs. concentration for the aligned and random electrospun PDS fiber orientations.

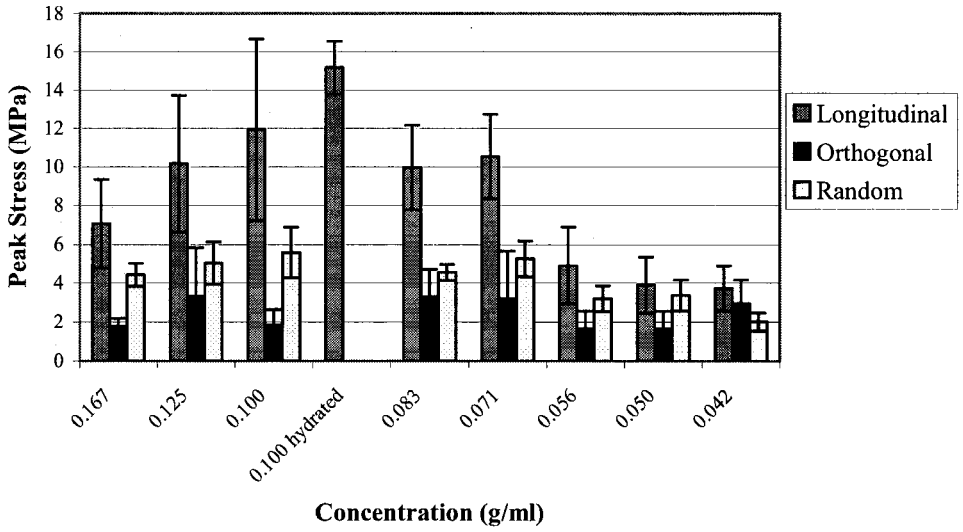

Figure 26. The results of the mechanical testing, dry and hydrated, are illustrated in terms of peak stress vs. concentration for the aligned and random electrospun PDS fiber orientations.

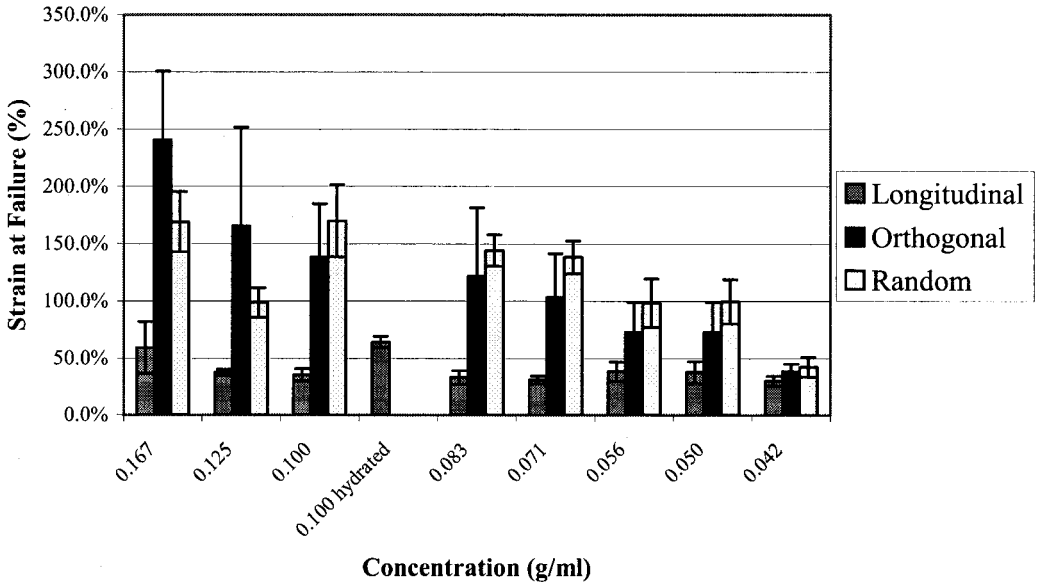

Figure 27. The results of the mechanical testing, dry and hydrated, are illustrated in terms of strain at failure vs. concentration for the aligned and random electrospun PDS fiber orientations.

In general, the values for modulus, peak stress, and strain at failure were highest for the aligned fibrous structures. A similar trend was evident as the fiber diameter increased.

More specifically, the analysis of the modulus data (Figure 25) indicated that the aligned moduli for the fibrous structures produced from the 71-167 mg/ml concentrations were significantly different from the aligned 42-56 mg/ml concentration structures with no differences amongst the groups. Dunn's method was used in the pair-wise statistical analysis of orthogonal and random moduli. The orthogonal 56 and 42 mg/ml derived structures were significantly different from the orthogonal 167 mg/ml structures. The randomly spun 167 and 125 mg/ml fibrous structures were significantly different than 42-71 mg/ml structures. Depending on if the data passed a normality test, Tukey's test or Dunn's method was performed for pair-wise comparisons of the moduli of an orientation within a solution concentration. Finally, the aligned fibrous structures of each concentration were significantly different than the orthogonal fibers of the same concentration.

The peak stress data is presented in Figure 26. Tukey's test was used to perform a pair-wise statistical analysis comparing the aligned peak stresses. The aligned 71-167 mg/ml derived fibrous structures were significantly different from the aligned 42-56 mg/ml fibrous structures. A pair-wise statistical analysis comparing the orthogonal peak stresses was performed using Dunn's method. The only significant difference detected in these data was that the orthogonal 56 mg/ml fibers were only significantly different from the 167, 100 and 50 mg/ml fibrous structures. A pair-wise statistical analysis comparing the random peak stresses was performed using Tukey's test. The random 42 mg/ml

concentration fibrous structure was significantly different from the other random fibrous structures except for the 56 mg/ml structure. Again, Tukey's test or Dunn's method was performed for pair-wise comparisons of the peak stresses of an orientation within a solution concentration depending on if the data passed a normality test. The aligned fibrous structures except for the 56 mg/ml concentration were significantly different than the orthogonal fibrous structures of like concentrations.

The strain at failure data is presented in Figure 27. Dunn's method was used in the pair-wise statistical analysis of aligned and orthogonal strain at failure. For the aligned fibrous structures, only the 167 mg/ml fibrous structure's strain at failure was significantly different than the 83, 71, and 42 mg/ml derived structures. The orthogonal 100-167 mg/ml derived structures were significantly different from the aligned 56 and 42 mg/ml fibrous structures. Again, depending on if the data passed a normality test, Tukey's test or Dunn's method was performed for pair-wise comparisons of the strain at failure for an orientation within a solution concentration. The aligned fibrous structure of each concentration was significantly different than the orthogonal fibrous structures of the same concentration.

The final data presented in Figures 25-27 are the hydrated values of structures electrospun from 100 mg/ml PDS/HFP. This evaluation was performed due to the concerns of the mechanical properties of the electrospun PDS structures being altered upon hydration, which would be the state of material during the majority of biomedical applications. The hydration of the samples did not significantly change the modulus or the peak stress during uniaxial testing when compared to the dry samples. However, the

strain at failure for the hydrated sample increased significantly from 35.6 ± 5.3% to 64.3 ± 5.1% for the dry and hydrated structures, respectively. This is an 81% increase in the strain at break indicating an increase in the plasticity of the hydrated structures.

DISCUSSION

Polydioxanone was successfully electrospun from solutions with HFP to form fibrous mats. Both aligned and random mats were capable of being produced as illustrated in Figure 5. As previously reported with electrospun polymers, a strong linear relationship exists between the electrospinning solution concentrations and the diameter of the fibers produced. A similar linear relationship is seen with the pore areas although the correlation is not as precise (Figure 22). It is hypothesized that pore area is a function of both fiber diameter and translation speed of the target mandrel. Since the translation speed is a fixed variable with the current electrospinning device, this parameter cannot be controlled as closely. Two other calculated parameters are very important in predicting the success of an electrospun polymer structure (i.e. tissue-engineering scaffold) are porosity, percent open area, and the surface area to volume ratio. These calculated values are depicted in Figures 23-24. Percent open area is a measure of porosity of the scaffold and serves as a predictor of cellular densities that can be obtained within the scaffold. The surface area to volume ratio can predict the extent of cellular interaction with the scaffold.

The physical characteristics of electrospun PDS scaffolds indicate that they possess high porosity, high surface to volume ratios, and can be comprised of sub-micron

diameter fibers. Once it has been determined that a scaffold can be produced to meet the physical characteristics desired of a biomedical application, traditional engineering principals such as stress and strain may ultimately govern the success of an implanted structure (8). The mechanical properties of interest in this study were the modulus (Figure 25), peak stress (Figure 26), and strain to failure (Figure 27). We believe that these are the key characteristic properties that must be addressed in the design of a biomedical structure and are commonly reported for various soft tissues.

It should be noted that hydration of the 100 mg/ml PDS in HFP sample did not significantly adversely change its mechanical performance as often seen with natural materials (76, 77, 118). Additionally, 4 mm inner diameter tubes were also prepared from 100 mg/ml PDS in HFP. These tubes were left on a stainless steel mandrel overnight to attempt to enhance an initial structural memory. The initial observation was that these tubes did display a degree of shape memory when removed and was for the most part maintained after being hydrated for 24 hours. Conceptually, this could lead to kink and crush resistance as a vascular scaffold material. Additional testing is underway to elicit cellular compatibility, suture retention and suitability as a scaffold for a tissue engineered blood vessel.

In all cases, the visualized orientation achieved during electrospinning has been confirmed by uniaxial mechanical testing. As expected, the longitudinal direction was significantly stronger (peak stress – longitudinal vs. orthogonal for all cases) and more rigid (modulus and strain to failure - longitudinal vs. orthogonal for all cases except the 42 mg/ml concentration) than the orthogonal direction. However, the randomly aligned

fibrous structures typically demonstrated properties similar to either the longitudinal or orthogonal values, which illustrate a potential lack of control over the fiber orientation throughout the structures.

Finally, it has been the experience of our laboratory and others that cell interaction improves and immune response decreases with decreases in fiber diameter of synthetic materials (16, 97). It is speculated that down stream biochemical processes are beneficially altered when focal adhesions form on surfaces with small radii of curvature. This phenomenon has also been demonstrated with improved cell adhesion on textured metal surfaces (116) so it appears to be independent of substrate. While not completely understood, it could provide progress in developing tissue engineering scaffolds from synthetic materials.

CONCLUSION

Polydioxanone is readily electrospun to produce fibers with diameters ranging from about 0.18 to 1.4 μm as a direct function of the concentration of the spinning solution. The fiber scale achieved was one to two orders of magnitude smaller than commercially available suture. Orientation of the electrospun mats was achieved using a rotating collection plate. Mechanical testing revealed anisotropic properties of the oriented mats. Future cell culture experiments will be needed to confirm that creating smaller diameter PDS fibers in a structure will improve phenotypic expression or construct viability in a manner similar to other synthetic bioresorbable materials.

Chapter 5 Electrospinning Collagen Type II

The following manuscript appeared in the Journal of Bioactive and Compatible Polymers, 2003, volume 18, pages 125-134 (76). The author's portion of this work included demonstration that the relationship between solution concentration and fiber diameter continues to be linear when electrospinning collagen type II. In addition, the author assisted in demonstrating the suitability of culturing chondrocytes on electrospun Collagen type II.

Electrospinning of Collagen Type II: A Feasibility Study

Jamil A. Matthews and Eugene D. Boland
Department of Biomedical Engineering
Virginia Commonwealth University
Richmond, VA 23298-0698

Gary E. Wnek
Department of Chemical Engineering
Virginia Commonwealth University
Richmond, VA 23298-3028

David G. Simpson
Department of Anatomy and Neurobiology
Virginia Commonwealth University
Richmond, VA 23298-0709

Gary L. Bowlin
Department of Biomedical Engineering
Virginia Commonwealth University
Richmond, VA 23298-0694

Abstract

Collagen is the natural scaffolding found in all tissues and has been explored extensively for use as a tissue engineering scaffold with limited success. In this feasibility study, the electrospinning of collagen type II and subsequent chondrocyte seeding was investigated for potential use in cartilage tissue engineering. The electrospinning process utilized lyophilized, chicken sternal cartilage collagen type II suspended in 1,1,1,3,3,3 hexaflouro-2-propanol and demonstrated that collagen type II could be electrospun to form non-woven fibrous mats composed of type II fibers that ranged from 110nm to 1.8 μm diameter. The fiber diameter was dependant on the type II concentration in solution with a higher concentration producing the larger diameters. The preliminary chondrocyte

seeding studies demonstrated that electrospun collagen type II scaffolds support cell growth and are readily infiltrated. In conclusion, the feasibility of collagen type II electrospinning has been demonstrated and the novel scaffolds produced are composed of nano- to micron-scale fiber diameters that have been shown to be compatible with chondrocytes.

KEY WORDS: collagen type II, electrospinning, tissue engineering, scaffolding.

Introduction

The field of tissue engineering has attempted to utilize a variety of synthetic and natural polymers and processing methods in attempts to fabricate scaffolds for the regeneration of tissue/organs (113). The electrospinning of collagen type I and III to form tissue engineering scaffolds composed of nanofibers has been previously presented (21, 77) and has tremendous potential for the production of ''ideal'' scaffolds. This manuscript will present the electrospinning of collagen type II for use in tissue engineering such products as articular cartilage and interverteberal disks (patents bending).

Articular cartilage is the connective tissue, composed of primarily type II collagen, which covers the ends of long bones and functions in load bearing (shock absorber) and joint lubrication (71). Type II collagen is a homotrimer composed of three identical α chains [α1(II)]3 that form less than 80nm diameter fibers (93, 111). It has been shown that fibrocartilage (combination of cartilage and fibrillar collagen), which is composed of mainly type I collagen and chondrocytes (undifferentiated) is not capable of handling the loads normally carried by articular cartilage (93). Thus, the application of electrospun collagen type I in the fabrication of articular cartilage would not be feasible due to the mechanical limitations of the material. Collagen type II accounts for 50–80% of the dry weight (90% of the total collagen content) of articular cartilage and forms a complex, interconnected, three-dimensional network (93). More specifically, the ultrastructure of articular cartilage can be divided into four zones: (1) the superficial tangential zone accounts for 10–20% of the overall thickness, (2) the middle zone which

accounts for 60% of the thickness, (3) the deep zone that is 30% of the thickness, and (4) the calcified cartilage zone where the cartilage interfaces with the bone (83). Each of these zones contains different collagen organization as well as different amounts of proteoglycans. Briefly, the superficial zone has fine collagen fibers that are aligned parallel to the articular surface. The middle zone has larger collagen fibers that are randomly arranged. Finally, the deep zone has woven collagen fibers, bundles, which are organized perpendicular to the articular surface (83). Interspersed throughout this collagen network are proteoglycans which function in the hydration of the tissue, substantially adding to the load bearing properties of this connective tissue that allows the chondrocytes (less than 5% of the tissue volume) to properly differentiate and subsequently to allow the tissue to possess significant load-bearing capabilities (71, 93). Thus, the illustration of the importance of the application of collagen type II in the engineering of cartilage tissue. In this study, we describe an electrospinning strategy to fabricate a cartilage prosthetic.

We have employed the electrospinning process to process a variety of both synthetic and natural polymers as scaffolds for cell and tissue growth (18, 20, 66, 77). The basic electrospinning system consists of a charged polymer solution that is fed through a small nozzle. Because of its charge, the solution is drawn toward a grounded collecting plate as a jet. During the jet's travel, the solvent gradually evaporates, and a charged polymer fiber is left that accumulates on the grounded target. The charges on the fibers eventually dissipate as they are neutralized by the surrounding environment (67). The final product of the process is a non-woven fiber mat (scaffold) that is composed of

fibers with diameters on the order of nanometers to microns. Details of the electrospinning apparatus used in this experimentation have been described previously (77).

Experimental Section

Collagen electrospinning

The feasibility study to demonstrate electrospinning and chondrocytes compatibility utilized lyophilized, chicken sternal cartilage collagen type II suspended in 1,1,1,3,3,3 hexaflouro-2-propanol (HFP). All reagents purchased through Sigma Aldrich unless noted. For this study, the collagen was electrospun at two concentrations (0.04 and 0.1 g/mL). The collagen solution was loaded into a 1.0mL syringe plunger with an 18-gauge stub-end needle placed on the syringe to act as the nozzle and charging point for the contained collagen solution. The filled syringe was placed on a syringe pump set to dispense the solution at rate of two mL per hour. The positive lead from the high voltage supply was attached to the stub-end metal portion to charge the collagen solution to 22 kV. A 303 stainless steel mandrel (0.1 cm W x 0.6 cm H x2 cm L) was used as a ground target and was placed four inches from the tip of the needle. The collagen solution was electrospun to form a fibrous, microporous mat (approximately 300μm thick) on the grounded mandrel. After electrospinning, the collagen mat was removed from the mandrel and processed for scanning electron microscopy (SEM) and chondrocytes seeding evaluation.

Scaffold seeding

Chondrocytes were seeded onto electrospun scaffolds of Type II collagen to evaluate the biophysical properties of this material. In these studies, a 100mg sample of collagen type II was placed in HFP at a concentration of 0.10 g/mL and electrospun. Once the entire volume (1 mL) of type II collagen solution was spun, its resultant electrospun mat was removed from the mandrel and fixed in a 3% glutaraldehyde vapor chamber for 15 h at room temperature. The constructs were soaked in 70% isopropyl alcohol for 5 min followed by three washes in sterile phosphate buffered saline [2]. Normal human articular chondrocytes (Clonetics Corp.), second passage, were suspended in culture media (1,000,000 cells in 1 mL) and plated onto scaffolds for 3 h in a seeding chamber. The seeding chambers consisted of a round, hollow stainless steel cylinder with an inside diameter of 6.4 mm, total length 7 cm. Seeding chambers were rotated at 1/8 rpm. The culture media was composed of 67% Dulbecco's Modified Eagle Medium (DMEM; high glucose with L-glutamine, sodium pyruvate and pyridoxine hydrochloride), 22% F-12 Nutrient Mixture, 15% fetal bovine serum, and 1% Penicillin-Streptomycin (10,000 Units/mL each). All media components were purchased from Gibco BRL Life Technologies. The mats were removed from the seeding chambers and cultured for 1 and 2 weeks, respectively, in a rotary cell culture system (RCCS) (Slow Turning Lateral Vessel (STLV); Synthecon, Inc., Houston, TX) that simulates microgravity (scaffold in continuous free-fall). This environment provides high mass transfer of nutrients in a buoyant, low shear environment under conditions that has been shown to foster cell–cell and cell–extracellular matrix (ECM) interactions (44, 45).

Results and Discussion

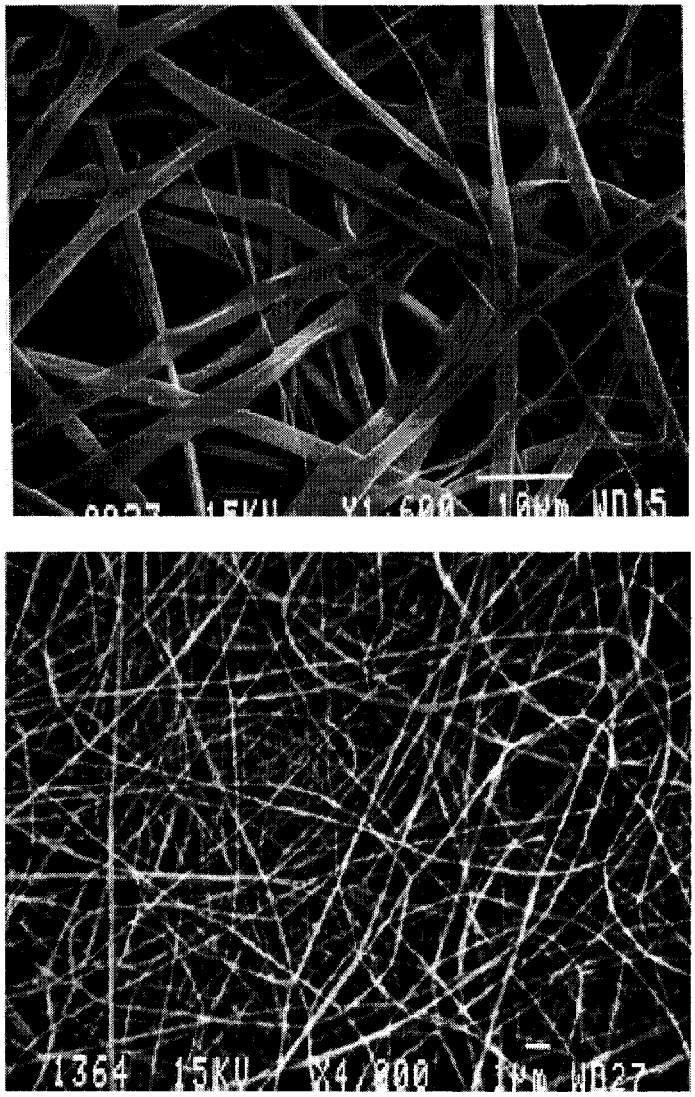

Figure 28. (Top) Scanning electron micrograph of an electrospun type II collagen matrix prior to seeding. The collagen type II ribbon-like fibers were electrospun from 100 mg/mL HFP and have widths from 0.30 to 3.59 μm (1.75 ± 0.86 μm). (Bottom) Collagen type II fibers spun from 40 mg/mL HFP illustrating the structure composed of 0.06–0.27 μm (0.11 ± 0.03 μm) fibers.

The SEM micrographs (Figure 28) of electrospun collagen type II reveal scaffolds composed of polymerized collagen fibers with an average diameter of 1.75 ± 0.9 μm and 0.11 ± 0.09 μm for the electrospun solutions of 0.1 and 0.04 g/mL, respectively. The mats produced from 1mL of starting solution were approximately 300 μm thick; increasing or decreasing the volume of polymer solution or the dwell time of any given domain of a target mandrel can modulate this parameter. Fiber diameter is modulated in electrospinning as a function of the identity and concentration of the polymer (18, 33). The 110nm electrospun fibers fabricated in this study approach the 80nm diameter of Type II collagen fibrils observed in native tissue. It should also be noted that electrospun mats of collagen type II possess substantial structural integrity and withstand manual manipulation, with glutaraldehyde vapor fixed scaffolds of this material being stable in the cell culture environment (77). Extensive structural analysis and mechanical testing of the dry and hydrated electrospun collagen type II structures are currently being performed.

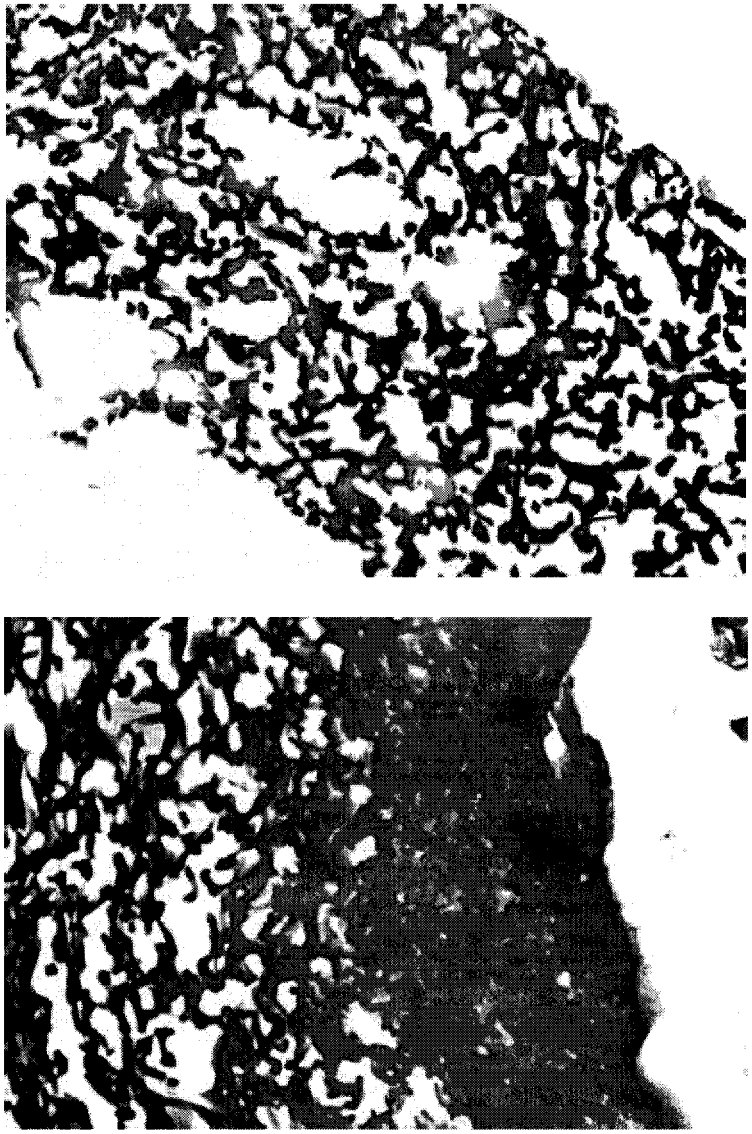

Figure 29. (Top) Type II after 1 week in culture with chondrocytes demonstrating a low chondrocyte concentration, even distribution, and limited remodeling across the scaffold. (Bottom) Chondrocytes on type II collagen matrix after 2 weeks in culture demonstrating increased cell infiltration and scaffold remodeling compared to week 1.

Chondrocyte seeding studies demonstrated that these electrospun collagen scaffolds support cells growth and are readily infiltrated. Samples of the histological sections used in this analysis are presented in Figure 29. SEM analysis, (Figure 30), of

seeded electrospun scaffolds after one week in a growth chamber revealed a sub-confluent layer of chondrocytes on the external surface of the matrix.

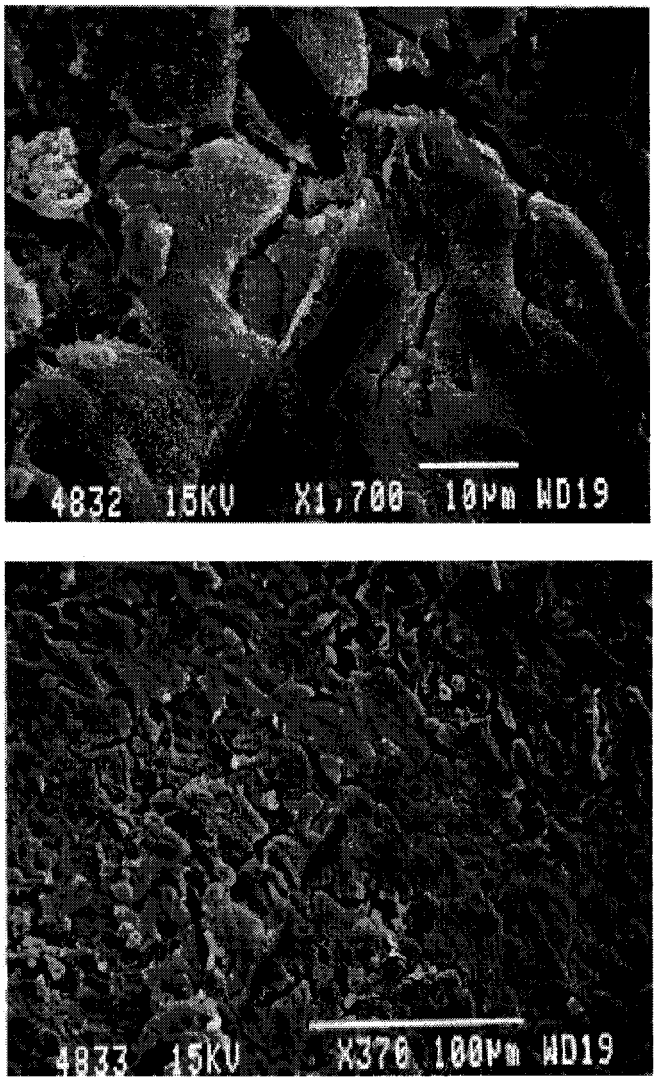

Figure 30. (Top) Scanning electron micrograph of type II collagen after 1 week in culture with chondrocytes demonstrating almost complete matrix coverage (Seeded surface). (Bottom) Seeded layer of the type II collagen mat under low magnification showing confluent cell coverage of the seeded surface after two weeks in culture.

Histological evaluation of the scaffolds revealed chondrocytes were evenly distributed across the scaffold thickness with no overt changes in the structure of the matrix. After

two weeks of culture, SEMs revealed a nearly confluent layer of cells on the external seeded surface of the scaffold. Histological examination of internal domains of the scaffolds indicated that substantial degree of remodeling transpires as the cells penetrate the matrix. This data demonstrates that chondrocytes can freely penetrate an electrospun matrix of Type II collagen. At present, the processes that mediate cellular infiltration remain to be defined, however, the chondrocyte cells appear to actively degrade and redeposit collagen as they penetrate this type of matrix.

One of the attractive aspects of the electrospinning process is that scaffolds of various shapes and sizes can be constructed while at the same time precisely controlling fiber orientation, composition (blended fibers, one can add other proteins (i.e. Type I collagen in an appropriate proportion), and dimensions. With electrospinning, a biomimetic cartilage scaffold with four zones, as previously described, composed of natural materials can be replicated. Complex constructs can be fabricated to closely replicate the structural and chemical composition of the native articular cartilage. For example, electrospinning can be used to prepare a cartilage construct with an inner central domain composed of random arrays of collagen fibrils. This inner domain can be supplemented with glycosaminoglycans, hyaluronic acid, keratin sulfate, chondrotoin sulfate, and aggregan complexes to promote hydration. The outer layers composed of relatively pure collagen can be electrospun along the required unique and predetermined axis (83). Another key advantage to the electrospinning process is that for those scaffolds, that one can make a mold for, will be seamless, 3-D scaffolds. Also, the ability to co-spin polymers with various additives (e.g., proteoglycans) offers the possibility of

tailoring the scaffold to a specific site and application. Thus, with electrospinning it may be possible to create ideal scaffoldings for the bioengineering of cartilage that could be generic or customized by the creation of a 3-D, biomimetic cartilage scaffold mold from such data as an X-ray or MRI rendering. In closing, at present, it will be necessary to empirically determine the exact composition necessary to promote the formation of bioengineered cartilage.

Conclusion

In conclusion, it may now be possible to construct a truly ''biomimicking'' fibrous scaffoldings for tissue engineering of cartilage and interverteberal disks using the process of collagen type II electrospinning to form a variety of composite structures. Of particular interest, with articular cartilage, will be the replication of the fibrous architecture of the native tissue that can be approximated with control over fiber orientation and diameter during the electrospinning process to create the composite scaffolds.

Acknowledgement

The authors would like to thank the Whitaker Foundation (RG—98-0465) for the financial support of this research. We would also like to thank Ms. Judy Williamson for obtaining the SEM micrographs.

Chapter 6 Hydrochloric Acid Pretreatment of Electrospun Poly(glycolic acid)

The following manuscript has been accepted for publication in the Journal of Biomedical Materials Research, Part B: Applied Biomaterials (16). This manuscript has been included as an example of modifying electrospun poly(glycolic acid) through pretreatment in a strong acid to improve biocompatibility through both *in vitro* and *in vivo* testing. Furthermore, the observation that biocompatibility improved as fiber diameters diminished was explored. Additional details about the chemistry, biodegradation and uses of poly(glycolic acid) can be found in Appendix A.

Utilizing Acid Pretreatment and Electrospinning to Improve Biocompatibility of Poly(glycolic acid) for Tissue Engineering

Eugene D. Boland[1], Todd A. Telemeco[2], David G. Simpson[2], Gary E. Wnek[3], and Gary L. Bowlin[1]

[1.] Department of Biomedical Engineering
Virginia Commonwealth University
Richmond, VA 23298-0694

[2.] Department of Anatomy
Virginia Commonwealth University
Richmond, VA 23298-0709

[3.] Department of Chemical Engineering
Virginia Commonwealth University
Richmond, VA 23298-3028

Abstract

Poly (glycolic acid) (PGA) has a long history as a bioresorbable polymer. Its biocompatibility is widely accepted yet PGA is often rejected as a soft tissue scaffold due to fibrous encapsulation. The goal of this study was to improve the soft tissue biocompatibility of PGA by producing scaffolds composed of small diameter fibers through electrospinning and subjecting these scaffolds to a concentrated hydrochloric acid (HCL) pretreatment. The theory is that small diameter fibers will illicit a reduced immune response and HCl treatment will improve cellular interactions. Scaffolds were characterized in terms of fiber diameter and pore area via image analysis software. Biocompatibility was assessed through a WST-1 cell proliferation assay (*in vitro*) using rat cardiac fibroblasts and rat intramuscular implantations (*in vivo*). Fibers produced ranged in diameter from 0.22 to 0.88 μm with pore areas from 1.84 to 13.22 μm^2. The

untreated scaffolds composed of 0.88 μm fibers was encapsulated *in vivo* and supported the lowest rates of cell proliferation. On the contrary, the acid pretreated scaffold with 0.22 μm fibers was incorporated into the surrounding tissue and exhibited proliferation rates that exceeded the control populations on tissue culture plastic. In conclusion, this study has shown the ability to improve the biocompatibility of PGA through acid pretreatment of scaffolds comprised of submicron fiber diameters.

Key Words: poly(glycolic acid), electrospinning, tissue engineering, scaffold, biocompatibility

Introduction

Poly(glycolic acid), or PGA, is a biodegradable aliphatic polyester currently exploited in a variety of medical applications. PGA possesses a compact, regular repeat unit that is terminated by a hydroxyl group on one end and a carboxyl group on the other with no side chains. This structure leads to a moderate degree of crystallinity, high melting point, and low solubility in organic solvents. That not withstanding, monofilaments of PGA can be degraded *in vivo* in as little as 2 to 4 weeks due to its hydrolytic degradation (119).

PGA's acceptance as a biomaterial began as a suture and wound dressing in the 1970's. It was found to have better than average biocompatibility, good strength and knot retention and a very predictable degradation rate. Upon implantation, PGA is characterized by a steady decrease in strength, an increase in localized pH, and fibrous capsule formation (119). These characteristics may be acceptable for a burn dressing or a suture, however, these material properties have limited the usefulness of PGA as a tissue engineering scaffold material for soft tissue applications.

Commercially available PGA products are comprised of braided, woven or knitted materials. These materials are produced from fibers that have a current minimum diameter of 10 μm although most are significantly larger (5, 119). This is a physical limit due to the mechanical stress induced during the melt spinning or extrusion processes employed during fiber manufacturing. While these fibers are small, they may be an order of magnitude larger than the native cells that will come in contact with the materials after implantation. Observationally, this size limit may be important since native protein fibers

in the extracellular matrix typically have diameters as small as 50 nanometers. With the current trends in tissue engineering to produce biomimicking scaffolds, this size constraint could further limit the acceptance of traditionally processed PGA for tissue engineering.

We have previously described how electrospinning can be used to produce PGA fibers with diameters as small as 110 nanometers (18). In that study, we showed that fiber diameter was directly proportional to the electrospinning solution concentration. Briefly, electrospinning is accomplished by inducing a large electric potential (15 to 30 kilovolts DC) in a polymer solution or melt and separating that polymer from an oppositely charged target. This creates a static electric field. As the field strength grows, the charge separation overcomes the surface tension of the solution and a thin jet (entangled polymer chains) is ejected from the polymer reservoir. This jet then travels toward the target. Instabilities within the charged jet define its orientation in space (condition previously described as whipping). By the time the jet reaches the target, a dry fiber is collected in the form of a non-woven mat. The focus of our laboratory is the utilization of these mats for tissue engineering applications with both synthetic and natural polymers (18, 20, 66, 76, 77, 106, 118).

The ability to generate non-woven PGA scaffolds comprised of sub-micron diameter fibers has addressed only one criticism of PGA as a tissue engineering scaffold for soft tissue applications. In an attempt to alter the surface properties and charge characteristics of electrospun PGA, we have hypothesized that a hydrochloric acid pretreatment can be used to manipulate the hydrophilic nature of the polymer and thereby

improve cell adhesion and migration. Previous literature suggests that cellular adhesion improves with hydrophilicity (47, 50) and we believe that improved cellular adhesion might reduce the inflammatory response typically observed with PGA-based materials. The improvements in hydrophilicity and adhesion may be due to hydrolysis.

To test these hypotheses, various concentrations of PGA were electrospun to form non-woven scaffolds. The scaffolds were characterized in terms of fiber diameter, approximate pore area, percent open area and surface area to volume ratios. Half of these scaffolds were treated with concentrated hydrochloric acid and the other half were not. These scaffolds were then used as a substrate for an *in vitro* cellular proliferation assay using rat cardiac fibroblasts or an *in vivo* host response evaluation in a rat model.

Methods

Electrospinning

For this study, PGA obtained from Alkermes, Inc. (Cincinnati, OH) was dissolved in 1,1,1,3,3,3 hexafluoro-2-propanol (HFP, Sigma Aldrich Chemical Co.) at concentrations of 67 mg/ml, 100 mg/ml and 143 mg/ml. These concentrations were chosen from previous work by the authors to demonstrate small, mid-sized and large fibers. The solutions were then loaded into a Becton Dickinson 5.0-ml syringe and placed in a KD Scientific syringe pump for metered dispensing between 8-14 ml/hr. The positive output lead of a high voltage supply (Spellman CZE1000R; Spellman High Voltage Electronics Corp.), set to 22 kV, was attached to a blunt 18 gauge needle on the syringe as depicted diagrammatically in Figure 31.

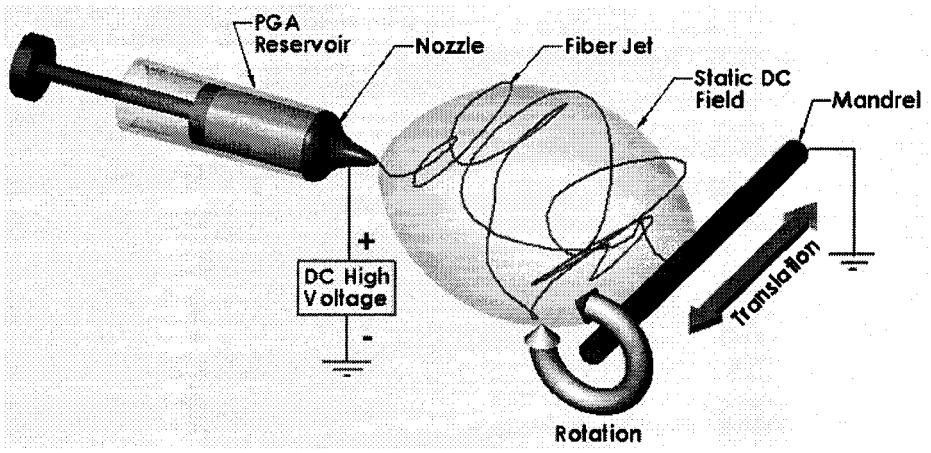

Figure 31. Diagrammatic representation of the electrospinning process. A syringe is used as the reservoir, a blunt 18 gauge needle as the nozzle and a high voltage power charging the solution to 15 - 30 kilovolts.

For the cell proliferation assay, a grounded target (1" Wide × 4" Long × 1/8" Thick; 303 stainless steel) was placed 11 inches from the needle tip and revolved at 500 revolutions per minute (RPM) to evenly coat the mandrel but not impart a large degree of alignment of the deposited fibers. For the host response evaluation, a 2 mm diameter x 150 mm long stainless steel mandrel was used to create seamless tubes with a 2 mm internal diameter (ID). Again, the mandrel was rotated at 500 RPM.

Scaffold characterization

After the scaffolds were electrospun, samples were cut from each mat for characterization. A representative sample from each was sputter coated in gold (Electron Microscope Sciences model 550) for scanning electron microscopy (SEM) (JEOL JSM-

820 JE Electron Microscope) and evaluated at 1000 to 4000 times magnification. The images were digitized with a flat bed scanner (Hewlett – Packard Scanjet 6200C) and analyzed by ImageTool 3.0 (Shareware provided by University of Texas Health Science Center in San Antonio) to determine the average fiber diameters (average and standard deviation calculated from 60 measurements per micrograph) in the various scaffolds. All measurements were calibrated using the scale on the micrograph as a reference to avoid errors in calculating the magnification after digitization. In addition to fiber diameter, pore areas were also calculated. This was done by a subjective approximation of surface pores in the SEM micrographs that were at least 15 μm deep. Current quantitative methods for determining porosity of electrospun scaffolds are in development. Percent open area and surface area to volume ratios were calculated knowing the supplied material density (1.5 g/cm^3), mass of the electrospun scaffolds, volume of the electrospun scaffold and calculated average fiber diameter using the following equations:

$$Percent\,Open\,Area = \frac{(1 - calculated\,scaffold\,density)}{(known\,material\,density)} * 100\%$$

$$Equivalent\,Fiber\,Length = \frac{(measured\,mass\,of\,scaffold)}{(known\,material\,density) * \pi * (average\,fiber\,radius)^2}$$

$$Surface\,Area\,to\,Volume\,Ratio = \frac{(equivalent\,fiber\,length) * 2 * \pi * (average\,fiber\,radius)}{(calculated\,scaffold\,volume)}$$

Acid pretreatment / sample preparation

Scaffold samples were die cut to 15 mm diameters to match the base diameter of a 24 well microtiter plate for the cell proliferation assay and the 2 mm diameter tubes were

cut to 15 mm lengths for implantation. After cutting, the scaffolds were disinfected in 70% ethanol for 10 minutes then subjected to three 10 minutes rinses in sterile water while agitated. For the acid pretreated specimens, the scaffolds were submerged in 11.7 Molar hydrochloric acid for 5 minutes. The scaffolds were then rinsed by submersion in sterile phosphate buffered saline for 2 minutes while agitated. This rinsing procedure was repeated three times. For the control group scaffolds, after disinfection, they were subjected to the identical rinsing procedure. The pH of the final rinse solution for all scaffolds was measured to confirm neutralization or removal of all acid during the rinsing procedure. All scaffolds were then placed in media containing 10% Fetal Bovine Serum for two hours prior to use and held in an incubator at 37°C, 5% CO_2 and constant humidity.

Cell culture

Cardiac fibroblasts (FBs) were emzymatically dissociated from three to four day old neonatal rats using a method previously described by Teraccio, et al. (108). These cells were cultured utilizing standard cell culture protocol in Dulbecco's Modified Eagle Medium (DMEM) and F12 Nutrient Mixture (F12) (2:1–DMEM:F12) supplemented with 10% Fetal Bovine Serum (FBS) and 1.2% antimycotic-antibiotic (Invitrogen Corporation). Culture medium specific to the cellular proliferation assay and host response evaluation will be discussed in the respective methods section.

Cell proliferation

Cell proliferation was measured using a WST-1 assay (Chemicon International) (31). This assay is based on a water soluble tetrazolium salt (slightly red) which is cleaved to formazan (dark red) by mitochondrial enzymes. The amount of formazan dye formed directly correlates to the number of metabolically active cells in the culture. To utilize this assay for analyzing tissue engineered scaffolds, six 15 mm diameter x 100 μm thick die cut scaffold specimens (three acid pretreated scaffolds and three control scaffolds) at each electrospinning concentration were placed in a separate well of the microtiter plate with $5x10^4$ FBs in 1 ml of tissue culture media to seed the scaffolds. To remove the confounding effects of growth factors, serum-free media (Dulbecco's Modified Eagle Medium and F12 Nutrient Mixture (2:1–DMEM:F12) supplemented with 10% ITS+1 (Insulin-Transferrin-Sodium Selenite media supplement with linoleic acid) (Invitrogen Corporation) was used in the cellular proliferation assay. Additionally, $1x10^3$, $5x10^3$, $1x10^4$, $2.5x10^4$, $5x10^4$, and $1x10^5$ cells were plated on standard tissue culture wells to serve as proliferation controls (no matrix). Into one well without cells was added 200 μl of standard tissue culture media to serve as a background control. The plates were cultured for 94 hours. After the incubation period, the culture media was aspirated and 200 μl of fresh media was added along with 20 μl of the Cell Proliferation Reagent WST-1. Two control groups (each group consisting of wells plated at $1x10^3$, $5x10^3$, $1x10^4$, $2.5x10^4$, $5x10^4$, and $1x10^5$ cells) to develop a standard curve were plated with 200 μl of fresh media and 20 μl of the Cell Proliferation Reagent WST-1. This plate was then incubated for an additional 2 hours on a 37°C shaker table. After agitation, 100

µl of solution from each well was transferred into a well on a new 96 well microtiter plate where the absorbance of the samples against the background control on a microtiter plate reader (Molecular Devices SpectraMax Plus) was obtained at a wavelength of 450 nm with a reference wavelength of 610 nm.

Host response

Due to the previous experience of the authors, a rat muscle implantation model was chosen for the preliminary *in vivo* evaluation. One hour prior to implantation, six scaffold tubes, 2 mm ID x 200 µm wall thickness x 15 mm length (one at each condition), were heat sealed at one end with forceps heated to 250°C (above PGA melting temperature) in a salt bath. The lumen of the cylinder was then filled with a Kregs-Ringer Bicarbonate (KRB) solution to avoid inducing an immune response from an air – tissue interface. The open end was then heat sealed and the sealed tube was placed in KRB until implanted. The goal of this host reaction study was to begin preliminary evaluation of the two variables present in this study, namely fiber diameter and acid pretreatment. Fiber diameter was chosen as the independent variable (varies between animals) with acid treatment as the dependent variable (varies within the animal). Three (n=3) adult male Sprague-Dawley rats between 300 and 450 grams were implanted with two scaffolds each (i.e. a 143 mg/ml scaffold with acid pretreatment was placed in the left hind leg and a 143 mg/ml scaffold without acid pretreatment was placed in the right hind leg of the same animal). To implant the scaffolds, the hindquarters of the rats were

washed in betadine and shaved, and a small channel was prepared within the belly of the vastus lateralis by blunt dissection (see Figure 32).

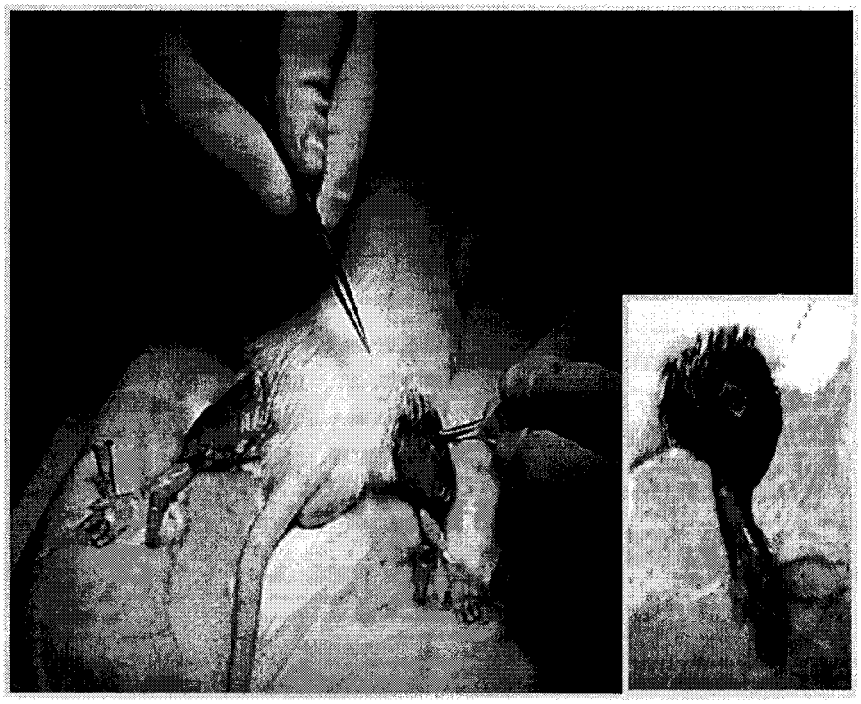

Figure 32. Bilateral scaffold implantation into Vastus Lateralis of adult male rat.

The scaffold was then inserted into this channel between the muscle and fascia untethered and the fascia and skin were sutured closed with 6-0 Prolene (Ethicon Corporation) to identify the implant site. The surgical site was sutured shut and the animals were returned to individual cages and allowed to ambulate. After 1 week, the scaffolds were removed, fixed in a 4% glutaraldehyde solution, and prepared for transmission electron microscopy (TEM) (Zeiss EM-10) and histology utilizing hematoxylin and eosin staining as well as Masson's Trichrome staining. NIH guidelines for the care and use of

laboratory animals (NIH Publication #85-23 Rev. 1985) have been observed and carried out under Virginia Commonwealth University's Institutional Animal Care and Use Committee (IACUC) protocol 9904-2635 approved 06/29/99.

Statistics

Unless otherwise noted, all statistics are based on a Kruskal-Wallis one way analysis of variance on ranks then subjected to a pairwise multiple comparison procedures (Tukey Test). The *a priori* alpha value is set at 0.05 with significance defined as $P \leq 0.05$. This methodology was chosen to address uneven sample sizes and distributions that may not be normal.

Results

Physical scaffolds characterization

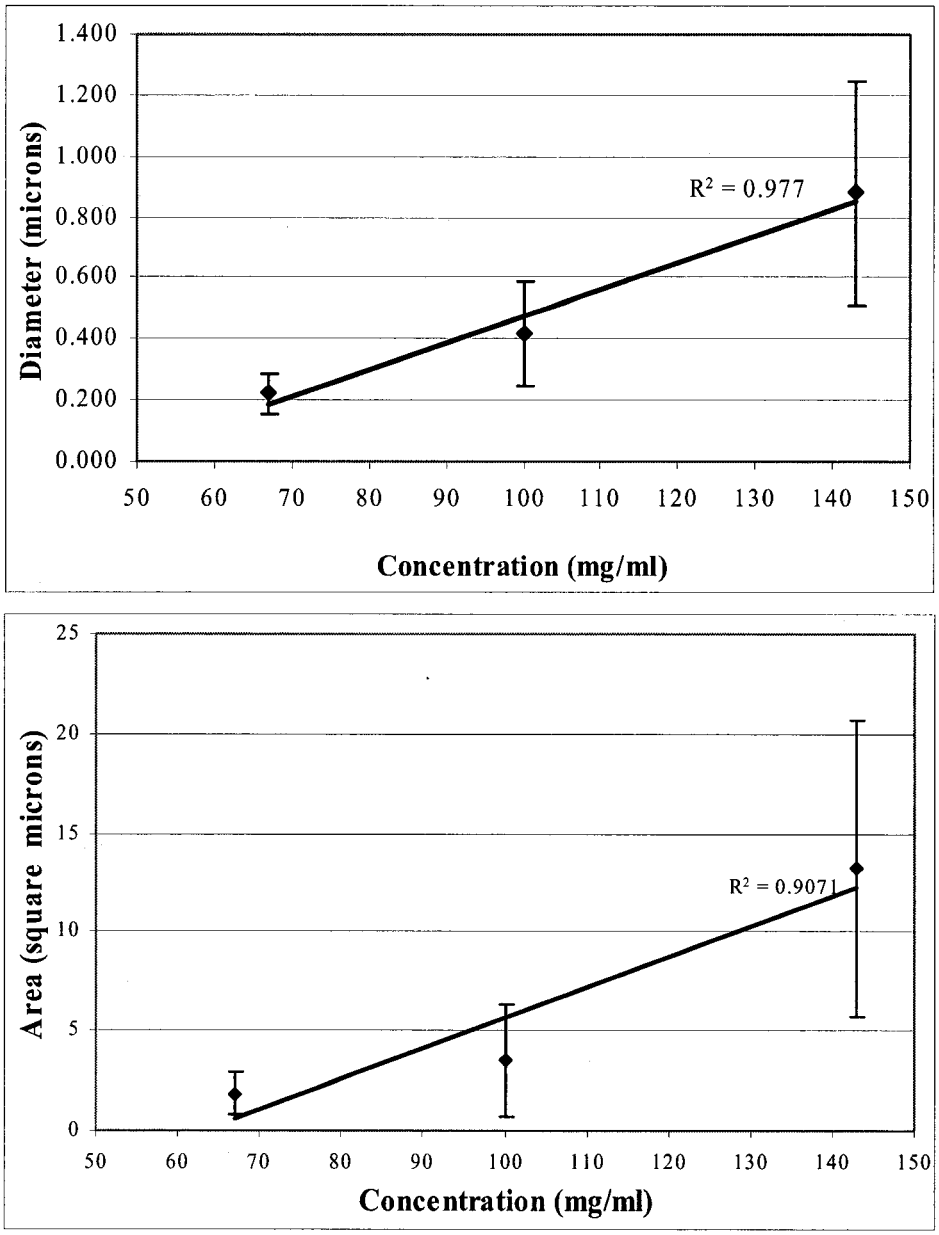

Figure 33. Line graphs depicting the relationship between PGA electrospinning concentration and fiber diameter (top graph) and PGA electrospinning concentration and pore area (bottom graph). All values are statistically different ($P<0.05$) from each other in pairwise testing.

A strong linear relationship between the electrospinning solution concentration and the measured fiber diameters was seen (Figure 33). These values closely compare with previous work by the authors (18, 20, 66, 76, 77, 106, 118). Dry fibers produced ranged in diameter from 0.22 to 0.88 μm at concentrations of 67 mg/ml PGA concentration and 143 mg/ml PGA concentration, respectively (excluding beads as depicted in Figure 34).

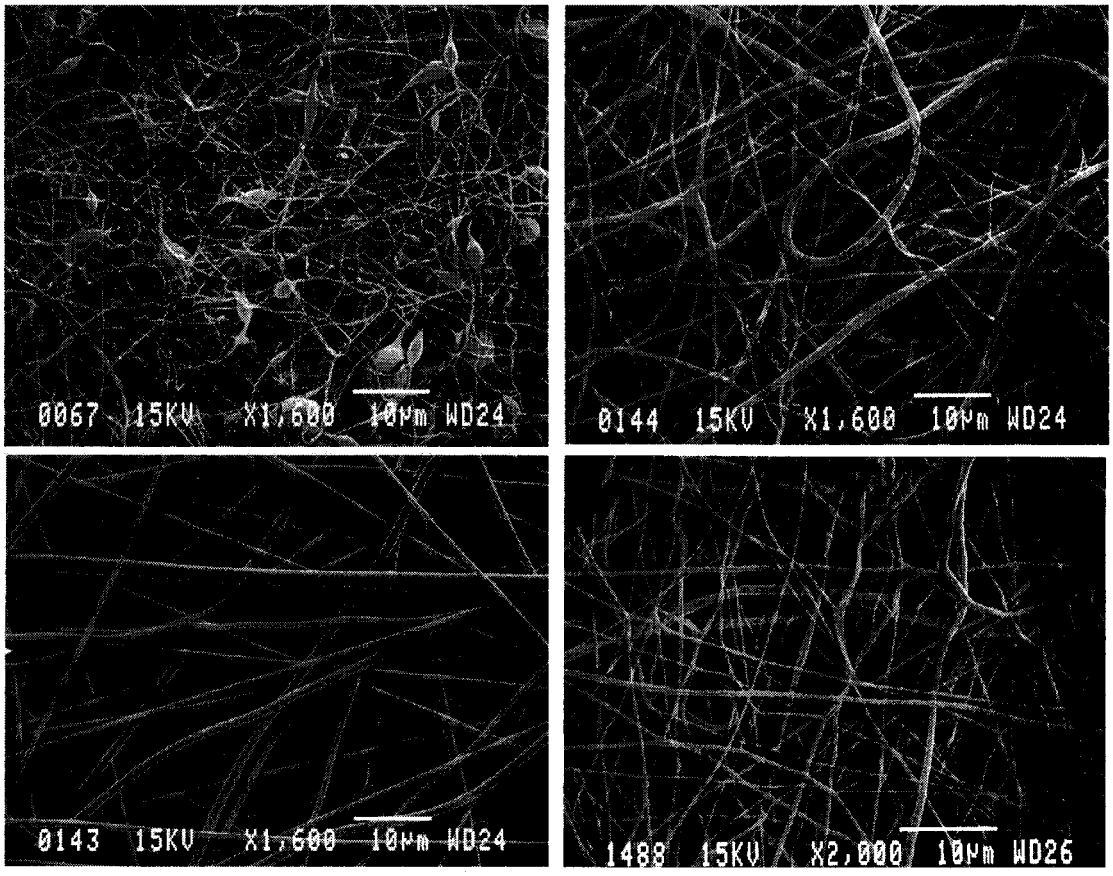

Figure 34. Scanning electron micrographs of control group electrospun PGA at 1600 times magnification and 100 mg/ml acid pretreated electrospun PGA (Bottom right) at 2000 times magnification. Top left: 67 mg/ml with 0.22 ± 0.07 μm fibers (excluding beads) and1.84 ± 1.08 μm^2 pores. Top right: 100 mg/ml with 0.42 ± 0.17 μm fibers and 3.53 ± 2.78 μm^2 pores. Bottom left: 143 mg/ml with 0.88 ± 0.37 μm fibers and 13.22 ± 7.45 μm^2 pores. Bottom right: 100 mg/ml with 0.41 ± 0.13 μm fibers and 3.71 ± 2.15 μm^2 pores.

A SEM micrograph of an acid pretreated 100 mg/ml PGA scaffold is also included in Figure 34 to illustrate that no gross morphological differences are seen after the acid pretreatment process. The bead formation in the 67 mg/ml PGA scaffold is caused by electrospinning near the transition concentration between electrospinning and electrospraying (no chain entanglement resulting in the formation of discreet droplets). Although the beads are present, they do not appear to adversely affect the compatibility of the scaffolds. Pore area, however, does not appear to follow the same linear trend as seen in Figure 33. Pore areas ranged from to 1.8 μm^2 to 13 μm^2 for the 67 mg/ml PGA concentration and the 143 mg/ml PGA concentration, respectively. This testing (and previous unreported data) support the hypothesis that pore area is related to concentration but approaches a minimum value that is dictated by mandrel rotation and translation speeds.

The scaffolds produced by electrospinning are easily handled and manipulated, yet are highly porous. The calculated porosities of the scaffolds are 83%, 85% and 81% respectively for the 67 mg/ml, 100 mg/ml, and 143 mg/ml concentrations. Related to the high porosity is a high surface area to volume ratio. The values, based on average fiber diameter, are 30,000, 14,000 and 8,800 cm^2/cm^3 respectively for the 67 mg/ml, 100 mg/ml, and 143 mg/ml concentrations. This high degree of void space and large surface area to volume ratio would seem to imply that the scaffolds would be good candidates for tissue engineering applications. As seen in the micrographs presented in Figure 34, the

fibers are randomly arranged with the greatest variability in fiber diameter (as a function of the mean) expressed at a concentration of 100 mg/ml.

Cellular proliferation assay

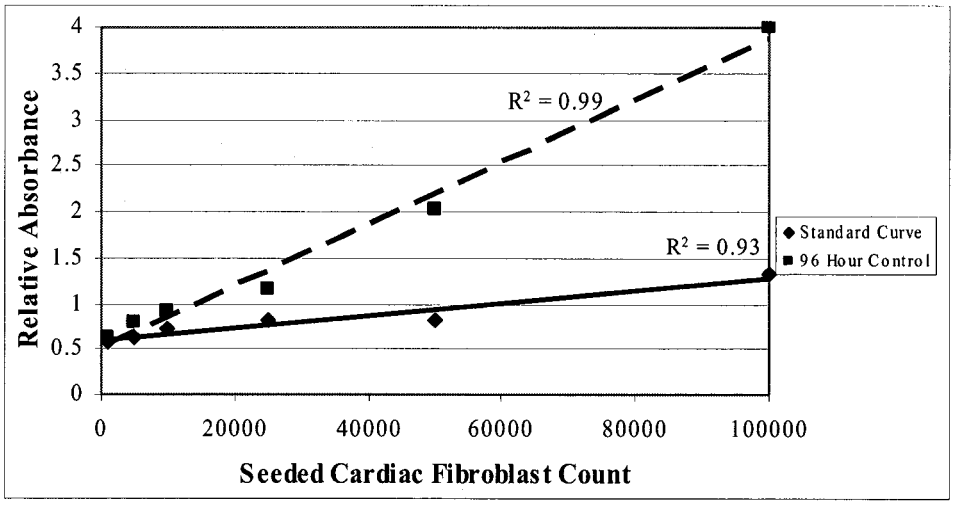

Figure 35. Line graft showing the control curves for the 96 hour cell proliferation assay. R^2 value for the 96 hour control (dashed) was 0.99 with $R^2 = 0.93$ for the standard curve (solid).

The WST-1 assay determines relative rates of proliferation by measuring mitochondrial activity. The controls in Figure 35 demonstrate the linearity of the assay results from 5000 to 100,000 seeded FBs. The R^2 value for the linear fit of the standard curve was 0.93 and the R^2 value for the 96 hour control curve was 0.99. This testing provided support for the hypothesis that acid treatment would improve the biocompatibility of electrospun PGA by increasing cellular proliferation. The proliferation assay data in Figure 36 show two trends in the data.

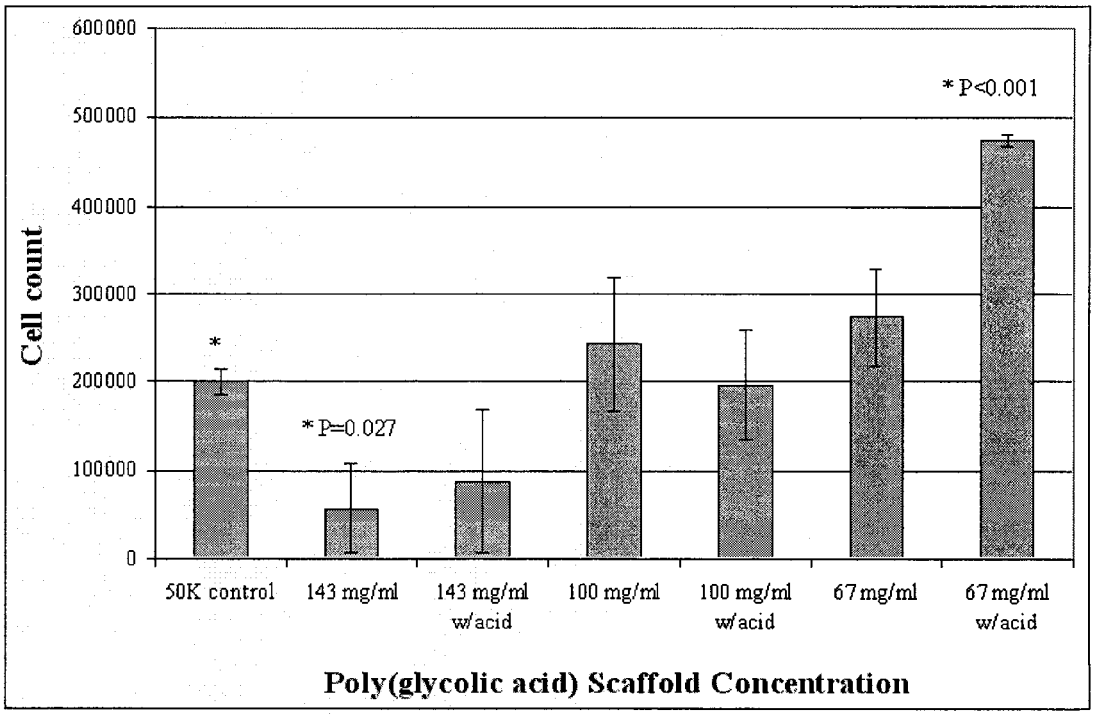

Figure 36. Bar graph depicting the 96 hour cell proliferation assay in terms of total cell count (based on standard curve) for each scaffold condition as well as the control sample. Significance was shown with respect to 50K control. For all possible two-way comparisons, refer to table 1. Note: Two of the three acid treated samples at a concentration of 67 mg/ml saturated the detector; the actual cell count may be higher than expressed.

The first is that proliferation increases as fiber size decreases. The second trend is that acid pretreatment within the smallest fiber group (0.22 microns at 67 mg/ml PGA concentration) significantly increased proliferation (p=0.007). Statistical differences (P values) for all pairwise comparisons can be seen in Table 2.

P values for statistical differences from pairwise comparisons (criteria alpha = 0.05 and P<0.05)								
67 acid	-	<0.001	0.002	<0.001	<0.001	<0.001	<0.001	<0.001
67 no acid	0.007	-	none	none	0.013	0.003	none	0.001
100 acid	<0.001	none	-	none	none	none	none	0.027
100 no acid	0.002	none	none	-	0.048	0.013	none	0.004
143 acid	<0.001	0.013	none	0.048	-	none	none	none
143 no acid	<0.001	0.003	none	0.013	none	-	0.027	none
50k control	<0.001	none	none	none	none	0.027	-	0.008
50k standard	<0.001	0.001	0.027	0.004	none	none	0.008	-
	67 acid	67 no acid	100 acid	100 no acid	143 acid	143 no acid	50k control	50k standard

Table 2. Table of P values from pairwise comparisons of the absorbance values recorded from the cell proliferation assay.

If the comparison failed the original criteria ($\alpha = 0.05$ and $P<0.05$) the word "none" is reported in the table. The 67 mg/ml acid pretreated sample was the only sample significantly higher than the 50,000 cell control ($P<0.001$) and the 143 mg/ml sample without acid pretreatment was the only sample significantly lower than the 50,000 cell control ($P=0.027$). This further supports the hypothesis that acid pretreatment of small diameter electrospun PGA fibers does have a beneficial cellular response *in vitro* over the 96 hour duration of this test.

Host response

The goal of the implantation study was to determine if the knowledge gained in the *in vitro* cellular proliferation assay could be extrapolated into a small animal model. After the implantation; redness, swelling and animal locomotion were evaluated at days one, two and four based on a subjective 0-5 scale rating where zero would correspond no redness, swelling or limits to locomotion, three would be noticeable from outside the cage and slightly impairing the animal and a five would be extreme redness and swelling

and cause an inability of the animal to use the limb. All animals had zero scores with no unusual redness or swelling by day four and were ambulating normally after day 2 (scores below 3). Upon excision of the scaffolds, the injury sites were evaluated for inflammation and degree of tissue ingrowth. The most pronounced inflammation was seen in the 143 mg/ml sample without acid pretreatment. This scaffold delaminated from the surrounding muscle tissue at recovery. At the other extreme, the 67 mg/ml sample looked well integrated into the surrounding tissue and was only identifiable at gross inspection by the sutures placed near the end of the scaffold. These sutures were for identification only and provided no anchoring to the surrounding tissue. The transmission electron micrographs presented in Figure 4 illustrate the 143 mg/ml sample without acid pretreatment, the 100 mg/ml sample without acid pretreatment and the 67 mg/ml sample with acid pretreatment.

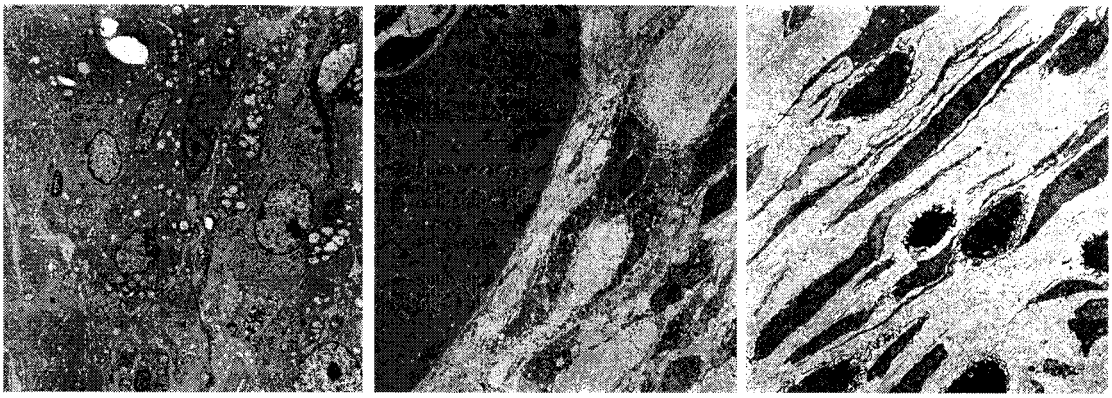

Figure 37. TEM micrographs of the scaffolds after one week implantation. Micrographs, left to right, are from 67 mg/ml PGA in HFP (no capsule seen – cells throughout entire cross-section), 100 mg/ml PGA in HFP (smaller capsule at border with native muscle), and 143mg/ml PGA in HFP (note large fibrotic capsule in white).

Observationally the first micrograph (Figure 37, left) is from the wall midsection of the 67 mg/ml acid pretreated sample, again the tube was collapsed but no clear demarcation was evident from one wall to the other. These scaffolds were densely populated with cells from the surrounding tissue. These cells exhibited active golgi and intermingled with well ordered thin collagen fibrils (banded fibers evident between cells). The vacuoles evident in this image reflect lysed mitochondria that were damaged as a result of poor penetration of the fixative, the density of this tissue appeared to impede fixation. The 100 mg/ml sample (Figure 37, center) did not appear to be as densely populated as the 67 mg sample; however, the cells were intercalated within fibrils of the electrospun matrix. A clear band of collagen fibers was visible between the native muscle on the left and the scaffold on the right, indicating a degree of fibrosis. The lumen of the collapsed cylinder exhibited a low density of cells that resembled adiposites. The 143 mg/ml sample (Figure 37, right) exemplifies the fibrous capsule formation that is commonly seen surrounding PGA implants. There was a low density of fibroblasts in the scaffold with excessive deposits of collagen (seen in white) and no cells within the lumen of the tube. Trichrome staining also confirms the presence of abundant collagen production within all the scaffolds again with collagen capsules associated with the higher electrospinning solution concentrations. Also, the presence of multinucleated immune cells decreased with decreasing fiber diameter or acid pretreatment from 1-2 cells per field at 100 times magnification for the 143 mg/ml concentration of PGA without acid pretreatment to none detected in six cross-sections of the 67 mg/ml concentration of PGA with acid pretreatment.

Discussion

The previously described (18) linear relationship between PGA electrospinning solution concentration and fiber diameter was reproduced in this study. The ability to produce fibers that are more than an order of magnitude smaller than any traditional fiber forming process remains as one of the most significant advantages to electrospinning for tissue engineering. We also observed that pore area did not vary as linearly as fiber diameter; the underlying reasons for this result remain to be explained. Pore area may turn out to have combined dependence on solution concentration (fiber diameter) and mandrel motion. Our current electrospinning apparatus does not allow for precise rotation and translation speed control that would be necessary to test this interdependence. These two controls are currently being implemented in a new electrospinning apparatus. Upon completion, the control of pore area will be addressed to further enhance the biomimicking capability of electrospun scaffolds.

Two other parameters become readily apparent when looking at the characterization data. The first parameter is the large void volume within the scaffold (greater than 80%). This open area provides potential space for cell infiltration while providing three-dimensional support for the cells. The other consideration is the significant surface area within the volume of the scaffold. These two parameters, together with the small fiber size, may help explain the improvement in biocompatibility seen in this study. As previously hypothesized, small fibers elicit a diminished immune response as compared to larger fibers possibly through the sensing of membrane curvature (95, 97). As cells attach to multiple thin fibers, membrane curvature may

enhance signal transduction. Since there is no native cell binding site on PGA, cell adhesion appears to be regulated by relatively non-specific cell-fiber interactions that are facilitated by the acid pretreatment.

The surface hydrolysis of ester bonds, exposing carboxylic acid and alcohol groups (17), resulting from the acid pretreatment (seen schematically in Figure 38) may improve vitronectin binding thus improving the ability of cells to adhere to the surface.

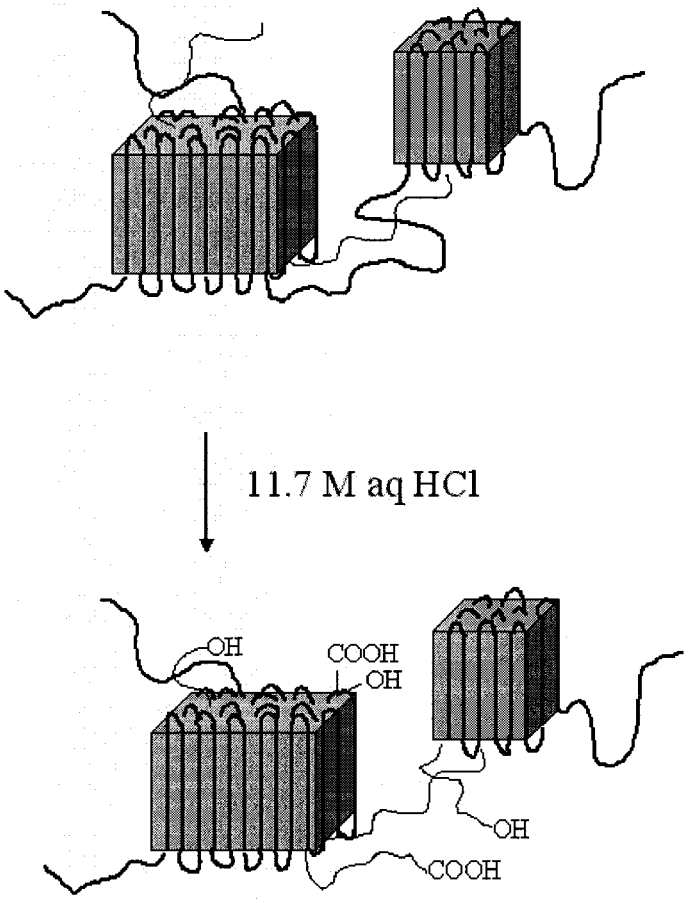

Figure 38. Diagrammatic representation of PGA hydrolysis due to pretreatment with 11.7 Molar aqueous hydrochloric acid. The hydrolysis of the ester bonds expose carboxylic acid and alcohol groups on the surface of the fibers.

The concept of hydrolyzing ester bonds to improve cell adhesion is not new. Gao et al. used 1M sodium hydroxide (NaOH) to hydrolyze PGA scaffolds and expose carboxylic acid and hydroxyl groups. These results demonstrated a linear decrease in fiber diameter with exposure time and an increase in cell seeding densities as a function of both hydrolysis and serum exposure (47). Due to the submicron starting diameters in this study, HCl was chosen to hydrolyze the surface since it produces no significant reduction in fiber diameter. We suspect that HCl, like NaOH, produced no changes in the bulk polymer properties (47). One result of surface hydrolysis is an anticipated increase in wettability. Nikolovski et al. have shown that vitronectin in serum rich media preferentially binds to PGA as a function of hydrophilicity (86). Further work by Webster et al. have shown surface roughness also plays a role in vitronectin binding (116). It could be speculated from this work and others (109) that surface hydrolysis of polymers may cause topology changes on the same scale as a 15 nanometer vitronectin molecule that are critical to its binding and subsequent cell adhesion (109, 116). Further detailed testing would be necessary to illicit the complete effect of acid pretreatment. Methods described by Webster (116) and Thapa (109) including electron spectroscopy for chemical analysis (ESCA), atomic force microscopy (AFM) and a modified surface-enhanced Raman scattering technique (SERS) could be incorporated into future work to more accurately determine the mechanism of binding as well as protein quantity and identity on the surface after exposure to serum.

Another possible explanation to the improved *in vivo* response could be a reduction in the localized pH decrease typically seen in the extracellular space at the

onset of PGA hydrolysis. It is often that this local acidosis is blamed for the poor tissue incorporation of PGA. *In vivo* degradation of PGA begins at the surface of the polymer in amorphous regions (17). It could be speculated that the acid pretreatment attacks the same amorphous regions thus releasing the initial burst of PGA monomers and oligomers prior to implantation. This theory could be tested in the future by evaluating crystallinity using differential scanning calorimetry before and after acid pretreatment.

It is often cited that cells will not migrate through holes below 10 μm in diameter (78.6 μm^2 area), yet the histology and TEM images from this study show clear cellular penetration within the one week implantation. This could be due to the absolute unique nature of the process. Since the fibers are collected as a dry, non-woven mat, cells may be able to push individual fibers from their path during migration. Even though the samples are hydrated prior to implantation, no crosslinking agents are used that would bind the fiber network and restrict mobility. This could reconcile the apparent contradiction seen in our laboratory with previously published results that dealt with rigid structures at the cellular level (82). Further work is needed to support this idea, although observationally, it appears to be correct.

Acknowledgements

The authors would like to thank the Whitaker Foundation (RG-98-0465) for the support of this research, as well as Alkermes, Inc. for the donation of the PGA used in this study. We would also like to thank Ms. Judy Williamson for her assistance obtaining the SEM and TEM micrographs.

Chapter 7 Review of Electrospinning in Tissue Engineering

The term "Tissue Engineering" was coined at a National Science Foundation sponsored meeting in 1987 and later defined as "the application of principles and methods of engineering and life sciences toward fundamental understanding of structure-function relationships in normal and pathological function". The central theme is a structure – function relationship that leads to the importance of understanding the native extracellular matrix (ECM) (85). In most tissues and organs, the ECM plays an important role in controlling cell behavior. The ECM is composed of structural, elastic and sequestering proteins and glycosaminoglycans that exhibit physical and chemical crosslinking to retain their shape. All of these structures are in the nanometer size range. Although the individual structures are significantly smaller than the cells, the ECM organizes cells in space. In addition, the ECM provides cells with environmental signals to direct specific cellular regulation and provides boundaries that separate one tissue space from another (58). The idea that such small structures can influence cellular function is not new. Researchers as early as 1960s claimed that nanometer sized features could influence cell behavior (94). More recently, it was reported that cells attach and organize around fibers with diameters smaller than the diameter of the cells through transmembrane and surface receptors on the cell (61).

Biomimetics and Effects of Fiber Size

Ideally, a synthetic ECM should mimic the structural and functional profile of the materials found in the native ECM. This is critical in order to mimic cell-cell and cell-matrix interactions and the expression of normal cellular phenotype. With the rapid developments in the field of bionanotechnology, the ability to produce synthetic nanofiber scaffolds has captured the interest of many researchers in the field of tissue engineering. The potential of applying nanofiber technology to solve tissue engineering challenges is revolutionary. Not only can nanofiber scaffolds mimic the nano-sized dimension of natural ECM, but they can also form a defined architecture to guide cell growth and development as needed. The ''contact guidance'' theory of cell-substrate interaction illustrates that a cell has the maximum probability of migrating in preferred directions which are associated with chemical, structural and/or mechanical properties of the substrate (36). Dunn reported that the arrangement of cells in controlled two- and three-dimensional architecture had beneficial effects on cell differentiation, proliferation and functional longevity (36).

The idea of using nanofiber scaffolds has not been met with the initial optimism one would expect. Many implantable biomaterials have been subjected to chronic inflammation and fibrous encapsulation if they possessed small pores. In fact, there has been considerable research showing that vascular grafts, for example, need pores greater than 30 μm to ensure incorporation into the surrounding tissues (82). Other cell types have been shown to behave in similar manners although the exact value of the pore size varies. Davila, in the late 1960's, suggested that fiber dimension may play as important a

role in tissue response as pore size (30). He went on to develop a scissoring model for fiber-cell interactions whereby cells trapped in acute angles between rigid fibers would be pinched with micro-motion of the implant. Since the relative stiffness of large filaments would be significantly higher than cell membranes, cells would be unable to resist this motion. He showed a strong correlation between inflammatory tissue responses and the ratio of porosity to the fiber diameter. These chronic effects may have lead to the unfavorable response of large fiber – small pore implants. It is important to note that this work was conducted on fibrous materials where the fiber diameters ranged from 39 to 161 μm. Even a small fiber in this study is many times larger and presumably stiffer than fibers produced by electrospinning. To date, the most controlled testing of tissue response to fiber diameter has been conducted by Sanders (97). In that study, polypropylene fibers between 2 and 27 μm were produced in the laboratory through rapid drawing of molten material. Fibers were grouped into four ranges: 2.1 – 5.9 μm, 6.5-10.6 μm, 11.1 – 15.8 μm, and 16.7 – 26.7 μm (97). Individual fibers from the four groups were randomly fixed onto polycarbonate frames with spacing between the fibers adequate to prevent interactions between adjacent fibers (previously determined experimentally). These frames were then implanted subcutaneously in adult Sprague – Dawley rats (400 gram) for 5 weeks to access fiber induced responses. Two important findings came from this study. First, small diameter fibers produced significantly lower immune responses (as determined by the number of activated macrophages) and thinner capsules. Secondly, all fibers, regardless of diameter, that were within 13 μm of blood vessels had smaller capsule formations (97).

The reduction in inflammation appeared to be more of a threshold mediated response than a graded response. No correlation was found between capsule thickness and fiber size that would indicate a gradual improvement. Because of the controls put in place, it was believed that surface curvature was the controlling parameter (97). It has previously been shown by Rovensky and others that many internal cellular functions are affected by membrane curvature either through up-regulation of focal adhesion related processes or directly through tension sensing (95, 97). Although this work was based on single fibers, it would be reasonable to expand this line of reasoning to cover fibrous mats comprised of loose nanofibers.

Since the application of electrospinning to tissue engineering is a relatively recent endeavor, many research groups have only begun to experiment with electrospinning synthetic polymers. While the focus of our tissue engineering research group has been both natural and synthetic polymers (14-16, 18, 20, 21, 76, 77, 118), this review will focus other tissue engineering research attempts that utilize electrospinning to produce scaffolds.

Cell Culture and Tissue Specific Applications

The first step in assessing the suitability of electrospun mats for tissue engineering scaffolds is cell culture. In one such study, Bhattarai introduced a novel electrospun biodegradable block copolymer for evaluation as a tissue engineering scaffold. This block copolymer (polydioxanone – poly(L-lactic acid) – poly(ethylene glycol)) was found to be a better biodegradable matrix than previously studied copolymers of poly(L-

lactic acid) (PLLA) and poly(ethylene glycol) (PEG) due to the random exchange of polydioxanone (PDS) segments for PLLA segments (10). They have investigated the effects of some control parameters on the electrospinning of the copolymer and found that a 20 weight percent solution of PDS:PLLA:PEG (20:70:10 ratio) electrospun from a 25:75 blend of dichloromethane and dimethylformamide produced uniform fibers with an average diameter of 350 nm (10). The nonwoven fibrous scaffolds were collected on a rotating mandrel. The target application for this electrospun scaffold was a tissue-engineering matrix. To explore this application, electrospun scaffolds were examined by scanning electron microscope (SEM), by uniaxial mechanical testing, by mercury porosimetry to determine their porosity and pore volume, and by cell culture with fibroblasts to determine cell proliferation, morphology, and cell–scaffold interaction after seeding.

Pore diameter distribution, total pore volume, pore area, and porosity of the electrospun scaffolds were measured by the AutoPore IV 9500 V1.05 mercury porosimeter (Micrometritis Instrument Co., Nacross, GA). This analysis demonstrated the porosity of the electrospun copolymer scaffold was greater than 80%. The median pore size was 8 μm, and the total pore area was 5 m^2/g. Although the largest pores measured were up to 200 μm, majority of the pores were less than 10 μm (10).

The electrospun copolymer scaffolds showed the maximum breaking strength of 1.4 MPa in the direction of mandrel rotation and 1.3 MPa perpendicular to the direction of rotation. In both cases, the elongation was 15–20% (10). Past experience with

electrospinning on a revolving mandrel would indicate that the rotational velocity was insufficient to induce a significant degree of alignment (18).

To assess cell proliferation, morphology, and cell–scaffold interaction; 2.6 cm rectangular samples of 200–350 μm thick electrospun scaffolds were sterilized by ethylene oxide gas for 2 hours. Fibroblast cells (1 x 10^5 cells) were seeded onto the surface of the scaffolds and grown in the RPMI-1640 medium with 10% Fetal Bovine Serum. In this study Bhattaria found that cells seeded on the nanofibrous scaffold had appropriate interactions with their environment based on the following observation. First, the cells maintained a normal phenotypic shape, suggesting that cells function biologically within this structure. Second, the adherent cells demonstrated significant proliferation during the study and the surface of the scaffold was completely covered by day five. Third, visual evidence that the cells physically cross-link the nanofiber scaffolds by branching or attaching to multiple fibers to form a multi-fiber cellular network (10). These observations indicated that the nanofibrous scaffolds of the copolymer positively promote cell–matrix interactions; however, the lack of cellular penetration was of some concern.

Cell interaction studies have also been performed with other cell types including bone marrow derived cells. Jin previously reported the capability to electrospin scaffolds from aqueous silkworm silk (Bombyx mori) solutions with poly(ethylene oxide) PEO (65). Fiber sizes ranged from 500 nm to 1 μm which are about 40 times smaller than degummed native silk fibroin. The purpose of his most recent study was to investigate

stromal cell responses on these fibers to determine the potential utility of this novel silk fibroin protein matrix as a tissue engineering scaffold.

Electrospun non-woven mats from silk/PEO blends were immersed into a 90/10 (v/v) methanol/water solution for 10 min to induce an amorphous to β-sheet conformational transition in the silk protein. After this treatment, the mats were washed with water for 48 h at 37°C to remove the PEO. Two groups of electrospun mats were studied for cell interactions. In one group, the PEO was washed out prior to testing and in the other group, the Silk/PEO blend was treated with methanol and rinsed but the PEO was not extracted. The electrospun fibers appeared to be randomly distributed in all the scaffolds. Even after PEO extraction, surface morphology was maintained and the scaffolds were found to be composed of fine uniform fibers with 700 ± 50 nm average fiber diameters (64).

After methanol treatment of electrospun mats, the modulus of elasticity, tensile strength and elongation values were 624.9 ± 0.9 MPa, 13.6 ± 1.4 MPa and 4.0 ± 2.0%, respectively (64). The β-sheet structure formation of electrospun silk fibroin during methanol treatment was evident by increased elastic modulus and strength and decreased elongation in the mat as compared to a mat before methanol treatment. PEO extraction decreased all mechanical properties due to the brittleness previously shown in regenerated silk fibroin films. Mechanically, the addition of PEO was effective in improving the properties of these electrospun mats. Even with decreased elongation, the mats were significantly tougher before PEO extraction than after extraction. Overall, this

empirical evidence supports the ability of these materials to be used as scaffolds for tissue engineering.

Jin proceeded with cellular interaction studies utilizing bone marrow stromal cells (BMSCs). Briefly, human unprocessed whole bone marrow aspirates were obtained from 25 year old donors (Clonetic-Poietics, Walkersville, MD), resuspended in Dulbecco's Modified Eagle Medium (DMEM) supplement with 10% Fetal Bovine Serum (FBS), 0.1 mM nonessential amino acids, 100 U/ml penicillin and 100 mg/l streptomycin, and 1 ng/ml basic fibroblast growth factor and plated at 8 ml aspirate/cm^2 in tissue culture polystyrene. Non-adherent hematopoietic cells were removed with the culture medium during medium exchange after 4 days. Matrices with and without PEO were seeded with cells (25,000 cells/cm^2) by pipetting the cell suspension directly onto the matrices then culturing under standard static conditions (64).

Cell numbers, as determined by treating the scaffolds with trypsin and counting the released cells using a hemocytometer, were significantly increased at day 7 when compared with day 1. Cell numbers on PEO extracted mats were significantly higher, approximately 88%, then on the non-extracted silk mats. Even though PEO supplied good mechanical properties to the electrospun mats, initially, the presence of PEO inhibited cell adhesion and proliferation. However, within 3–4 days in culture, the PEO was extracted and proliferation appeared to accelerate. Nearly the entire surface of both the PEO extracted and nonextracted mats were densely populated with BMSCs after 7 days of cultivation. After 14 days of incubation, the electrospun silk mats supported extensive BMSC proliferation and complete matrix coverage. Overall, Jin concluded that

the ability of electrospun silk matrices to support BMSC attachment, spreading and growth *in vitro*, combined with a biocompatibility and biodegradable properties of the silk protein matrix, suggested that these biomaterial matrices could be used as scaffolds for tissue engineering (64, 81, 120).

Many researchers have moved beyond these preliminary cell–matrix interaction studies to evaluate tissue-like structures produced *in vitro* from electrospun matrices. One such tissue of interest is the small diameter vascular graft since clinical outcome of other synthetic materials is often unacceptable (51). Researchers at the National University of Singapore are experimenting electrospinning a copolymer of 75% PLLA and 25% PCL to produce scaffolds with fibers of 550 ± 120 nm (81, 120). To evaluate the suitability of the copolymer, scaffolds were prepared for seeding with smooth muscle cells (SMC) and endothelial cells (EC) (81). Scaffolds were prepared either as randomly deposited mats (81) or highly aligned mats (120). For the random scaffolds, human ECs and SMCs were seeded independently (cultures expanded separately) onto sterilized scaffolds that were prewetted in ethanol for two days then immersed in DMEM containing 10% FBS (81). The sterilization technique was not specified. After 1 and 7 days, scaffolds were harvested and EC phenotype was studied by immunohistology and laser scanning confocal microscopy. Antibodies again EC surface marker CD-31 were used for identification and cell count (SMCs do not express CD-31) (81). By day 7, all cell counts were significantly higher (with and without CD-31 marker) then day 1. Also, a new matrix, presumably created by the cells on the scaffold was visible. Again, it should be noted that no specific testing was done to determine the makeup of the new

matrix. At the completion of the experiment, the cells almost reached confluence on the surface of the scaffold with spreading more pronounced with SMCs (81). With aligned fibers, the focus was shifted to SMC orientation and cellular interaction (120). Phase contrast microscopy images revealed SMC's began to adhere to the aligned scaffold within the first hour and spread in exactly the direction of the fibers. By 5 hours, most of the SMCs had attached and extended themselves along the aligned fibers to develop a spindle-shaped appearance. This shape is characteristic of the native bipolar spindle shape indicative of the contractile phenotype. After 3 days, the cells reached 50% confluence on the surface and no longer had perfect alignment along the fibers. In SEM micrographs, short and thin fibrous structures perpendicular to the cell body attached to the nearest fiber forming a ''bridge'' between the cell body and adjacent nanofibers. Cell – cell junctions were not reported. The dimension of the bridge structures were between 0.5–2 μm. The authors indicated that these results were similar in dimension and appearance to focal contacts reported previously reported in the literature (120). Further research is needed to determine the exact nature of the cell-matrix adhesions between the SMCs and the aligned nanofibers and to determine the role and composition of the bridging structures and to determine if they are functional focal contacts. They were, however, similar to the dimension of focal contacts reported in previous studies. Again, it needs to be noted that these scaffolds did not promote cellular ingrowth. Numerous other researchers have seen the same level of success with electrospun materials (15, 18, 20, 80, 106, 124).

The use of electrospun scaffolds in tissue engineering applications is still in its infancy. Our laboratory, like many others, are just now testing cellular compatibility and cell growth dynamics on these nano to micro-scale fibrous materials. The most advanced work reported in the literature is a contractile cardiac graft developed by Shin, et al (99). Polycaprolactone was electrospun from a 10 wt% solution of equal parts chloroform and methanol to produce typical fiber diameters from 100 nm to 5 μm. The average fiber diameter in this study was 250 nm with occasional outliers of up to 10 μm (99). SEM analysis of the scaffolds revealed that some of the fibers were fused at intersections and form physical crosslinks. Generally, the mesh had an interconnected, open structure with pore sizes well above that of the fiber diameters. The non-woven fibrous meshes were collected on nickel-chrome wire rings. During cell culture, these rings would act as passive stretching devices to condition and mature the cardiac myocytes. After electrospinning, the scaffolds were stored in desiccators for several days to allow ample time for solvent outgassing. For sanitization, the scaffolds were placed in 70% ethanol overnight. Following the alcohol treatment, the scaffolds were coated with a purified type 1 collagen solution (Cohesion Technologies, Palo Alto, CA) prior to cell seeding to promote binding. To assess the scaffold's potential as a cardiac graft, neonatal rat cardiomyocytes were seeded on the PCL meshes. After two weeks of *in vitro* culture, the grafts were characterized using immunohistology and SEM (99).

Immunohistochemical staining for tropomyosin was used to assess the fraction of cardiac myocytes in the grafts and verify that the grafts were not overgrown with fibroblasts. Staining against Cardiac troponin I and connexin 43 was used to verify

cardiac myocyte phenotype and the presence of gap junctions. Muscle specific cardiac actin was organized into numerous myofibrils. Cross-striations were also visible throughout the graft. The cardiac myocytes did stain positively for tropomyosin and showed spindle, round, and multiangular morphologies with striations that are indicative of the sarcomeric structures of muscle cells. The cardiac myocytes also stain positively for cardiac troponin-I and diffuse gap junctions were observed. Overall, a high density of cardiac myocytes were observed throughout the entire graft (99).

Both SEM and immunohistochemical analysis revealed that the surface of the graft was confluent with multiple cell layers but, unlike other studies reported here, cells were found throughout the graft. The cell density was lower in the midsection. It was believed that the elastic nature of the PCL and the support given by the ring provided sufficient stability and resistance for the cardiac myocytes and this resistance allowed the cells to mature and spontaneously contract from day 3 to the termination of the experiment on day 14 (99). While an individual 10 μm graft would not provide clinically significant support for a ventricular defect which is often over 1 cm thick, additional research into stacking grafts is underway and may provide insight into designing thicker patches. One item not discussed in this work was the random nature of the starting scaffold. Since the ring did provide passive tension, contraction could be coordinated in a grossly radial direction. The interrelationship between direction of tension and fiber orientation must be addressed in future designs to provide cues necessary to direct the expression of the correct cardiac phenotype.

Although electrospinning would seem well suited to produce these fibrous mats to serve as tissue engineering scaffolds, some would argue against the technique. Ma and Smith contend that the process is too difficult to control and produces fibers of unacceptable variations in diameter (73, 102). They claim that electrospun fibers can be produced only at the very upper limit of native ECM fiber diameters (50 – 500 nm) and quite often exist in the micron size range rather than the nanofiber range. Additionally, they site the inability to control fiber deposition and design three dimensional pore structures as reasons to choose a competing technology such as phase separation (73, 102). The additional electrospinning control capabilities described in the following sections will address many of these concerns. While the process of electrospinning may not be perfect, there is considerable evidence indicating that tissues can be successfully engineered utilizing this methodology.

Chapter 8 Novel Electrospinning Apparatus: Preliminary Details

This manuscript has been submitted to the Association for the Advancement of Medical Instrumentation's journal titled Biomedical Instrumentation and Technology as part of a young investigator competition in 2003 that was won by the author. This manuscript outlines the preliminary research involved in designing the next generation electrospinning apparatus.

AUTOMATED ELECTROSTATIC PROCESSING DEVICE FOR TISSUE ENGINEERING APPLICATIONS

Eugene D. Boland

Department of Biomedical Engineering
Virginia Commonwealth University
P.O. Box 980694

Richmond, VA 23298-0694

Abstract

The specific aim of this project is to develop an automated electrostatic processing apparatus that is capable of controlling the three-dimensional architecture of a tissue engineering scaffold. Electrostatic processing, or electrospinning, is based upon simple concepts of charge separation. A charged polymer solution (or melt) is fed through a small opening or nozzle (usually a needle or pipette tip), and because of its charge, the solution is drawn towards a grounded collecting plate (usually a metal screen, plate, or rotating mandrel) as a jet. During the jet's travel, the solvent gradually evaporates, and the polymer fiber is formed (50 nanometer to 10 micron) and deposited on the plate. The proof of concept of using this technique has been well documented and can be adapted to produce tissue engineering scaffolds.

The apparatus described in this application incorporates multi-axis controls that will allow for repeatable fabric densities and fiber alignment. Fiber alignment and scaffold density are controlled by rotating a mandrel (at a precise speed) along one axis, translation along that same axis, and rotation around the second axis perpendicular to the electrospun fiber stream. This control is accomplished with a PC based "supervisory" control program written in the LabVIEW® programming language. Scaffold thickness and fiber diameters are determined by the syringe metering pump flow rate, material being electrospun and solution concentrations.

Through extensive laboratory analysis (mechanical testing and both optical and electron microscopy), parameters such as fiber orientation, diameter and mechanics will be predictive from specific polymer setups. Our laboratory has also demonstrated the ability to electrospin natural polymers such as collagen, elastin, and fibrinogen, with or without the addition bioresorbable polymers. This will allow us to tailor scaffolds to meet specific tissue engineering needs by creating a truly biomimicking synthetic extracellular matrix.

Introduction

Tissue engineering is an interdisciplinary field that blends classical engineering and the life sciences. The field by name is still in its infancy, yet the basic principles are as old as interventional surgery. The desire to restore, maintain or improve tissue function remains the end goal but a new set of tools and techniques are emerging. The study of structure – function relationships in both normal and pathological tissues has been coupled with the development of biologically active substitutes or engineered materials (8). The focus of this manuscript will be a tissue engineering approach designed to create scaffolding that is capable of mimicking native tissue. The target structures are those of the extra-cellular matrix (ECM). Ideally, the synthetic scaffold should mimic the structural and functional profile of the materials found in the native ECM. This is critical in order to mimic cell-matrix interactions and the expression of normal cellular phenotype.

Synthetic ECMs or scaffolds must be designed to conform to a specific set of requirements. The first requirement is that the material must be biocompatible and function without interrupting other physiological processes. This functionality includes an ability to promote normal cell growth and differentiation while maintaining three-dimensional orientation/space for the cells. Secondly, the scaffold should not promote or initiate any adverse tissue reaction (51). In addition, for clinical and commercial success, scaffold production should be simple yet versatile enough to produce a wide array of configurations to accommodate the size, shape, strength and other intricacies of the target tissue (51, 54, 55, 82, 105, 113). Once implemented, *in vitro* or *in vivo*, the material

should either be removed though degradation and absorption or incorporated though native remodeling mechanisms leaving only native tissue. Beyond these generalized requirements, the interactions of single native cells with its immediate surroundings must also be analyzed. Cells are neither autonomous entities kept in proximity to each other by the ECM nor do cells "communicate" only with other cells. Cells and the ECM have a three-dimensional interrelationship that is kept in balance and influenced by both internal and external stimuli. This model requires that any scaffold material must be able to interact with cells in three dimensions and facilitate this communication. The goal is to create a synthetic ECM that will duplicate all the essential intercellular reactions and promote native intracellular responses. In the native tissues, the structural ECM proteins are 1 to 2 orders of magnitude smaller that the cell itself, thus, allowing the cell to be in direct contact with many fibers defining its three dimensional orientation (87). This property may be a crucial factor in determining the success or failure of a tissue-engineering scaffold.

We believe that electrospinning represents an advantageous processing method to meet both the general material requirements as well as the potential size issues raised above. In this manuscript, we will first discuss a brief history of the technique, and follow that with a simple electrospinning process that can and has been performed in the laboratory. Once the process is established, we will focus on the work done in our laboratories to improve this process and establish processing parameters for a variety of commercially available bioresorbable polymers to create a wide variety scaffolds for tissue engineering.

Brief History of Electrospinning

Electrospinning traces its roots to electrostatic spraying, which was first described by Lord Rayleigh more than 100 years ago. He theorized, and later determined through experiments, that if a sufficiently large electrical charge can be applied to a droplet at the tip of a nozzle, it would overcome surface tension and be ejected in a stream (13, 91). The droplets formed by injecting charge into a liquid, typically to 5-30 kV, from an electrode. The charged liquid is attracted to a second electrode of opposite polarity some distance away. Droplets are dispersed from the cone tip when electrostatic repulsions within the liquid exceed its surface tension.

Many years later, Taylor studied and explained the events that occur at the nozzle as the electric field deformed the fluid and formed a stream (33, 91). The initial charge injection causes the droplet at the nozzle to form a hemispherical surface. As the electric charge is increased, the surface undergoes a shape change from hemispherical to spherical and eventually to conical. These changes are due to the balancing of the increasing solution charge with its surface tension, and the final conical shape is known as the Taylor cone (35). Countless experiments since have shown that when the liquid possesses any conductivity the stable cone configuration described by Taylor becomes a cone with a thin column or jet of liquid emerging from the tip. Even so, such "cone-jet" configurations are commonly referred to as "Taylor cones" even though Taylor did not predict the formation of these jets. If the concentration of the polymer in the charged solution is sufficiently high to cause chain entanglement, a fiber rather than a droplet is drawn from the tip of the Taylor cone (Figure 39). Such is the case for electrospinning.

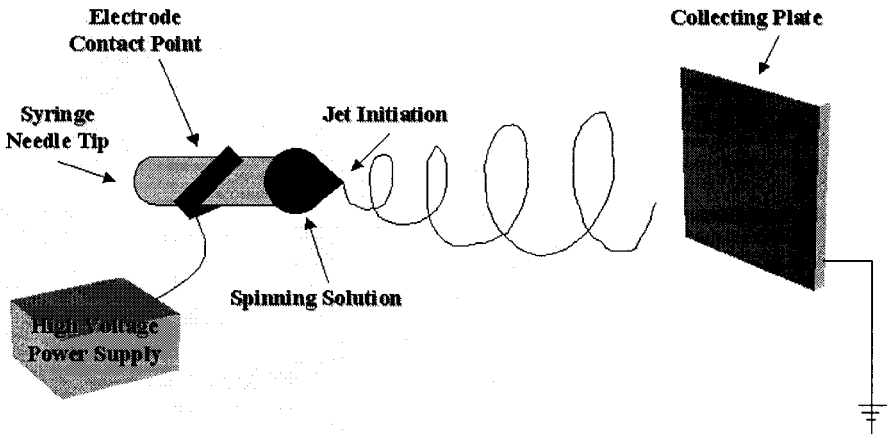

Figure 39. A schematic of an electrospinning device illustrating the "cone-jet" phenomenon.

The first patent (U.S. Patent 1,975,504) in electrospinning was granted to Formhals in 1934 for a process that produced fine fibers from a cellulose acetate solution (41). He was later granted related patents (U.S. Patents 2,116,942; 2,160,962; and 2,187,306) in 1938, 1939, and 1940. This work focused on electrospinning as a method of making artificial thread for textile mass production.

Recent Research in Electrospinning

In the last 10 to 15 years, there has been a resurgence of interest in the electrospinning process. Srinivasan and Reneker dissolved Kevlar® (poly (p-phenylene terephthalamide)) in sulfuric acid and were able to obtain fibers with diameters of 1.3 μm that exhibited some crystallization properties similar to that of commercial Kevlar® fibers spun from the liquid crystalline state (104). For these experiments, the fibers were collected in a grounded water bath, which allowed for removal of residual acid. This

group was also able to produce carbon nanofibers with diameters from 100-500 nm by electrospinning a polyacrylonitrile solution containing molten mesophase pitch (29, 40).

Doshi and Reneker demonstrated the electrospinning of poly (ethylene oxide) (PEO) in water to obtain fibers with diameters in the range of 0.5-5.0 μm (91). Other groups have also succeeded in electrospinning fibers from PEO and biodegradable materials such as Poly (lactic acid) (PLA) (32, 33). Bognitzki formed PLA fibers with an average diameter of one micron from a solution containing tetraethyl benzylammonium chloride (TEBAC). TEBAC, which is an organosoluble salt, facilitated a decrease in fiber diameter by decreasing solution surface tension and increasing electrical conductivity (13).

Until recently, few researchers have critically analyzed the electrospinning process variables. Deitzel et al. have detailed the effects of solution concentration and spinning voltage on fiber morphology (33). Gibson et al. have studied transport properties of the fibers and fiber mats (33, 48, 49) and Reneker et al. have recently detailed a mathematical model describing the travel of the fiber jet (92).

From these bodies of work, we know that diameter, morphology, and orientation of the resultant fibers are a function of the many variables involved. The properties of the solution, including its molecular weight, chemistry and nature can greatly alter the ability to electrospin a polymer. The ratio of polymer to specific solvents can vary the diameters of the fibers produced by effecting viscosity, surface tension and conductivity. Voltage appears to play a role in determining fiber uniformity through jet stability. Ideally, the fibers should be dry when collected to prevent fusing or the appearance of

"solvent welded" beads where fibers cross. The higher the polymer concentrations with respect to solvent volumes, the drier the fiber produced (33, 34). Solution infusion rates into the system and distances between the initiation tip and collecting plate also affect fiber dryness (13, 33, 34). However, the principal variable in fiber dryness is solvent volatility. Solvent volatility computations must account for the temperature, environmental conditions, and distance to maximize fiber dryness and, therefore, minimize the formation of bead defects (35).

Automated Apparatus for Electrospinning

Much of the previous work was accomplished using an electrospinning device much like the prototype device in our laboratory. This process involves drawing the electrospinning solution into a plastic syringe and placing it in a syringe pump for metered dispensing. The positive output lead of a high voltage supply (Spellman CZE1000R; Spellman High Voltage Electronics Corp.), set to 15-25 kV, is attached to a blunt 18-gauge needle on the syringe. A grounded target (1" x 4" x 1/8" 303 Stainless Steel) is placed 4-12 inches from the needle tip to collect the fibers. This grounded target may be stationary or rotating. The target can also translate back and forth in front of the needle to uniformly coat a larger target. These simple motions can be used to create non-woven fibrous mats that can be used as tissue engineering scaffolds in our laboratory. This can produce randomly aligned fibers by holding the target stationary or marginally aligned fibers (depending on rotational speed) but only in the direction of rotation. This

method has limited repeatability and scalability. Figure 40 depicts scanning electron micrographs (SEMs) of random and aligned scaffolds using this system.

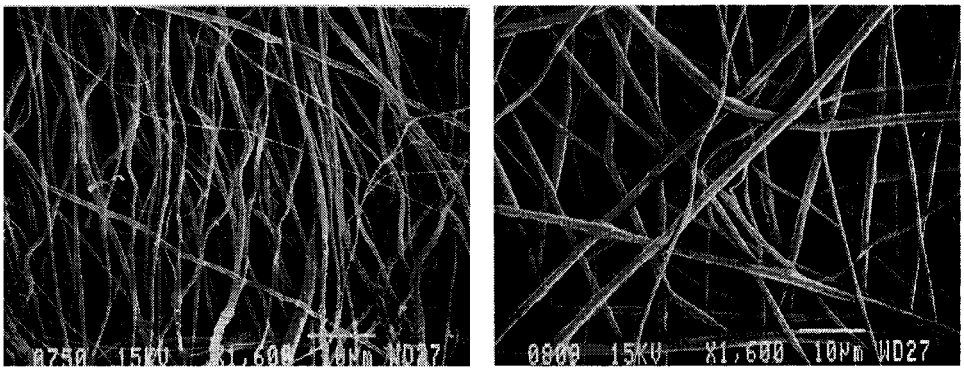

Figure 40. Electrospun poly(glycolic acid) at a concentration of 143 mg/ml in 1,1,1,3,3,3 Hexafluoro-2-propanol produced an aligned scaffold (left) and a random scaffold (right), both photos are at 1600x magnification and have a 10μm inset bar [21].

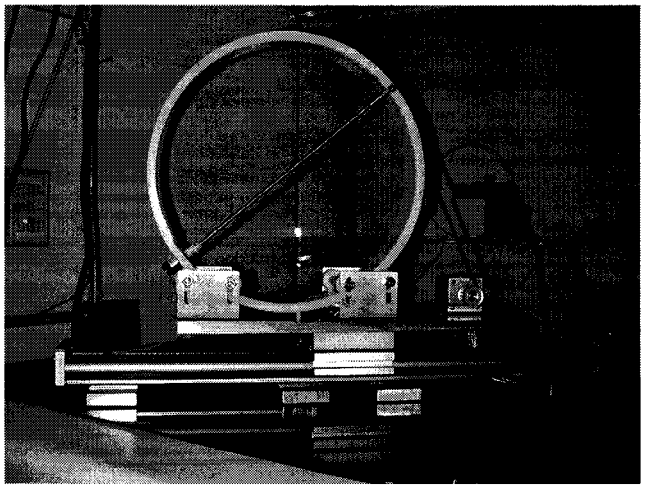

Figure 41. Novel electrospinning device designed and fabricated by the author.

To date, no targeting system allows for the controlled orientation of the collected fibers. This new automated electrospinning device (depicted in Figure 41.) addresses this need by incorporating multi-axis motion that will allow for repeatable fabric densities and fiber

alignment. Fiber alignment is controlled by rotating a mandrel (at a precise speed) along one axis, translation along that same axis, and rotation around the second axis perpendicular to the electrospun fiber stream. The software that controls this device is capable changing the translational speed, rotational speed and pitch of the target mandrel during electrostatic processing. The software was written in such a manner as to provide supervisory control of multiple single-axis motor controllers for the movement of the apparatus. This is accomplished by having the software develop and download programs to each independent motor controller. The software also acquires feedback from the controller to verify proper execution of the program. By doing this, the software coordinates or synchronizes the motion of the individual motion controllers to allow precise orientation of the fibers being deposited on the target mandrel. This control will allow the process to be more repeatable and reproducible.

In addition to controlling the axis motion controllers, this software prompts the user to enter other process information including, but not limited to: material and solvent, applied voltage, mandrel information, nozzle to mandrel distance and injection flow rate. This information, along with the motion control specifications and operator name, will be exported to a time / date stamped file for archival record keeping.

The software is written in the National Instruments LabVIEW® programming language in such a manner to present the operator with an easy to follow menu system built into a graphical user interface. The software is designed to run on an IBM PC compatible computer with appropriate communication hardware.

Validation and Test Methods

Once the software design and programming has been completed, system testing will be done to confirm the accuracy and repeatability of the motions. Translation distance will be evaluated using a steel scale with an accuracy of greater that 0.5 mm. A distance of ± 1 mm from the expected will be the acceptance criteria. Translational speed will be measured from a return trip motion (from one end to the other and back). An accuracy of ± 2 seconds is required and will be based on the programmed acceleration, deceleration, velocity, and reversal dwell time. This will be tested across the full useful range of translational speeds. The timing device will have an accuracy of greater that ± 0.1 seconds. Mandrel rotation will be measured by a digital stroboscope with an accuracy of greater than ± 10% of reading. This accuracy will match the acceptance criteria. Mandrel pitch will be measured manually with a protractor with an acceptance criterion set at ± 5 degrees.

After motion controls are confirmed, the ability to control fiber orientation needs to be verified. The first step is to confirm the previously seen dependence of fiber diameter on solution concentration (18). Poly(glycolic acid) will be used during this phase of testing. The reason for using poly(glycolic acid), or PGA, is that it is one of a group of biodegradable aliphatic polyesters currently exploited in a variety of medical applications. PGA possesses a moderate degree of crystallinity, a high melting point, and low solubility in organic solvents. PGA's inception as a biomaterial came in the 1970's as a degradable suture material. It was found to have better than average tissue compatibility, reproducible mechanical properties such as strength, elongation and knot

retention, and predictable bioabsorption (119). These properties make PGA well suited for tissue engineering applications and therefore an appropriate validation polymer for this device.

Solution concentrations of 67 mg/ml, 100 mg/ml and 143 mg/ml of PGA in 1,1,1,3,3,3 hexafluoro-2-propanol (HFP) will be electrospun at identical processing parameters to determine the fiber diameter – solution concentration relationship independent of voltage, distance, solvent volatility and orientation. These values were chosen from past experiments conducted in our laboratory to determine the concentration range that will produce consistent fibers (18). The fibrous mats or scaffolds will be visualized by scanning electron microscopy. The resulting micrographs will be digitized and analyzed using Uthscsa's ImageTool 3.0 (National Institutes of Health shareware developed by the University of Texas Health Science Center in San Antonio) to determine the average fiber diameters (average and standard deviation calculated from 60 measurements per micrograph) in the various mats. All measurements will be calibrated using the scale on the micrograph as a reference to avoid errors in calculating the magnification of the scanned photos.

The second hypothesis to be addressed is whether the control software can cause specific fiber alignment. As previously mentioned, our prototype electrospinning apparatus could marginally control fiber orientation my varying the mandrel rotational speed. A more rigorous test involving the two variables, mandrel rotation speed and mandrel translation, will be implemented. The mandrel is capable of rotating between 0 and 8000 revolutions per minute (RPM) and the translation slide capable of 0 to 800

inches per minute. A test matrix will be set up that varies each parameter in 25% increments. Alignment will be verified in a twofold process. First, the resultant scaffolds will be visualized with the SEM and alignment will be described qualitatively. Secondly, uniaxial tensile testing will be implemented. The uniaxial tensile test will be able to "interrogate" the scaffolds to find the principle orientation. Test specimens adhering to the American Society of Testing and Materials method D412 (ASTM D412 – Tensile Testing of Rubber and Thermoplastic Elastomers) will be cut at various angles with respect to the primary axis of revolution for the mandrel. This method was chosen over method D5035 (Test Method for Breaking Force and Elongation of Textile Fabrics) due to the elastic nature of the prepared scaffolds and to facilitate comparison to other data in the literature. Since the fibers are dry when collected, the individual fibers will contribute to the total mechanical property. If scaffolds are stretched along the principle fiber axis, high stiffness and low extension to failure is expected. The inverse is true when the mats are stretched perpendicular to the principle fiber axis. This testing should compliment the visual analysis to confirm the primary fiber orientation and the degree of orientation (higher degree of orientation should yield larger variation between stretching along the principle fiber axis and stretching perpendicular to that axis). All statistics will be based on either a one-way or multiway ANOVA (depending on comparison) with the *a priori* significance level will be set at $\alpha = 0.05$.

Preliminary Results and Discussion

Because this investigation is on going at this time, I will present the preliminary data adhering to the described methods but collected with our prototype setup. This apparatus has a fixed translation speed of 80 inches per minute and mandrel rotation that was set at either 100 RPM for random scaffolds or 1000 RPM for aligned scaffolds. Five (n = 5) test specimen were tested in each of the following orientations; Longitudinal – along the principal fiber direction in the aligned mat, Orthogonal – perpendicular to the principal fiber orientation in the aligned mat, and Random – taken from the random mat. Tests were repeated for the 67 mg/ml, 100 mg/ml, and 143 mg/ml concentrations of PGA in HFP.

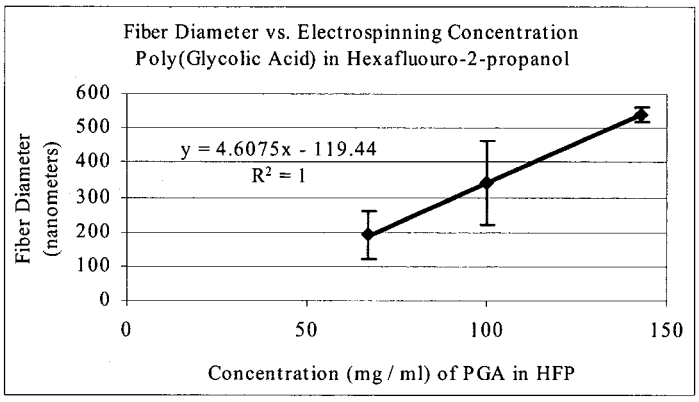

Figure 42. A linear regression of fiber diameter in nanometers as a function of electrospinning concentration (18).

The first hypothesis of this experimental protocol was to test the effect of solution concentration on fiber diameter. The graph in Figure 42 depicts the linear relationship seen for PGA in HFP. Even the largest diameters produced by electrospinning are more

than 10 times smaller then those that can be extruded to manufacture braided thread and woven mats (18).

Uniaxial material testing was performed on a MTS Bionix 200 mechanical testing system incorporating a 100N load cell with an extension rate of 1.0 mm/minute to failure (MTS Systems Corp.; Eden Prairie, MN). The specimens were cut out of the mats using a "dog-bone" shaped template to assure uniformity and to isolate the failure point away from the grips (18). The specimens had a width of 2.75 mm, a gauge length of 11.25 mm and thicknesses that ranged from 0.6 to 1.25 mm. The material properties chosen for comparison were the elastic modulus (tangential method automatically selected by the MTS TestWorks 4.0 software) and the strain to failure (also calculated automatically by the software) (18).

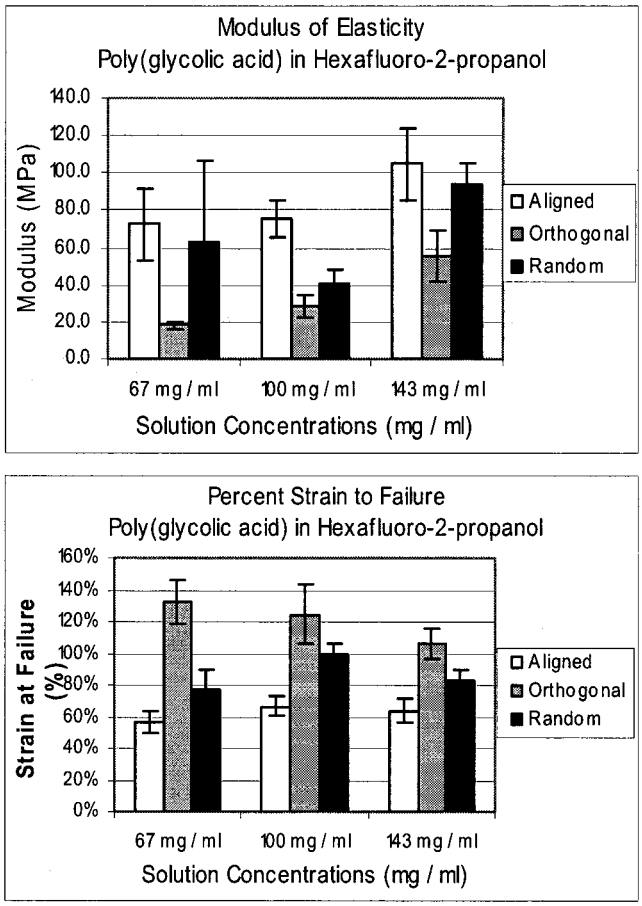

Figure 43. The modulus of elasticity and percent strain to failure of the three test concentrations of PGA in HFP (18).

The two charts in Figure 43 illustrate the relationship between orientation and both the elastic modulus of the scaffold as well as its strain to failure. In all cases tested, a significant difference was calculated between the longitudinal and orthogonal directions using the Students T Test with a significance level of $P<0.01$.

This preliminary data suggests that orientation will be predictive of the stress / strain relations of a specific polymer and the strength of these electrospun scaffolds will make them good candidates for tissue engineering applications. Additionally, solution concentration can be predictive of fiber diameter and nano-scale fiber diameters are possible with this system.

Conclusion

The significance of this research goes to the core principles of tissue engineering; create an engineered material that can mimic the natural structure of the extra-cellular matrix. These structures vary greatly from tissue to tissue; therefore an apparatus for mimicking these structures must be versatile. This newly developed automated electrospinning apparatus, when coupled with the extensive electrospinning experience gained in our laboratory (18, 20, 66, 76, 77, 106, 118), promises to provide the level of control, reproducibility, and flexibility needed in designing scaffolds from straight parallel fibers for skeletal muscle applications to the intricate helical arrangement of cardiac muscle. It will also provide the ability to design multi-layered tissue scaffolds for complex structures such as blood vessels, or to rapidly produce scaffolds useful for the topical wound healing of patients with burns and ulcers. From data collected during this study and an understanding of the mechanical requirements of specific tissues, the framework for a new generation of tissue-engineered scaffolds can emerge. These new scaffolds could revolutionize the treatment of injury and disease thereby reducing complications and improving the patient's quality of life after treatment.

Chapter 9 Design and Control of the Novel Electrospinning Apparatus

As illustrated routinely in the past sections, electrospun mats tend to have a high degree of variability in thickness and fiber orientation. The pioneering work in the utility of electrospun materials was done by Formhals in the 1930's as devices to collect synthetic thread (41-43). While these devices did isolate fiber deposition, the principle focus was to collect enough microfibers to make a larger nonwoven thread. This thread would then be capable of being processed in a manner similar to other commercially manufactured threads for the textile industry. The principle idea of the new design being described here is to create a finished electrospun product rather than just processing a raw material into a manufacturing component. In this case, the electrospun product will be a scaffold to serve as a synthetic extracellular matrix (ECM). To understand the design requirements, one must first understand the "design" of the native ECM. For most tissues the ECM is critically arranged to provide support, mechanical cues of orientation and stress, and sequester molecules to provide an appropriate microenvironment (58, 61, 74, 112, 113). That being established, it is understandable that electrospinning may not be ideally suited to produce tissue engineering scaffolds without adequate control over fiber collection. The idea for this novel electrospinning apparatus culminated from the need to induce more control over the fibrous mat produced from the electrospinning process and the desire to make the process more repeatable.

Mechanical

This novel electrospinning apparatus operates on a simple principle; fiber alignment can be induced through rotation and translation of the target. For the basic apparatus setup, two different targets or mandrels have been incorporated into the design. The first mandrel is a 4 mm diameter cylindrical stainless steel (400 series stainless steel). This mandrel will be used as a template for a small diameter vascular graft. This diameter produces a surface length (circumference in this example of a circular cross-section) of 12.57 mm. This surface length will be used to assess the velocity of the mandrel surface to compare this value to the measured and predicted value for jet traveling at 1.8 to 3.7 meters per second (6). Since the individual fine fibers produced by electrospinning are fragile, it is important that the mandrel rotation velocity is such that the major force acting on the fibers is electrical rather mechanical draw. The following equation governs the relationship between linear velocity and rotational velocity of a mandrel.

*Linear velocity = (rotational velocity) * (surface length)* (1)

For this size mandrel, the equivalent mandrel velocity would be 8,594 and 17,666 RPM, respectively for a jet velocity of 1.8 and 3.7 m/s. The exact value for a particular setup would be useful but the numbers reported by Baumgarten should predict an adequate starting point for future refinement. Since these rotational values would match the jet velocity, one would need to stay below these values to assure that the fibers would not be drawn. This becomes more important if larger mandrels are used. The second test mandrel that accompanied this design was a stainless steel square stock (400 series

stainless steel) with an edge length of 0.75 inches. This mandrel will be used primarily for collecting electrospun fibers to be used in mechanical testing or to make flat sheets for cell culture studies. This mandrel has a surface length of 76.2 mm. Assuming the same jet velocity, the equivalent mandrel velocity would be between 1,417 and 2,913 RPM. This simple exercise comparing rotational velocity to surface velocity illustrated the importance in knowing the exact size of a rotating mandrel when trying to align fibers. For this reason, the design criterion for mandrel rotation was set at 8000 RPM. Another aspect to fiber alignment in a physiologically significant manner would involve translation of the mandrel. Translating the mandrel back and forth in front of the electrospinning jet can accomplish two things. This first would be that it would ensure that the mandrel is evenly coated with electrospun fibers. The second, and possibly more important from a physiology standpoint, is that translation can produce pitch. With few exceptions, no tissue in the body has a perfectly aligned ECM. Since the main focus of our laboratory is blood vessel tissue engineering, pitch control is necessary to replicate the natural helical pattern in a vascular ECMs. If the translational velocity of the mandrel matches the rotational velocity, fibers should theoretically be collected at a 45° angle with respect to the radial direction of the mandrel. Assuming the 4 mm cylindrical mandrel is being revolved at 8000 RPM, the surface velocity of the mandrel would be 1.68 m/s. This would necessitate a translation velocity of 1.68 m/s for a 45° pitch as determined in the following equation.

*(translational velocity) = (surface velocity) * tangent (pitch angle)* (2)

It should be noted that these calculations are only theoretic approximations based on fibers being picked up on the mandrel without slipping and with an initial direction normal to the mandrel surface. Based on this theory, the design criterion was to induce up to a 20° pitch when using the 4 mm diameter mandrel. This pitch angle would require a translational velocity of 0.61 m/s.

Having the design criteria established (0 – 8000 RPM rotation and 0 – 0.61 m/s translation) a physical design could be made. Before continuing one additional control motion was hypothesized. This motion would be rotational about the electrospinning jet axis which will be defined as mandrel pitch. This rotation could provide two benefits. First, adding pitch control to the mandrel could accommodate more complex shapes and potentially add another orientation option. The second, and more practical for vascular applications, would be that mandrel pitch can theoretically increase the translation speed of the mandrel past the jet. The following equation relates the effective velocity, actual translational velocity and mandrel pitch:

$$effective\ velocity = \frac{1}{\cos(pitch)} * (translational\ velocity) \tag{3}$$

Pitch was included as a design requirement; however, no actual angular requirements were set due to foreseeable mechanical constraint.

With the design criteria set, a thumbnail sketch was made as seen in Figure 44.

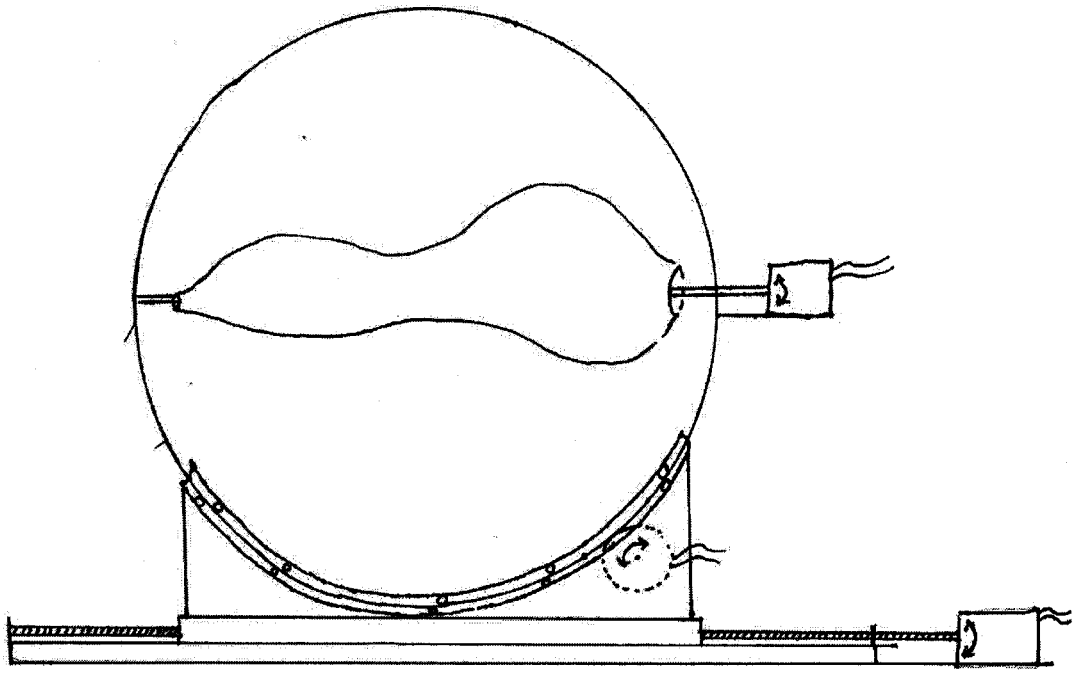

Figure 44. Thumbnail sketch of a new electrospinning apparatus capable of providing adequate control to develop a biomimicking vascular graft as well as other tissue engineering applications.

From this sketch, a detailed 3-D model was drawn using SolidWorks 2001plus (SolidWorks Corporation, MA). The rendered picture seen in Figure 45 is the finished assembly and the basis for the drawings and bill of materials included in Appendix B.

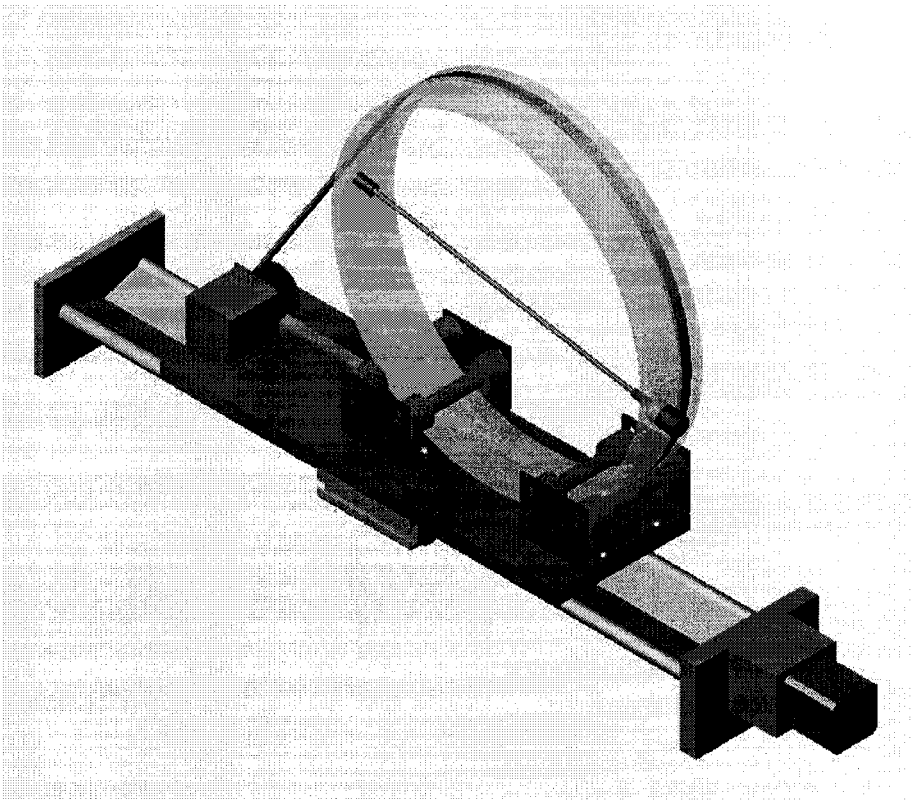

Figure 45. Rendered assembly of the components necessary to build the new electrospinning apparatus described in this document.

The design includes a constant velocity servo motor (MicroMo 1724T024SR motor) with a 512 step encoder and variable current power supply to assure even motion with varying loads. The specifications of the motor include a 0-8600 RPM no load speed. Since the rotational control motor is mounted directly to the support ring, the decision was made to sacrifice speed for size. The motor as selected weighs less than 2 ounces. The motor is coupled to the mandrel by a non-conductive adaptor for electrical isolation. The opposing end of the mandrel is supported by a graphite bushing to provide a conductive path to either ground or charge the mandrel. For translation, a linear screw drive with a 1.2 inch pitch and zero backlash nut in a rigid support stage (Dolphin Guide: 24 inch

travel / 1.2" pitch - Stage manufactured by Pacific Bearing) was coupled to a hybrid stepper motor with a dedicated software based controller (Applied Motion Products P/N HT23-401-001 hybrid stepper motor, - Applied Motion Products P/N Si3540 programmable step controller). A hybrid stepper motor has the advantage of micro-stepping to produce smoother, higher velocity motion than a standard stepper motor. Hybrid motors are more prone to internal slippage if the torque is excessively high so careful operating parameters must be chosen. For this application, the motor will operate at 20,000 steps per revolution (0.018° per step) which is controlled by a square wave output at a specific frequency and duty cycle generated by the step controller. The torque requirement had been estimated based on the lead screw pitch and the weight of the moving components but its performance had to be assessed in the final assembly. Pitch is controlled by a second stepper motor (Applied Motion Products P/N HT17-075 with a Superior Electric SLO/SYN SS2000MD4 translation drive) and a belt drive around the supporting ring which allows for ± 35° rotation. Since no requirements were made for this aspect of the design, the final performance was assessed on the basis of repeatability. Based on the effective velocity equation, a 35° pitch would effectively increase the translational velocity by 22%. The completed device in an acrylic chamber can be seen in the photographs in Figure 46.

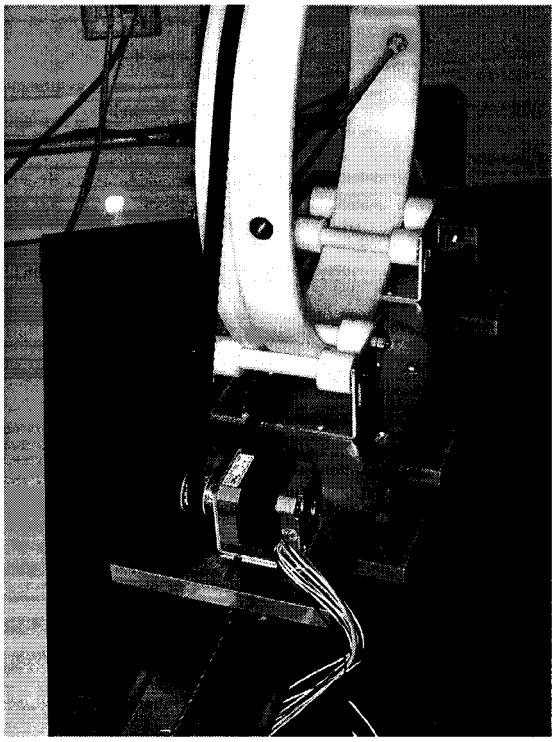

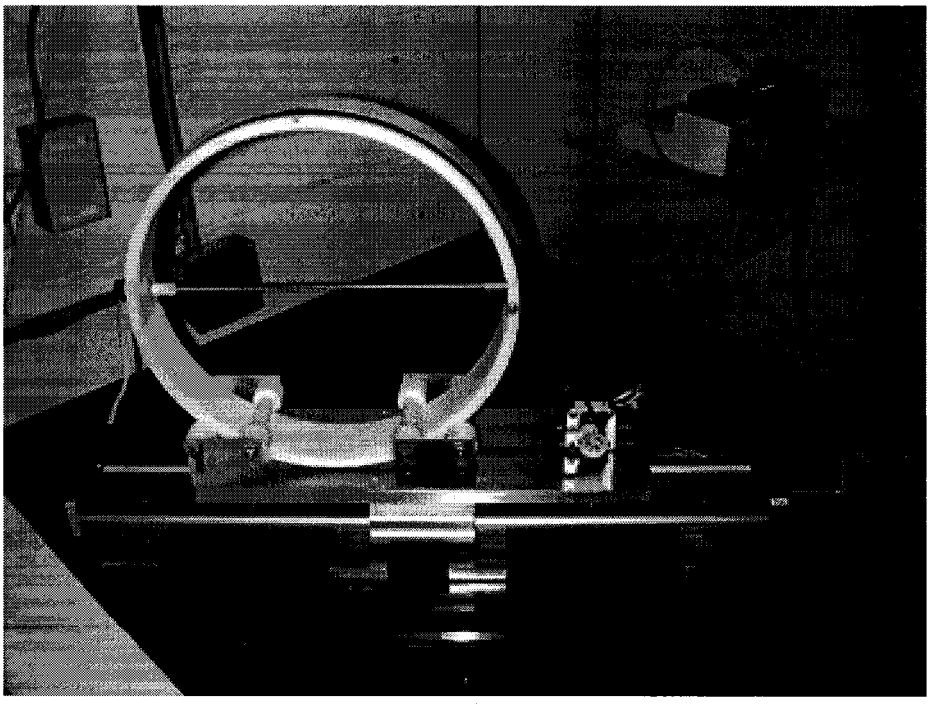

Figure 46. Photographs of novel electrospinning apparatus.

Software

One aspect of the design criteria was to make the process more repeatable. The software control added to this system was designed to accomplish this task in two different ways. The first part of the software, written in LabVIEW® (National Instruments, TX), has a user input screen, as seen in Figure 47, prompting for a polymer type and concentration, syringe type and volume, needle size, infusion pump flow rate, voltage, nozzle to target distance, mandrel velocity, translation velocity, and translation distance.

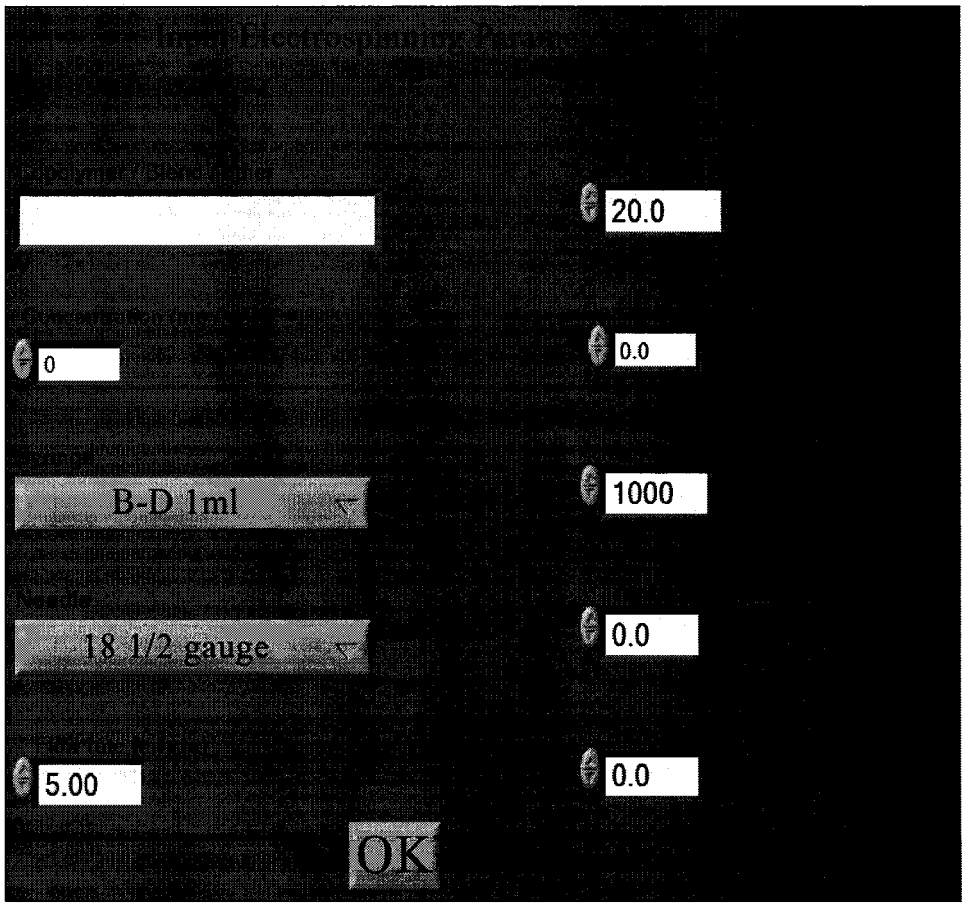

Figure 47. User input screen for the control software.

At the present time, only the mandrel velocity input will control the device. At the completion of the data entry step, this information is written to a data file as a two line tab delimited text file on the computer for future reference. The user can either select an existing file and append the data to the end or create a new file. The name and location of this file is user editable. For motion control, the LabVIEW® program uses serial commands sent to the respective motion controllers and in turn receives feedback from those controllers. All real time control is handled by the individual axis motion controllers. During the LabVIEW® program execution, the real time mandrel velocity is displayed as seen in Figure 48.

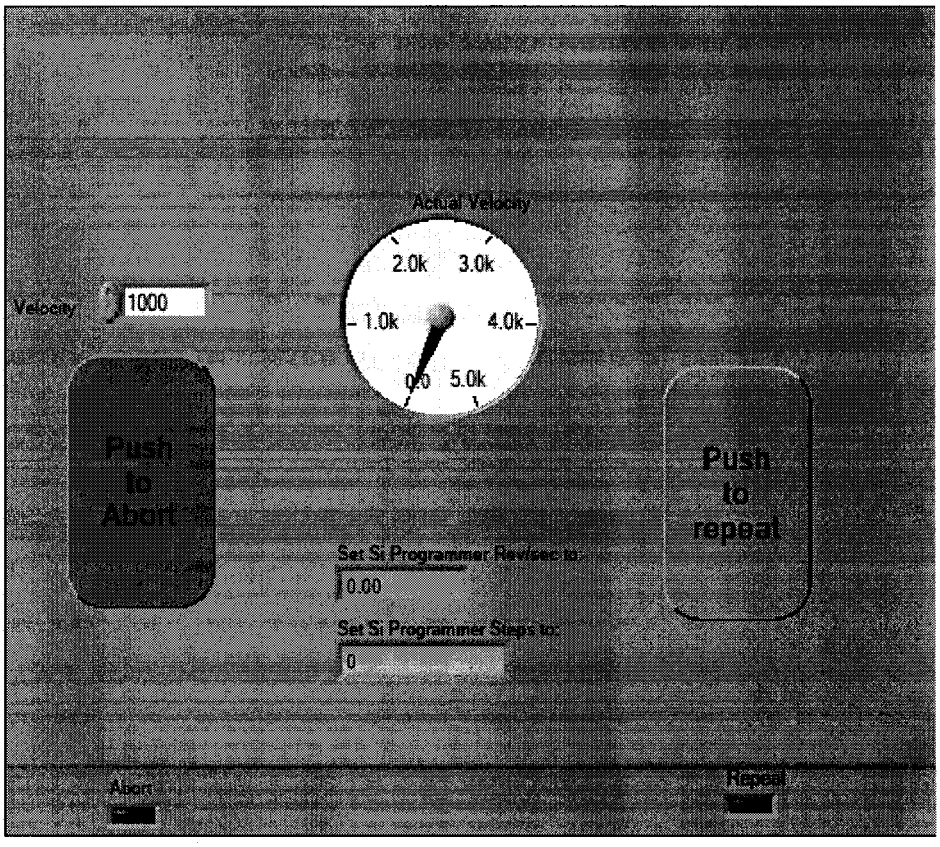

Figure 48. Mandrel Velocity screen from the control software.

This give the user the ability to know if the program specifications are being met since the velocity and the velocity set point are displayed. Some rotational resistance can be overcome since the motor is a constant velocity servo but excessive resistance will slow the motor since current is limited to prevent motor damage. This screen also gives the user the ability to repeat the process and go back to the user input screen for an additional run or abort and exit the program. The final values displayed on this screen are the two set points for the translation control software based on the user input translation distance and velocity. The complete LabVIEW® program can be found in appendix C.

The translation control is accomplished through a program called Si Programmer (Applied Motion Products) that was supplied with the Si 3540 Programmable Step Controller. This software allows the user to define a motion in terms of revolutions per second, step count, current, acceleration, deceleration, and return speed then downloads that program to the controller. When the Si Programmer software is launched, the following default values should be verified on that screen: Output set to 3.0 A/phase, Idle Current set to 50%, Steps/Rev set to 20000, and the communication port set to COM1. As previously mentioned, the main LabVIEW® program will calculate and display the appropriate step count and revolution per second values to correspond to the values entered on the startup screen. The Si Programmer uses a one step input (select line one in programming list) named "move and return". After selecting move and return from the popup window, the user will input the step count calculated by LabVIEW as the Step value and the calculated Rev/Sec velocity for both the Rev/Sec value and the return speed. For all cases, the acceleration and deceleration values should be 100 rev/sec/sec.

After modifying the program, if necessary, the program is downloaded to the translation controller and SI Programmer should be exited. Whenever the translation drive is powered on, except when the Si Programmer software is running, the resident program will be executed. This will reduce the need to routinely reprogram the translation controller, however, care must be taken to prevent damage or injury. This one line program will provide adequate ability to control translation. The pitch is also controlled through LabVIEW® with a user selectable pitch angle that is converted to a step count and downloaded to the pitch axis controller. An integrated multi-axis control board may be necessary in the future to better synchronize the motion and have all motion controlled through a single software program.

Testing and Future Direction

Testing began with the mandrel rotation. To confirm the velocity, a digital stroboscope (Extech Instrumentation) was used with a reflective marker placed either on the motor shaft or directly on each of the mandrels placed within the system. The set points were entered into the computer program and velocity readings were taken after 20 seconds, after 1 minute and after 15 minutes. This was repeated 4 times at each velocity setting for each mandrel to test stability and repeatability. The averaged data can be seen in Table 3 on the following page. It should be noted that at low speed, below 500 RPM, the mandrels are very susceptible to binding if the shaft couplings are not centered. For items marked with an asterisk, accurate velocities could not be determined due to this binding. As these velocities are only useful for random fiber alignment, the oscillating motion would be of no practical consequence.

Mandrel rotation			
No load		4 mm diameter shaft	3/4 in. square shaft
Set point (RPM)	Actual (RPM)	Actual (RPM)	Actual (RPM)
100	100.0 ± 0.0	*	*
250	250.0 ± 0.0	250.0 ± 0.1	235.0 ± 12.4*
500	500.1 ± 0.1	499.8 ± 0.1	499.7 ± 0.2
750	750.0 ± 0.0	750.2 ± 0.1	749.4 ± 0.5
1000	1000.1 ± 0.1	1000.0 ± 0.0	1000.0 ± 0.2
1250	1250.0 ± 0.1	1249.7 ± 0.4	1249.8 ± 0.3
1500	1500.2 ± 0.2	1499.2 ± 0.3	1499.4 ± 0.3
1750	1749.9 ± 0.1	1750.0 ± 0.1	1750.1 ± 0.1
2000	2000.0 ± 0.1	1999.4 ± 0.2	2000.1 ± 0.1
2250	2250.0 ± 0.0	2249.8 ± 0.1	2249.8 ± 0.2
2500	2500.3 ± 0.1	2499.7 ± 0.1	2500.0 ± 0.2
2750	2749.8 ± 0.1	2750.0 ± 0.0	2749.8 ± 0.3
3000	3000.0 ± 0.0	3000.1 ± 0.1	2999.6 ± 0.6
3250	3250.0 ± 0.1	3248.9 ± 0.3	3250.0 ± 0.3
3500	3499.7 ± 0.2	3499.7 ± 0.1	3499.8 ± 0.5
3750	3749.8 ± 0.3	3749.2 ± 0.2	3642.6 ± 4.6
4000	4000.2 ± 0.2	3998.8 ± 0.3	*
4250	4250.0 ± 0.1	4250.0 ± 0.4	*
4500	4499.2 ± 0.2	4499.2 ± 0.4	*
4750	4747.8 ± 0.5	4748.8 ± 0.7	*
5000	4998.2 ± 0.4	4998.4 ± 0.9	*

Table 3. Table reporting averaged data for mandrel rotation. Each reported point is an average of 12 measurements (± 1 standard deviation). Items marked with an asterisks hesitated while revolving and accurate results could not be measured.

Testing was terminated at 5000 RPM due to significant slowing of the mandrels at set points above that value. Initial specifications called for 8000 RPM and this motor may still be capable of producing those speeds after speaking to the manufacturer who said it may be possible to use a higher current power supply thereby increasing the available

torque of the motor. This may cause increased heating of the motor and premature failure. The risks of motor damage will have to be weighed against any possible benefit of the increased rotational velocity in the future.

The second test was to determine that translational velocity range and repeatability. Current was set to the maximum value for the motor and acceleration, deceleration, and constant velocity rates were systematically changed to determine the performance window for the complete system. Since the mandrel is 250 mm long, the requirement would be to have a 250 mm region of constant velocity or avoid discrepancies along the length of the mandrel. The overall design of the system allows for at least 450 mm of motion. Therefore, a stroke distance of 18 in. was chosen for the experiment (Si Programmer uses English units). The requirement for success would be no internal motor slippage for a typical 30 minute sample run with a 50% increase in stage weight. The increased stage weight was used to simulate inertial changes due to mandrel changes or friction from fiber buildup during a run. The maximum acceleration and deceleration values were determined to be 120 in/s^2 (3.05 m/s^2) and the maximum constant velocity was determined to be 25.4 in/s (0.64 m/s). No variation in either acceleration or velocity could be measured within the non-slipping range using a manual stopwatch even when measured over multiple cycles. It was determined that once the motor slips, it will not re-engage until the system is stopped and restarted. This slippage behavior can provide some assurance of movement accuracy if the system is run while unattended.

For general usage, the acceleration and deceleration value should be held constant and the steady velocity set-point could be changed. The operating window can be seen in the chart in Figure 49. In that figure, the new electrospinning device is compared to the current prototype device.

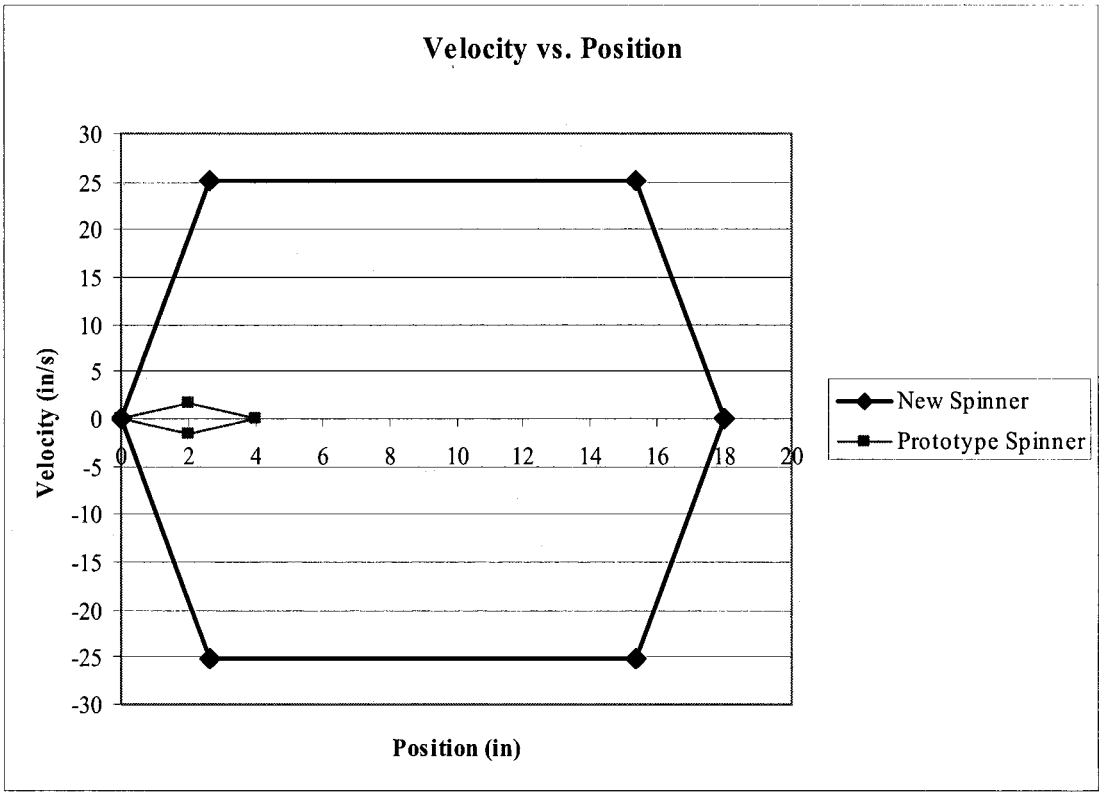

Figure 49. Performance (velocity vs. position) comparison between the new electrospinner and the existing prototype design.

Since the pitch control must match the translation, the requirements for pitch is to change from 0 to 35° in the positive direction to 0 to 35° in the negative direction during the time it takes the stage to reverse direction and get back to constant velocity. This time has been calculated as 0.47 seconds (deceleration time + reversal time + acceleration time). The pitch control motor was capable of accomplishing this task, however, a better timing

mechanism could be developed in the future to make the synchronization easier. Currently, careful user intervention during startup is required to assure the two motors are synchronized.

After system verification and testing, preliminary tests were conducted to begin to verify theoretical fiber control. Electrospinning of PGA at 100 mg/ml was chosen for this testing because of the authors experience and its applicability to tissue engineering. The following two test conditions were established. 1.) High velocity rotation – low velocity translation (3500 rpm, 1 in/s), defined as aligned and 2.) High velocity rotation – high velocity translation (3500 rpm, 25.2 in/s), defined as pitched. The square stock mandrel was used as the target to facilitate mechanical testing of the mats after electrospinning. SEM micrographs of the representative mats can be seen in Figure 50.

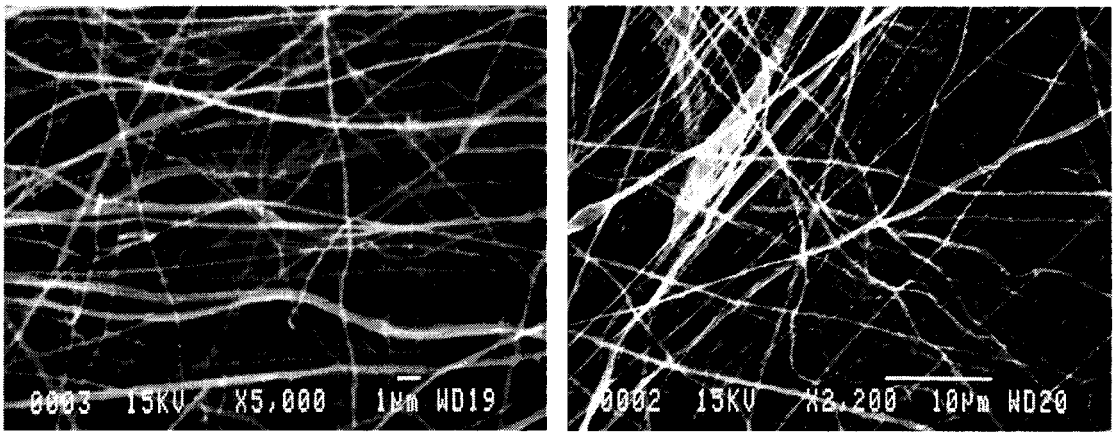

Figure 50. SEM micrographs of 100 mg/ml PGA electrospun from HFP. The image on the left (5000x magnification) is the aligned mat with 0.197 ± 0.017 micron diameter fibers and 0.611 ± 0.111 micron^2 pores. The image on the left (2200x magnification) is the pitched mat with 0.217 ± 0.011 micron diameter fibers and 3.085 ± 0.495 micron^2 pores. Values are reported as mean ± standard error.

Physical examination of the mats by previously reported means (16) was conducted to determine fiber size and pore area, values are reported as mean ± standard error. For the aligned mat, the fiber diameter is 0.197 ± 0.017 microns with pore areas of 0.611 ± 0.111 microns^2. For the pitched mat, the fiber diameter is 0.217 ± 0.011 microns with pore areas of 3.085 ± 0.495 microns^2. Two interesting observations can be made from these findings. The pitched mat has significantly larger pores ($P<0.001$ by Mann-Whitney rank sum) and there appears to be fewer fibers that deviate from the two principle orientations. Both conditions may be explained by the increased relative velocity of the mandrel with respect to the jet. Estimation of the pitch angle is between 30° and 40° instead of a predicted value of 10°. Further experimentation will be necessary to determine the cause for the increased pitch angle.

Uniaxial mechanical testing was performed on the aligned mat to confirm alignment (18). Modulus of elasticity, peak stress and strain to failure were chosen to characterize the mats. These results, seen in Figures 51-53 confirm that a high degree of anisotropy is present and the results support the predicted principle fiber direction. Until a more accurate measure of fiber alignment can be developed, uniaxial mechanical testing provides the most detailed evaluation of the underlying fiber structure. Incomplete alignment or inter-fiber bonding is evident in these scaffolds due to the high peak stress in the orthogonal direction. At present, these two conditions cannot be isolated beyond observation of the SEM micrographs. It is my opinion that incomplete alignment is the more likely candidate in this test setup.

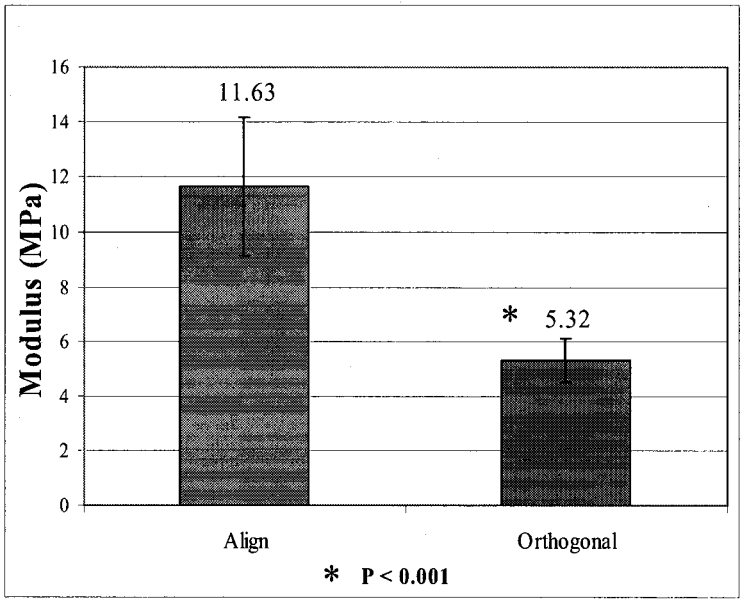

Figure 51. Modulus of elasticity comparing specimens (n=10) cut in the aligned direction of the mat to specimens cut in the orthogonal direction of the mat. Graphed as average ± 1 standard deviation. Statistical conclusion based on Student's t-test (α = 0.05).

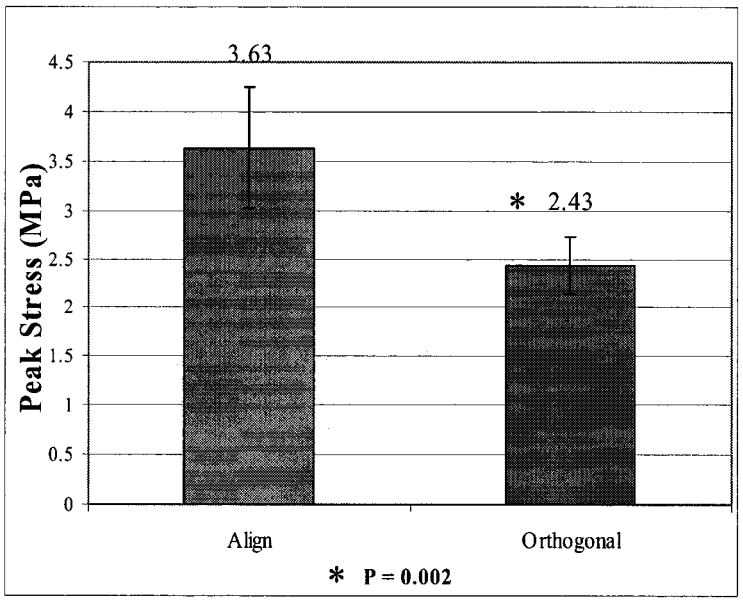

Figure 52. Peak stress comparing specimens (n=10) cut in the aligned direction of the mat to specimens cut in the orthogonal direction of the mat. Graphed as average ± 1 standard deviation. Statistical conclusion based on Student's t-test (α = 0.05).

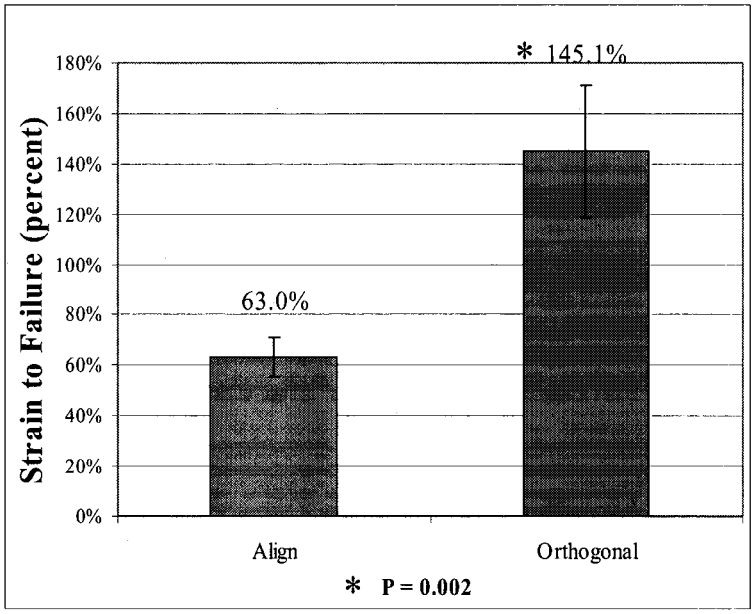

Figure 53. Strain to failure comparing specimens (n=10) cut in the aligned direction of the mat to specimens cut in the orthogonal direction of the mat. Graphed as average ± 1 standard deviation. Statistical conclusion based on Student's t-test ($\alpha = 0.05$).

In conclusion, the computer control of this electrospinning apparatus has been demonstrated to impart a high level of accuracy and precision into the motion of the electrospinning target. In addition, the data file generated will aid in the repeatability of the electrospinning process by tracking most of the user dependent variables. The increased translation velocity of this system has been able to demonstrate a new level of fiber alignment that the previous system could not induce. Although the orientation did not exactly follow the theoretical calculations, a larger degree of pitch was observed and I believe that a more accurate prediction can be developed with additionally experimentation. This ability should provide a necessary step forward to develop a truly biomimicking scaffold. Another benefit that may be derived from this tool is the ability to isolate fiber size from pore area since pore area was seen to increase with pitch. This

could allow researchers to probe cellular interactions with electrospun matrices as either a function of fiber size or pore area. I would predict that some cell types, such as chondrocytes, would prefer larger pores to allow cells to cluster in a looser matrix while other cells, such as myocytes, would prefer smaller pores to enhance cell – fiber contacts and mechanotransduction.

Literature Cited

Literature Cited

1. PDS II (Polydiaxonone). The Veterinarian's Suture Guide. Auburn University.

2. 2001. Current Good Manufacturing Practices for Medical Device Manufacturers. In *Code of Federal Regulations.*

3. Alcock H, F. L. 1981. *Contemporary Polymer Chemistry*. Englewood Cliffs: Prentice-Hall. 599 pp. 3-94.

4. Babanalbandi A, Hill DJT, O'Donnell JH, Pomery PJ. 1996. An electron spin resonance analysis on [gamma]-irradiated poly(glycolic acid) and its copolymers with lactic acid. *Polymer Degradation and Stability* 52: 59-66.

5. Barrows T. 1991. Synthetic Bioabsorbable polymers. In *High Performance Biomaterials: A Comprehensive Guide to Medical and Pharmaceutical Applications*, ed. S M, pp. 243-57. Lancaster: Technomics.

6. Baumgarten PK. 1971. Electrostatic spinning of acrylic microfibres. *Journal of Colloid and Interface Science* 36: 71-9.

7. Belenkaya B, Sakharova V, Sinevich E, Belousov S, Kuptsov A. 1999. Synthesis and biodegradation of modified polyglycolide. *Polymer Preprints* 39: 164.

8. Bell E. 1991. Tissue engineering: a perspective. *Journal of Cellular Biochemistry* 45: 239-41.

9. Bennett S, Connolly K, Lee DR, Jiang Y, Buck D, et al. 1996. Initial biocompatibility studies of a novel degradable polymeric bone substitute that hardens in situ. *Bone* 19: 101S-7S.

10. Bhattarai SR, Bhattarai N, Yi HK, Hwang PH, Cha DI, Kim HY. 2004. Novel biodegradable electrospun membrane: scaffold for tissue engineering. *Biomaterials* 25: 2595-602.

11. Boenisch M, Mink A. 2000. Clinical and histological results of septoplasty with a resorbable implant. *Archives of Otolaryngology--Head & Neck Surgery* 126: 1373-7.

12. Bognitzki M, Frese T, Steinhart M, Greiner A, Wendorff JH, et al. 2001. Preparation of fibers with nanoscaled morphologies: Electrospinning of polymer blends. *Polymer Engineering and Science* 41: 982-9.

13. Bognitzki M, Frese T, Wendorff JH, Greiner A. 2000. Submicrometer shaped polylactide fibers by electrospinning. *Abstracts of Papers of the American Chemical Society* 219: U491-U.

14. Boland ED, Bowlin GL, Simpson DG, Wnek GE. 2001. Electrospinning of tissue engineering scaffolds. *Abstracts of Papers of the American Chemical Society* 222: U344-U.

15. Boland ED, Matthews JA, Pawlowski KJ, Wnek GE, Simpson DG, Gary LBFFM. 2004. Electrospinning collagen and elastin: preliminary vascular tissue engineering. *Frontiers in Bioscience* 9: 1422-32.

16. Boland ED, Telemeco TA, Simpson DG, Wnek GE, Bowlin GL. 2004. Utilizing Acid Pretreatment and Electrospinning to Improve Biocompatibility of Poly(glycolic acid) for Tissue Engineering. *Journal of Biomedical Materials Research Part B: Applied Biomaterials* In Press.

17. Boland ED, Wnek GE, Bowlin GL. In Press. Poly(Glycolic Acid). In *The Encyclopedia of Biomaterials and Biomedical Engineering*, ed. GL Bowlin, GE Wnek. New York: Marcel Dekker, Inc.

18. Boland ED, Wnek GE, Simpson DG, Pawlowski KJ, Bowlin GL. 2001. Tailoring tissue engineering scaffolds using electrostatic processing techniques: A study of poly(glycolic acid) electrospinning. *Journal of Macromolecular Science-Pure and Applied Chemistry* 38: 1231-43.

19. Bonnet D, Patkai J, Tamisier D, Kachaner J, Vouhe P, Sidi D. 1999. A new strategy for the surgical treatment of aortic coarctation associated with ventricular septal defect in infants using an absorbable pulmonary artery band. *Journal of The American College of Cardiology* 34: 866-70.

20. Bowlin GL, Pawlowski KJ, Stitzel JD, Boland ED, Simpson DG, et al. 2002. Electrospinning of polymer scaffolds for tissue engineering. In *Tissue Engineering and Biodegradable Equivalents: Scientific and Clinical Applications*, ed. K Lewandrowski, D Wise, D Trantolo, J Gresser, M Yaszemski, D Altobelli, pp. 165-78. New York: Marcel Dekker, Inc.

21. Bowlin GL, Wnek GE, Simpson DG, Terracio L. 2003. *United States Patent No. 6,592,623.*

22. Browning A, Chu CC. 1986. The effect of annealing treatments on the tensile properties and hydrolytic degradative properties of polyglycolic acid sutures. *Journal of Biomedical Materials Research* 20: 613-32.

23. Buchko CJ, Chen LC, Shen Y, Martin DC. 1999. Processing and microstructural characterization of porous biocompatible protein polymer thin films. *Polymer* 40: 7397-407.

24. Cady RB, Siegel JA, Mathien G, Spadaro JA, Chase SE. 1999. Physeal response to absorbable polydioxanone bone pins in growing rabbits. *Journal of Biomedical Materials Research* 48: 211-5.

25. Chatani Y, Suehiro K, Okita Y, Tadokoro H, Chujo K. 1968. Structural studies of polyesters I. Crystal structure of polyglycolide. *Die Makromolecular Chemistry* 133: 215-29.

26. Chu CC. 1981. The in-vitro degradation of poly(glycolic acid) sutures--effect of pH. *Journal of Biomedical Materials Research* 15: 795-804.

27. Chu CC, Browning A. 1988. The study of thermal and gross morphologic properties of polyglycolic acid upon annealing and degradation treatments. *Journal of Biomedical Materials Research* 22: 699-712.

28. Chu CC, Campbell ND. 1982. Scanning electron microscopic study of the hydrolytic degradation of poly(glycolic acid) suture. *Journal of Biomedical Materials Research* 16: 417-30.

29. Chun I, Reneker DH, Fong H, Fang X, Deitzel JM, et al. 1999. Carbon Nanofibers from Polyacrylonitrile and Mesophase Pitch. *Journal of Advanced Materials* 31: 36-41.

30. Davila JC, Lautsch EV, Palmer TE. 1968. Some physical factors affecting the acceptance of synthetic materials as tissue implants. *Annals of The New York Academy of Sciences* 146: 138-47.

31. Decker T, Lohmann-Matthes M-L. 1988. A quick and simple method for the quantitation of lactate dehydrogenase release in measurements of cellular cytotoxicity and tumor necrosis factor (TNF) activity. *Journal of Immunological Methods* 115: 61-9.

32. Deitzel JM, Beck Tan NC, Kleinmeyer JD, Rehrmann J, Tevault D. 1999. *Generation of Polymer Nanofibers through Electrospinning. Rep. ARL-TR-1989*, Army Research Laboratory Technical Report.

33. Deitzel JM, Kleinmeyer J, Harris D, Tan NCB. 2001. The effect of processing variables on the morphology of electrospun nanofibers and textiles. *Polymer* 42: 261-72.

34. Deitzel JM, Kosik W, McKnight SH, Tan NCB, DeSimone JM, Crette S. 2002. Electrospinning of polymer nanofibers with specific surface chemistry. *Polymer* 43: 1025-9.

35. Doshi J, Reneker DH. 1995. Electrospinning Process and Applications of Electrospun Fibers. *Journal of Electrostatics* 35: 151-60.

36. Dunn GA. 1982. Contact guidance of cultured tissue cells: a survey of potentially relevant properties of the substratum. In *Cell Behavior*, ed. R Bellairs, A Curtis, G Dunn, pp. 247-80. Cambridge: Cambridge University Press.

37. Eilbert JB, McKinney PW, Conn J, Jr, Binder P, Beal JM. 1971. Polyglycolic acid synthetic absorable sutures. *American Journal of Surgery* 121: 561-5.

38. Feng JJ. 2003. Stretching of a straight electrically charged viscoelastic jet. *Journal of Non-Newtonian Fluid Mechanics* 116: 55-70.

39. Fong H, Chun I, Reneker DH. 1999. Beaded nanofibers formed during electrospinning. *Polymer* 40: 4585-92.

40. Fong H, Chun I, Reneker DH. 1999. *Carbon Nanofibers*. Presented at 24th Biennial Conference on Carbon.

41. Formhals A. 1934. *United States Patent No. 1,975,504.*

42. Formhals A. 1939. *United States Patent No. 2,160,962.*

43. Formhals A. 1940. *United States Patent No. 2,187,306.*

44. Freed LE, Vunjak-Novakovic G. 1997. Microgravity tissue engineering. *In Vitro Cellular & Developmental Biology. Animal* 33: 381-5.

45. Freed LE, Vunjak-Novakovic G, Langer R. 1993. Cultivation of cell-polymer cartilage implants in bioreactors. *Journal of Cellular Biochemistry* 51: 257-64.

46. Fridrikh SV, Yu JH, Brenner MP, Rutledge GC. 2003. Controlling the fiber diameter during electrospinning. *Physical Review Letters* 90: 144502.

47. Gao J, Niklason L, Langer R. 1998. Surface hydrolysis of poly(glycolic acid) meshes increases the seeding density of vascular smooth muscle cells. *Journal of Biomedical Materials Research* 42: 417-24.

48. Gibson PW, Schreuder-Gibson HL, Pentheny C. 1999. Electrospinning Technology: Direct Application of Tailorable Ultrathin Membranes. *Journal of Coated Fabrics* 28: 63-72.

49. Gibson PW, Schreuder-Gibson HL, Rivin D. 1999. Electrospun Fiber Mats: Transport Properties. *AIChE Journal* 45: 190-5.

50. Gong J, Shao C-L, Yang G-C, Pan Y, Qu L-Y. 2003. Preparation of ultra-fine fiber mats contained $H_4SiW_{12}O_{40}$. *Inorganic Chemistry Communications* 6: 916-8.

51. Greisler HP, Gosselin C, Ren D, Kang SS, Kim DU. 1996. Biointeractive polymers and tissue engineered blood vessels. *Biomaterials* 17: 329-36.

52. Hohman MM, Shin M, Rutledge G, Brenner MP. 2001. Electrospinning and electrically forced jets. I. Stability theory. *Physics of Fluids* 13: 2201-20.

53. Holder WD, Jr, Gruber HE, Moore AL, Culberson CR, Anderson W, et al. 1998. Cellular ingrowth and thickness changes in poly-L-lactide and polyglycolide matrices implanted subcutaneously in the rat. *Journal of Biomedical Materials Research* 41: 412-21.

54. How TV, Guidoin R, Young SK. 1992. Engineering design of vascular prostheses. *Proceedings of the Institution of Mechanical Engineers. Part H, Journal of Engineering in Medicine* 206: 61-71.

55. Hsu S, Kambic H. 1997. On matching compliance between canine carotid arteries and polyurethane grafts. *Artificial Organs* 21: 1247-54.

56. Huang L, McMillan RA, Apkarian RP, Pourdeyhimi B, Conticello VP, Chaikof EL. 2000. Generation of synthetic elastin-mimetic small diameter fibers and fiber networks. *Macromolecules* 33: 2989-97.

57. Huang Z-M, Zhang Y-Z, Kotaki M, Ramakrishna S. 2003. A review on polymer nanofibers by electrospinning and their applications in nanocomposites. *Composites Science and Technology* 63: 2223-53.

58. Hubbell JA. 2002. Matrix Effects. In *Principles of Tissue Engineering*, ed. R Lanza, R Langer, J Vacanti, pp. 237-50. San Diego: Academic Press.

59. Hurrell S, Cameron RE. 2001. Polyglycolide: Degradation and drug release. Part I: Changes in morphology during degradation. *Journal of Materials Science: Materials in Medicine* 12: 811-6.

60. Hurrell S, Cameron RE. 2001. Polyglycolide: Degradation and drug release. Part II: Drug release. *Journal of Materials Science: Materials in Medicine* 12: 817-20.

61. Hynes RO. 2002. Integrins: Bidirectional, Allosteric Signaling Machines. *Cell* 110: 673-87.

62. Ibnabddjalil M, Loh IH, Chu CC, Blumenthal N, Alexander H, Turner D. 1994. Effect of surface plasma treatment on the chemical, physical, morphological, and mechanical properties of totally absorbable bone internal fixation devices. *Journal of Biomedical Materials Research* 28: 289-301.

63. Ishaug-Riley SL, Okun LE, Prado G, Applegate MA, Ratcliffe A. 1999. Human articular chondrocyte adhesion and proliferation on synthetic biodegradable polymer films. *Biomaterials* 20: 2245-56.

64. Jin H-J, Chen J, Karageorgiou V, Altman GH, Kaplan DL. 2004. Human bone marrow stromal cell responses on electrospun silk fibroin mats. *Biomaterials* 25: 1039-47.

65. Jin H-J, Fridrikh SV, Rutledge GC, Kaplan DL. 2002. Electrospinning Bombyx mori silk with poly(ethylene oxide). *Biomacromolecules* 3: 1233-9.

66. Kenawy ER, Bowlin GL, Mansfield K, Layman J, Simpson DG, et al. 2002. Release of tetracycline hydrochloride from electrospun poly(ethylene-co-vinylacetate), poly(lactic acid), and a blend. *Journal of Controlled Release* 81: 57-64.

67. Kim BS, Reneker DH. 1999. Mechanical Properties of Composites Using Ultrafine Electrospun Fibers. *Polymer Composites* 20: 124-31.

68. Kitchens WH. 1997. Legal issues involved in tissue engineering: FDA regulation of tissue engineering. In *Synthetic Biodegradable Polymer Scaffolds*, ed. A Atala, D Mooney, JP Vacanti, R Langer, pp. 33-49. Boston: Birhauser.

69. Kontio R, Suuronen R, Salonen O, Paukku P, Konttinen YT, Lindqvist C. 2001. Effectiveness of operative treatment of internal orbital wall fracture with polydioxanone implant. *International Journal of Oral And Maxillofacial Surgery* 30: 278-85.

70. Kricheldorf HR, Damrau D. 1998. Polylactones 42: Zn L-lactate-catalyzed polymerizations of 1,4-dioxan-2-one. *Macromolecular Chemical Physics* 199: 1089-98.

71. Kuettner KE. 1992. Biochemistry of articular cartilage in health and disease. *Clinical Biochemistry* 25: 155-63.

72. Lee KH, Kim HY, Khil MS, Ra YM, Lee DR. 2003. Characterization of nano-structured poly(ε-caprolactone) nonwoven mats via electrospinning. *Polymer* 44: 1287-94.

73. Ma PX, Zhang R. 1999. Synthetic nano-scale fibrous extracellular matrix. *Journal of Biomedical Materials Research* 46: 60-72.

74. MacKenna D, Summerour SR, Villarreal FJ. 2000. Role of mechanical factors in modulating cardiac fibroblast function and extracellular matrix synthesis. *Cardiovascular Research* 46: 257-63.

75. Martin GE, Cockshott ID. 1977. *United States Patent No. 4,043,331.*

76. Matthews JA, Boland ED, Wnek GE, Simpson DG, Bowlin GL. 2003. Electrospinning of Collagen Type II: A Feasibility Study. *Journal of Bioactive and Compatible Polymers* 18: 125-34.

77. Matthews JA, Wnek GE, Simpson DG, Bowlin GL. 2002. Electrospinning of collagen nanofibers. *Biomacromolecules* 3: 232-8.

78. McIntire LV, Greisler HP, Griffith L, Johnson PC, Mooney DJ, et al. 2002. Tissue Engineering Research. World Technology Evaluation Center.

79. Middleton JC, Tipton AJ. 1998. Synthetic biodegradable polymers as medical devices. *Medical Plastics and Biomaterials*: 30.

80. Min B-M, Lee G, Kim SH, Nam YS, Lee TS, Park WH. 2004. Electrospinning of silk fibroin nanofibers and its effect on the adhesion and spreading of normal human keratinocytes and fibroblasts in vitro. *Biomaterials* 25: 1289-97.

81. Mo XM, Xu CY, Kotaki M, Ramakrishna S. 2004. Electrospun P(LLA-CL) nanofiber: a biomimetic extracellular matrix for smooth muscle cell and endothelial cell proliferation. *Biomaterials* 25: 1883-90.

82. Mooney DL, R. 1995. Engineering biomaterials for tissue engineering: the 10 - 100 micron size scale. In *The Biomedical Engineering Handbook*, ed. J Bronzino, pp. 1609-18. Boca Raton: CRC Press.

83. Mow VC, Zhu W, Ratcliffe A. 1991. Structure and Function of Articular Cartilage and Meniscus. In *Basic Orthopaedic Biomechanics*, ed. VC Mow, WC Hayes, pp. 143-98. New York: Raven Press.

84. Nelson D, Cox M. 2000. Carbohydrate biosynthesis. In *Lehninger: Principles of Biochemistry*, ed. D Nelson, M Cox, pp. 722-64. New York: Worth Publishers.

85. Nerem R. 2000. The Challenge of Imatating Nature. In *Principles of Tissue Engineering*, ed. R Lanza, R Langer, CA Vacanti, pp. 9-15. San Diego: Academic Press.

86. Nikolovski J, Mooney DJ. 2000. Smooth muscle cell adhesion to tissue engineering scaffolds. *Biomaterials* 21: 2025-32.

87. Olsen BR. 1997. Matrix Molecules and Their Ligands. In *Principles of Tissue Engineering*, ed. R Lanza, R Langer, W Chick, pp. 47-65: R. D. Landes Company.

88. Pezzin APT, Alberda van Ekenstein GOR, Duek EAR. 2001. Melt behaviour, crystallinity and morphology of poly(p-dioxanone). *Polymer* 42: 8303-6.

89. Ray JA, Doddi N, Regula D, Williams JA, Melveger A. 1981. Polydioxanone (PDS), a novel monofilament synthetic absorbable suture. *Surgery, Gynecology & Obstetrics* 153: 497-507.

90. Rayleigh L. 1882. On the Equillibrium of Liquid Conducting Masses Charged with Electricity. *The London, Edinburgh and Dublin Philosophical Magazine and Journal of Science* 44: 184-6.

91. Reneker DH, Chun I. 1996. Nanometre diameter fibres of polymer, produced by electrospinning. *Nanotechnology* 7: 216-23.

92. Reneker DH, Yarin AL, Fong H, Koombhongse S. 2000. Bending instability of electrically charged liquid jets of polymer solutions in electrospinning. *Journal of Applied Physics* 87: 4531-47.

93. Riesle J, Hollander AP, Langer R, Freed LE, Vunjak-Novakovic G. 1998. Collagen in tissue-engineered cartilage: types, structure, and crosslinks. *Journal of Cellular Biochemistry* 71: 313-27.

94. Rosenberg MD. 1963. Cell guidance by alterations in monomolecular films. *Science* 139: 411-2.

95. Rovensky Y, Samoilov VI. 1994. Morphogenetic response of cultured normal and transformed fibroblasts, and epitheliocytes, to a cylindrical substratum surface. Possible role for the actin filament bundle pattern. *Journal of Cell Science* 107 (Pt 5): 1255-63.

96. Rudert M, Hirschmann F, Schulze M, Wirth CJ. 2000. Bioartificial cartilage. *Cells, Tissues, Organs* 167: 95-105.

97. Sanders JE, Stiles CE, Hayes CL. 2000. Tissue Response to Single-Polymer fibers of Varing Diameters: Elavuation of fibrous encapsulation and macrophage density. *Journal of Biomedical Materials Research* 52: 231-7.

98. Santavirta S, Konttinen YT, Saito T, Gronblad M, Partio E, et al. 1990. Immune response to polyglycolic acid implants. *The Journal of Bone And Joint Surgery. British Volume* 72: 597-600.

99. Shin M, Ishii O, Sueda T, Vacanti JP. 2004. Contractile cardiac grafts using a novel nanofibrous mesh. *Biomaterials* 25: 3717-23.

100. Shin YM, Hohman MM, Brenner MP, Rutledge GC. 2001. Electrospinning: A whipping fluid jet generates submicron polymer fibers. *Applied Physics Letters* 78: 1149-51.

101. Shin YM, Hohman MM, Brenner MP, Rutledge GC. 2001. Experimental characterization of electrospinning: the electrically forced jet and instabilities. *Polymer* 42: 9955-67.

102. Smith LA, Ma PX. 2004. Nano-fibrous scaffolds for tissue engineering. *Colloids and Surfaces B: Biointerfaces* In Press, Corrected Proof.

103. Spivak AF, Dzenis YA, Reneker DH. 2000. A model of steady state jet in the electrospinning process. *Mechanics Research Communications* 27: 37-42.

104. Srinivasan G, Reneker DH. 1995. Structure and Morphology of Small-Diameter Electrospun Aramid Fibers. *Polymer International* 36: 195-201.

105. Starke GR, Douglas AS, Conway DJ. 1999. An Integral Mathematical Approach to Tissue Engineering of Vascular Grafts. In *Tissue Engineering of Prosthetic Vascular Grafts*, ed. P Zilla, HP Greisler, pp. 441-59: R.G. Landes Company.

106. Stitzel JD, Pawlowski KJ, Wnek GE, Simpson DG, L. BG. 2001. Arterial smooth muscle cell proliferation on a novel biomimicking, biodegradable vascular graft scaffold. *Journal of Biomaterials Applications* 15: 1-12.

107. Taylor G. 1969. Electrically Driven Jets. *Proceedings of the Royal Society of London Series A* 313: 453-75.

108. Terracio L, Rubin K, Gullberg D, Balog E, Carver W, et al. 1991. Expression of collagen binding integrins during cardiac development and hypertrophy. *Circulation Research* 68: 734-44.

109. Thapa A, Webster TJ, Haberstroh KM. 2003. Polymers with nano-dimensional surface features enhance bladder smooth muscle cell adhesion. *Journal of Biomedical Materials Research* 67A: 1374-83.

110. Tomihata K, Suzuki M, Ikada Y. 2001. The pH dependence of monofilament sutures on hydrolytic degradation. *Journal of Biomedical Materials Research* 58: 511-8.

111. Trentham DE, Townes AS, Kang AH. 1977. Autoimmunity to type II collagen an experimental model of arthritis. *The Journal of Experimental Medicine* 146: 857-68.

112. Tyagi SC. 2000. Physiology and homeostasis of extracellular matrix: cardiovascular adaptation and remodeling. *Pathophysiology* 7: 177-82.

113. Vacanti JP, Vacanti CA. 1997. The Challenge of Tissue Engineering. In *Principles of Tissue Engineering*, ed. R Lanza, R Langer, W Chick, pp. 1-5: Academic Press.

114. Vasenius J, Vainionpaa S, Vihtonen K, Makela A, Rokkanen P, et al. 1990. Comparison of in vitro hydrolysis, subcutaneous and intramedullary implantation to evaluate the strength retention of absorbable osteosynthesis implants. *Biomaterials* 11: 501-4.

115. von Wild KR. 1999. Examination of the safety and efficacy of an absorbable dura mater substitute (Dura Patch) in normal applications in neurosurgery. *Surgical Neurology* 52: 418-24; discussion 25.

116. Webster TJ, Schadler LS, Siegel RW, Bizios R. 2001. Mechanisms of enhanced osteoblast adhesion on nanophase alumina involve vitronectin. *Tissue Engineering* 7: 291-301.

117. Williams DF, Mort E. 1977. Enzyme-accelerated hydrolysis of polyglycolic acid. *Journal of Bioengineering* 1: 231-8.

118. Wnek GE, Carr M, Simpson DG, Bowlin GL. 2003. Electrospinning of nanofiber fibrinogen structures. *Nano Letters* 3: 213-6.

119. Wong WH, Mooney DJ. 1997. Synthesis and properties of biodegradable polymers used as synthetic matrices for tissue engineering. In *Synthetic Biodegradable Polymer Scaffold*, ed. A Atala, D Mooney, JP Vacanti, R Langer, pp. 50-82. Boston: Birhauser.

120. Xu CY, Inai R, Kotaki M, Ramakrishna S. 2004. Aligned biodegradable nanofibrous structure: a potential scaffold for blood vessel engineering. *Biomaterials* 25: 877-86.

121. Yao L, Haas TW, Guiseppi-Elie A, Bowlin GL, Simpson DG, Wnek GE. 2003. Electrospinning and stabilization of fully hydrolyzed poly(vinyl alcohol) fibers. *Chemistry of Materials* 15: 1860-4.

122. Yarin AL, Koombhongse S, Reneker DH. 2001. Bending instability in electrospinning of nanofibers. *Journal of Applied Physics* 89: 3018-26.

123. Yarin AL, Koombhongse S, Reneker DH. 2001. Taylor cone and jetting from liquid droplets in electrospinning of nanofibers. *Journal of Applied Physics* 90: 4836-46.

124. Yoshimoto H, Shin YM, Terai H, Vacanti JP. 2003. A biodegradable nanofiber scaffold by electrospinning and its potential for bone tissue engineering. *Biomaterials* 24: 2077-82.

125. Zeleny J. 1914. The electrical discharge from liquid points, and a hydrostatic method of measuring the electric intensity at their surface. *The Physical Review* III: 69-91.

126. Zeleny J. 1917. Instability of electrified liquid surfaces. *The Physical Review* X: 1-8.

127. Zong X, Kim K, Fang D, Ran S, Hsiao BS, Chu B. 2002. Structure and process relationship of electrospun bioabsorbable nanofiber membranes. *Polymer* 43: 4403-12.

128. Zong X, Ran S, Fang D, Hsiao BS, Chu B. 2003. Control of structure, morphology and property in electrospun poly(glycolide-co-lactide) non-woven membranes via post-draw treatments. *Polymer* 44: 4959-67.

APPENDIX A

Appendix A includes an encyclopedia chapter titled Poly(glycolic acid) included in The Encyclopedia of Biomaterials and Biomedical Engineering edited by Gary L. Bowlin and Gary E. Wnek (17). This work provides greater details about the processing, degradation and medical uses of poly(glycolic acid).

Poly (Glycolic Acid)

Eugene D. Boland[1], Gary E. Wnek[2] and Gary L. Bowlin[1]

[1] Department of Biomedical Engineering
Virginia Commonwealth University
Richmond, VA 23298-0694

[2] Department of Chemical Engineering
Virginia Commonwealth University
Richmond, VA 23298-3028

KEYWORDS: Poly(glycolic acid), PGA, bioresorbable, ester, biodegradation, polymer

INTRODUCTION

Poly (glycolic acid) (PGA) is a synthetic polymer that degrades to natural metabolic waste products. The chemical structure of glycolic acid can be written as $HOCH_2COOH$, noting that the molecular termination is by a hydroxyl group on one end and by a carboxyl group on the other. Glycolic acid, also known as hydroxyacetic acid, is found naturally in young plants and in green fruits. Glycolate, which is the ester or salt form of the acid, is produced from ribulose 1,5 bisphoshate (a Calvin cycle initiator) in chloroplasts and transferred to peroxizomes where it is oxidized to glyoxylate, which can be transaminated to the amino acid glycine. It is further processed in the mitochondria, passed back to the peroxisome for transamination and reduction then finally passed back

to the chloroplast as glycerate where adenosine tri-phosphate (ATP) phosphorylates it. The 3-phospho-glycerate can then re-enter the Calvin cycle for sugar production. This process, called photorespiration, is a seemingly wasteful side reaction of photosynthesis that consumes both oxygen and ATP and produces carbon dioxide and hydrogen peroxide. In human metabolism, the specific glycolic acid oxidase is not present but it may be slowly oxidized and transaminated to glycine in a similar manner. This slow metabolism would lead to localized build up of glycolic acid, the ramifications of which will be discussed later as pertaining to the *in vivo* tissue response.

SYNTHESIS OF PGA

After one has sufficient quantity of monomer from either an extraction and purification from plants (84) or synthesis in the laboratory, the polymer can be synthesized. Two different methods can be employed to produce the polymer. The first is polycondensation. In condensation reactions, the monomer subunits react and release a small molecule such as water (3). Since glycolic acid contains two functional groups that can participate in a condensation reaction, it can self-polymerize (3, 119). The basic reactions involve creating dimers from two monomers, tetramers from two dimers, and so on, to eventually form polymer (see Scheme 1).

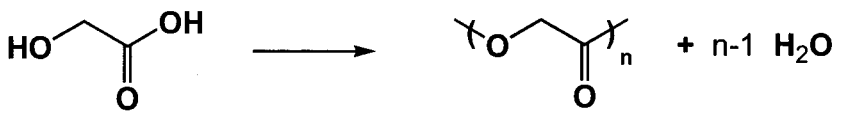

Scheme 1. Condensation polymerization of glycolic acid to PGA. Note that the number of repeating units, n, in the polymer is an average number

The reaction is characterized by the early disappearance of monomers from the solution and the slow increase of high molecular weight species. Due to the random nature of the polymer formation, there is a broad molecular weight distribution throughout the reaction and significant concentrations of high molecular weight polymers are difficult to achieve (3, 119). Adding to the difficulty, common commercial esterification catalysts such as antimony trioxide also catalyze the reverse reaction, namely depolymerization (119). Moreover, glycolic acid has a great tendency to cyclodimerize to glycolide (see Scheme 2), thus ending its reactivity in condensation reactions.

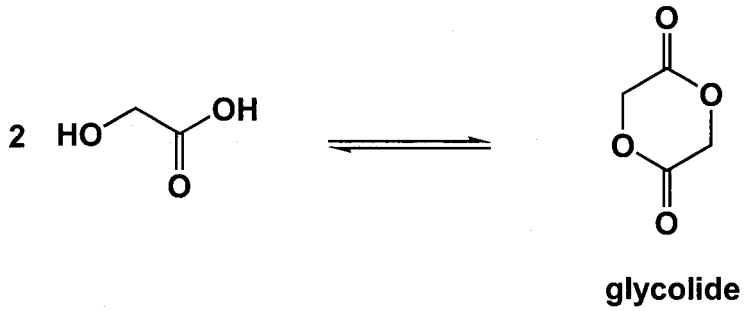

glycolide

Scheme 2. Dimerization of glycolic acid to glycolide

Due to these drawbacks, a second method of preparing PGA is preferred, namely, ring opening polymerization (ROP) of glycolide, (see Scheme 3) (119).

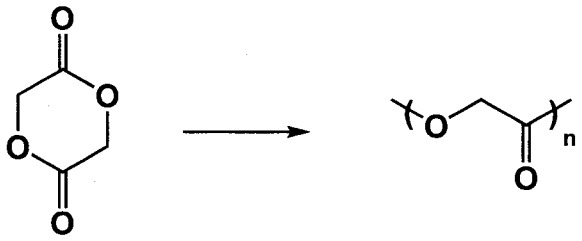

Scheme 3. Ring-opening polymerization of glycolide to PGA

Depending on the catalyst used, these polymerization reactions can be anionic, cationic, or involve insertion mechanisms. Of these mechanisms, insertion using metal alkoxides or carboxylates as catalysts is the most commercially viable and therefore will be the only method discussed. The tin (see Scheme 2) octoate catalyst is the most commonly used due to its acceptance by the U.S. Food and Drug Administration (FDA) as a food stabilizer (119). The polymerization of glycolide is typically carried out in bulk at 220°C for 4 hours. This results in a 96% conversion to polymer with molecular weights ranging from 10^4 to 10^6 Daltons (119). As is the case with polyesters in general, equilibration reactions such as ester interchange and chain unzipping may take place, the effects of which would be the formation of shorter chains and low molecular weight species such as cyclic dimers, trimers and, to a lesser extent, cyclic oligomers and even monomers (3, 119). These species can drastically affect the mechanical properties of the final products and their production must be carefully monitored and avoided if possible. This ROP method can also be employed to form copolymers with other α-hydroxy acids (of the general form $-[-O-CH(R)-CO-]-$). Other copolymerization methods include ABA block copolymer formations with a monoester group of poly (ethylene glycol) or fatty acids (7). These various copolymers of glycolide also have significant uses in medicine.

PGA CHARACTERIZATION

The regularity of the PGA backbone and its rather compact repeat unit suggests that the polymer will tend to at least partially crystallize. Indeed, early x-ray diffraction work reveals that the unit cell contains two anti-parallel polymer chains, and that these

chains have a sheet-like molecular arrangement of planar 'zig-zag' conformations. Also, the C=O groups of adjacent polymers in the unit cell overlap (see Figure 1.)

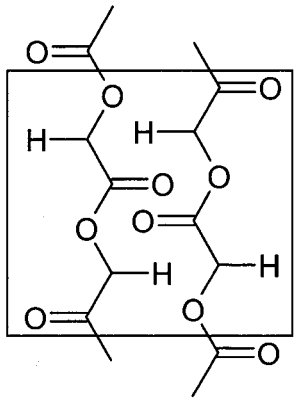

Figure 1. Crystal Structure of Polyglycolide

The density of the crystal was determined to be rather high at 1.69 grams per cm^3. It was suggested that the close approach of ester groups, resulting in tight molecular packing, produces the abnormally high melting temperature and insolubility of the polymer (25).

PGA DEGRADATION

Biodegradation is the destruction of one or more chemicals by biological processes. PGA is not removed by biodegradation alone but also mechanisms of hydrolytic degradation, erosion and bioabsorption. Hydrolytic degradation is the breakdown of a material by physical or chemical interactions with water and bioabsorption is the uptake of material by a cell. Hydrolytic degradation is the predominant mechanism of PGA breakdown resulting in the loss of mechanical strength (59).

There have been many theories about the hydrolytic degradation of PGA. All the theories have had two central dogmas: first, the amorphous region of the polymer is quickly degraded which results in a significant loss of mechanical properties in a matter of days to weeks, and secondly, the crystalline region of the remaining fragments degrade more slowly yet crystallinity remains measurable until the material is completely degraded. One such theory was formulated from a detailed multi-time point analysis described by Hurrell and Cameron (6), they employed analysis techniques that included small and wide angle X-ray scattering (SAXS and WAXS, respectively), mass measurement, differential scanning calorimetry, pH measurement and UV-spectrophotometry. One key finding was that as the degradation proceeded, the intensity of the crystal peaks on the WAXS profiles increased with respect to the amorphous halo (59). This confirms earlier findings that the amorphous region degrades first leaving the crystalline regions intact (119). This observation continued over the first 10 days, at which time the crystallinity leveled off and the amorphous halo was only faintly visible. Again this observation is supported by clinical findings that PGA sutures lose most of their strength in the first two weeks (119). Another valuable observation is the rapid drop in the glass transition temperature over the first 6 hours and then it continues to drop at a much slower rate. This rapid drop may indicate that water had diffused to the center of the sample in the first 6 hours – this corresponds well with the previously reported diffusion constant of $5.0 \pm 1.0 \times 10^{-9}$ cm^2 s^{-1} of water into PGA (59). A final observation showed a dramatic drop in pH after about 10 days despite being in a buffered solution (59) which indicated that glycolic acid is released during the first 10 days but the rate of

release may increase dramatically around the 10-day point. In all the techniques applied to analyzing PGA degradation, a dramatic change in rate or morphology was noted at the 10-day point.

These observations and calculations helped devise the following four-stage degradation profile:

- The first stage of the degradation process is characterized by homogeneous diffusion of the hydrolytic solution into the sample. A sharp drop in the glass transition temperature characterizes this stage. For their model, this stage occurred over the first 6 hours.
- The second stage is that of homogeneous hydrolysis. During this stage there is solution absorbed and relatively low mass loss. The chain hydrolysis reduces the polymer fractions to a critical molecular weight that is capable of diffusing from the solid. This stage took place over the first 10 days.
- The end of the second stage and beginning of the third stage is marked by a significant drop in the localized pH. This pH drop is a function of oligomer diffusion from the construct. Cameron theorizes that as oligomers diffuse out and additional fluid diffuses in, a reaction-erosion front forms on the surface (59). This would expedite the degradation of the sample and address crystal breakdown. Due to the observation that cracks originate on the surface and proceed inward during hydrolysis, it is believed that these fronts proceed inward via hydrodynamic forces and eventually reach the opposing front at the center.

- The time at which these fronts meet is the onset of stage four. During stage four, only small crystalline fragments remain within the implant site. There is no structural integrity left in the implant and the stage concludes at the removal of all traces of the PGA (59).

With hydrolytic degradation of polyesters, changing the pH of the hydrolytic media can significantly alter the rate of degradation. This would be an interesting aside if one were to assume all bodily tissues and fluids remained at a pH near 7.4. While this may be true for the majority of bulk tissues and fluids, it is certainly not the rule. Localized pH values of 1 are common in the stomach but the pH in the small intestine and bladder often exceed 10. In addition to regional pH differences, one must be aware of the local affects of inflammatory and foreign body responses. Depending on the cells recruited, local effectors can either raise or lower the pH depending on the proteins involved. To compare pH effects, an experiment was developed to degrade PGA suture material in three different buffered solutions. The three different buffer solutions were maintained as acidic (pH=5.25), slightly alkaline (pH=7.44) and strongly alkaline (pH=10.09). During the degradation process, samples were tested for strength retention (standard uniaxial fiber testing in a controlled environmental chamber) (26). Other experimentation added scanning electron microscopy (SEM) to evaluate surface morphology during degradation (26, 28). Initial results found that the suture material degraded significantly faster in the strong alkaline solution than in either of the less alkaline solutions. In fact, there was no significant difference in the degradation behavior of the acidic or slightly alkaline treated samples prior to 21 days of immersion. Two

possible factors could be responsible for differences seen in this study: the so-called "cage-effect" in the crystalline regions and the pH effect on the ability to form hydrogen bonds (26).

The hydrolysis of simple organic esters in acidic media follows the general mechanism in Scheme 4.

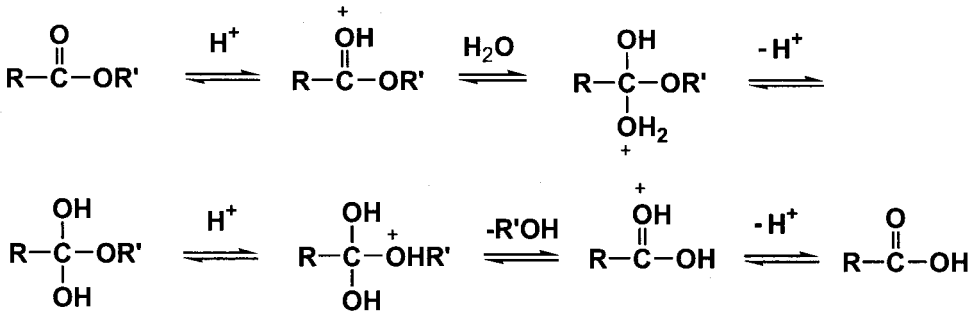

Scheme 4. Acid-catalyzed ester hydrolysis

It is believed that the reversal process of two fragmentary ends rejoining in the amorphous region is insignificant due to chain mobility, but this cannot be said about the crystalline regions. Two chains held in a crystal lattice that are separated by hydrolytic cleavage have a greater chance to recombine. This is the so-called "cage effect". If this does indeed exist, it could slow down the degradation in acidic or near neutral pH buffer conditions. The cage effect may not even be restricted to the crystalline regions. If sufficiently immobile polymers, either due to high viscosity or high molecular weights, a cage could be created in amorphous regions as well (26, 28).

The same cannot be said in the presence of a strong alkaline-buffered solution due to the irreversibility of hydrolysis (26, 28, 110). Alternatively, it has been reported that

the capability of adjacent polymer chains to form hydrogen bonds is significantly reduced or even lost at higher pH levels. Since hydrogen bonding was previously identified as a contributing factor to PGA's crystallinity and stability (25), it would stand to reason that the elimination of those bonds could accelerate degradation. A relatively "looser" structure would be more open to attack (110).

It is likely that both of these mechanisms contribute to the hydrolytic degradation of PGA. The cage effect would be more pronounced in acidic or neutral attacks and the reduction of pH dependent hydrogen bonding would be more pronounced in strong alkaline attacks. The former mechanism preserves the crystalline regions while the latter rapidly degrades the amorphous regions. These mechanisms are closely tied to the experimental observations if we accept a chain scission model. This model states that chain scission during hydrolytic degradation begins at tie-chain segments at the point where the rigid crystals tie into the amorphous chains (26, 28, 33). These ends carry the load in the bulk polymer and are most susceptible to move during hydrolytic cleavage in acidic or neutral attacks. The tie-chains are also theorized to participate in extensive hydrogen bonding with the crystal lattices and are therefore prone to dissociate with strong alkaline attacks. Both outcomes can predict the loss of mechanical strength and elasticity observed experimentally (26, 110).

Localized pH is not the only effectors that can change degradation rates *in vivo*. The role of enzymes has also been identified as contributing to the degradation of PGA. As stated earlier, humans do not possess the specific glycolic acid oxidase that can expedite breakdown and removal of PGA but we do possess a number of non-specific

esterases and proteases that may be expressed by cells recruited in a foreign body response to implanted polymers (110). Experiments have demonstrated that certain families of enzymes increased the rate of degradation of PGA *in vitro* (117). Specifically, the presence of bromelain, esterase, or leucine animopeptidase reduced the complete degradation time of PGA sutures to less than 1 week from the previously reported values ranging from 2-4 weeks (7, 117, 119). This *in vitro* work prompted an *in vivo* exploration of implant sites. Large quantities of acid phosphatase and leucine animopeptidase were found at the implant sites of orthopedic PGA fixatives. While the biodegradation properties of leucine animopeptidase were seen *in vitro*, acid phosphatase did not enhance *in vitro* degradation (117). The role of the acid phosphatase is unclear, but it has been speculated to play a role in absorption (117).

PGA APPLICATIONS

As previously mentioned, PGA is a semi-crystalline material with a high melting temperature and low solubility. In fact, the only known means of solvent processing PGA is in hexafluoroisopropanol or hexafluoroacetone sesquinhydrate in carbon tetrachloride (59, 60). Both of these solvents, however, have high toxicity levels appropriate for yarn or fabric production but not for drug delivery, since the drug may react with the solvent or trace amounts of the solvent could be incorporated into the end product. Melt processing is the typical commercial method, specifically, hot drawn fibers or melt pressed molding. With the former technique, fiber diameters as low as 10 μm can be produced and the latter is capable of larger sized constructs typically for orthopedic applications (5, 119). These fibers can then be further processed through winding,

weaving and braiding techniques to produce currently marketed products such as suture and wound dressings (5, 37, 119). Several products have been commercially available since the early 1970's and have paved the way for new advances in PGA processing and products.

Current medical research involving PGA is in four key areas: drug delivery, orthopedic fixation, degradable sutures and tissue engineering. As previously stated, PGA has many drawbacks as a drug delivery device except its rapid and predictable degradation. To avoid toxicity of solvents, scientists sought a drug that was thermally stable at temperature compatible with melt processing PGA (60). For this study, their drug of choice was Theophylline, a bronchodialator that is used in the treatment of chronic asthma and pulmonary disease. The drug is water soluble, weakly basic and sublimes without degradation at temperature above PGA's processing temperature (60). Even at low concentrations, its inclusion prevented crystal formation in PGA, which may be evidence of even distribution throughout the polymer, and should give a more even dosage. Both of these theories proved correct, illustrating the strength of PGA as a drug delivery polymer. A rather steady dispensing of the drug from day 6 to day 15 was observed (60) which provided additional support to their previous theory on the four-stage degradation process of PGA.

The second area of interest is in orthopedic fixation devices, namely, rods, plates, and screws. Two different uses are emerging: The first is as a binding agent with other polymers such as calcium phosphate fibers (62), and the second is as a self reinforced polymer (114). In the former application, PGA is used to provide initial support that is

gradually reduced until the calcium phosphate is carrying the full load. Nevertheless, a material with a two-week degradation time may not be adequate for bone repair. To slow the rate of hydrolytic degradation, researchers chose a novel surface plasma treatment (CH_4 and Parlene®) to make the surface more hydrophobic (62). In doing so, they slowed the rate of media uptake and therefore slowed the first stage of degradation, which appears to be pivotal in the overall degradation rate. These plasma coatings were found to be non-toxic and thus provide a new method to decrease the degradation rate of PGA to counter the many factors that can increase the rate of degradation. Along a similar methodology, a method of coating self-reinforced PGA (sintered suture) with another slower degrading polymer is presented (114). The constructs were briefly submerged in chloroform containing polydioxanone, poly-hydroxybutyric acid, or poly(lactic acid). This was done to form a thin, slowly degrading coating that would prevent water uptake by the PGA construct. The idea may have been sound but the application suffered cracking and delamination and was eventually ruled out since it did not statistically decrease the degradation rate of the constructs *in vivo*. It was concluded by this group that self-reinforced PGA materials degrade too rapidly to be effective internal fixatives for cortical bone fractures (114).

The third area of interest returns to sutures. As long as surgeons are cutting into the body, there will be a quest for the perfect suture. One that can be used anywhere, has strong knot retention, retains strength long enough for complete closure and avoids adverse affects on healing. This has led researchers to re-evaluate modifications to PGA that affect its strength and degradation rate. One such approach has been to anneal the

suture material for different lengths of times and at different temperatures while subjecting the suture to a slight axial load (22). The idea is that the crystalline regions will align along the long axis of the suture and polymer chains in the amorphous regions will straighten to increase strength and decrease the degradation rate. This was the response elicited from the testing. A very complex relationship emerged that linked annealing temperature and load with hydrolytic degradation and mechanical properties (22). Further evaluation will be necessary to test the limits of these relationships.

The emerging discipline of tissue engineering is reaching into many aspects of anatomy and physiology, from wound closure to full organ replacement. Electrospinning is the deliberate charging of a polymer, either in solution or melt, by applying a high voltage potential between that solution and a grounded target. The phenomenon of combining electrospinning with tissue fabrication, which occurs when electrical forces at the surface of the polymer solution overcome the surface tension, creates a polymer solution jet. This jet produces fibers with diameters from microns to nanometers (down to 50 nm) (33). Many factors can affect the morphology of electrospun fibers, although these variables have only recently been examined with PGA.

As described earlier, PGA can be tailored into many different scaffold configurations utilizing electrospinning. Electrospinning uses a static electric field to draw the polymer fibers out of solution rather than a mechanical drawing or ejection system previously described for fiber formation. PGA fibers can be produced from 1.2 ± 0.4 μm diameters at a 140-mg/ml concentration in hexafluoroisopropanol to 110 ± 40 nm diameters at a 50-mg/ml concentration. Fiber diameter varied linearly with concentration.

Fiber alignment, as depicted in the micrograph in Figure 2, was achieved through rotation and translation of the grounded target. Fibrous mats produced in this manner demonstrated significant mechanical strength and anisotropic properties related to fiber orientation. It is speculated that these relationships can be exploited to develop a wide variety of biomimicking tissue engineering scaffolds (18).

PGA REGULATORY ISSUES

Regulatory pathways have not always been as critical. The United States federal government did not tightly regulate initial PGA products (approved for sale prior to medical device amendment to the Food, Drug and Cosmetic Act in 1976), however, new devices or drugs will be much more thoroughly scrutinized for compliance to specific parts of the Good Manufacturing Practices as outlined in CFR title 21 (2, 68). Even with this scrutiny, similar products can still be expedited through the regulatory process. And as often the case, the first product approved becomes the standard to which all others are measured. Outside the United States, the European Union has established the European Medicines Evaluation Agency (EMEA) to regulate the marketing of medical products as either a medical device or medicinal product. Similarly, the Japanese Pharmaceutical and Medical Safety Bureau (PMSB) requires demonstration of safety and efficacy of medical products regulated as either medical devices or pharmaceuticals. Regulation of PGA products are increasingly hard to characterize as devices, drugs or biologics and approval for use must be sought on a case by case, country by country basis. Further information about issues facing tissue engineered products can be found in a World Technology Evaluation Center (WTEC) report on tissue engineering research (78).

One area that is always a concern of the regulatory bodies is the sterilization of products. Gamma irradiation is becoming a popular method to sterilize everything from latex gloves to lunchmeats. Care should be taken before applying this technology to PGA constructs. It has been reported that gamma irradiation can significantly affect the degradation properties of PGA. Utilizing the techniques of electron spin resonance (ESR) analysis and scanning electron microscopy, chain scission and degradation were monitored *in vitro*. Gamma irradiation of ester groups can enhance the susceptibility to form chain scissions even at a normal sterilization dose of 25 kilograys (kGy) (4). At this dosage, total mechanical strength is lost during the first 10 days in buffered media. Significant decrease in the molecular weight after irradiation was measured and ESR confirmed many chain scission radicals in the polymer chains. Although initial SEM analysis showed no difference before placing the samples in media, it became quickly apparent that irradiated samples degraded at a much faster rate and appeared to degrade by the same mechanism. This provides confirmation that merely inspecting for cracks cannot accurately predict damage caused by gamma irradiation. It would be advisable to select an alternate means of sterilization (4).

PGA *IN VIVO* TISSUE RESPONSE

In addition to regulatory issues, such as sterilization, the greatest hurdle is often tissue compatibility. Work has been done to describe the immune response to PGA implants. In general, they are very acceptable. The principle cell type found in effusion samples around PGA implants was a small lymphocyte, although a few monocytes were also found (98). This could be interpreted as a slight foreign body response to the implant

but the absence of neutrophils supports a non-infectious response, possibly a lymphocyte-mediated immunological reaction (98). These data can be taken to show PGA is relatively inert immunologically, however, inert may not be good enough for the next generation of tissue engineering materials. It would be desirable to create materials that are bioactive, that is to say they cause a biological response. The desired response would be that of natural healing and incorporation not encapsulation.

Many groups are racing to find the "magic" material that promotes natural healing, augments native tissues (if desired), or is capable of replacing native tissue with a new tissue construct. One such approach was to take highly porous PGA matrices of non-woven 12 micron diameter fibers and implant them subcutaneously in a rat model to see if native tissue would grow into the matrix and form a new tissue mass. Initially, the matrices were encapsulated, but with time, the capsule thinned and cells migrated into the matrix. Histological examination showed the cells migrated from the skeletal muscle rather than from the skin or adipose tissue (53). Much to researchers' dismay, the tissue receded as the matrix degraded. Upon complete degradation of the matrix, no trace of the cells that had previously ingrown could be found and no internal scar was evident even though a fibrous capsule previously existed in that location. When comparing PGA to other matrix material, less neo-vascularization was noticed. It was postulated that the rapid release of glycolic acid into the local environment dropped the localized pH and down regulated vascular formation (53).

Another approach taken with a PGA based product was pre-hydrolyzing the surface to promote cell adhesion (47). The premise of this research is that short-term

exposure to an alkaline solution will begin hydrolyzing the surface of the matrix and improve its wetting behavior and ultimately make it a more suitable cell culture surface. SEM analysis revealed surface erosion without crack formation from this processing. A 50% mass reduction in the fibers of the matrix was targeted (13 μm diameter fibers reduced to 9μm). Wetting behavior was also effected by this treatment by changing the surface composition from 51% carbon and 49% oxygen to 49% carbon and 51% oxygen as measured by XPS (47). This increase in oxygen on the surface could account for the increased hydrophilic nature of the surface. Through this experimental technique, they were able to devise a way to improve static, *in vitro* cell seeding densities (47). They did not expand to animal trials nor did they do long term seeding studies to see if the trend continued.

The final method to be presented is work being done to enhance the usefulness of PGA as a tissue-engineering polymer. The focus of this work can be surmised as encapsulation versus incorporation. Many researchers have shown that PGA is encapsulated by collagen during the degradation process. This may be acceptable for sutures but not a tissue scaffold. Building on work with electrospun PGA presented earlier, one would want to look at cellular response to the material/matrix construct. Scientists have described a size scale for tissue engineering claiming that cells cannot migrate through pores under 20 to 50 microns. They maintain that small pores promote encapsulation and large pores promote incorporation (82). Nevertheless, unpublished data seems to contradict this dogma. Figures 3 and 4 are two transmission electron

micrographs that show cells within an electrospun PGA matrix with pore sizes below 5 microns and below 0.8 μm, respectively.

Observationally, the micrograph in Figure 3 shows a typical capsule formation by actively secreting fibroblasts where as the micrograph in Figure 4 shows no capsule and high cell densities laying down orderly matrices. The difference between the two is that the first is 1-μm fibers and the second is 0.2μm fibers that were pretreated in 11.7 molar hydrochloric acid. While other research presented claimed no difference in degradation with acidic versus neutral pH buffers, the material was not exposed to as strong an acid. These preliminary findings, if supported by additional analytical and animal experimentations, may bring PGA back into the forefront as a bioabsorbable polymer for medicine, specifically tissue engineering.

APPENDIX B

Appendix B contains the bill of materials to construct the novel electrospinning apparatus described in this document.

Next Generation Electrospinner: Bill of Materials

Quantity	Part / Drawing	Description
1 ea	Drawing: Base	Spinner base
1 ea	Drawing: Base Spacer Block	spacer between spinner base and stage
1 ea	Drawing: Bearing Shaft Adaptor	interface between shaft and free bearing
1 ea	Drawing: Motor Shaft Adaptor	interface between shaft and shaft motor
2 ea	Drawing: Roller Flange (drawn flat)	flange for aligning supports for spinner ring
1 ea	Drawing: Shaft	mandrel for electrospinning
1 ea	Drawing: Spinner Ring	frame for holding and revolving mandrel
1 ea.	Drawing: Stepper Base	Stepper Motor support
4 ea	Drawing: Support Shaft	roller to support spinner ring
4 ea	Drawing Support Shaft Bolt	center support and fastening of support shaft
1 ea	Dolphin Guide: 24 inch travel/1.2" pitch	Stage manufactured by Pacific Bearing
con't	NEMA 23 motor and controller (included)	motor and controller provided by Pacific Bearing (SDP-SI part)
1 ea	SDP-SI P/N S9117M-S18HT / with controller	Stepper Motor from Stock Drive Products
1 ea	MicroMo 1724T024SR motor	Motor and MVP2001 controller for mandrel rotation
1 ea	Stepper Motor driver and controller	McMaster-Carr PN's 6134K61 and 6134K91
1 ea	SDP-SI P/N A 6A 3-12DF03706	aluminum timing pulley (machine ID to match motor)
1 ea	SDP-SI P/N A 6B 3-230037	timing belt for rotary control - 43.2" length
1 ea	.375" ID x .500" OD x 0.5" graphite bushing	couple spinner ring and bearing shaft adaptor
4 ea	#10-32 x 1.25" flat head cap screws	secure base to stage
8 ea	1/4 -20 x 0.375" button head cap screws	secure roller flanges to base
4 ea	#6-32 x 0.5" flat head cap screw	mounting screws for stepper base to base
8 ea	SDP-SI P/N A 7Y55 ESS6225	extended inner race bearings for support shaft
8 ea	1/4 - 20 locking nuts	fastening of Support Shaft Bolts to Roller Flange
6 ea	M1.6 x 3mm socket head cap screw	mounting screws for motor to spinner ring
1 ea	#4-40 x .125 socket head set screw (soft point)	secure bearing shaft adaptor to shaft
1 ea	#2-56 x .125 socket head set screw (soft point)	secure motor shaft adaptor to motor shaft

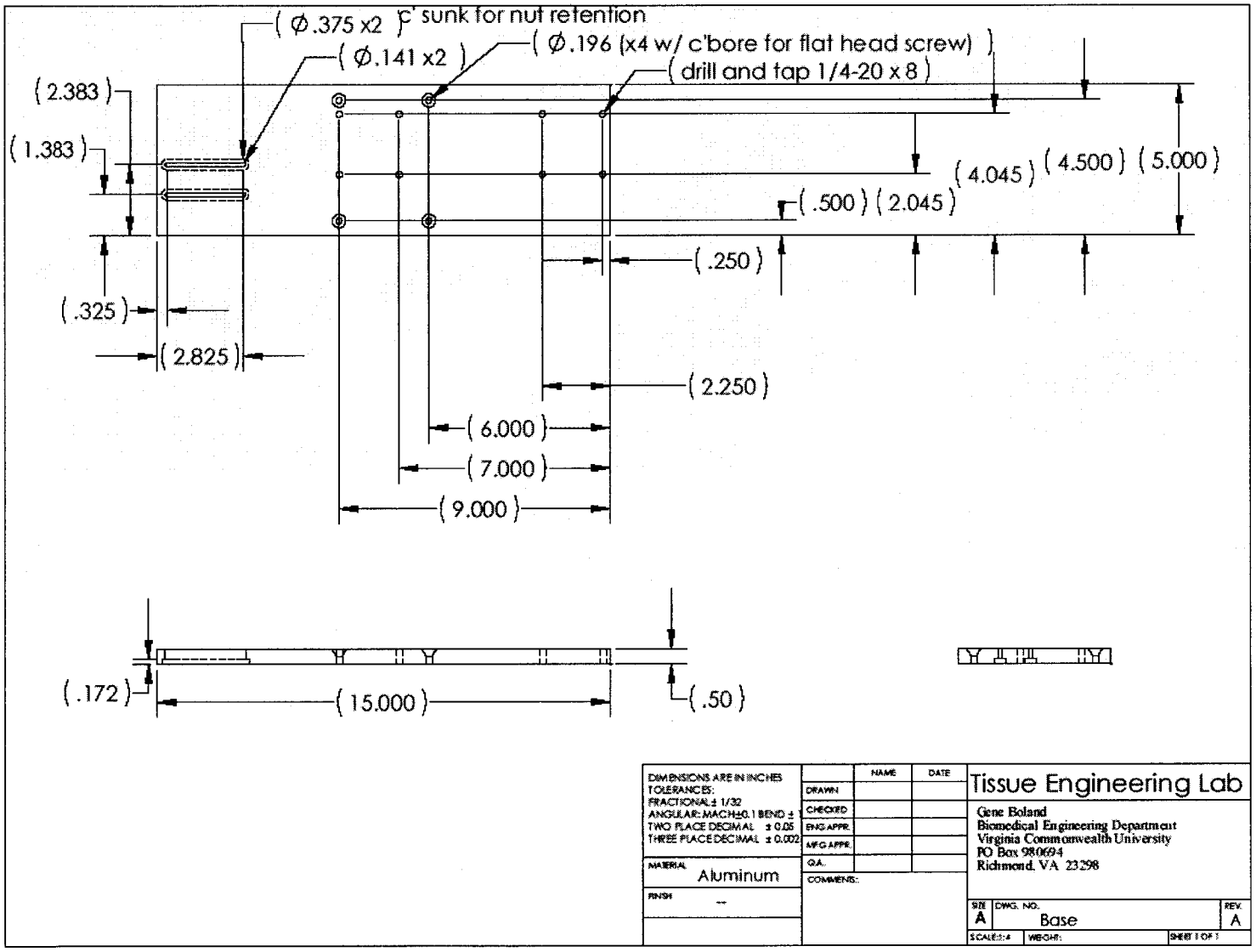
(Ø.375 x2 C' sunk for nut retention
(Ø.141 x2)
(Ø.196 (x4 w/ c'bore for flat head screw))
(drill and tap 1/4-20 x 8)
(2.383)
(1.383)
(4.045) (4.500) (5.000)
(.500) (2.045)
(.250)
(.325)
(2.825)
(2.250)
(6.000)
(7.000)
(9.000)
(.172)
(15.000)
(.50)
DIMENSIONS ARE IN INCHES
TOLERANCES:
FRACTIONAL ± 1/32
ANGULAR: MACH ±0.1 BEND ±
TWO PLACE DECIMAL ± 0.05
THREE PLACE DECIMAL ± 0.002
MATERIAL Aluminum
FINISH --
NAME DATE
DRAWN
CHECKED
ENG APPR.
MFG APPR.
Q.A.
COMMENTS:
Tissue Engineering Lab
Gene Boland
Biomedical Engineering Department
Virginia Commonwealth University
PO Box 980694
Richmond, VA 23298
SIZE A
DWG. NO. Base
REV. A
SCALE: 1:4
WEIGHT:
SHEET 1 OF 1

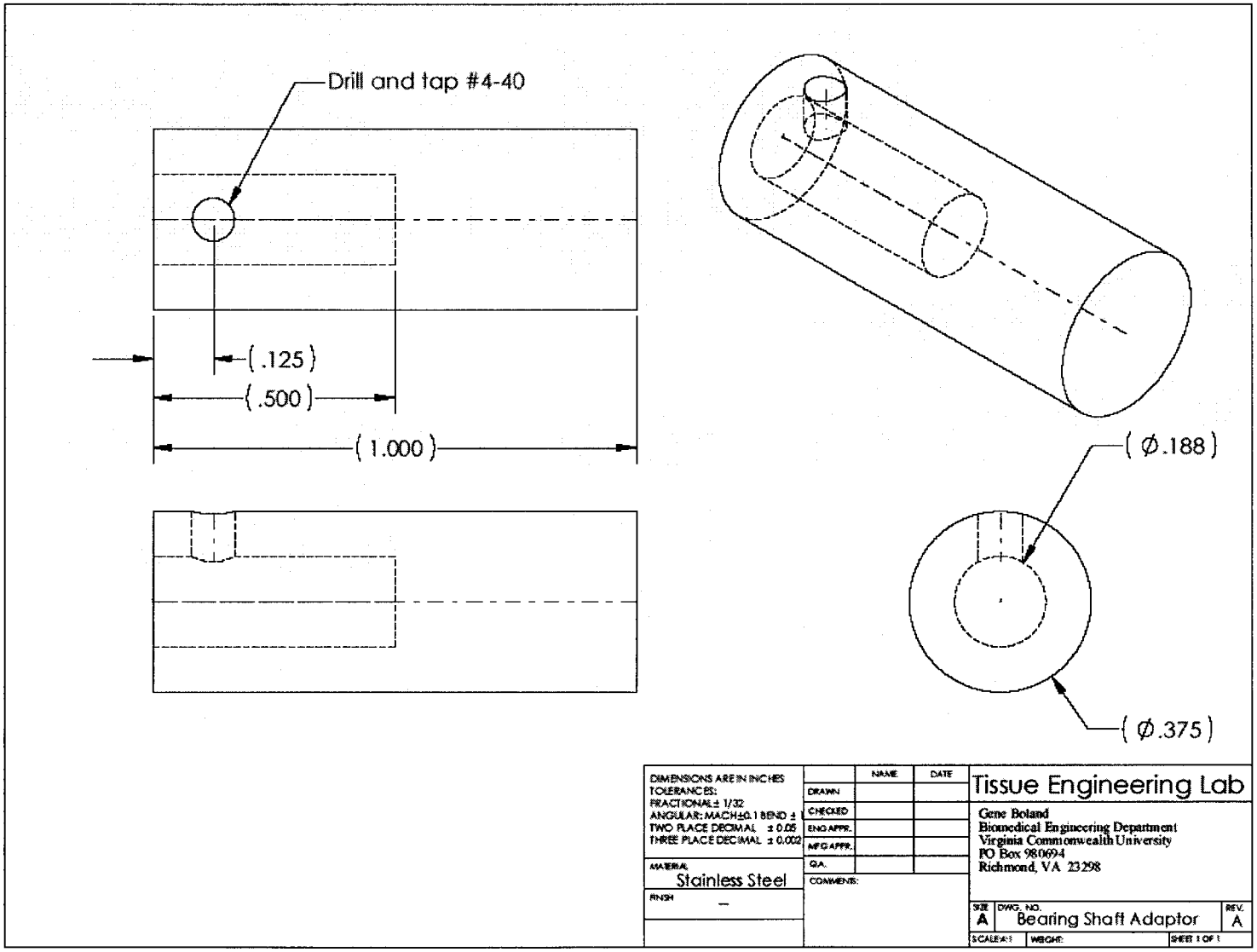
Drill and tap #4-40
(.125)
(.500)
(1.000)
(Ø.188)
(Ø.375)
DIMENSIONS ARE IN INCHES
TOLERANCES:
FRACTIONAL ± 1/32
ANGULAR: MACH ±0.1 BEND ±
TWO PLACE DECIMAL ± 0.05
THREE PLACE DECIMAL ± 0.002
MATERIAL
Stainless Steel
FINISH
—
NAME
DATE
DRAWN
CHECKED
ENG APPR.
MFG APPR.
QA.
COMMENTS:
Tissue Engineering Lab
Gene Boland
Biomedical Engineering Department
Virginia Commonwealth University
PO Box 980694
Richmond, VA 23298
SIZE
A
DWG. NO.
Bearing Shaft Adaptor
REV.
A
SCALE: 4:1
WEIGHT:
SHEET 1 OF 1

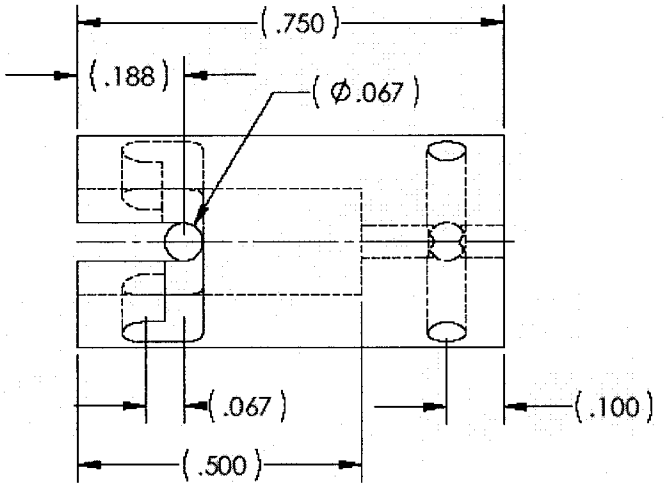

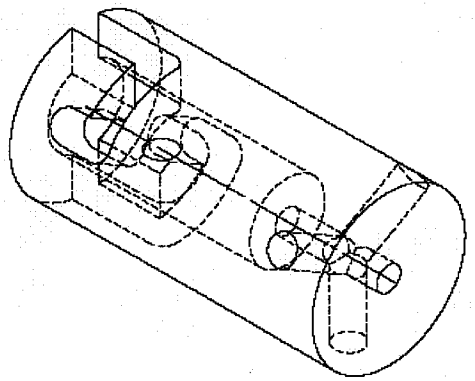

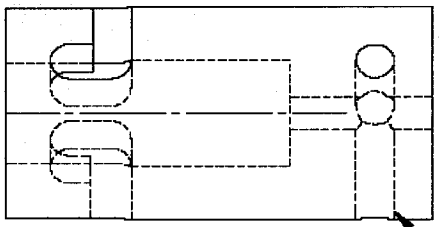

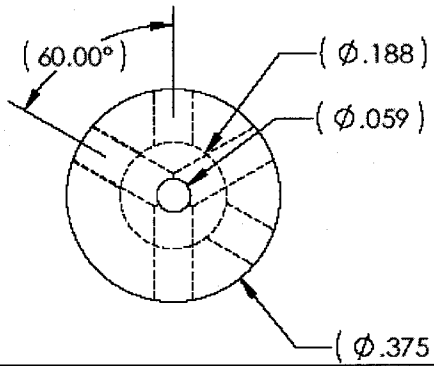

DIMENSIONS ARE IN INCHES TOLERANCES: FRACTIONAL ± 1/32 ANGULAR: MACH ±0.1 BEND ± TWO PLACE DECIMAL ± 0.05 THREE PLACE DECIMAL ± 0.002		NAME	DATE
	DRAWN		
	CHECKED		
	ENG APPR.		
	MFG APPR.		
	Q.A.		
MATERIAL Acetal (delrin)	COMMENTS:		
FINISH —			

Tissue Engineering Lab

Gene Boland
Biomedical Engineering Department
Virginia Commonwealth University
PO Box 980694
Richmond, VA 23298

SIZE	DWG. NO.	REV.
A	Motor Shaft Adaptor	A
SCALE: 1	WEIGHT:	SHEET 1 OF 1

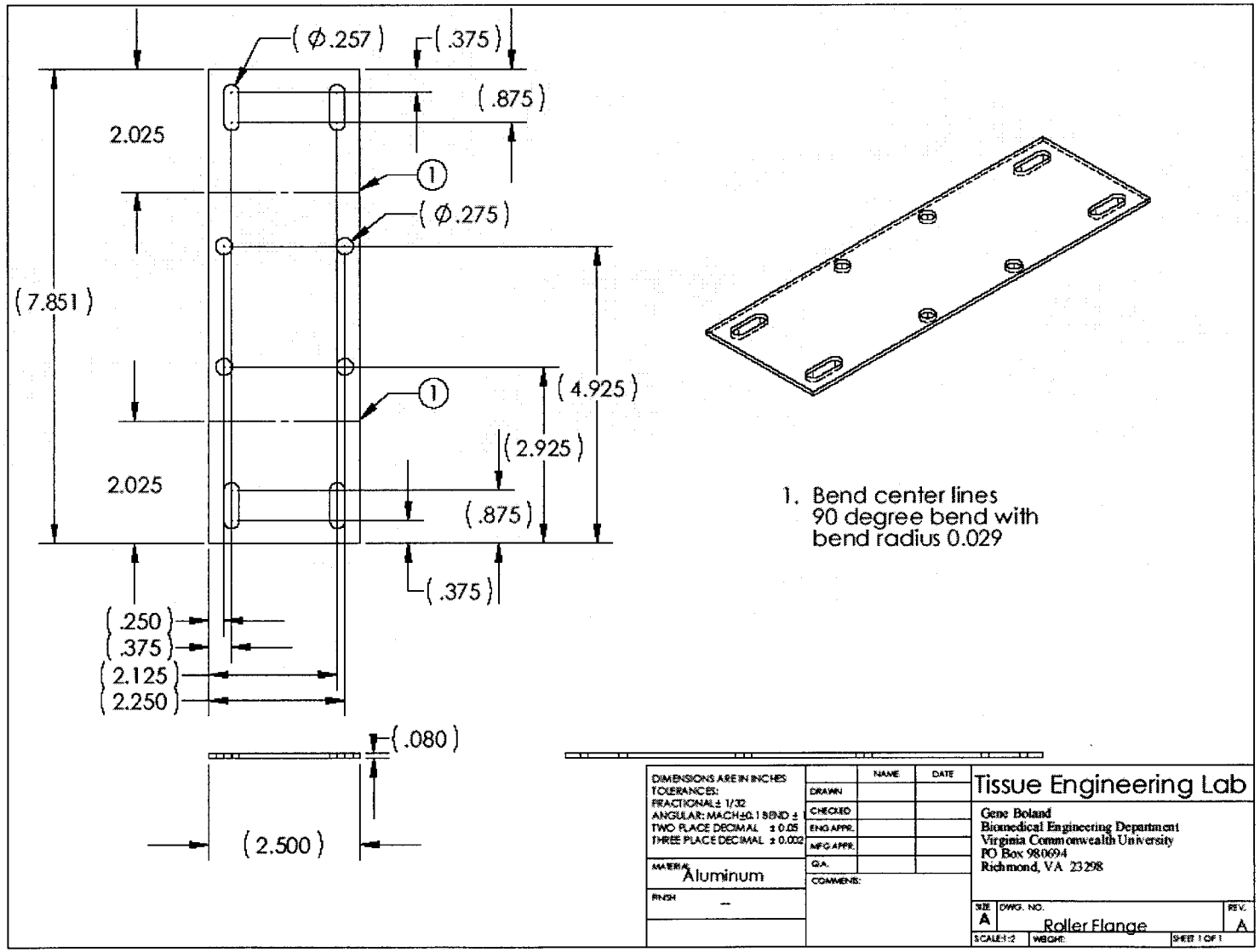
(Ø.257)
(.375)
(.875)
2.025
1
(Ø.275)
(7.851)
(4.925)
1
(2.925)
2.025
(.875)
(.375)
(.250)
(.375)
(2.125)
(2.250)
(.080)
(2.500)
1. Bend center lines
90 degree bend with
bend radius 0.029
DIMENSIONS ARE IN INCHES
TOLERANCES:
FRACTIONAL ± 1/32
ANGULAR: MACH ±0.1 BEND ±
TWO PLACE DECIMAL ± 0.05
THREE PLACE DECIMAL ± 0.002
MATERIAL Aluminum
FINISH —
NAME
DATE
DRAWN
CHECKED
ENG APPR.
MFG APPR.
Q.A.
COMMENTS:
Tissue Engineering Lab
Gene Boland
Biomedical Engineering Department
Virginia Commonwealth University
PO Box 980694
Richmond, VA 23298
SIZE A
DWG. NO. Roller Flange
REV. A
SCALE: 1:2
WEIGHT:
SHEET 1 OF 1

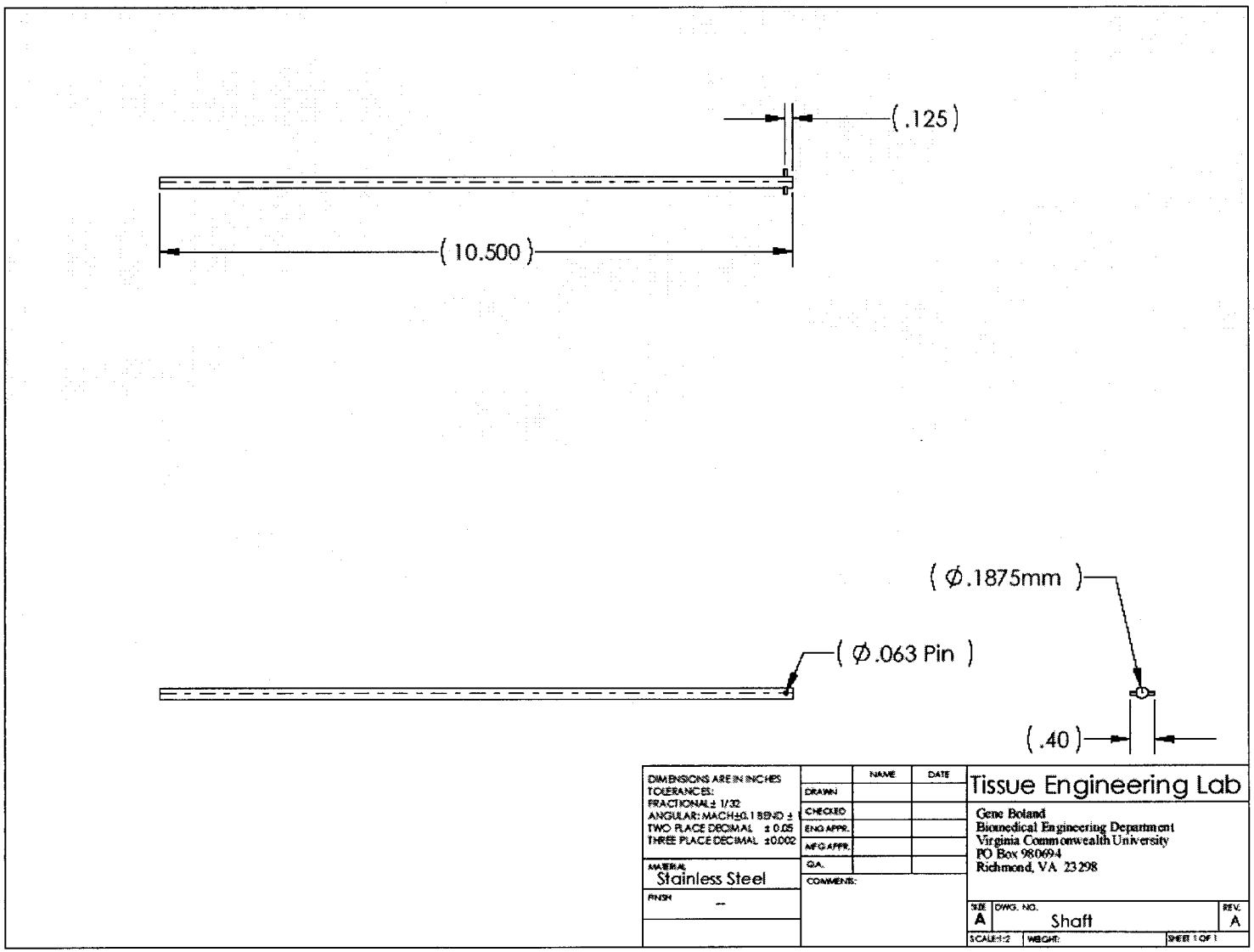
(.125)
(10.500)
(Ø.1875mm)
(Ø.063 Pin)
(.40)
DIMENSIONS ARE IN INCHES
TOLERANCES:
FRACTIONAL ± 1/32
ANGULAR: MACH ±0.1 BEND ±
TWO PLACE DECIMAL ± 0.05
THREE PLACE DECIMAL ±0.002
MATERIAL
Stainless Steel
FINISH
--
NAME
DATE
DRAWN
CHECKED
ENG APPR.
MFG APPR.
QA
COMMENTS:
Tissue Engineering Lab
Gene Boland
Biomedical Engineering Department
Virginia Commonwealth University
PO Box 980694
Richmond, VA 23298
SIZE
A
DWG. NO.
Shaft
REV.
A
SCALE:1:2
WEIGHT:
SHEET 1 OF 1

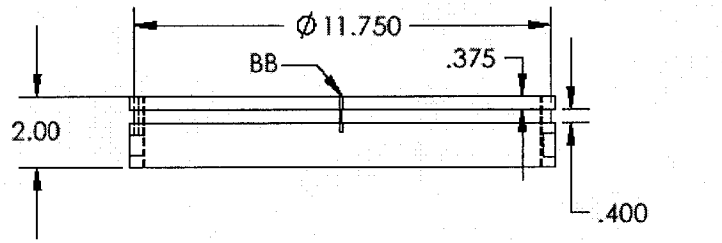

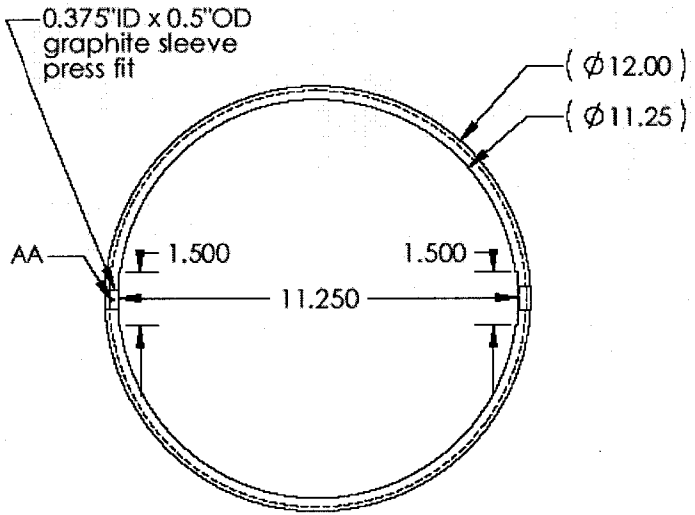

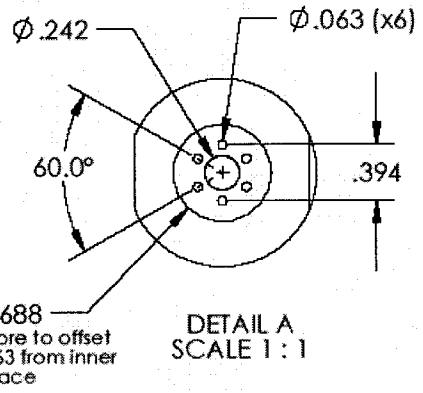

DETAIL A
SCALE 1 : 1

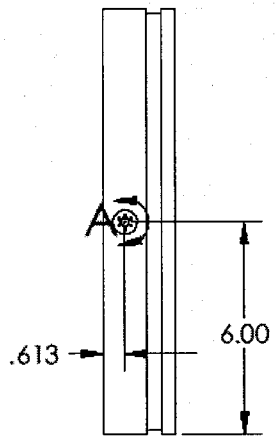

AA:
Drill and Tap 6-32 from back to inner hole, insert threaded stud to secure sleeve and grounding lug (expose 0.25" from rear)

BB:
Drill and insert 1/16" x 1" pin from back. Center hole 0.100" from outer rim.

DIMENSIONS ARE IN INCHES TOLERANCES: FRACTIONAL ± 1/32 ANGULAR: MACH ±0.1 BEND ± TWO PLACE DECIMAL ± 0.05 THREE PLACE DECIMAL ± 0.002		NAME	DATE
	DRAWN		
	CHECKED		
	ENG APPR.		
	MFG APPR.		
	Q.A.		
MATERIAL Acetal (Delrin)	COMMENTS:		
FINISH –			

Tissue Engineering Lab

Gene Boland
Biomedical Engineering Department
Virginia Commonwealth University
PO Box 980694
Richmond, VA 23298

SIZE	DWG. NO.	REV.
A	Spinner Ring	A
SCALE: 1:4	WEIGHT:	SHEET 1 OF 1

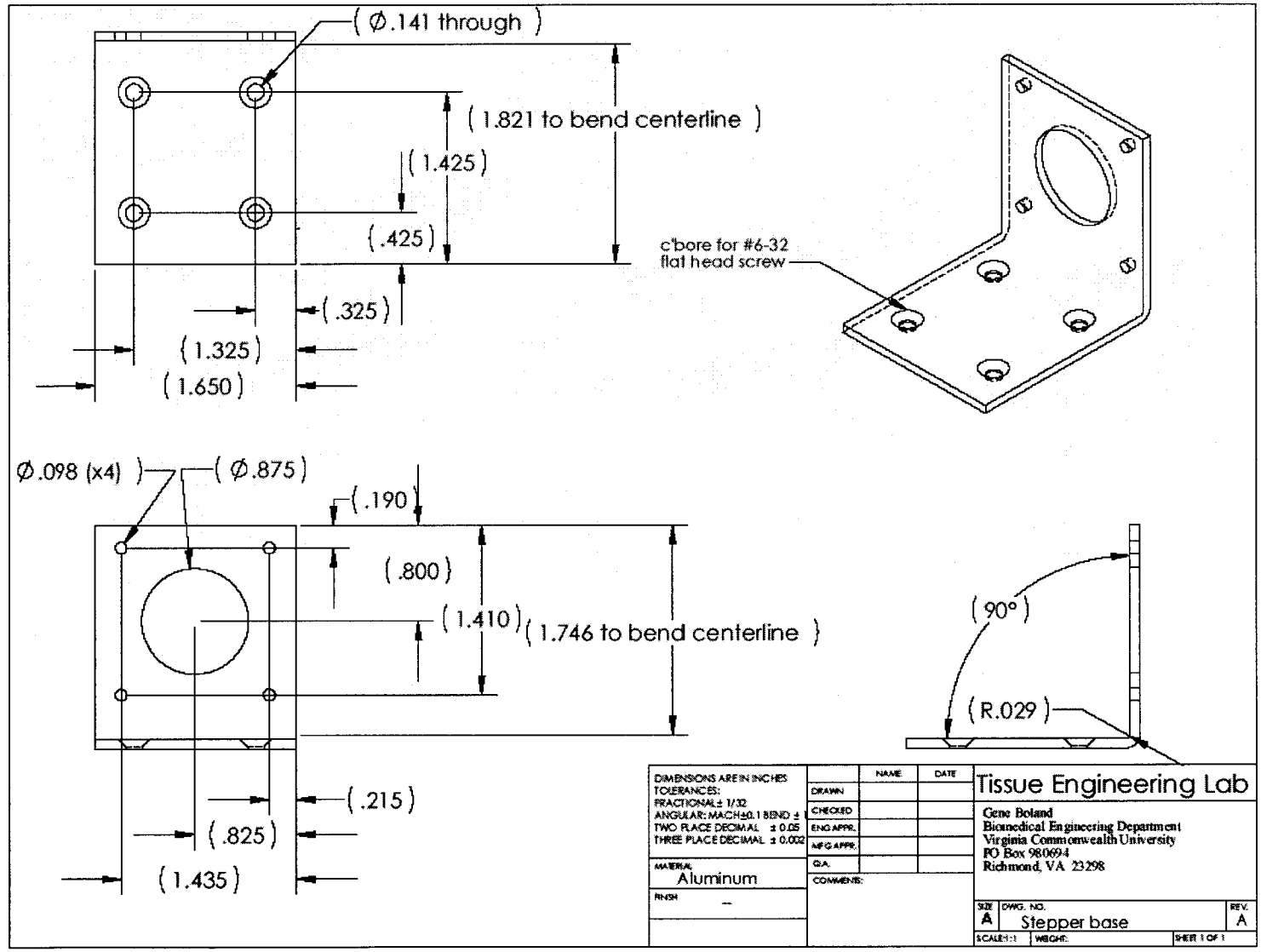
(Ø.141 through)
(1.821 to bend centerline)
(1.425)
(.425)
(.325)
(1.325)
(1.650)
c'bore for #6-32
flat head screw
Ø.098 (x4))
(Ø.875)
(.190)
(.800)
(1.410)
(1.746 to bend centerline)
(90°)
(R.029)
(.215)
(.825)
(1.435)
DIMENSIONS ARE IN INCHES
TOLERANCES:
FRACTIONAL ± 1/32
ANGULAR: MACH ±0.1 BEND ±
TWO PLACE DECIMAL ± 0.05
THREE PLACE DECIMAL ± 0.002
MATERIAL
Aluminum
FINISH
—
NAME
DATE
DRAWN
CHECKED
ENG APPR.
MFG APPR.
Q.A.
COMMENTS:
Tissue Engineering Lab
Gene Boland
Biomedical Engineering Department
Virginia Commonwealth University
PO Box 980694
Richmond, VA 23298
SIZE
A
DWG. NO.
Stepper base
REV.
A
SCALE: 1:1
WEIGHT:
SHEET 1 OF 1

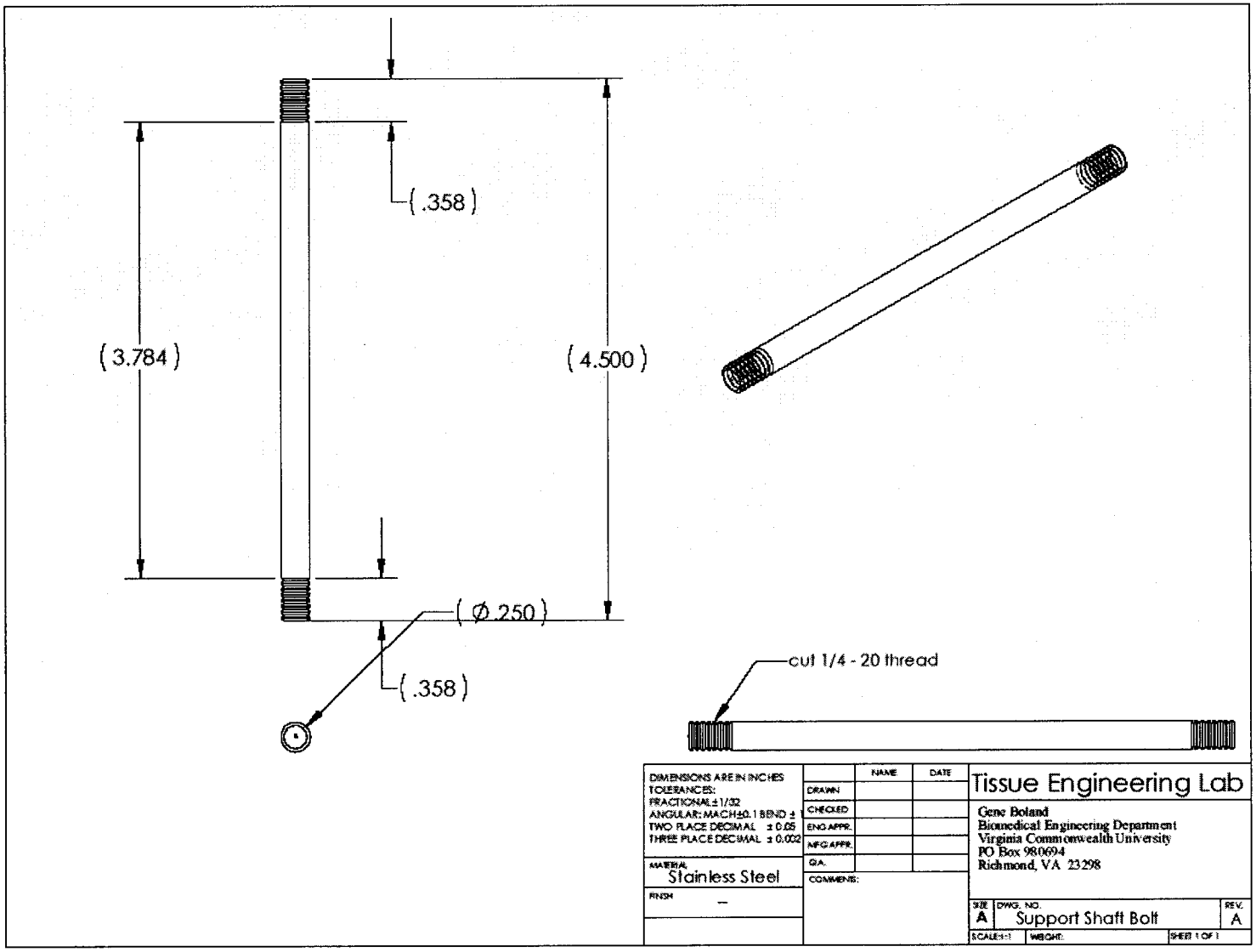
(.358)
(3.784)
(4.500)
(Ø.250)
(.358)
cut 1/4 - 20 thread
DIMENSIONS ARE IN INCHES
TOLERANCES:
FRACTIONAL ± 1/32
ANGULAR: MACH ± 0.1 BEND ±
TWO PLACE DECIMAL ± 0.05
THREE PLACE DECIMAL ± 0.002
MATERIAL
Stainless Steel
FINISH
—
NAME
DATE
DRAWN
CHECKED
ENG APPR.
MFG APPR.
QA
COMMENTS:
Tissue Engineering Lab
Gene Boland
Biomedical Engineering Department
Virginia Commonwealth University
PO Box 980694
Richmond, VA 23298
SIZE
A
DWG. NO.
Support Shaft Bolt
REV.
A
SCALE: 1:1
WEIGHT:
SHEET 1 OF 1

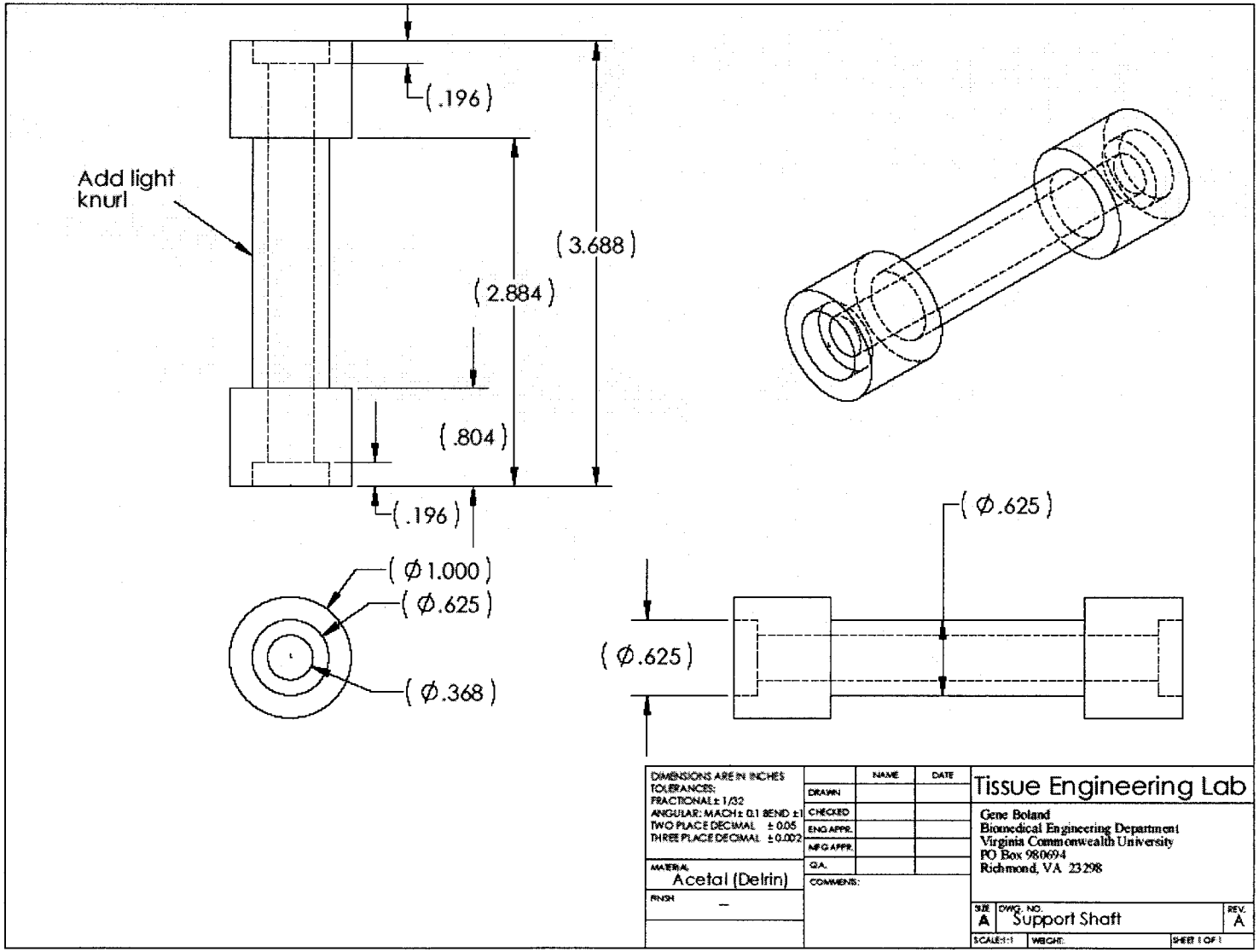

		NAME	DATE
DIMENSIONS ARE IN INCHES			
TOLERANCES:	DRAWN		
FRACTIONAL ± 1/32	CHECKED		
ANGULAR: MACH ± 0.1 BEND ±1	ENG APPR.		
TWO PLACE DECIMAL ± 0.05	MFG APPR.		
THREE PLACE DECIMAL ± 0.002	Q.A.		
MATERIAL: Acetal (Delrin)	COMMENTS:		
FINISH: —			

Tissue Engineering Lab

Gene Boland
Biomedical Engineering Department
Virginia Commonwealth University
PO Box 980694
Richmond, VA 23298

SIZE	DWG. NO.	REV.
A	Support Shaft	A
SCALE: 1:1	WEIGHT:	SHEET 1 OF 1

APPENDIX C

Appendix C contains the LabVIEW® control software used for controlling rotation and user input information for this electrospinning device.

Connector Pane

Front Panel

Controls and Indicators

Block Diagram

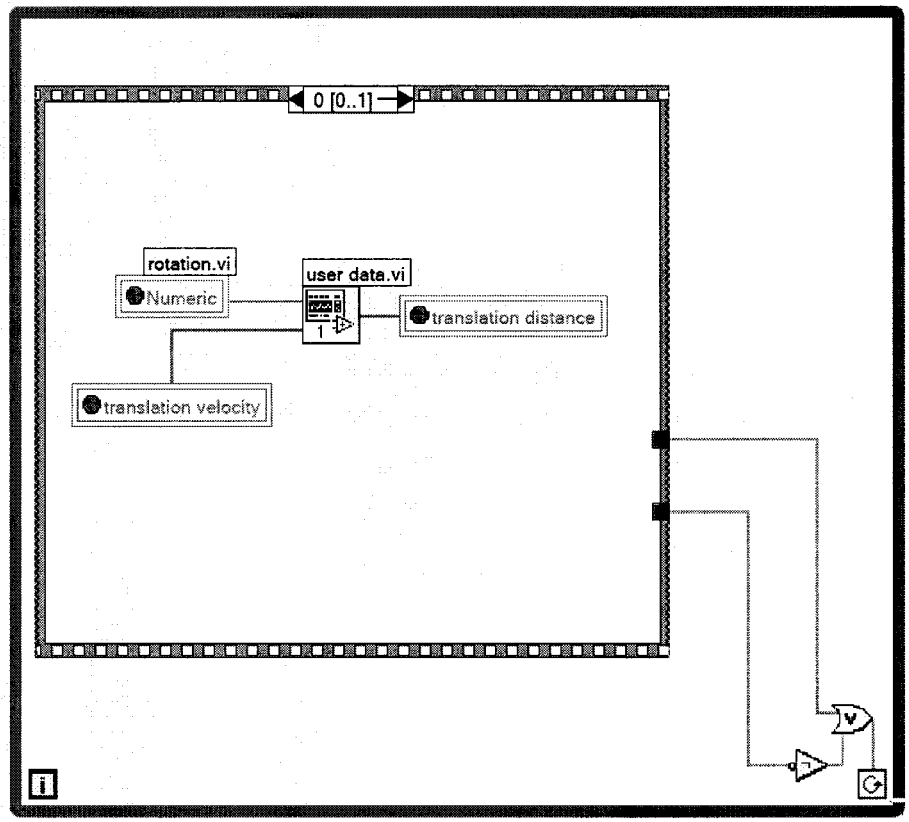

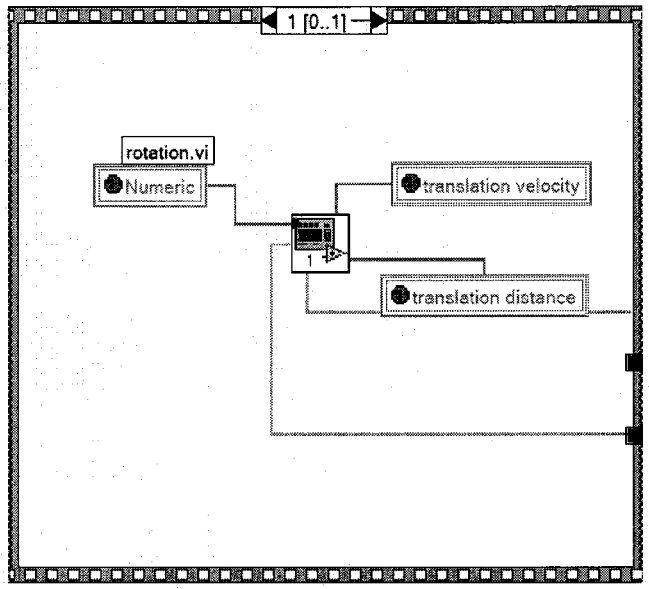

Position in Hierarchy

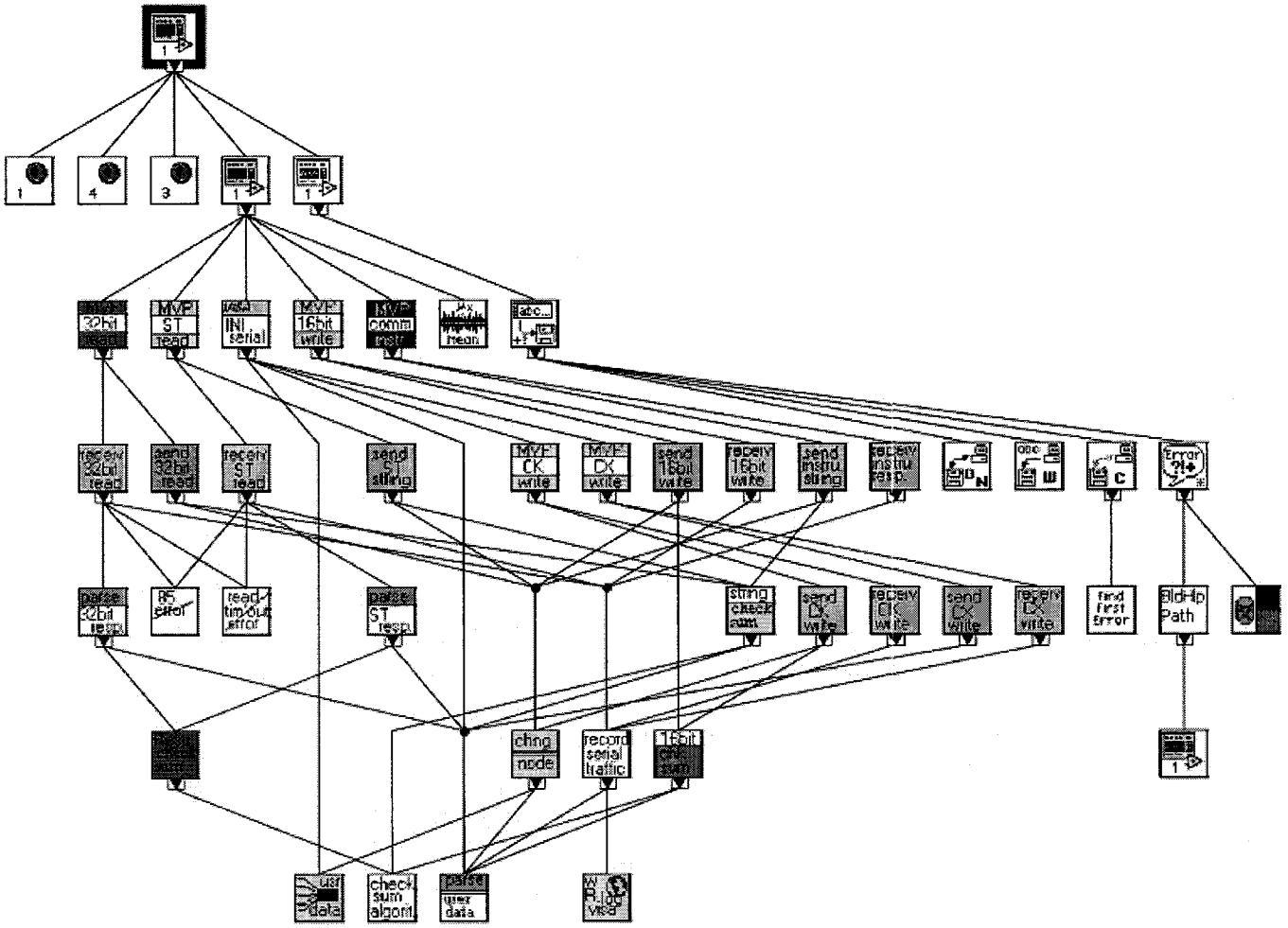

List of SubVIs

user data.vi
F:\eboland\labview\Spinner.llb\user data.vi

mandrel velocity 2.vi
F:\eboland\labview\Spinner.llb\mandrel velocity 2.vi

rotation.vi
F:\eboland\labview\Spinner.llb\rotation.vi

trans speed.vi
F:\eboland\labview\Spinner.llb\trans speed.vi

trans distance.vi
F:\eboland\labview\Spinner.llb\trans distance.vi

History

"control.vi History"
Current Revision: 5

Connector Pane

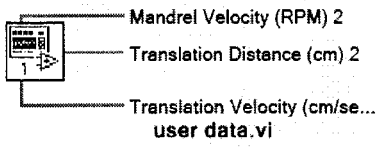

Front Panel

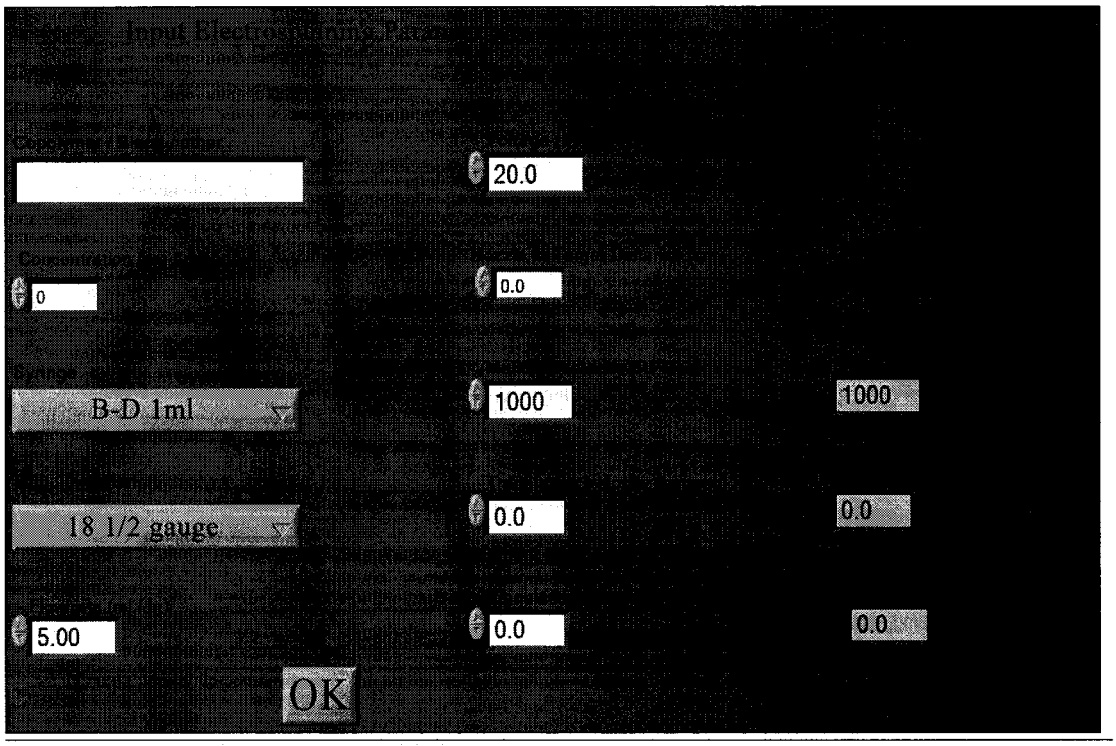

Controls and Indicators

- **Copolymer / Blend / other**
- **Voltage (kV)**
- **Flow rate (ml / hr)**
- **Nozzle to Target Distance (cm)**
- **Mandrel Velocity (RPM)**
- **Translation Velocity (cm/sec)**

I16 Syringe
I8 Needle
TF OK Button
DBL Concentration (mg / ml)
DBL Translation Distance (cm)
DBL Mandrel Velocity (RPM) 2
DBL Translation Velocity (cm/sec) 2
DBL Translation Distance (cm) 2

Block Diagram

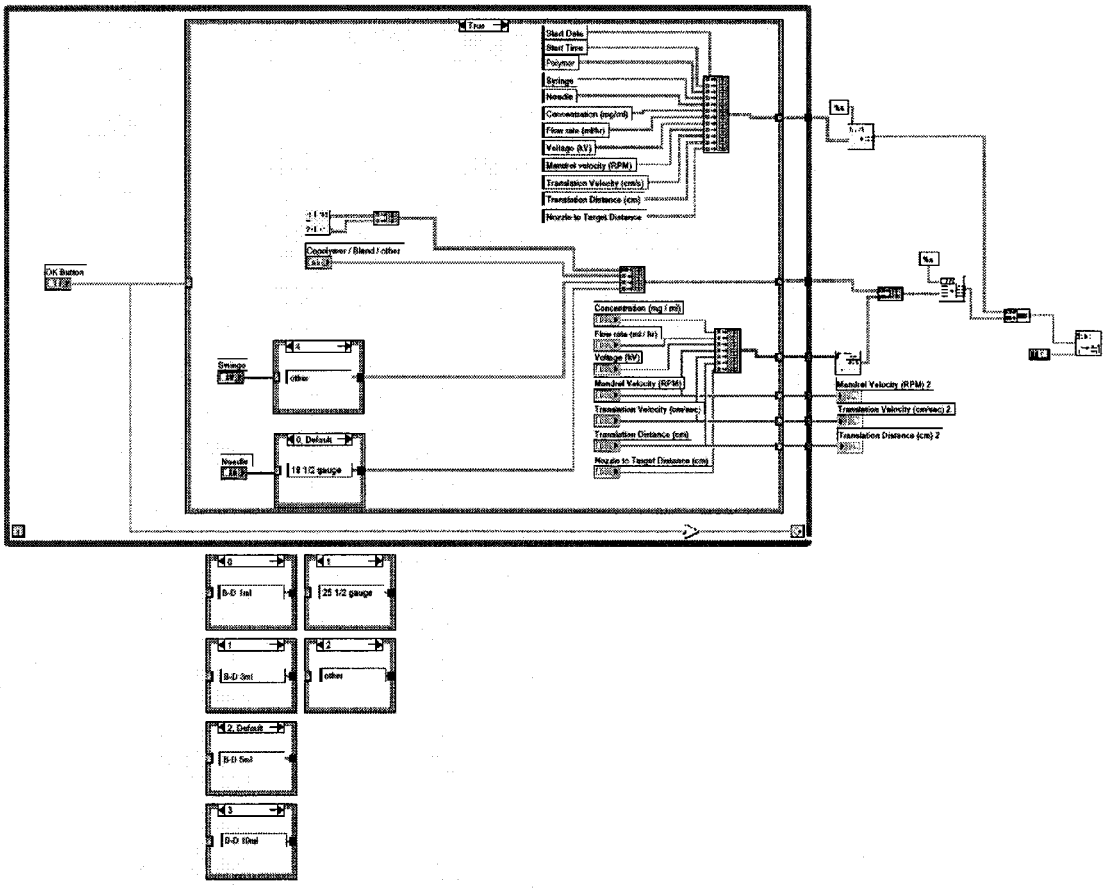

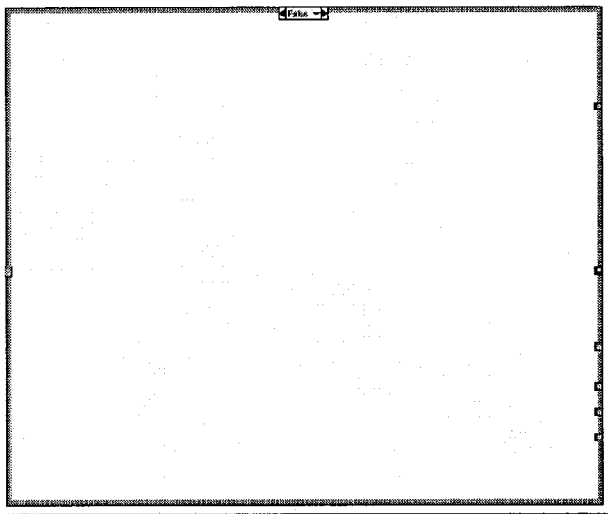

Position in Hierarchy

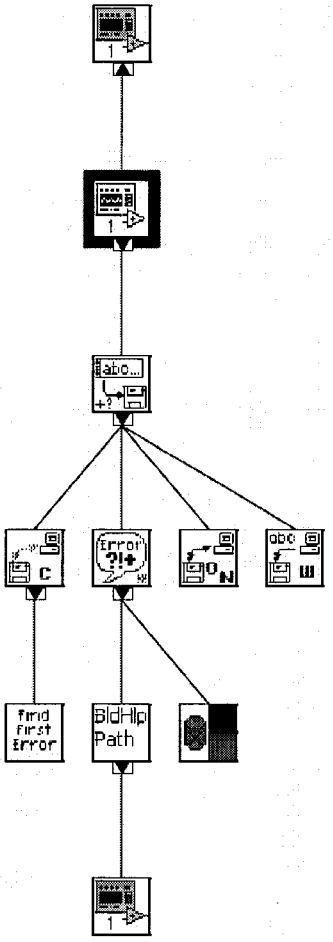

List of SubVIs

Write Characters To File.vi
C:\Program Files\National Instruments\LabVIEW 6.1\vi.lib\Utility\file.llb\Write Characters To File.vi

History

"user data.vi History"
Current Revision: 14

Connector Pane

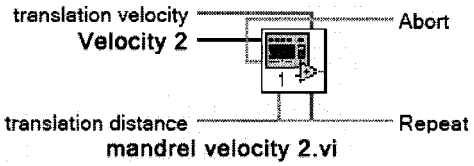

Front Panel

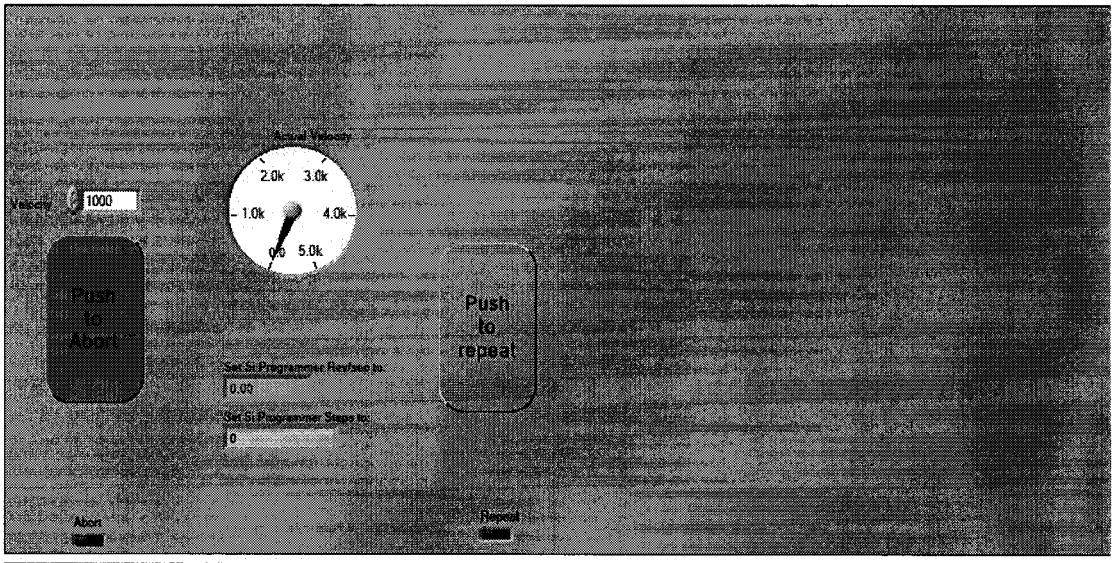

Controls and Indicators

- **Deceleration**
- **Abort deceleration**
- **Abort action code**
  0=disable drive
  1=stop and servo
  2=decelerate and stop
- **Acceleration**
- **Velocity 2**
- **Abort**
- **Setup Cluster**
  - **VISA in**
    this is the VISA ID for this VISA session
  - **serial port**
    Here we select the serial port

Address node
Here you can select the MVP2001 node number.
-1=no change in the previous selection
0=select all 63 MVP2001 controllers on this RS485 line
1-63=select one of the MVP2001 controllers on the RS485 line

The node number identifies the MVP2001.
Note:
On the MVP2001 front panel switches 5 through 10 are used to assign a node number for that MVP2001.
Least sigificant bit: switch 5
Most significant bit: switch 10

for example, node 4 would be selected on the front panel of the MVP2001 by
5=ON
6=ON
7=OFF
8=ON
9=ON

checksum
Here you can select whether the MVP2001 should use checksum during serial communications.
Default: checksum=YES

baud rate
Here you can set the baud rate of the serial communication. Make sure that, you set the MVP2001 to the same baud rate!
On the MVP2001 switches 3 and 4 are used to select the baud rate.
9600bps: 3=on; 4=on
19200bps: 3=on; 4=off
38400bps: 3=off; 4=on
57600bps: 3=off; 4=off
For the new baud rate to take effect, the power must be removed from the MVP2001 and after a few second, turned back on!

log serial data
Here you can select whether the MVP2001 should keep a record of the sent command strings and the received response strings. When the "record serial data option" is set to " YES" the arrays in the global variable called "Global-Visa Write and Read.vi"
This feature is useful during code development but can slow down the execution of your application!
If the the "record serial data option" is set to " YES" the array in the global are getting larger and larger with each command and response!

serial timeout
The serial time out is a VISA variaable. NI-VISA will wait this long before the serial communication operation is terminated.

Wait_after_send
0-255 [mSec]
Here you can set the leght of time the driver will wait after sending out a command to the MVP2001. each count is equal to one millisecond. the maximum length is 127 millisecons.
Note:
Under certain circumstances it is necessary to allow some time between sending a command to the MVP and attampting to read back the response. Even sending out commands that do not produce a respone might require some wait time between sending these kind of commads one after the other.

U8 **max.re-sends**
When the checksum feature is ON, this parameter determines how may times the commad will be re-sent to the MVP2001 upon failure os the checksum test or when the legth of the response is zero.
When the checksum feature is OFF, the command will be re-sent if the length of the response is zero.

DBL **translation velocity**

DBL **translation distance**

TF **Repeat**

TF **Abort 2**

U32 **loop time**

Status

TF **0: Moving**
Bit 0 : 1=move in progress; 0=not commanded to move

TF **1: In Position**
Bit 1 : 1=Motor is in position; 0=motor is not in position

TF **2: Vel/Pos. Mode**
Bit 2 : 1=MVP2001 is in velocity mode; 0= MVP2001 is in Position mode

TF **3:AMN (J2-1)**
Bit 3 : 1=Indicates that, trajectory percentage complete (defined by the "T" command) is achieved
0=indicates that the trajectory complete percentage is not yet achieved

TF **4: T% Done**
Bit 4 : 1=an error has occurred; 0=everything is OK

TF **5: DeviceNet Mode**
Bit 5 : 1=module is in DeviceNet mode; 0=module is not in DeviceNet mode

TF **6: DeviceNet Error**
Bit 6 : 1=a DeviceNet message error has occurred in one or more packets
0=the DeviceNet message pockets are OK

TF **7: Excess FE**
Bit 7 : 1=the current move is off its program trajectory by more than the allowed amount
0=current move is going OK
(the allowed fallowing error is set by the FD command)

TF **8: Motor Disabled**
Bit 8 : 1=motor is not enabled or has been disable by some error; 0= motor is enabled

TF **9: Soft Limit**
Bit 9 : 1=you have reached the program range limit set by the LL command
0=move is within range limit

TF **10: Local Mode**
Bit 10: 1=Local Mode is active; 0=Remote mode is active

TF **11: E.. Stop (J2-4)**
Bit 11: Emergency stop flag (1=active)

TF **12: XEv#1(J2-8)**
Bit 11: Emergency stop flag (1=active)

TF **13: + HLim(J2-5)**
Bit 13: Positive limit flag (1=active)

TF **14: XEv #2(J2-7)**
Bit 14: External event #2 (1=active)

TF **15: - HLim(J2-6)**
Bit 15: negative limit flag (1=active)

TF **In position 5 times**

TF **1: In Position**

U32 **loop timetime**

I32 **Position readings**

error out

TF **status**
The status boolean is either TRUE (X) for an error, or FALSE (checkmark) for no error or a warning.

The pop-up option Explain Error (or Explain Warning) gives more information about the error displayed.

I32 **code**
The code input identifies the error or warning.

The pop-up option Explain Error (or Explain Warning) gives more information about the error displayed.

abc **source**
The source string describes the origin of the error or warning.

The pop-up option Explain Error (or Explain Warning) gives more information about the error displayed.

I32 **Actual Velocity**

DBL **Set Si Programmer Rev/sec to:**

DBL **Set Si Programmer Steps to:**

TF **Abort**

TF **Repeat**

Block Diagram

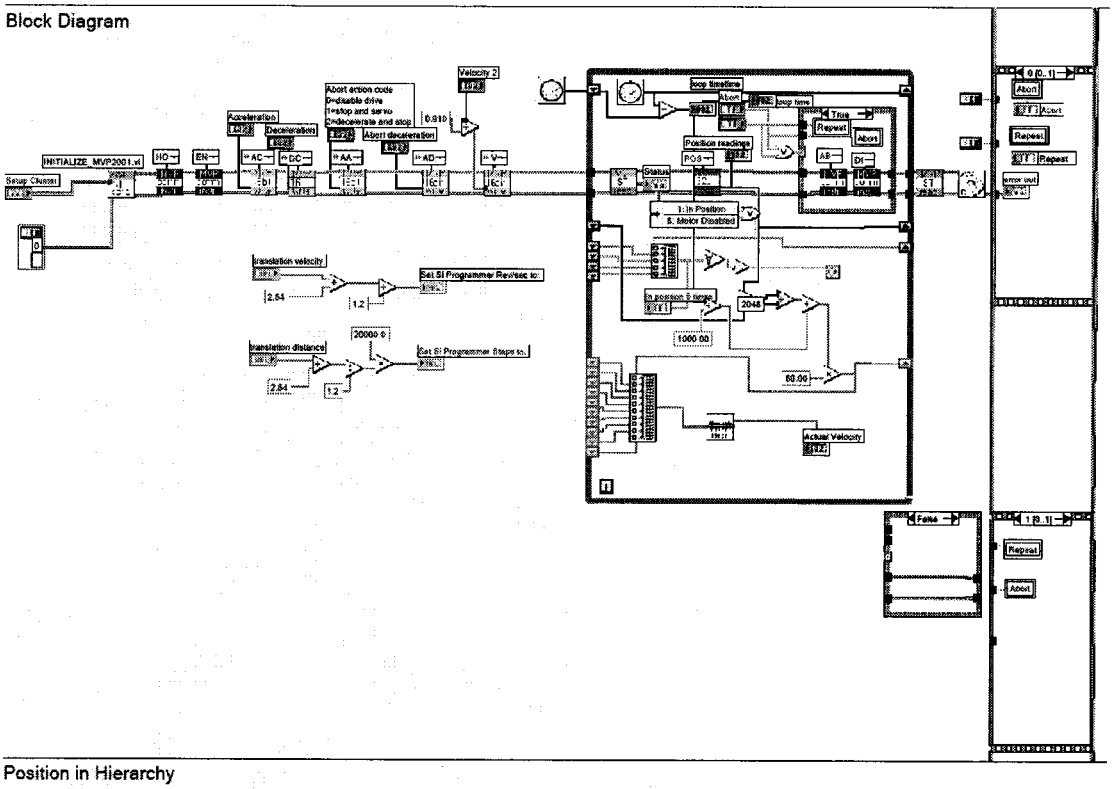

Position in Hierarchy

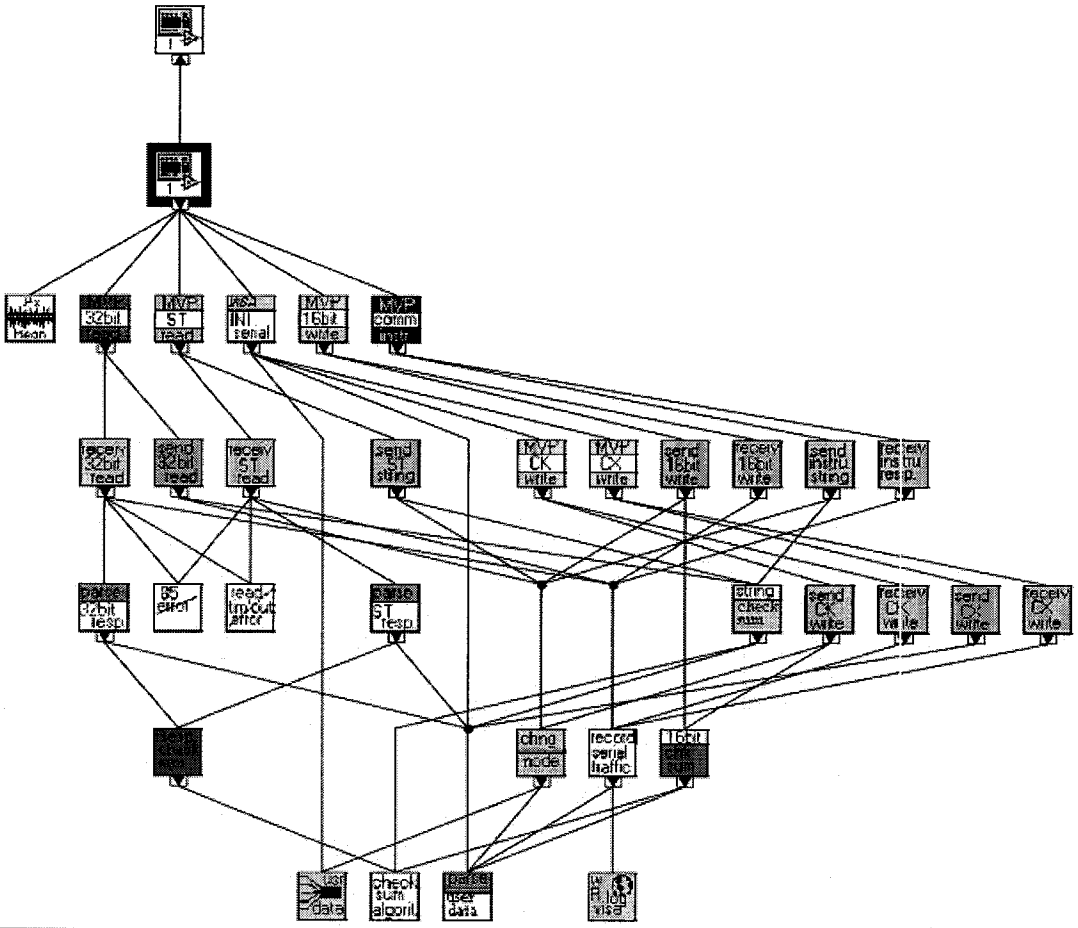

List of SubVIs

INITIALIZE_MVP2001.vi
C:\Program Files\National Instruments\LabVIEW 6.1\vi.lib\MVP2001\INITIALIZE_MVP2001.vi

comm(16bit_Write).vi
C:\Program Files\National Instruments\LabVIEW 6.1\vi.lib\MVP2001\comm(16bit_Write).vi

Comm(instruction).vi
C:\Program Files\National Instruments\LabVIEW 6.1\vi.lib\MVP2001\Comm(instruction).vi

comm(ST).vi
C:\Program Files\National Instruments\LabVIEW 6.1\vi.lib\MVP2001\comm(ST).vi

comm(32bit_Read).vi
C:\Program Files\National Instruments\LabVIEW 6.1\vi.lib\MVP2001\comm(32bit_Read).vi

Mean.vi
C:\Program Files\National Instruments\LabVIEW 6.1\vi.lib\Analysis\baseanly.llb\Mean.vi

---

History

"mandrel velocity 2.vi History"
Current Revision: 32

Connector Pane

rotation.vi

Front Panel

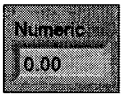

Controls and Indicators

Numeric

Block Diagram

Position in Hierarchy

List of SubVIs

History

"rotation.vi History"
Current Revision: 0

Connector Pane

trans speed.vi

Front Panel

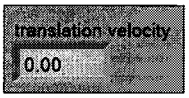

Controls and Indicators

DBL translation velocity

Block Diagram

Position in Hierarchy

List of SubVIs

History

"trans speed.vi History"
Current Revision: 1

Connector Pane

trans distance.vi

Front Panel

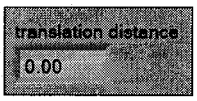

Controls and Indicators

translation distance

Block Diagram

Position in Hierarchy

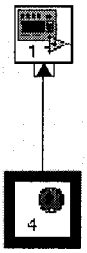

List of SubVIs

History

"trans distance.vi History"
Current Revision: 1

VITA

Eugene David Boland was born in Munising, Michigan on August 21, 1971 and is a United States Citizen. He graduated from Neenah High School in Neenah, Wisconsin in 1989 then received a bachelor's degree in Biomedical Engineering in 1994 from Marquette University in Milwaukee, Wisconsin. While at Marquette University, he received the Engineering Cooperative Education Student of the Year award and a Certificate of Achievement in Biomedical Engineering from the Department of Veterans Affairs in 1994. After graduating, he went to work for St. Jude Medical, Inc. - Heart Valve Division in St. Paul, Minnesota. He then worked for Cordis Corporation, A Johnson and Johnson Company in Warren, New Jersey. After a year, he left and went to work for Cryolife, Inc. in Kennesaw Georgia. He returned to school in 2000 to pursue his Ph.D. in Biomedical Engineering at Virginia Commonwealth University in Richmond, Virginia. He conducted his research in the Tissue Engineering Laboratory of Gary L. Bowlin, Ph.D. While at Virginia Commonwealth University, he received the Alex M. Clarke Award of Excellence in Biomedical Engineering and an American Heart Association Pre-doctoral fellowship.

CURRICULUM VITAE

PERSONAL INFORMATION:

Eugene David Boland

United States Citizen

Home Address:

Office Address:

LICENSURE:

Engineer-in-Training, (PE eligible)

EDUCATION:

Ph.D., Biomedical Engineering (exp. May 2004) – Virginia Commonwealth University

Dissertation: Novel Apparatus to Control Electrospinning Fiber Orientation for the Production of Tissue Engineering Scaffolds.
Advisor: Gary L. Bowlin, Ph.D.

Post-Baccalaureate Certificate (April 2003) – Virginia Commonwealth University

Preparing Future Faculty in the Professions (PFFP)
Course work includes:Seminar: The Academic Profession
Seminar: College Teaching
Seminar: Teaching the Professions
Seminar: Professing the Applied Physical Sciences
Internship: Professional Education

B.S., Biomedical Engineering (1994) - Marquette University

Emphasis: Biomechanics
Advisor: John Linehan, Ph.D.

ACADEMIC APPOINTMENTS:

Teaching Assistant (Aug. 2000-Dec. 2000)
Virginia Commonwealth University
Department of Mechanical Engineering
Richmond, VA 23298

Teaching Assistant / Instructor (Dec. 2000-Present)
Virginia Commonwealth University
Department of Biomedical Engineering
Richmond, VA 23298

INDUSTRIAL EXPERIENCE:

Process / Manufacturing Engineer (May 1998 – Aug. 2000)
Cryolife, Inc. - Kennesaw, GA

Responsible for daily process functions in laboratory operation. Direct supervision of all process changes and improvements in the bioprosthetics laboratory which included the technology transfer from R&D to develop pilot manufacturing of a tissue engineered heart valve.

Senior Research Engineer (May 1997 – May 1998)
Cordis, A Johnson and Johnson Co. - Warren, NJ

Managed the Advanced Research evaluation laboratory which was responsible for the development of physiologically significant *in vitro* test method for cardiovascular devices. Served as technical advisor on various FDA 483 response teams and for the New Business Development and Marketing departments.

Research Engineer (July 1994 – May 1997)
St. Jude Medical, Inc – Heart Valve Division - St. Paul, MN

Served as the principal engineer in the R&D Engineering Test Lab. Responsibilities included design and improvement of heart valve testing, coordinating hydrodynamic testing for regulatory submissions of new devices, automation of tissue processing systems and mechanical characterization of heart valve tissue after chemical treatments.

MEMBERSHIPS - SCIENTIFIC, HONORARY, AND PROFESSIONAL SOCIETIES:

Biomedical Engineering Society (BMES)
Virginia Academy of Science (VAS)
Tissue Engineering Society International (TESI)

MEMBERSHIP IN COMMUNITY ORGANIZATIONS:

Ancient Order of Hibernians – Divisional Recording Secretary

SPECIAL AWARDS:

Awards: University/School:

Engineering Cooperative Education Student of the Year: Marquette University, 1994
Alex M. Clarke Award of Excellence in Biomedical Engineering, Department of Biomedical Engineering, Virginia Commonwealth University, 2003.

Other Honors; National/International:

Certificate of Achievement in Biomedical Engineering: Department of Veterans Affairs Hospital – North Chicago, IL, 1994
"On the Spot" service award: Johnson and Johnson, 1998: $100
Association for the Advancement of Medical Instrumentation Young Investigator Award, 2003, approximate value $3000

External Grants:

Pre-doctoral Fellowship: "Development of an Automated Electrostatic Processing Device for Tissue Engineering Applications." American Heart Association – Mid-Atlantic Affiliate – Reference number 0315255U, awarded 7/1/2003 - 6/30/2004: $20,000.

Internal Grants:

Travel Grant: VCU School of Graduate Studies, 2001: $300
Student Research Grant-in-Aid: VCU School of Graduate Studies, 2001: $1000
Travel Grant: VCU Graduate Student Association, 2003: $150

INVITED SEMINARS:

Fall 1997 – Marquette University, Guest Lecturer – Frontiers of Biomedical Engineering
"Testing and Design of Interventional Cardiology Devices"

Fall 1995 – Marquette University, Guest Lecturer – Frontiers of Biomedical Engineering
"Role of Biomedical Engineer in Prosthetic Heart Valve Industry"

Fall 1994 – Marquette University, Guest Lecturer – Frontiers of Biomedical Engineering
"Testing and Design of Prosthetic Heart Valves"

SERVICE:

Reviewer:

Encyclopedia of Biomaterials and Biomedical Engineering, Marcel Dekker, Inc.
Journal of Biomedical Materials Research Part B: Applied Biomaterials

OTHER SIGNIFICANT SCHOLARLY EXPERIENCE:

Undergraduate Students Supervised:

Mahesh Datla (Senior, September 2002 – May 2003)
Senior Design Project: "Developing a PLA – Elastin Vascular Construct by Electrospinning"

Larry Campbell (Senior, September 2002 – May 2003)
Senior Design Project: "Developing a PLA – Elastin Vascular Construct by Electrospinning"

Allison L. Faucette (Summer Intern, May - August 2001)
Project: "Electrospinning Biodegradable Polymers for Tissue Engineering Scaffolds."

Tara R. George (Summer Intern, April - August 2001)
Project: "Electrospinning Biodegradable Polymers for Tissue Engineering Scaffolds."

Danielle C. Knapp (Summer Intern, April - August 2001)
Project: "Electrospinning Biodegradable Polymers for Tissue Engineering Scaffolds."

Jared A. Hoover (Summer Intern, May - August 2001)
Project: "Electrospinning Biodegradable Polymers for Tissue Engineering Scaffolds."

Teaching Assignments

1.) **EGRB 403 – Tissue Engineering** (Spring 2003)
Co-Instructor (under guidance of Dr. Gary Bowlin)
Study of the design, development and clinical application of tissue engineered components for use in the human body. Analysis of biology, chemistry, material science, engineering, immunology and transplantation as pertains to various tissue engineered components including blood vessels, bone, cartilage, pancreas, liver and skin.
Course 4.08 / 5.0 Instructor 4.43 / 5.0

2.) **EGRB 310 – Biomechanics** (Spring 2001, 2002)
Laboratory Instructor
This first course in biomechanics will analyze the forces, stresses and strains in the human body during normal function. Emphasis will be placed on certain parts of the human body including hard (bone) and soft (cartilage, ligaments, and tendons) tissues. Knowledge of statics and the mechanics of deformable bodies is required as is a knowledge of calculus and differential equations. Exposure to human anatomy and physiology also is necessary; however, more in-depth anatomic study of the different parts of the body will be part of the material covered.

3.) **ENGR 101 – Introduction to Engineering** (Fall 2002)
Laboratory Instructor
Introduces basic circuits including resistors, diodes, transistors, digital gates and motors. Simple electromechanical systems are considered including motors, gears and wheels. The laboratory introduces fundamental circuit testing and measurement, and proper laboratory notebook writing; students are required to analyze, build and test a digitally controlled robot.

4.) **EGRM 300 – Mechanical Systems Design** (Fall 2000)
Teaching Assistant
Basic principles of applied mechanics and materials employed for the design of machine elements and mechanical systems; state of stress, deformation and failure criterion is applied to bearings, brakes, clutches, belt drives, gears, chains, springs, gear trains, power screws and transmissions.

5.) **EGRB 101 -- Biomedical Engineering Practicum I** (Spring 2003, 2004, Fall 2003)

Teaching Assistant

This course involves the introduction of clinical procedures and biomedical devices and technology to biomedical engineering freshman. Students will tour medical facilities, clinics, and hospitals and will participate in medical seminars, workshops, and medical rounds. Students will rotate among various programs and facilities including biomedical engineering, orthopedics, cardiology, neurology, surgery, otolaryngology, emergency medicine, pharmacy, dentistry, nursing, oncology, physical medicine, ophthalmology, pediatrics and internal medicine.

6.) **EGRB 427 – Biomaterials** (Fall 2002, 2003)

Lecturer (assisted Dr. Gary Bowlin)

Analysis of physical, chemical, thermal and physiological response factors associated with materials and implant devices used in the human body. Study of the properties of biomedical materials used as implants, prostheses, orthoses and as medical devices in contact with the human body. Computer modeling and experimental studies.

BIBLIOGRAPHY:

Papers Published:

1.) **Boland, E.D.**; Barnes, C.; Coleman III, B.D.; Wnek, G.E.; Bowlin, G.L. "Preliminary Mechanical Evaluation of Electrospun Polydioxanone for Tissue Engineering Applications." *In Preparation.*

2.) Barnes, C., **Boland, E.D.**, Pawlowski, K.J., Simpson, D.G., Wnek, G.E. and G.L. Bowlin**.** Electrospun Fibrinogen Hemostatic Bandages. *J. of Chemical Education, In Preparation.*

3.) **Boland, E.D.**, Pawlowski, K.J., Simpson, D.G., Wnek, G.E. and G.L. Bowlin. "Electrospinning: A Revitalized Polymer Processing Technique." J. of Chemical Education, *In Preparation.*

4.) **Boland, E.D**.; Bowlin, G. L. "Automated Electrostatic Processing Device for Tissue Engineering Applications." *Biomedical Instrumentation and Technology*, In Review.

5.) Telemeco, T.A.; Bowlin, G.L.; Wnek, G.E.; **Boland, E.D.**; Cohen, N.; Vaida, M.; Tang, D.G.; Baumgarten, C.M.; Matthews, J.A.; Terracio, L.; Wise, B.; Simpson, D.G. "Electrospun Collagen as a Surgical Biomaterial: Fabrication of a Skeletal Muscle Prosthetic." *Tissue Engineering*, In Review.

6.) **Boland, E.D.**; Telemeco, T.A.; Simpson, D.G.; Wnek, G.E.; Bowlin, G.L. "Utilizing Acid Pretreatment and Electrospinning to Improve Biocompatibility of Poly(glycolic acid) for Tissue Engineering." *Journal of Biomedical Materials Research: Part B, Applied Biomaterials*, In Press.

7.) **Boland, E.D.**; Matthews, J.A.; Simpson, D.G.; Wnek, G.E.; Bowlin, G.L. 2004. "Electrospinning Collagen and Elastin for Vascular Tissue Engineering and the Preliminary Development of a Three-Layered Construct." *Frontiers in Biosciences*, 9: 1422-1432.

8.) Matthews, J.A.; **Boland, E.D**.; Wnek, G.E.; Simpson, D.G.; and G.L. Bowlin. 2003. "Electrospinning of Collagen Type II: A Feasibility Study." *Journal of Bioactive and Compatible Polymers*, 18(2): 125-134.

9.) **Boland, E.D**.; Wnek, G.E.; Simpson, D.G.; Pawlowski, K.J. and G.L. Bowlin. 2001. "Tailoring Tissue Engineering Scaffolds Using Electrostatic Processing Techniques: A Study of Poly(Glycolic Acid)." *Journal of Macromolecular Science,* 38(12): 1231 – 43.

10.) Elizondo D.R., **Boland, E.D**., Ambrus, J.R., and J.L. Kurk. 1996. "Mechanical Cardiac Valve Prostheses: Wear Characteristics and Magnitudes of Three Bileaflet Valves." *Journal of Heart Valve Disease* 5: 115-123.

Book Chapters:

1.) **Boland, E.D.**; Espy, P.; Wnek, G.E.; G.L. Bowlin. 2004 "Tissue Engineering Scaffolds" In The Encyclopedia of Biomaterials and Biomedical Engineering. Bowlin and Wnek Eds. Dekker, Inc., In Press

2.) **Boland, E.D.**; Wnek, G.E.; G.L. Bowlin. 2004 "Poly(Glycolic Acid)" In The Encyclopedia of Biomaterials and Biomedical Engineering. Bowlin and Wnek Eds. Dekker, Inc., In Press

3.) Bowlin, G.L.; Pawlowski, K.J.; Stitzel, J.D.; **Boland, E.D**.; Simpson, D.G.; Fenn, J.B.; G.E. Wnek. 2002 "Electrospinning of Polymer Scaffolds for Tissue Engineering" In Tissue Engineering and Biodegradable Equivalents: Scientific and Clinical Applications. Lewandrowski, Trantolo, Gresser, Taszemski, and Altobelli Eds. Dekker, Inc., pp. 165-178.

Abstracts Published:

1. Matthews, J.A.; **Boland, E.D.**; Simpson, D.G.; Wnek, G.E.; and G.L. Bowlin. "Cellular Interaction with Electrospun Collagen Type I Scaffolds." Poster presented at the International Society for Applied Cardiovascular Biology (ISACB), Ninth Biennial Meeting, Savannah, GA, March 10-13, 2004.

2. **Boland, E.D.**; Simpson, D.G.; Wnek, G.E.; and G.L. Bowlin. "Cellular Response to Acid Treated Electrospun Poly(glycolic acid) Scaffolds for Tissue Engineering." Poster presented at the International Society for Applied Cardiovascular Biology (ISACB), Ninth Biennial Meeting, Savannah, GA, March 10-13, 2004.

3. Matthews, J.A.; **Boland, E.D.**; Simpson, D.G.; Wnek, G.E.; and G.L. Bowlin. "Electrospinning Collagen and Elastin: Preliminary Vascular Tissue Engineering." Poster presented at the International Society for Applied Cardiovascular Biology (ISACB), Ninth Biennial Meeting, Savannah, GA, March 10-13, 2004.

4. Anderson Jr., C.D.; **Boland, E.D.**; Wnek, G.E.; Simpson, D.G.; and G.L. Bowlin. "Electrospun Elastin for Tissue Engineering Scaffolds." Poster presented at the 8th Annual International Workshop on Tissue Engineering, Hilton Head, SC, March 6-10, 2004.

5. **Boland, E.D.**; McManus, M.C.; Wnek, G.E.; Simpson, D.G.; and G.L. Bowlin. "Electrospun Fibrinogen: Mimicking Nature's Degradable Scaffold." Presented as an Oral Presentation at the 8th Annual International Workshop on Tissue Engineering, Hilton Head, SC, March 6-10, 2004.

6. **Boland, E.D.**; Wnek, G.E.; Simpson, D.G.; and G.L. Bowlin. "Blending Electrospun Collagen and Polydioxanone for High Strength-High Elasticity Tissue Engineering Applications." Accepted at the 8th Annual International Workshop on Tissue Engineering, Hilton Head, SC, March 6-10, 2004.

7. Telemeco, T.A.; Bowlin, G.L.; Matthews, J.A.; **Boland, E.D**.; Wnek, G.E. and D.G. Simpson. "Electrospun Collagen as a Tissue-Engineering Scaffold: Fabrication of a Skeletal Muscle Prosthesis." Presented as an Oral Presentation at Tissue Engineering Society International – 2003 Annual Meeting, Orlando, FL, December 2003. (work presented by D. G. Simpson).

8. Matthews, J.A.; **Boland, E.D.**; Wnek, G.E.; Simpson, D.G.; and G.L. Bowlin. " Electrospinning of Collagen Type II Nano-fibrous Scaffoldings: Preliminary Cartilage Engineering." Presented as an Oral Presentation at Tissue Engineering Society International – 2003 Annual Meeting, Orlando, FL, December 2003. (work presented by G. L. Bowlin).

9. **Boland, E.D.**; Simpson, D.G.; Wnek, G.E. and G.L. Bowlin. "Acid Pretreatment of Electrospun Poly(glycolic acid) Nano-fibrous Scaffolds Improves Biocompatibility for Tissue Engineering Applications." Presented at the Tissue Engineering Society International – 2003 Annual Meeting, Orlando, FL, December 2003.

10. Wnek, G.E.; **Boland, E.D.**; Simpson, D.G. and G.L. Bowlin. "Electrospinning Tissue Engineering Scaffolds." Presented at the Materials Research Society Fall 2003 Meeting, Boston, MA, December 2003. (work presented by G.L. Bowlin).

11. **Boland, E.D.**; Wnek, G.E.; Simpson, D.G.; and G.L. Bowlin. "Electrospinning Micro- to Nano-scale Fibrous Tissue Engineering Scaffolds." Presented at the Biomedical Engineering Society 2003 Annual Fall meeting, Nashville, TN, October, 2003.

12. **Boland, E.D.**; Bowlin, G.L. "Novel Apparatus for the Electrospinning of Tissue Engineering Scaffolds." Presented at the Biomedical Engineering Society 2003 Annual Fall meeting, Nashville, TN., October 2003.

13. **Boland, E.D.**; Simpson, D.G.; Wnek, G.E.; Bowlin, G.L. "Electrospinning of Biopolymers for Tissue Engineering." Oral Presentation at the Division of Polymeric Materials: Science and Engineering. 226th American Chemical Society National Meeting, New York, NY, September 2003 (work presented by G.L. Bowlin).

14. **Boland, E.D.** "Automated Electrostatic Processing Device for Tissue Engineering Applications." Oral presentation at the Association for the Advancement of Medical Instrumentation Annual Conference, Long Beach, CA, June 2003.

15. **Boland, E. D.**; G. E. Bowlin. "Development of a Novel Electrostatic Processing Device for Tissue Engineering Applications." Oral presentation at the 81^{sr} Annual Meeting of the Virginia Academy of Science, Charlottesville, VA, May 2003.

16. Telemeco, T.A.; **Boland, E. D.**; Bowlin, G. L.; Wnek, G. E. and D. G. Simpson. "Integrin Mediated Regulation of the Substrate and Strain

Dependent Expression of Interstitial Matrix Metalloproteinases." Presented at TE-2003, 7th Annual Hilton Head Tissue Engineering Workshop, Hilton Head, SC, March 2003.

17. Telemeco, T.A.; **Boland, E. D.**; Matthews, J.A.; Bowlin, G. L.; Wnek, G. E. and D. G. Simpson. "Biocompatibility of Electrospun Type I Collagen, Gelatin, poly(glycolic acid) (PGA), poly(lactic acid) (PLA), and PGA/PLA co-Polymer." Presented at TE-2003, 7th Annual Hilton Head Tissue Engineering Workshop, Hilton Head, SC., March 2003.

18. Matthews J.A.; **Boland, E.D.**; Wnek, G.E.; Simpson, D.G. and G. L. Bowlin. "Electrospinning a Collagen Type II Tissue Engineering Scaffolding." Presented at TE-2003, 7th Annual Hilton Head Tissue Engineering Workshop, Hilton Head, SC., March 2003.

19. **Boland, E.D.**; Simpson, D.G.; Wnek, G.E. and G.L. Bowlin."Biocompatibility of Electrospun Poly (glycolic acid) Nanofiber Scaffolds." Presented at TE-2003, 7th Annual Hilton Head Tissue Engineering Workshop, Hilton Head, SC., March 2003.

20. Wnek, G.E.; Yao, L.; Kenawy, E.; Sanders, E.; Layman, J.M.; **Boland, E.D.;** Simpson, D.G.; Matthews, J.; Coleman, B.; G.L. Bowlin. 2002. "Microfiber and Nanofiber Polymer Scaffolds by Electrostatic Spinning: An Overview." *Polymeric Materials: Science and Engineering* 87: 455-456.

21. **Boland, E.D.**; Wnek, G.E.; G.L. Bowlin. "Utilizing Electrospinning to Control Fiber Diameters of Bioresorbable Polymers for Tissue Engineering Scaffolds." Oral presentation at the 80th Annual Meeting of the Virginia Academy of Science, Hampton, VA., May 2002.

22. **Boland, E.D.**; Wnek, G.E.; G.L. Bowlin. "Characterization of Electrospun Tissue Engineering Scaffolds Comprised of Poly(glycolic acid) Poly(lactic acid) and Polycaprolactone." Presented at the 5th Annual Graduate Research Symposium, Virginia Commonwealth University., April, 2002.

23. **Boland, E.D.**; Simpson, D.G.; Wnek, G.E. and G.L. Bowlin. 2002. "Methodology for Improving Tissue Incorporation Utilizing Electrospun Poly (Glycolic Acid)" *Cardiovascular Pathology* 11(1): 36. (Presented at the International Society for Applied Cardiovascular Biology Biennial Meeting, St. Gallen, Switzerland)

24. **Boland, E.D.**; Wnek, G.E.; G.L. Bowlin. "Electrospun Tissue Engineering Scaffolds Composed of Poly(Lactic Acid) and Polycaprolactone." Oral

presentation at TE2002: International Workshop on Tissue Engineering, St. Gallen, Switzerland. February, 2002.

25. **Boland, E.D.**; Wnek, G.E.; Simpson, D.G.; Telemeco, T. and G.L. Bowlin. 2001. "Engineering a Poly(Glycolic Acid) Tissue Scaffold by Employing Electrostatic Processing." *Annals of Biomedical Engineering* 29(1): S-144. (Biomedical Engineering Society Annual Fall Meeting, Durham, NC).

26. **Boland, E.D.**; Bowlin, G.L.; Simpson, D.G.; and G.E. Wnek. "Electrospinning of Tissue Engineering Scaffolds." Oral Presentation at the Division of Polymeric Materials: Science and Engineering. 222nd American Chemical Society National Meeting, Chicago, IL, August 2001 (work presented by G.E. Wnek).

27. Matthews, J.A.; Telemeco, T.A.; **Boland, E.D.**; Cohen, N.; Vida, M.; Bowlin, G.L. and D.G. Simpson. "Electroprocessing: Fabrication of Novel Biocompatible Materials." Presented at the 4th International Symposium on Frontiers in Biomedical Polymers, Williamsburg, VA, May 2001.

28. **Boland, E.D.**; Wnek, G.E.; Simpson, D.G.; Telemeco, T.A.; G.L. Bowlin. "Tailoring a Poly(Glycolic Acid) Tissue Engineering Scaffold by Utilizing Electrostatic Processing." Presented at the 4th International Symposium on Frontiers in Biomedical Polymers, Williamsburg, VA, May 2001.

29. **Boland, E.D.** and D.R. Elizondo. "Mechanical Heart Valve Prosthetics: In Vitro and In Vivo Wear Characteristics." Oral presentation at The American Ceramic Society Joint Fall Meeting., San Antonio, TX, October 1996.

PATENTS AND DISCLOSURES

Disclosures Filed

1.) "Electroaerosol Cell Seeding." Wnek, G., Lam, P., Bowlin, G.L., Simpson, D.G., Matthews, J., and E.D. Boland. Virginia Commonwealth University

2.) "Development of Tissue Engineered Heart Valves Utilizing and Electrospun Matrix." Bowlin, G.L., Simpson, D.G., Wnek, G. and E.D. Boland. Virginia Commonwealth University

3.) "Precision Winding Apparatus for Use with Electrostatic Processing." Boland, E.D., Bowlin, G.L., Simpson, D.G., and G.E. Wnek. Virginia Commonwealth University

4.) "Aqueous Electroprocessed Matrix." Simpson, D.G., Bowlin, G.L., Boland, E.D., Matthews, J.A., and G.E. Wnek. Virginia Commonwealth University.

5.) "Intervertebral Disc Prosthesis." Telemeco, T.A., Boland, E.D., Simpson, D.G., Bowlin, G.L., and G.E. Wnek. Virginia Commonwealth University.

6.) "Supervisory Control Software for a Precision Winding Apparatus for use with Electrostatic Processing." Boland, E.D. and Bowlin, G.L. Virginia Commonwealth University.

7.) "Electrospinning Collagen Type I from Acetic Acid." Bowlin, G.L., Simpson, D.G., Wnek, G. and E.D. Boland. Virginia Commonwealth University

8.) "Electrospinning Collagen Type I from Formic Acid." Bowlin, G.L., Simpson, D.G., Wnek, G. and E.D. Boland. Virginia Commonwealth University

9.) "Electrospinning Collagen Type I with Polydioxanone." Bowlin, G.L., Simpson, D.G., Wnek, G. and E.D. Boland. Virginia Commonwealth University